Universidade de Lisboa

Faculdade de Medicina

Focusing on metabolomic dysregulation and modulation of retinal metabolism to develop novel therapeutic strategies for Diabetic Retinopathy

Liliana Páris Pereira

Doutoramento em Medicina

Especialidade de Oftalmologia

2015

Universidade de Lisboa

Faculdade de Medicina

Focusing on metabolomic dysregulation and modulation of retinal metabolism to develop novel therapeutic strategies for Diabetic Retinopathy

Liliana Páris Pereira

Orientador: Professor Doutor Martin Friedlander, M.D./Ph.D

Co-orientador: Professor Doutor Luís Graça, M.D./Ph.D

Doutoramento em Medicina

Especialidade de Oftalmologia

Todas as afirmações efectuadas no presente documento são da exclusiva responsabilidade do seu autor, não cabendo qualquer responsabilidade à Faculdade de Medicina da Universidade de Lisboa pelos conteúdos nela apresentados

A impressão desta dissertação foi aprovada pelo Conselho Científico da Faculdade de Medicina de Lisboa em reunião de 23 de Junho de 2015

Acknowledgements

At the beginning of my PhD journey someone told me that I should be emotionally prepared to enjoy moments of great enthusiasm and to survive moments of profound despair and frustration, all rooted in my research project. This was indeed the case and thanks to the people who I am about to mention, I managed to overcome those bleak moments and to get back the motivation I needed to keep loving science and my own research projects ☺

I would like to start by expressing my very special thanks to my supervisor, Professor Martin Friedlander, for accepting me as a student in his laboratory, for his guidance, for always replying to my emails personally (even before he met me); for making me feel part of the 'family' from the moment I arrived (and even when I interviewed); for always meeting with me (despite his very busy schedule) when I had my 'scientific-existential panic attacks', for telling me that everything would be ok because "this is how science works"☺ and making me feel that I could do it; for introducing me to the Mactel project and to a large number of brilliant scientific minds; and finally for all the great pieces of advice on life. I would also like to thank Professor Friedlander and his family for their genuine care and concern from the very start, which made me feel more comfortable and less lonely when I first arrived, and also for their precious advice (and living example) on how to achieve a successful career and a happy and fulfilling family life.

I would also like to express my most sincere gratitude to my thesis committee members, Professor Luis Graça, Professor Luísa Coutinho-Santos, Professor João Ferreira and Professor Sérgio Dias for agreeing to be on my committee, for their genuine interest in my projects, for their brilliant and kind comments and suggestions, for their availability to help my work come to fruition and for their encouraging emails and continued support. Thank you so much for being there for me despite the physical distance and the time difference!

I owe a very important debt to two friends (1) Dr Peter Westenskow who patiently taught most of the molecular biology techniques I know, who accompanied and supervised me in my first experiments, who spent endless hours critically revieweing what I wrote, listening to my scientific hypothesis, doubts and preliminary presentations and discussing them with me afterwards; and (2) Michele Gerhart who, jointly with Dr Westenskow, helped me get settled in my new life, introduced me to the lifestyle of San Diego and took me for invigorating walks when I was feeling discouraged.

I would like to show my greatest appreciation to the members of my laboratory who have helped me immensely during this journey, and especially to: Dr Yoshi Usui, for his genuine interest in my projects, his excellent experimental suggestions and his optimistic and encouraging words of wisdom at all times; Dr Marin Gantner, for her friendliness and

encouraging comments, for sharing her expertise in metabolism with me, for her crucial assistance with metabolic experiments and for critically reviewing my manuscripts; Dr Edith Aguilar for continuous moral support and total availability for assistance with experiments, Dr Toshihide Kurihara, for his bright suggestions and technical help; Dr Lindsay Keir, Dr Salome Murinello, Dr Felicitas Bucher and Dr Susumu Sakimoto for their friendly advice, moral support and great experimental suggestions; Carli Wittgrove, Daniel Feitelberg and Regis Fallon for their assistance with experiments, friendliness and for their enthusiastic support.

I have greatly benefited from fruitful discussions with Professor Edward Holmes who kindly listened to my data presentations, provided insightful comments and suggested new directions based on his expert knowledge. These insights greatly contributed to improve my projects.

A special thanks goes to my incredibly amazing parents, sister and close family, who have given me all the support and love I could ever wish for despite the long periods without phone calls and quick emails; and to my lovely friends (especially Henrique, Nádia, João Mariana, Raul, Gwena, Marc, Elise, Vincent and Jessica) who kept checking on me despite my uncharacteristic aloofness. Their funny, caring and encouraging chats and emails helped me get through the “darkest times”.

Finally, I would like to show my greatest appreciation to the Institutions (Fundação Calouste Gulbenkian, FCT, Fundação Champallimaud) and people who made the PFMA IV program possible, and especially to the ones I had the chance to contact directly with, namely: Professor Leonor Parreira (founder of the program); Professor António Coutinho (Director of the IV Edition); Professor Thiago Carvalho and Professor João Ferreira who continuously supported me, sending emails with new articles and encouraging words of advice; and Professor Francisca Fontes,, whose constructive comments and warm encouragement greatly assisted me in writing my project proposal. I would also like to thank Dra Francisca Moura, Dra Teresa Burnay (at FGC) and Manuela Cordeiro (at Instituto Gulbenkian de Ciência) for making my life so much easier whenever I ran into administrative issues.

My deepest thanks to everyone who made this challenging yet rewarding PhD journey possible and if I have forgotten to mention someone, please forgive me and “blame it on my absentmindedness, not my intention”.

Table of contents

List of Figures

List of Tables

List of Abbreviations

ACCORD - The Action to Control Cardiovascular Risk in Diabetes

AGEs - Advanced glycation end products

AMD - Age-related macular degeneration

AMP – Adenosine monophosphate

Ang 1 - Angiopoietins 1

Ang 2 - Angiopoietins 2

BCVA – Best corrected visual acuity

bFGF – Basic fibroblast growth factor

BM – Bruch's membrane

BMI – Body Mass Index

BP – Blood pressure

BRB – blood retinal barrier

iBRB – inner blood retinal barrier

oBRB – outer blood retinal barrier

BVO - Branch vein occlusions

CAM - Chick chorioallantoic membrane

CC – Choriocapillaris

CCL2 (MCP-1) - Chemokine (C-C motif) ligand 2

CCR2 (CD 192) - C-C chemokine receptor type 2

CNS - central nervous system

CNV - Choroidal neovascularization

cGMP – cyclic GMP

Dll4 – Delta-like ligand 4

DCCT – The Diabetes Control and Complications Trial

DME – Diabetic macular edema

DR – Diabetic retinopathy

DT - Diphtheria toxin

iDTR – (inducible) Diphtheria toxin receptor

EC – Endothelial cells

ECM – Extracellular matrix

EPO – Erythropoietin

ERG – Electroretinogram

ETC – Electron transport chain

FGF - Fibroblast growth factor

GCL – Ganglion cell layer

GFAP – Glial fibrillary acidic protein glial

GFP – Green fluorescent protein

eGFR – (estimated) Glomerular filtration rate

GMP – Guanosine monophosphate

GPR91 – G-protein coupled receptor 91

HbA1C – Glycated Hemoglobin

HIFs – Hypoxia inducible factor (Includes HIF-1alpha and HIF-2alpha)

HPLC – High performance liquid chromatography

iBRB – Inner blood retinal barrier

iDTR – Inducible Diphtheria toxin receptor

IL-1 β – Interleukin-1β

ILM – Inner limiting membrane

INL – Inner nuclear layer

IMM – Inner mitochondrial membrane

IMP – Inosine-5'-monophosphate

IOP – Intraocular pressure

IPL – Inner plexiform layer

IRMA - Intraretinal microvascular abnormalities

IS – Inner segments (of photoreceptors)

ISH - *In situ* hybridizations

KLF 2 – Krüppel-like Factor

LC/MS – Liquid chromatography mass spectrometry

MacTel – Idiopathic Juxtafoveal Macular Telangiectasia (Type II)

MAP-2 - Microtubule-associated protein 2

M1 – Pro-inflammatory macrophages

M2 – Anti-inflammatory macrophages

METLIN – Software available online for putative identification of metabolites (Developed by the Siuzdak's lab at TSRI)

MS – Mass spectrometry

NADPH - Nicotinamide adenine dinucleotide phosphate

NFL – nerve fiber layer

NOS – Nitric oxide synthase

NO – Nitric oxide

NP-1 – Neuropillin 1

NPDR – Non-proliferative diabetic retinopathy

NV – Neovascularization

NVU – Neurovascular unit

oBRB – Outer blood retinal barrier

OCR - Oxygen consumption rate

OIR – Oxygen-induced retinopathy

OLM – Outer limiting membrane

ONL – Outer nuclear layer

OPs – Oscillatory potentials

OPL – Outer plexiform layer

ORF - Open reading frame

OS – Outer segments (of photoreceptors)

PAM - Peptidylglycine alpha-amidating monoxygenase

PDGF – Platelet derived growth factor

PDR – Proliferative diabetic retinopathy

PGC-1α - Peroxisome proliferator-activated receptor Y coactivator 1-α

PHD 1 - 3 – Oxygen-sensing prolyl hydroxylase domain proteins

PI3K/AKT - Phosphatidylinositol 3-kinase/Protein kinase B pathway

PKC - Protein kinase C

PRs – Photoreceptors

PRP - Panretinal photocoagulation

Ptf1a - Pancreas specific transcription factor 1 subunit alpha

RAP - Retinal Angiomatous Proliferation

RD - Retinal degeneration

RGC – Retinal ganglion cells

ROP – Retinopathy of prematurity

RPE – Retinal pigment epithelium

RTK - Receptor tyrosine kinases

RT-PCR/PCR – Real-time polymerase chain reaction

SD-OCT – Spectral domain optical coherence tomography

TNF-α – Tumor necrosis factor- α

TSRI - The Scripps Research Institute

TUNEL - Terminal deoxynucleotidyl transferase dUTP nick end labeling staining

UCB – University of California at Berkeley

UCSD - University of California at San Diego

UCSF – University of California at San Francisco

UKPDS - The UK Prospective Diabetes Study

VEGF – Vascular endothelial growth factor

VEGFR-1 (FLT-1) – Vascular endothelial growth factor receptor 1

VEGFR-2 (FLK-1; KDR) - Vascular endothelial growth factor receptor 2

VHL (pVHL) – Von Hippel Lindau suppressor gene product

VLDLR – Very low-density lipoprotein receptor

VMD2 - vitelliform macular dystrophy-2

VO – Vaso-obliteration (or vaso-obliterated)

WS – Wolfram syndrome

WFS1 – Wolfram syndrome type 1 gene

XCMS – Web-based platform to process untargeted metabolomic data (Software developed at the Siuzdak's lab, TSRI

Resumo

A retinopatia diabética (RD) é uma complicação neurovascular da diabetes que afecta 126.6 milhões de pessoas em todo o mundo (o que equivale a 34.6% da população diabética mundial) e que constitui uma das principais causas de cegueira em adultos com idade inferior a 65 anos, nos países industrializados.

De acordo com as características do fundo ocular, a RD pode ser classificada em não-proliferativa e proliferativa. A RD não-proliferativa corresponde à fase inicial da doença e é identificada pela presença de microaneurismas, hemorragias e exsudados intraretinianos. A RD proliferativa, por sua vez, caracteriza-se pela presença de uma rede neovascular patológica que se desenvolve na superfície retiniana em direcção ao humor vítreo, e reflecte a fase avançada da doença. Estes neovasos podem dar origem a descolamentos de retina, através da formação de membranas fibrovasculares na superfície retiniana e vítreo que exercem tracção sobre a neuro-retina e conduzem à sua separação do epitélio pigmentar que lhe está subjacente, e hemorragias vítreas. Estes fenómenos em conjunto com o edema macular diabético (que se pode desenvolver durante as fases iniciais ou tardias de RD), constituem as principais causas de perda de visão na população com RD.

Apesar da elevada prevalência mundial de RD, as estratégias preventivas e terapêuticas actualmente existentes são bastante limitadas. Presentemente, não existem biomarcadores específicos e validados capazes de prever a evolução da doença e as duas estratégias terapêuticas mais frequentemente utilizadas - fotocoagulação laser e injecções intraoculares de agentes anti-angiogénicos - são incapazes de evitar a sua progressão de modo eficaz e permanente em todos os doentes. Além disto, estas terapias são implementadas em fases já avançadas de RD e, devido ao seu modo de actuação “não-selectivo” e destrutivo, podem potencialmente induzir uma panóplia de efeitos adversos a nível retiniano (laser e agentes anti-angiogénicos) e até sistémico (agentes anti-angiogénicos).

Uma das causas que justifica a falta de progresso no que respeita ao desenvolvimento de novas estratégias terapêuticas para a RD é a ausência de um modelo animal roedor diabético capaz de reproduzir fielmente as características patológicas típicas das fases tardias da doença, nomeadamente a neovascularização pré-retiniana.

Nesta dissertação irei introduzir os seguintes conceitos que proporcionam uma visão integradora da RD e que poderão vir a ser úteis para o desenvolvimento de terapêuticas futuras mais eficazes e capazes de actuar mais precoce e selectivamente:

(**1**) A RD tem sido classicamente encarada como uma doença vascular e as linhas de orientação clínica actualmente vigentes ainda se baseiam neste pressuposto. Contudo, existe um acumular de evidência científica e clínica que demonstra que o compromisso da função neuronal retiniana (revelado por alterações electrofisiológicas, tais como: alterações de potenciais oscilatórios e redução da vasodilatação em resposta à estimulação "Flicker") ocorre mais precocemente do que as alterações vasculares do fundo ocular. Uma vez que (1) o funcionamento adequado da retina requer comunicações intercelulares estáveis entre neurónios, vasos e células da glia na unidade neurovascular, e que (2) a RD se caracteriza por compromisso neuronal e vascular, é provável que a desestabilização das interacções neurovasculares retinianas contribua activamente para o desenvolvimento e progressão da doença.

(**2**) Na investigação da patofisiologia da RD, a utilização de análises metabolómicas e de estudos focados no metabolismo energético retiniano tem sido surpreendentemente escassa. Um exemplo paradigmático desta situação é reflectido pelo facto do perfil metabolómico da RD permanecer desconhecido.

A diabetes tem origem num defeito metabólico que compromete profundamente a produção energética a nível celular. Por outro lado, a neuro-retina é um dos tecidos metabolicamente mais exigentes do organismo. Esta combinação é potencialmente catastrófica no que toca à função retiniana, pelo que identificar perturbações metabólicas na retina diabética poderá providenciar uma nova perspectiva em relação à RD.

(**3**) Apesar de se saber que a comunicação entre fotorreceptores, interneurónios, células da glia e vasos retinianos é mediada por metabolitos cuja produção se encontra comprometida em condições patológicas, os mecanismos precisos subjacentes a estas interacções neurovasculares permanecem desconhecidos. Aprofundar o conhecimento a este nível é crucial, pois as unidades neurovasculares retinianas são responsáveis pela regulação do fluxo sanguíneo

para as redes neuronais, assegurando assim o seu dinamismo e funcionamento adequados.

Além dos pontos previamente mencionados, também observações clínicas estiveram na génese do plano de investigação apresentado nesta dissertação; uma das observações mais relevantes consiste na existência de um sub-grupo de doentes diabéticos de longa duração que se encontra aparentemente protegido contra o desenvolvimento de estados avançados de RD (e que por vezes não desenvolve RD de todo) mesmo quando o controlo metabólico é desadequado. Porém, os mecanismos subjacentes a esta protecção permanecem desconhecidos. Estudar estes doentes proporciona uma excelente oportunidade para identificar factores protectores endógenos e também para alcançar uma melhor compreensão dos mecanismos envolvidos no desenvolvimento e progressão da RD.

Para adquirir conhecimentos mais aprofundados acerca (1) da existência de perturbações metabólicas locais e do seu impacto no desenvolvimento e progressão da RD, e (2) dos mecanismos que comprometem a comunicação neurovascular na retina diabética, a utilização de análises metabolómicas altamente sensíveis baseadas em espectrometria de massa constitui a estratégia experimental ideal. Neste trabalho esta tecnologia foi utilizada para analisar amostras clínicas de humor vítreo e de soro sanguíneo provenientes de pacientes diabéticos com diferentes graus de RD e de controlos não-diabéticos com o objectivo de: (1) obter uma visão global do perfil metabolómico característico das fases avançadas de RD; e de (2) identificar factores circulantes potencialmente protectores.

Na RD proliferativa (RDP) foi identificada uma grave desregulação nos níveis de amino-ácidos no humor vítreo, em especial daqueles envolvidos no metabolismo da arginina-prolina. Estes resultados sugeriram uma metabolização preferencial da arginina pela via da arginase em detrimento da via alternativa, a da sintase do óxido nítrico. Estudos subsequentes num modelo de ratinho não-diabético ("oxygen-induced-retinopathy mouse", OIR) que desenvolve características de retinopatia isquémica revelaram um perfil metabolómico idêntico ao observado no vítreo de doentes com RDP. Análises posteriores utilizando isótopos estáveis de azoto (^{15}N) com o objectivo de estudar mais detalhadamente o metabolismo da

arginina no olho do ratinho OIR confirmaram a hipótese previamente sugerida ao demonstrar uma hiperactividade da enzima arginase com produção preferencial de prolina. Desregulação a este nível pode potencialmente comprometer a comunicação neurovascular retiniana, pois o óxido nítrico (produto da via enzimática alternativa cuja actividade se encontra diminuída nestas condições) é um importante modulador das interacções celulares na unidade neurovascular.

O trabalho apresentado nesta dissertação identificou também novas funções para os interneurónios e fotorreceptores retinianos, ao revelar que estes desempenham um papel activo no desenvolvimento e manutenção dos vasos que os nutrem, sendo capazes de regular directamente o fluxo sanguíneo que recebem. Deste modo, estudar mais detalhadamente a disfunção dos (inter)neurónios retinianos nesta capacidade vaso-reguladora poderá proporcionar pistas adicionais para melhor compreender os mecanismos envolvidos na disrupção da comunicação neurovascular retiniana.

As análises metabolómicas efectuadas no soro de pacientes diabéticos com ou sem RDP revelaram que os doentes “protegidos” (i.e., diabéticos de longa duração sem RDP) tinham níveis significativamente mais elevados de inosina, um metabolito gerado durante o metabolismo das purinas. Para averiguar o seu potencial terapêutico na retinopatia isquémica, este metabolito foi injectado directamente no olho do ratinho OIR. A administração de inosina aumentou significativamente a revascularização das áreas retinianas isquémicas, reduzindo consequentemente o desenvolvimento de neovascularização patológica. Simultaneamente a estes efeitos fenotípicos benéficos, as injecções de inosina induziram também efeitos metabólicos vantajosos através dos seguintes mecanismos: (1) redução da produção de prolina, o que sugere um antagonismo da via metabólica da arginase que se encontra hiperactiva em condições de retinopatia isquémica; e (2) adaptação do metabolismo basal mitocondrial (oxidativo) às adversas condições metabólicas locais através da redução selectiva de consumo de oxigénio nas áreas retinianas isquémicas; este efeito pode potencialmente aumentar a tolerância dos neurónios retinianos ao ambiente hipóxico, graças à redução da discrepância entre oferta e utilização de recursos metabólicos nestas regiões retinianas vulneráveis.

Finalmente, as injecções intravítreas de inosina foram também responsáveis por moderar favoravelmente a resposta inflamatória na retina isquémica e este

fenómeno poderá ser consequência de uma melhoria global do estado metabólico.
Em resumo, o trabalho apresentado nesta dissertação recorreu a análises metabolómicas para responder a duas intrigantes questões relativas à RD:

(1) Qual é o perfil metabólico ocular característico da RDP?
(2) Quais são os potenciais factores circulantes endógenos responsáveis pela "protecção" de um subgrupo de doentes diabéticos de longa duração que não desenvolve RDP?

As respostas a estas questões, descritas em maior detalhe ao longo dos próximos capítulos, poderão vir a contribuir para o desenvolvimento de futuras terapias, mais selectivas, mais eficazes e de actuação mais precoce do que as actualmente existentes e poderão, potencialmente, revolucionar o tratamento da RD e melhorar a qualidade de vida dos doentes diabéticos.

Palavras-chave: Diabetes, Retinopatia isquémica; Neovascularização pré-retiniana; Metabolismo retiniano; Terapêuticas selectivas

Abstract

Diabetic retinopathy (DR) is a neurovascular complication of diabetes mellitus and a leading cause of blindness in adults below the age of 65, in industrialized nations. Currently there are 126.6 million people with DR worldwide (34.6% of the total diabetic population) and it is estimated that this number will increase to 191.0 million by 2030. Generally, DR is divided into two stages: non-proliferative diabetic retinopathy (NPDR), an earlier phase characterized by appearance of microaneurysms, dot and blot hemorrhages, capillary occlusions and nerve fiber layer infarcts and; and proliferative diabetic retinopathy (PDR), the late-stage disease, which is diagnosed when pathological neovascular changes are identified on the retinal surface and/or vitreous. Diabetic macular edema (DME) can develop at any stage and reflects a pathological increase in retinal vascular permeability.

Despite its high prevalence, current availability of preventive and therapeutic strategies is far from ideal. In fact, there are no reliable biomarkers to predict risk of developing DR and no effective, targeted and early-acting therapies to sustainably and safely prevent disease progression into its vision threatening stages: PDR and DME. The two main therapeutic options currently available for DR are laser photocoagulation and intravitreal injections of anti-vascular endothelial growth factor (VEGF) agents; these constitute “non-selective” and destructive (especially for laser therapy) approaches that are not only unable to effectively and sustainably arrest retinal disease progression in every case, but can also potentially induce a myriad of undesired off-target effects at the retinal level and even systemically, in the case of VEGF antagonists. Moreover, they act late in the disease course.

The lack of reliable rodent models - there is no diabetic mouse model that spontaneously recapitulates the late stages of DR - has greatly hindered research progress and development of novel and effective drugs for PDR, further contributing to the present therapeutic scenario.

In this dissertation I will introduce and present my experimental work in the context of the following concepts, which can potentially lead to development of targeted, earlier acting, less destructive and more effective future therapies for DR:

(**1**) DR has long been regarded as a vascular disease and present-day DR management guidelines are still based on this assumption. However, a growing body of evidence shows that retinal neuronal function becomes impaired before vascular changes can be detected; these findings along with those showing that adequate retinal functioning depends on stable intercellular interactions within neurovascular units, suggest that disrupting retinal neurovascular crosstalk may play a critical role in promoting disease development and progression.

(**2**) Metabolomic studies have been surprisingly neglected in the investigation of DR's pathophysiology, and this is clearly reflected by the fact that the metabolome of human DR remains unknown. Furthermore, the neuroretina is one of the most metabolically demanding tissues in the body per unit weight, and diabetes is triggered by a metabolic defect that profoundly impairs cellular energy production. These features constitute a potentially disastrous combination in regard to retinal functioning and suggest that studying retinal energy metabolism in DR is critical.

(**3**) Metabolic cycles of photoreceptors, interneurons and glial cells are still under debate and, even though it is known that intercellular communications within the neurovascular unit (NVU) are mediated by metabolites whose production becomes dysregulated under pathological conditions, the precise mechanisms underlying retinal neurovascular coupling are not fully identified. Gaining further insight into these interactions is pivotal because retinal NVUs are responsible for regulating blood flow for functionally dynamic retinal neuronal networks and, thus, for their proper functioning.

Besides the points stated above, additional clinical clues were considered to guide the research plan presented in this dissertation. One the strongest came from a subset of long-term diabetic patients who appear to be protected from developing late-stage DR, by an unknown mechanism. Studying these patients provides an excellent opportunity to identify protective factors and to further understand the mechanisms involved in progression of DR.

In order to better understand how metabolic dysregulation impacts development of DR, how neurovascular interactions become compromised in the diabetic retina, and to develop strategies to potentially restore homeostasis within the NVU, we decided to use metabolomic analyses. A highly sensitive metabolomics mass-spectrometry based approach was used in ocular and serum samples to identify the most prominent metabolic perturbations, to acquire a global overview of the

metabolomic landscape in late-stage DR and to identify potentially protective circulating factors.

At the ocular level, late-stage diabetic retinopathy was associated with severe dysregulation in amino acid levels; this was especially prominent in those generated during arginine metabolism, suggesting a preferential activity in the arginase pathway over the alternative Nitric Oxide Synthase (NOS) pathway; Studies in the Oxygen-Induced-Retinopathy (OIR) mouse, a non-diabetic model that develops features of ischemic retinopathy, revealed a very similar metabolic landscape and, *in vivo* global isotope analysis confirmed the presence of asymmetrical arginine metabolism by showing: (1) over-activity in the arginase pathway leading to enhanced proline production; and (2) reduced activity in the alternative NOS pathway, with potentially reduced NO production. Even though NO's role in DR and other retinopathies is not clearly understood, NO is known to be an important modulator of cellular interactions within the NVU and its lower availability in specific locations and/or time-points in pathological conditions may significantly contribute to the disruption of retinal neurovascular crosstalk.

The work presented in this dissertation has also described novel functions for interneurons (amacrine and horizontal cells) and photoreceptors within the NVU, by showing that these cells play an active role in regulating their primary vasculature and thus, their blood supply. Furthermore, it has also shown that dysfunction of retinal neurons in this capacity can directly alter their own blood supply, therefore providing additional clues for disrupted retinal neurovascular crosstalk.

Metabolomic analyses comparing serum samples from diabetic patients with or without PDR (long-term diabetic patients "protected" from late-stage DR versus those who were non-protected) revealed that "protected" patients had higher circulating levels of a purine metabolite, inosine. To assess its therapeutic potential in conditions of retinal ischemia, inosine was delivered to the eye of the OIR mouse where it enhanced effective revascularization of ischemic retinal areas, thus significantly reducing pathological neovascularization.

These effects were associated with a favorable modulation of the local pro-inflammatory response that could result from an improved overall retinal metabolic status. These beneficial effects on retinal metabolism induced by inosine injections were observed as: (1) a reduction in basal mitochondrial respiration in vaso-

obliterated areas (i.e., ischemic areas), which can potentially increase retinal neuronal tolerance to hypoxia by reducing the metabolic mismatch created by scarce metabolic supply and high neuronal demand; and (2) a reduction in proline production, suggesting antagonism of the arginase pathway (which is hyperactive in oxygen-induced-retinopathy and potentially in human PDR).

In summary, the work presented in this dissertation employed a metabolomic-focused approach with a strong focus on neurovascular crosstalk to answer two intriguing questions regarding DR:

(**1**) What is the characteristic ocular metabolic landscape of severe DR?

(**2**) Is the "protection" against severe DR (observed in some long-term diabetic patients) associated with differences in circulating metabolic factors?

The answers to these questions, presented below, could serve as the basis of future targeted, more effective and earlier acting therapeutics that would revolutionize DR patient management.

Identification of the most prominently affected metabolic pathways in eyes with severe DR has identified specific pathways of amino acid metabolism as potential targets for development of new drugs for DR. We have also identified a circulating protective factor, inosine, in "protected" patients and further investigated its ability to (1) prevent development of retinal ischemia and pathological neovascularization; (2) adjust retinal metabolism to the limited energy supplies in ischemic areas; and (3) counteract development of prominent metabolic dysregulation by potentially inhibiting the pathology-promoting arginase pathway. We believe that inosine can potentially become an effective, early-acting therapeutic agent to prevent progression of DR.

In addition, these metabolites could potentially be used as reliable biomarkers for monitoring response to therapy and for predicting risk of developing or progressing DR. Finally, the work presented in this dissertation supports the concept that early intervention for treating DR will restore balance and stabilize cellular interactions within the NVU, thereby reversing the chronic stressors (e.g., extreme conditions of metabolic insufficiency in retinal ischemic areas) that ultimately drive development and progression of retinal pathology.

Keywords: Diabetes; Ischemic retinopathy; Pre-retinal neovascularization; Retinal metabolism; Targeted therapies.

Chapter I: Introduction

Diabetes affects 382 million people worldwide and approximately 35% of diabetic patients develop diabetic retinopathy (DR), a retinal disease that constitutes a leading cause of blindness in adults below the age of 65 in industrialized nations[1].

Currently, there are no reliable biomarkers to assess risk of disease progression and the existing therapeutic strategies (laser photocoagulation and anti—vascular endothelial growth factor agents) act late and can induce potentially significant side effects, both at the retinal and systemic levels[2-4].

Even though neuronal dysfunction, identified by electrophysiological (ERG) testing, constitutes one of its earliest features, DR is still largely regarded as a disease of vascular origin. Clinical diagnosis and monitoring of disease progression continue to rely upon appearance and development of retinal vascular changes, which occur only later in the disease process[5]. This focus on the vasculature, which is commonly observed both in DR research and in the clinic, is highly limiting as it provides a restricted view of the disease effects on the retina and of its pathophysiology.

In order to avoid progression of diabetic retinopathy into its devastating late-stages and improve diabetic patient care, discovery of new biomarkers and therapeutic targets is imperative[6]. Achieving this goal requires adoption of a new, integrative perspective that takes into account the interdependence amongst the different retinal cell populations and focuses on the disruptive effects of diabetes on retinal neurovascular metabolic crosstalk.

To better understand the potential positive impact of this paradigm shift on development of new management strategies for DR, some essential ophthalmological, vascular and metabolic concepts will be discussed here in Chapter I, in the following sections:

- Anatomy of the eye
- Physiologic vascular development
- Retinal pathological neovascularization
- Diabetic retinopathy: state of the art
- The neurovascular unit (NVU)
- The role of metabolic factors in retinal disease

A. Anatomy of the Eye

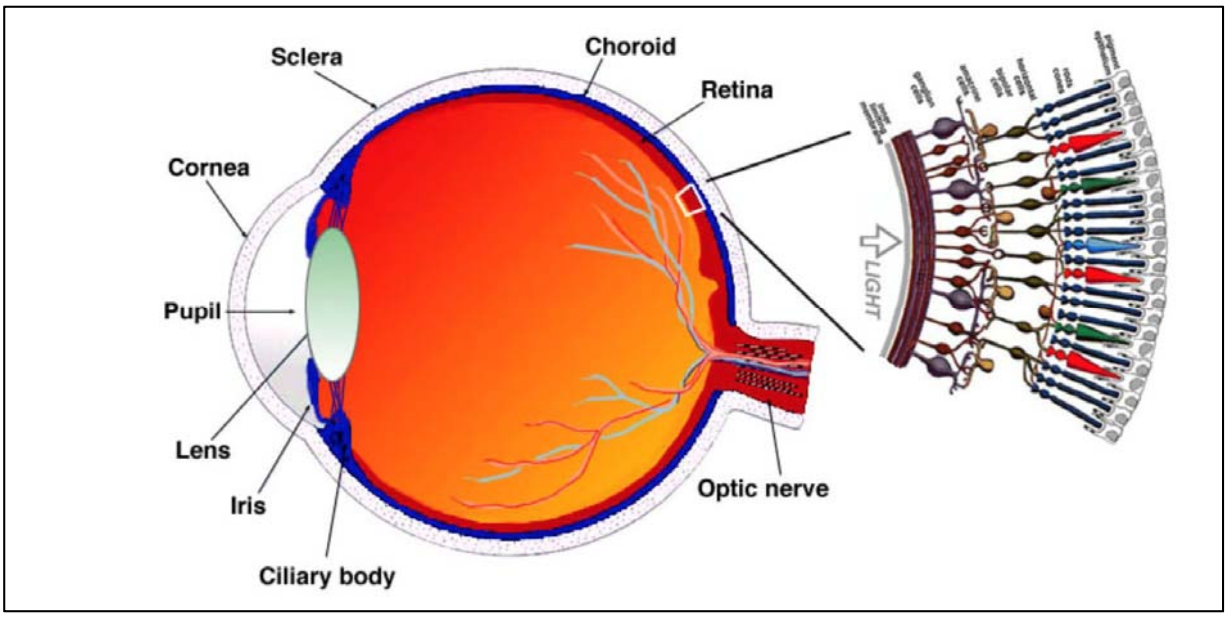

Figure 1 - Simplified representation of the human eye [7]

A.1. General Organization

The human eye is a highly complex structure composed of three different layers that enclose its fluid contents. The ***external layer*** is formed by the sclera, a meshwork of irregularly organized type I and III collagen fibers that provides shape and protection to the eye ball, and the cornea, an avascular and transparent structure consisting of highly ordered collagen fibers; the ***intermediate layer*** comprises the iris (its sphincter and dilator muscles control the diameter of the pupil), the ciliary body (that controls accommodation and produces aqueous humor), and the choroid (a layer of blood vessels that nourishes part of the eye); and the ***internal layer*** formed by the retina, which includes a light-sensitive portion (occupying 75% of its total area) responsible for phototransduction, and a small light-insensitive region (25%).

A.1.a. Anterior and Posterior Segment

From a clinical standpoint it is common to divide the eye into two principal anatomical segments, anterior and posterior, which are separated by an imaginary line just behind the lens (**Figure 1**). The anterior segment is formed by the cornea, iris, ciliary body and the anterior part of the sclera whereas the posterior segment extends from the lens to the back of the eye, including the vitreous body, the retina-choroid complex and the optic disc.

For the purpose of this work, we will be focusing on the posterior segment and more specifically on the retina and retinal pigment epithelium (RPE)-choroid complex.

A.1.b. The Fundoscopic Examination

The retina is the only readily visible portion of the central nervous system and the ocular fundus is the only location where vasculature can be directly visualized, providing a direct window on the patient's overall vascular status.

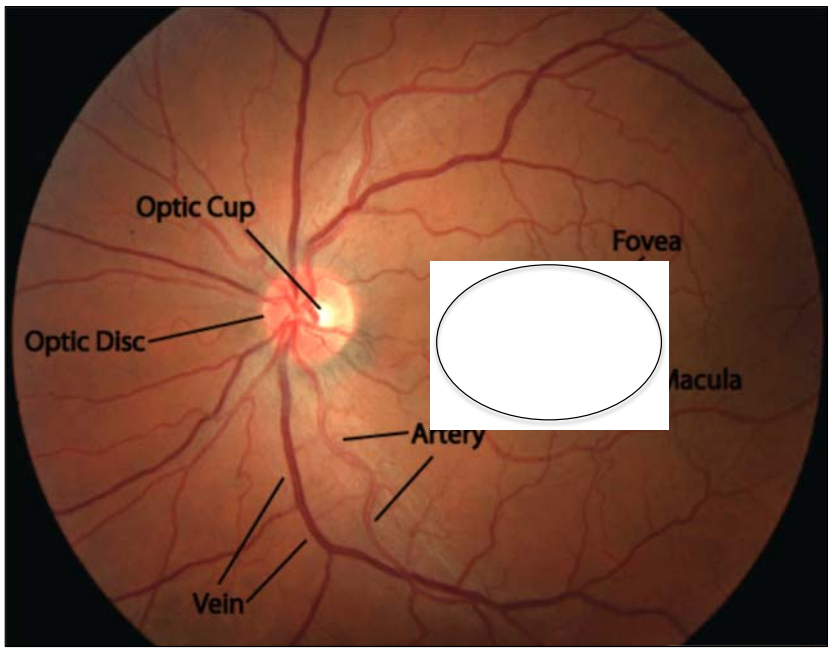

Figure 2 - Structures identified on fundoscopic examination[7]

When performing a fundoscopic examination, several retinal structures can be identified and assessed (**Figure 2**), namely:

- The *retinal vasculature*
    - The retinal artery and the retinal vein can be easily identified as part of the four retinal vascular arcades (superior temporal, inferior temporal, superior nasal and inferior nasal) that radiate from the optic nerve
- *Optic disc*
    - The optic disc (or optic papilla) is the region through which retinal ganglion cell (RGC) axons bundle together to leave the retina and form the optic nerve
    - A cup to disc ratio of 0.3 (cup occupying 1/3 of the diameter of the entire disc) is considered normal. When this ratio increases, however, it suggests a loss of neuroretinal tissue.

- *Macula and fovea*
    - The macula is a yellow-pigmented area located to the temporal side of the optic disc that includes the fovea, an avascular zone formed exclusively by cone photoreceptors concentrated at their maximal density and arranged at their most efficient packing density (hexagonal mosaic) for maximal visual efficiency. Maintenance of this highly ordered array of foveal cones is critical to ensure the highest resolution and best color vision.
    -

A.1.c. Components of the Retina-Choroid complex

The retina-choroid complex includes three main structures: the neuroretina, the retinal pigment epithelium (RPE) and the choroid.

A.1.c.i. Neuroretina

The noblest part of the eye is the retina, a highly specialized direct extension of the brain. The retina is a thin (0.5 mm) layer that covers the back of the eye and is composed by neurons, interneurons, glial cells and vasculature organized in a highly ordered fashion.[8] The retina has a discrete laminar structure, easily

identified on hematoxylin and eosin stainings (**Figure 3**), formed by the ganglion cell layer (GCL), the inner plexiform layer (IPL), the inner nuclear layer (INL), the outer plexiform layer (OPL), the outer nuclear layer (ONL) and the outer segments of photoreceptors (OS)[8].

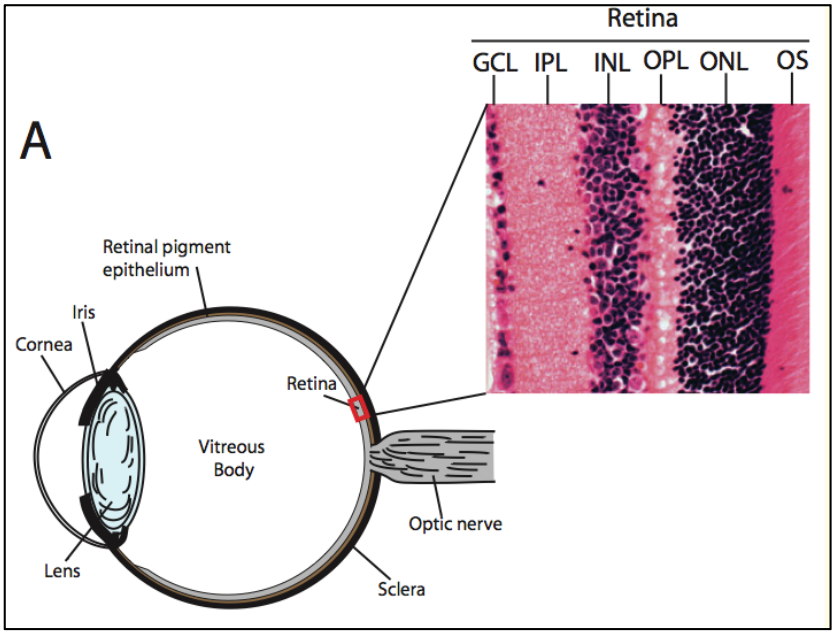

Figure 3 - Histological section of the human retina showing its different layers (the nuclei of the retinal cells are arranged in nuclear layers - ONL and INL – while their axons form the plexiform layers – IPL and OPL). Schematic representation of the gross anatomy of the eye[8]

Retinal neurons and phototransduction

The light-sensing photoreceptors (rods and cones) reside in the outermost layers of the neural retina, OPL and ONL, and form specialized apical extensions - the outer segments - that are crucial for visual processing because they contain the light sensitive photopigments and the phototransduction machinery (**Figure 4**).

Rods are highly sensitive photoreceptors (PRs) under scotopic conditions (i.e. in low light) whereas *cones* perform their functions under photopic conditions (i.e. in bright light), being responsible for our visual acuity and color vision.

The neural signals generated by photoreceptors in response to light are transferred to another neuronal cell type, the *bipolar cell,* present in the INL.

Amacrine and horizontal cells then act as inhibitory interneurons and modulate the neural signal within the INL. Finally visual information is transmitted to the dendrites of *retinal ganglion cells (RGC)* that send the information to the visual centers of the brain through their axons, which form the optic nerve[8].

In summary, the phototransduction process is initiated when light photons are captured by cone and rod photoreceptors in the outer retina, transformed into electric signals and passed on to bipolar cells. These transmit the electrical impulses to the retinal ganglion cells, which in turn send the integrated signal to the visual cortex. This process is modulated within the INL by amacrine and horizontal cells, which function as lateral inhibitory neurons.

Visual cycle (**Figure 4**)

In contrast to what would be expected, photoreceptor cells are more metabolically active under scotopic conditions. These cells depolarize in the absence of stimuli (e.g. light) and hyperpolarize in presence of light. Under scotopic conditions, cGMP levels are high and open cGMP-gated sodium channels, which create a steady inward current (the dark current) that maintains PR cells in a depolarized state and, hence, continually active[9].

Both in cones and in rods the absorption of light energy by their photopigments (formed by opsin and 11-cis retinal and present in the outer segments) initiates the same neural response, hyperpolarization. Photopigments must be continually recycled in order for visual activity to occur[10].

Rhodopsin is composed by the apoprotein, opsin, covalently linked to the chromophore 11-cis-retinal, by a protonated Schiff base[11]. Rhodopsin is the only photosensitive pigment present in rods. In cones, however, there are three different varieties of opsins covalently bound to 11-cis retinal; these opsins are distinguishable by their amino acid sequences, which modulate the absorption spectra of their associated chromophore (11-cis-retinal), thus determining the light absorption peaks in the blue, green and red portions of the visible light spectrum. All three opsins coexist in every cone but the predominance of one type of opsin defines the cone type[10]. Most humans have trichromatic vision due to presence

of three types of cones, the S cones (for short wavelength – 420 nm), the M-cones (for medium wavelength – 530 nm) and the L-cones (for long wavelength – 560 nm). However, some humans do not develop the three functional cone types, becoming colorblind; alternatively they can develop four or more, becoming tetrachromatic[12].

Opsins and rhodopsin are G-protein coupled receptors.

The visual cycle has been thoroughly described in rod PRs (the classical visual cycle) where it is initiated by light photons that activate these cells and induce photoisomerization of 11-cis retinal into all-trans retinal. This biochemical reaction changes the conformation of rhodopsin, closes cGMP-gated channels and causes subsequent hyperpolarization of the PR cell. In order for the visual cycle to continue, 11-cis retinal must be regenerated and this occurs through a step-wise process divided between rods and RPE cells. All-trans retinal is reduced to all-trans retinol in rods and then shuttled back to the RPE where it is reconverted to 11-cis retinal via two enzymatic reactions[9,13].

Cones are less dependent upon the RPE and have a different recycling pathway that relies mainly on Mueller glia[14]. Additionally, cones also express many of the enzymes required for chromophore reconversion and are actually able to regenerate 11-*cis* retinal from 11-*cis* retinol.

In cones, the all-trans retinol generated during visual activity is transported to Mueller cells, isomerized to 11-cis retinol and then transported back to the inner segments of cone PRs where it is oxidized to its active form (11-cis retinal)[14].

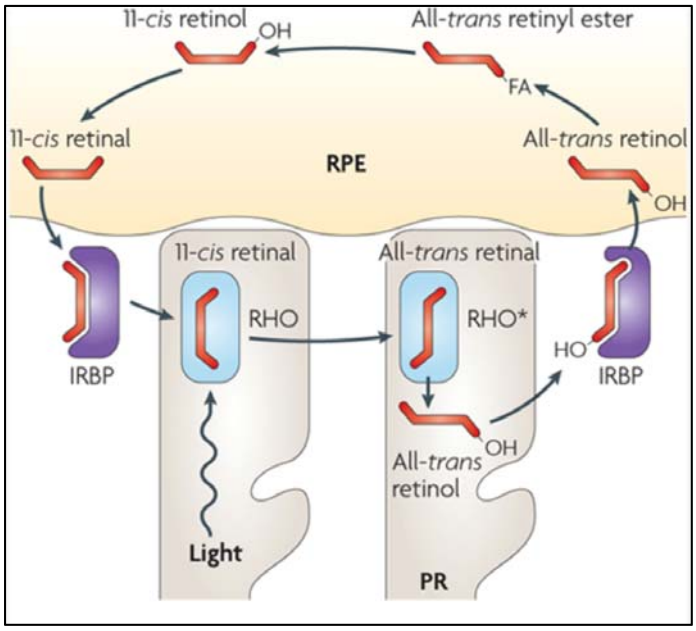

Figure 4 - Simplified version of the rod photoreceptor visual cycle[15] (RHO = rhodopsin; RHO* = activated rhodopsin; IRBP = interphotoreceptor retinoid-binding protein)

Macroglial cells

The macroglial cells of the retina, Mueller cells and astrocytes, play an important supportive role and are crucial for maintaining retinal homeostasis.

Mueller cells, the main macroglial cell of the retina, are the only cell type to span the entire thickness of the tissue (**Figure 5A&B**) and provide structural and functional support to the neuronal population.

Mueller cells contain intermediate filaments (composed by glial fibrillary acidic protein (GFAP)) that following trauma to the retina (e.g. retinal detachment; abnormal Intraretinal vascular growth) become massively upregulated throughout the cell. GFAP is therefore used as a marker for Mueller cell activation (**Figure 5B**). The 'zonula aherens' between Mueller cells and PRs forms the outer limiting membrane (OLM) of the retina, whereas Mueller cell endfeet (that project towards the retinal surface) and the basement membrane at the inner retinal surface form the inner limiting membrane (ILM).

Figure 5 – Retinal architecture. (**A**) Schematic representation of the cellular organization in the retina, including its individual cell types.[8]; (**B**) Retinal cross-section from the VLDLR -/- mouse showing Mueller glial cells specifically activated around the abnormal intraretinal vessels, spanning the entire retina **[16]** (**RPE** - retinal pigment epithelium; **OS** – outer segments; **OLM** – outer limiting membrane; **ONL** – outer nuclear layer; **OPL** – outer plexiform layer; **INL** – inner retinal layer; **IPL** – inner plexiform layer; **GCL** – ganglion cell layer; **NFL** – nerve fiber layer)

Astrocytes are the other glial cell type present in the retina but, rather than originating locally from the retinal neuro-epithelium, they enter the developing retina from the brain simultaneously with the developing optic nerve. Their cell processes, which contain high amounts of intermediate filaments such as GFAP, cover the superficial retinal blood vessels that run in and amongst the retinal ganglion cell bundles, thus reinforcing the selective metabolic exchange function of the inner blood retinal barrier.[7]

Microglial cells

Microglial cells are the resident macrophages of the retina and are responsible for maintaining tissue homeostasis. They play an important role during development, wound healing and in conditions of retinal degeneration and retinal auto-immunity[17]. Their immunoregulatory function is also critical for maintenance of retinal health. Upon retinal insult microglial cells become rapidly activated, initiate production of cytokines and acquire motile properties; however, these cells are also able to limit subsequent inflammation avoiding further tissue damage[18].

A.1.c.ii. Retinal pigment epithelium (RPE) and choroid

The Retinal pigment epithelium (RPE) is a single layer of pigmented cells interposed between the light-sensitive photoreceptor outer segments and choriocapillaris (the choriocapillaris is the vascular plexus part of the choroid, which also consists of choroidal blood vessels and extracellular matrix; **Figure 6**). The RPE rests, on its basal surface, on Bruch's membrane, a penta-laminar structure consisting of a central elastin core sandwiched between two collagen layers that provides mechanical separation and ensures selective transport of substances between the fenestrated choroidal vasculature and the highly ordered PR layer. On its apical side, the RPE contacts with the interphotoreceptor matrix that contains molecules responsible for retinoid exchange, disk phagocytosis and physical stabilization, providing an interface for communication with PR outer segments.

The RPE cells perform multiple indispensible roles for maintenance of proper visual function, namely: regulation and transport of ions, water, growth factors and nutrients to the outer portions of the PRs (transepithelial transport) as well as trafficking of metabolic waste from the photoreceptors in the opposite direction, phagocytosis of PR outer segments, recycling of the visual pigments, maintenance of PR cell adhesion (essential for maintenance of high spatial resolution of PR cells), absorption of light (absorbance of light scatter through its melanin pigment, to improve optical image quality), maintenance of the ion composition of the subretinal space and secretion of cytokines, immune modulators and growth factors.[19,20]

The RPE and the neuroretina constitute a functional unit that is already of importance during embryonic development, as both structures depend on each other for adequate tissue differentiation and maturation. A paradigmatic example of this interdependence is Leber congenital amaurosis, an ophthalmological condition in which PR degeneration results from mutations in genes expressed in the RPE[21].

After full development of the RPE-choroid complex, this functional unit continues to be crucial as the RPE fulfills a multitude of tasks that are essential for proper photoreceptor functioning and consequent visual processing.[19]

Retinal and choroidal circulation

Since the retina is the most metabolically active tissue in the body per unit weight, proper visual function is heavily dependent on its vasculature and highly vulnerable to even subtle changes in vascular supply[22].

The mammalian retina receives blood supply from two different sources, the choroidal circulation and the retinal circulation. Choroidal vessels receive the majority of the systemic blood flow (65-85%) and are responsible for nourishing the outer retina (especially the photoreceptors)[23]. On a full thickness cross-section of the eye, both large choroidal vessels and the choriocapillaris can be identified (**Figure 6**).

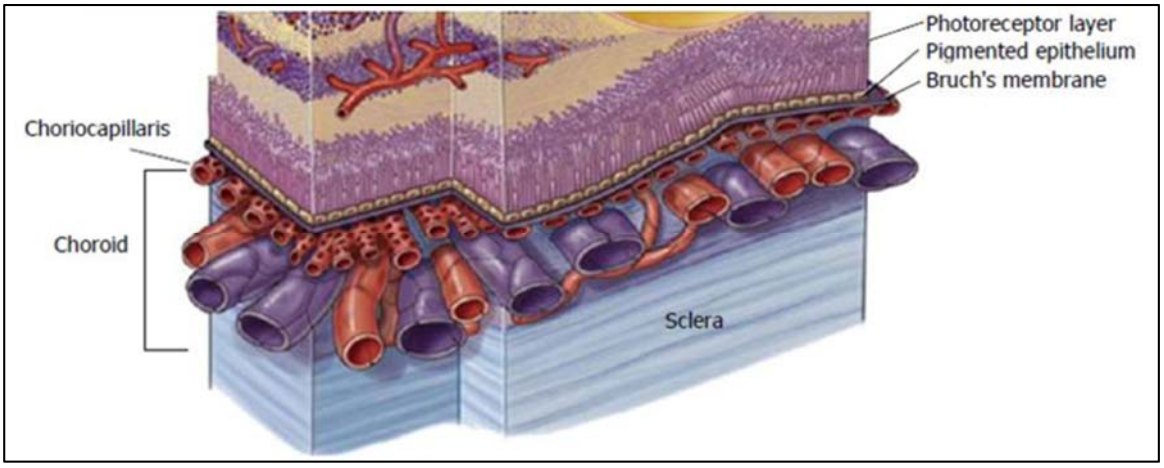

Figure 6 - Schematic representation of the RPE-choroid complex[24]

The retinal vasculature receives 20-30% of the systemic blood flow and is responsible for providing metabolic supply to the inner retinal layers.[7] It is composed of three vascular plexuses, superficial, intermediate and deep, which are easily identified on retinal cross-sectional views (**Figure 7**).

In order for the retina to regulate its environment in response to varying metabolic demands and to maintain its immunoprivileged condition, the retinal vasculature possesses barrier properties similar to those seen in the brain.

A blood retinal barrier (BRB) surrounds retinal vascular plexuses and is induced by Mueller glia and astrocytes during development. It is composed of two parts, the

inner retinal barrier (iBRB), which relies on tight junctions between retinal capillary endothelial cells; and the outer retinal barrier (oBRB), formed by tight junctions between the retinal pigment epithelium cells. [25]

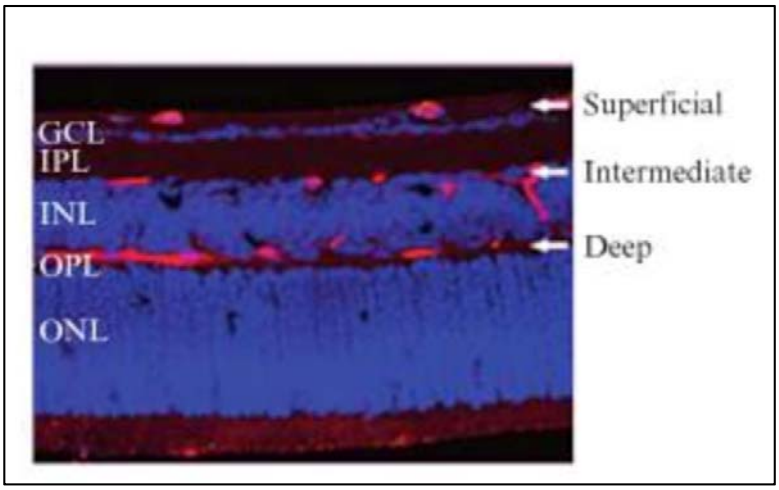

Figure 7 - Retinal cross-section illustrating the three retinal vascular plexuses [26]

Disruption of the iBRB characterizes DR and leads to development of diabetic macular edema (DME), which is currently the leading cause of vision loss in diabetic patients[27]. In addition, the pathological pre-retinal neovessels that constitute the hallmark feature of the devastating late-stage of diabetic retinopathy (proliferative diabetic retinopathy - PDR), are also leaky and further contribute to retinal edema. The exact mechanisms driving development of these vascular changes under diabetic conditions remain unclear.

To gain further knowledge into this area, it is important to review the main processes and factors involved in systemic and retinal vascular development.

B. Physiologic Vascular Development

B.1. General Concepts

Vascular development comprises three main processes:

- Vasculogenesis

- Angiogenesis
- Arteriogenesis

Vasculogenesis is the process through which new vessels are formed '*de novo'* from assembly of mesoderm-derived endothelial precursors (angioblasts) into primitive vascular tubes. This process is generally responsible for vascularization of tissues of endodermal origin and occurs in the embryo[28].

After this primary network is laid out, new vessels are formed by sprouting from pre-existing ones. This process in called *angiogenesis* and primarily vascularizes tissues of ectodermal and mesodermal origin, such as the retina, the brain and the kidney[23]. Additionally, angiogenesis is the predominant process responsible for neovascularization in pathological settings such as proliferative diabetic retinopathy (PDR) and wound healing.

Arteriogenesis, which is essential for creation of mature vessels, subsequently follows; once the vessel network is developed, pericytes and vascular smooth cells are recruited to ensheath the nascent endothelial cell tubules, thus providing blood vessels with stability and capacity to regulate their own perfusion (auto-regulation).

B.1.a. Angiogenic sprouting: Tip and Stalk Cell Phenotypes

Although vessels are typically quiescent in adulthood, their endothelial cells (EC) retain high plasticity, which allows them to sense and respond to pro-angiogenic cues. This ability to maintain their sprouting capacity becomes interesting in pathological conditions, where it can either be advantageous (e.g. in limb ischemia) or deleterious (e.g. in the eye following ischemic pathology)[28].

When pro-angiogenic signals dominate the environment, ECs regain their migratory and invasive capacities and vascular sprouting occurs. During vascular branching there are two crucial EC types: *tip cells*, which direct the growth of new sprouts by probing the environment for guidance cues through their filopodia; and *stalk cells*, which proliferate to sustain sprout elongation. The terms tip and stalk EC do not designate stable cell fates but rather transient phenotypes determined during a dynamic process that is tightly regulated by vascular endothelial growth factor (VEGF) and Notch signaling pathways (**Figure 8**) [28,29].

During the sprouting process, there is constant competition for the tip cell phenotype. VEGF exposure upregulates delta like ligand 4 (Dll4) in all EC and the ones that start expressing it earlier or at higher levels, are at a competitive advantage, consequently becoming tip cells. Simultaneously, these tip cells activate notch signaling in neighboring ECs to ensure that they will become stalk cells.[28]

Tip cells guide elongation of the growing sprout by expanding or retracting their filopodia in accordance to environmental cues through ligand-receptor interactions. Some signaling pathways involved in tip cell attraction include VEGF – VEGF Receptor-2(Flk-1)/Neuropilin-1 (NP-1)[30] and Stromal derived factor 1 (SDF-1) – CXCR4[31]; while those pathways involved in tip cell repulsion include Semaphorin 3A – Plexin D1[32], Netrin - Netrin receptor UNC5B and Roundabout receptor 4 (ROBO4) – UNC5B[33,34].

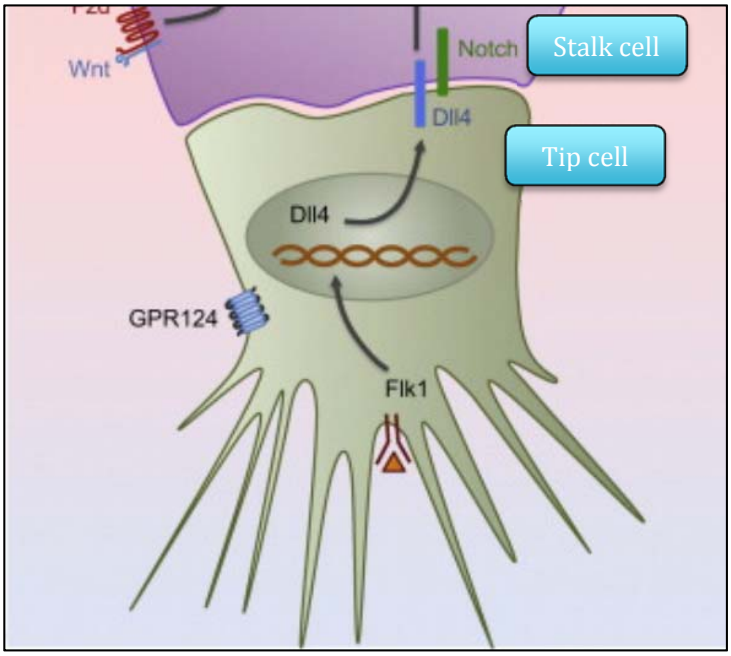

Figure 8 – Notch/Dll4 signaling regulates tip (green) and stalk (purple) cell fate[29]

B.1.b. Vessel Stabilization and Maturation

The process of *vessel stabilization* is initiated when two tip cells fuse with one another via a VE-cadherin mediated interaction between their respective filopodia. This branch anastomosis is supported by macrophages that accumulate locally and induce stalk cell stabilization. Additionally, stalk cells also lay the foundations for vessel perfusion by being responsible for lumen formation and by participating in subsequent vascular remodeling in response to flow[28].

In perfused vessels, shear forces determine a change of shape in stalk cells and upregulate the Kruepper-like 2 (KFL2) transcription factor that promotes EC quiescence by downregulating VEGF signaling (downregulating VEGFR2/Flk-1) and upregulating thrombomodulin and endothelial Nitric Oxide Synthase (eNOS) expression[35]. The latter ones ensure formation of patent vessels (Nitric oxide, NO, is a vasodilator) with an antithrombogenic endothelium (thrombomodulin exerts an anti-thrombotic effect). In non-perfused vessels, endothelial stalk cells are not subject to shear forces, levels of KLF-2 are low and the cell undergoes apoptosis. This ensures that the vascular network is only formed by perfused vessels.

Finally, *vessel maturation* takes place through: (1) recruitment of pericytes to the previously stabilized vessels (mediated by Platelet derived growth factor β (PDGF) and its receptor); (2) formation of N-cadherin junctions between adjacent ECs and (3) deposition of basement membrane. Mature vessels acquire a *phalanx EC phenotype* characterized by expression of oxygen sensors[36] (via Prolyl Hydroxylase Domain protein 2 – PHD2 - and Hypoxia inducible factor signaling – HIFs) that allow them to regulate vessel perfusion according to oxygen delivery and metabolic demands. In addition, mature EC adopt survival strategies such as autocrine expression of VEGF, which activates the PI3Kinase/AKT survival pathway to ensure that vessel integrity is maintained. Other non-autocrine factors such as Fibroblast growth factor (FGF), Notch, Angiopoetin 1 (Ang1)/Tie2 signaling and effects of blood flow/shear stress are also involved in sustaining EC survival in perfused vessels.[28]

B.2. Retinal Vascular Development

The vascular network supplying the adult retina undergoes major remodeling during development:

1. During the *early developmental stages*, the choroidal circulation ensures viability of the outer retina, while the inner retina is supplied exclusively by the hyaloid vasculature, an arterial network that extends all the way across the vitreous, from the optic nerve to the anterior segment of the eye.
2. Around *mid-gestation* (in humans) or *around birth* (in mice), the hyaloid vessels regress and are replaced by an emerging retinal vascular network that emanates from the optic nerve.
3. In the adult retina, the mature retinal vasculature is composed of three plexuses, superficial, intermediate and deep. Since avascularity of the outer retina is crucial to ensure adequate visual function, these vascular networks are restricted to the inner retina[23].

Investigating formation and maturation of the retinal vascular network is not possible in humans, where it is fully developed at birth; however it can be easily studied in the mouse, where it occurs during the first three postnatal weeks.

Retinal vascular development occurs by sprouting angiogenesis in a step-wise fashion and relies on generation of radial and 'in-depth' VEGF-A gradients.
Vascularization of the retinal surface occurs first and follows a radial centrifugal pattern. After this is completed, vascular growth shifts to a three-dimensional pattern and sprouting vessels dive vertically towards the OPL, where they form the deep plexus. Finally, a new VEGF gradient is established and nascent vessels turn back to the IPL to form the intermediate plexus.
Full development of the three parallel and interconnected vascular networks is observed at approximately three weeks after birth (in the mouse), with complete development of the superficial plexus by postnatal day (P) 7; of the deep plexus by P14 and of the intermediate plexus by P21[37].

B.2.a. Astrocytes: Contribution to Retinal Vascular Development

Astrocytes are believed to provide the template over which the superficial retinal vascular plexus develops. [38,39] Supporting this view are the following observations:
a) Both in primate and in non-primate mammal retinas, astrocytes are restricted to vascularized areas.
b) Astrocytes can provide extracellular matrices for organized vascular growth.
c) Astrocytes invade the retina prior to retinal vascular development. There is a complete astrocytic template covering the entire retina at the time of birth (in mice).
d) Astrocytes may promote and guide retinal angiogenesis through hypoxia induced VEGF-expression as well as expression of selected adhesion molecules that can interact with ECs, such as R-cadherin
e) Astrocytes have been shown to be important in maintaining vascular integrity and may prevent misdirected migration of the retinal vasculature into the vitreous[38].
The current mechanistic concept suggests that astrocytes act as guides for vascular development in the retina by experiencing hypoxia, which leads to creation of a centrifugal VEGF gradient that attracts tip and stalk endothelial cells from nascent vessels. Upon binding R-cadherin expressed on astrocytes,

endothelial cell filopodia become stabilized and lead further EC growth along the preexisting astrocytic template (**Figure 9**). As the vascular network expands over them, astrocytes acquire a more mature phenotype, proliferation ceases, GFAP is upregulated and VEGF is downregulated. Since astrocytes act as promoters of vascular growth, this creates a negative feedback loop that stabilizes numbers of astrocytes and vascular density in the retina.[38,40]

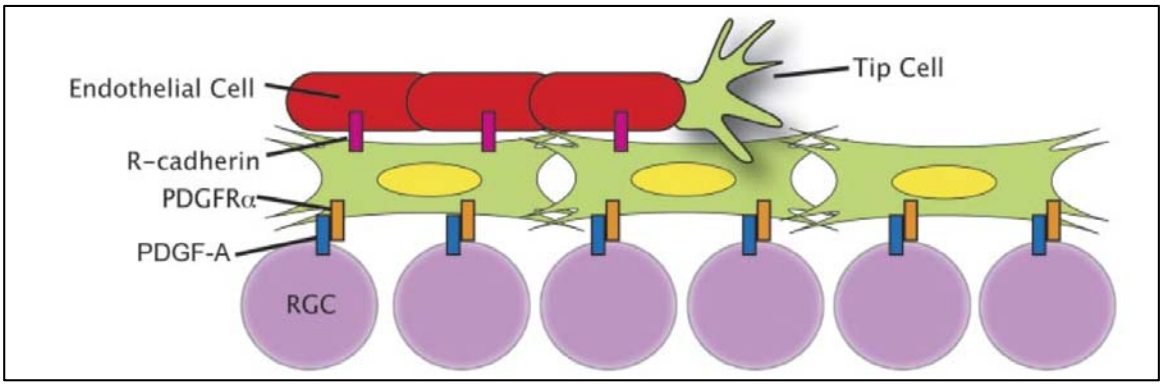

Figure 9 - Retinal vascular development depends on interactions between: (1) EC and astrocytes (stabilized by R-cadherin); and (2) RGC and Astrocytes (via PDGF-α/PDGFR-α signaling)[40]

Despite the important role played by the astrocytic template in physiological retinal vascular development, studies performed in transgenic mice that are not able to express VEGF in astrocytes revealed that astrocyte-derived VEGF is not indispensable for the process, suggesting that other cell types and/or growth factors can play a compensatory role.

In contrast, hypoxia induced astrocyte derived VEGF is critical for development of pathological retinal neovascularization[41] and for stabilization of the developing retinal vasculature. Studies in Oxygen Induced Retinopathy (OIR) mice have shown that VEGF deletion in astrocytes leads to vascular collapse under hyperoxia conditions due to regression of smooth muscle coated radial arteries and veins.[42]

Besides astrocytes, retinal neurons and myeloid cells have also been described to play a significant role in retinal vascular growth.

B.2.b. Retinal neurons: Contribution to Retinal Vascular Development

Retinal neurons play a major role in retinal vascular development as they:

a) Are the only source of retinal VEGF-A during embryogenesis → VEGF-A is critical to maintain the hyaloid vasculature and to guarantee nourishment of the inner retina at this early stage.[43,44]

b) Express VEGFR2 (Flk-1) → Activation of this receptor by VEGF in the first postnatal week appears to be fundamental for maintaining neuroretinal cells in an undifferentiated state as retinal progenitor cells and post-mitotic progenitors [45]. Additionally, VEGFR2 expression in retinal neurons plays a paramount role in ensuring completion of the initial radial growth along the GCL, preventing premature vertical growth towards the neuroretinal, by regulating extracellular VEGF-A protein levels, through VEGFR2-mediated endocytosis.[43]

c) Act as hypoxia sensors → Retinal ganglion cells (RGC) act as key sensors of hypoxic stress both in physiologic (during retinal vascular development) and pathological conditions (for example in ischemic retinopathies). When hypoxia inducible factor 1alpha (HIF-1α) is activated in RGC, VEGF-A is produced and contributes to formation of the gradient that guides nascent vessels. Retinal ganglion cells and their ER stress response have also been shown to significantly influence pathological neovascularization in a model of OIR[46] and, given their location and capacity to produce VEGF, they may play a compensatory role in driving and facilitating physiological retinal vascular development when the astrocytic hypoxic response is compromised.

Furthermore, the invasion of the retina by astrocytes early during development is intimately associated with RGC via PDGF-α/PDGFR-α signaling. Astrocytes express PDGFR-α and travel on top of PDGF-α expressing RGC, when migrating from the optic nerve to the retinal periphery to finally form the retinal astrocytic template (**Figure 9**).[47]

B.2.c. Macrophages and Microglia: Contribution to Retinal Vascular Development

The (1) intimate association between macrophages and the vasculature along with (2) the correlation between reduced microglial cell numbers and retinal vascular

scarcity (associated with hyperoxic conditions) suggest that these cells can modulate vascular development, remodeling and maturation in the retina under both physiologic and pathological conditions[39]. Ablation of macrophages (through cell-specific expression of diphtheria toxin or by injection of clodronate liposomes[44,48]) inhibits regression of the hyaloid vasculature and genetic deletion of angiopoietin-2 or elements in the Wnt signaling pathway (Norrin, FZD4 and LPR5) in macrophages disrupts formation of the deep retinal plexus.

The deep vascular plexus is known to develop independently of retinal astrocytes but little is known about the specific cellular and molecular mechanisms governing its formation.

The phenotypes induced by loss of Wnt signaling in macrophages and loss of VEGFR2 signaling in neurons (previously described in the text), suggest that neurons and myeloid cells can cooperate to regulate formation of the deep vascular retinal plexus[43].

Although much has been reported on the different cellular and molecular mechanisms involved in retinal vascular development, formation of the intermediate plexus remains elusive and the work present here in **Chapter IV A** will provide further knowledge on this matter[49].

B.3. The pivotal role of VEGF in Vascular Development and Pathological Neovascularization

Several pro-angiogenic factors (e.g. PDGFα and β and its receptors; angiopoietins, FGF, TGF-β and its receptors) have been shown to contribute to vascular development and pathological neovascularization, however Vascular Endothelial Growth Factor (VEGF) has gained the most attention and is currently considered the most critical one.

B.3.a. VEGF superfamily

VEGFs are fundamental regulators of vascular development during vasculogenesis and angiogenesis. In mammals the VEGF family includes five members: VEGF-A, B, C, D and PIGF (placental growth factor), which bind in a

partially overlapping pattern to VEGF receptors [VEGFR-1(Flt-1), VEGFR-2(Flk-1) and VEGFR-3(Flt-4)] and co-receptors (heparan sulphate proteoglycans and neuropilins)[50].

VEGF-A, the most extensively studied family member, acts as a specific EC mitogen, induces vascular permeability with very high potency (10.000 times more potent than histamine) and is chemotactic for macrophages. Alternative splicing of the VEGF-A gene generates its different isoforms[50].

B.3.b. VEGF-A isoforms

Alternative splicing of the VEGF-A gene gives rise to different isoforms with diverse biological activities. In humans five isoforms of VEGF-A have been identified: VEGF 121, VEGF 145, VEGF 165, VEGF 189 and VEGF 206. In mice, however, only three isoforms have been reported: VEGF 120, VEGF 164 and VEGF 188. These are one amino acid residue shorter than their corresponding human ones.[23]

The different isoforms are expressed in a tissue-specific fashion during embryogenesis and in the adult organism. Their different amino acid lengths define distinct heparin-binding properties, which in turn determine their level of interaction with the cell surface and with extracellular matrices. VEGF 120 is not able to bind heparin and is freely soluble; VEGF 164 moderately binds heparin and can be found both in its soluble form or bound to the extracellular matrix; VEGF 188 strongly binds heparin and practically does not exist in the soluble form, being sequestered on the cell surface and extracellular matrix.

In addition, the isoforms also differ (1) in their biological potency, with VEGF 164 inducing a 100-fold higher proliferative response in EC than VEGF-120, and (2) in their capacity to bind Neuropilin-1 (NP-1, a co-receptor), with VEGF-164 being the only isoform able to do so.

This functional diversity is evident in studies with transgenic mice that only produce specific isoforms. Transgenic mice that only produce VEGF 120, a more freely diffusible form, show a flattened VEGF gradient and delayed retinal vascular growth. Although these mice live to term, they die within the first two weeks of postnatal life due to severe vascular defects[51].

Similarly, VEGF 188 mice show abnormal vascular remodeling in the lungs and in the retina, with defective development of the primary plexus and persistent hyaloid vasculature. Furthermore the formation of retinal arteries is compromised whereas retinal veins develop normally[52].

Mice expressing only VEGF164, however, display a normal retinal vessel network, which shows that this isoform is sufficient to guarantee adequate retinal vascular development[52].

These findings demonstrate that VEGF–A isoforms do not perform interchangeable functions and rather play functionally distinct roles during vascular development (with only VEGF-164 being sufficient on its own).

B.3.c. VEGF Receptors (VEGFRs)

VEGFRs are receptor tyrosine kinases (RTK) that when activated lead to receptor auto-phosphorylation, which induces recruitment of interacting proteins and activation of several downstream signaling pathways. VEGFR activation can induce cellular processes, such as cell migration, survival and proliferation that are shared with many other growth factors but can also promote unique responses, such as formation of a 3D vascular structure and control of vascular permeability.[50]

Negative regulation of VEGFRs is important to limit exaggerated responses on target cells and can be achieved by two mechanisms: rapid dephosphorylation of the receptors by tyrosine-specific phosphatases or rapid degradation in the proteasome.

VEGF-A can bind and activate VEGFR-1 (Flt-1) and VEGFR-2 (Flk-1)[50]. It can also bind neuropilin-1, a transmembrane glycoprotein that acts as a co-receptor for VEGF in angiogenesis but lacks VEGF catalytic function[30].

VEGFR-2 is expressed on EC during physiological vascular development and pathological neovascularization, where it mediates VEGF-A's proliferative effects. However, in normal adult retinas populated by quiescent vessels, it is mainly found in non-vascular cells, such as neurons, where it titrates VEGF-A levels in the outer retina, ensuring maintenance of its avascularity[43].

VEGFR-1 is expressed in EC, pericytes and mononuclear cells throughout development and in the adult retina. It positively regulates monocyte and macrophage migration and negatively regulates VEGFR2-mediated EC proliferation through its soluble variant (sVEGFR-1). VEGFR-1, therefore, appears to be an important vascular regulator during embryogenesis by acting as a ‘physiologic trap’ for VEGF-A, restricting its access to VEGFR-2. [50]

B.3.d. Hypoxia-driven VEGF expression

Retinal neurons and glial cells can sense oxygen levels in the retina and produce VEGF under hypoxic conditions, in an attempt to restore adequate nutrient and oxygen delivery to cells in order to avoid metabolic insufficiency.

Interestingly, the molecular mechanisms underlying physiologic retinal vascularization and pathological retinal neovascularization are largely indistinguishable, except for their magnitude, and hypoxia-induced production of VEGF acts as the main driver in both cases [23,53].

Hypoxia-inducible transcription factors (HIFs: HIF-1 and HIF 2) are pivotal for the process and aim at adjusting oxygen supply and demand by regulating gene networks involved in survival, metabolism and angiogenesis[28]. HIF activity is regulated by the Von Hippel Lindau tumor suppressor gene product (pVHL) via activation of oxygen-sensing prolyl-hydrolase domain proteins (PHDs 1-3).

In *normoxia* (ambient oxygen conditions), PHD proteins hydroxylate HIFs and target them to proteasomal degradation. In contrast, in *hypoxia*, PHD proteins are inactive, HIFs escape degradation and bind to hypoxia responsive elements (HRE) on target genes, such as VEGF-A, promoting their transcription and subsequent actions.

Experimental studies and clinical evidence from Von Hippel Lindau patients have demonstrated that HIF-1α plays a crucial role in retinal neovascular diseases and in physiological vascularization. Using mouse models, it has been shown that an increase in HIF-1α expression correlates with VEGF-A expression during physiologic and pathologic retinal vascularization[54]. In addition, studies performed on transgenic mice where HIF-1α was silenced in different retinal cells types have confirmed HIF's essential role in regulating VEGF expression in the retina[23].

C. Retinal Pathological Neovascularization

In the adult retina, under normal circumstances, quiescence of the retinal vasculature is the norm and this is critical for maintenance of a functional tissue architecture and adequate visual function. However, a pathological stimulus, such as ischemia, is capable of inducing a potent and disorganized vaso-proliferative response that leaves visual function at risk.

Pathological neovascularization in the posterior segment of the eye is classified into three types depending on the vascular bed from where it originates. The three types are: choroidal neovascularization (CNV), intra-retinal neovascularization and pre-retinal neovascularization.

C.1. Types of Neovascularization affecting the Posterior segment

C.1.a. Choroidal Neovascularization (CNV)

Pathological outgrowth of new vessels from the choroid is characteristic of the exudative (neovascular) form of age-related macular degeneration (AMD). In these cases, choroidal vessels grow towards the retina, break Bruch's membrane and enter the subretinal space, where accumulation of fluid or blood can lead to RPE or retinal detachment.

Increased VEGF-A expression occurs in proliferative RPE and inflammatory cells. Even though VEGF-A overexpression is necessary for full development of CNV, as shown by studies where antibody mediated neutralization of VEGF reduced its formation and progression[55], it is not sufficient to ensure invasion of BM or the RPE[56], i.e. invasive CNV. However, sub-retinal injections of viral vectors expressing VEGF-A were able to reproduce invasive CNV[57,58], which suggests that damage to BM and the inflammatory response (here, iatrogenically induced by sub-retinal injection) are critical for development of the neovascular process.

Therefore, development of invasive CNV requires both elevated expression of VEGF-A and rupture of Bruch's membrane (BM), the latter being facilitated by aging-induced alterations in the BM's structure.

Basic FGF (bFGF) has also been implicated in CNV development, being detected in surgically excised CNV membranes. However studies in bFGF null mice have shown that it is not necessary for formation of experimental CNV[59] and a direct role for this growth factor in CNV progression has not been clearly established. Nevertheless other studies have shown that overexpression of bFGF by laser-damaged PRs induces CNV if prior disruption of BM's occurs[60], suggesting that its pro-angiogenic potential is dependent on cellular injury and release into the extracellular space.

Non-exudative (dry) AMD, which is characterized by localized degeneration of RPE cells associated with atrophy of regional PRs and choriocapillaris (CC), may also progress onto the exudative form. As such, it constitutes an important 'model' for studying the initial events that lead to CNV, including potential disruptions in the neuronal-RPE-vascular crosstalk amenable for therapeutic targeting.

During development and in adulthood the relationship between choroidal vessels and the RPE is crucial as RPE cells secrete VEGF-A that acts as a survival factor to maintain a viable and quiescent CC, which in turn ensures proper PR functioning.[61,62]

With age, an increasing structural disorganization and thickening of BM occurs and renders it less permeable to RPE-derived VEGF-A. As such, VEGF-A does not diffuse normally into the CC, which undergoes atrophy, resulting in localized PR hypoxia and subsequent VEGF-A overexpression that leads to secondary neovascularization (CNV).

C.1.b. Intraretinal Neovascularization

Intraretinal neovascularization is characterized by abnormal vascular proliferation in the inner retina that, over time, expands into the subretinal space disrupting the normally avascular outer retina and visual function. This type of neovascularization is observed in macular telangiectasia (MacTel), an uncommon retinal disease; and in retinal angiomatous proliferation (RAP), a sub-type of AMD where CNV appears

to be preceded by intraretinal neovascularization. Both conditions are accompanied by glial cell abnormalities and PR dysfunction, which from studies in mouse models, appear to be secondary to neovascular changes[16].

Intraretinal NV that expands towards the subretinal space has been induced (1) by overexpressing VEGF-A in photoreceptors[63]; (2) by disrupting EC migration via R-cadherin[38] blockade; and (3) by deleting the gene for Very Low Density Lipoprotein receptor (VLDLR).[64]

Although the driving mechanism of this type of neovascularization remains unclear, a necessary role for VEGF-A has been demonstrated in mice, by using an anti-VEGF agent that suppressed the vascular phenotype in VLDLR null rodents[16]. Despite this, anti-VEGF agents have not shown consistent effects in MacTel patients.

C.1.c. Pre-retinal Neovascularization

Rapid vessel proliferation arising from the superficial retinal plexus occurs during pathological conditions characterized by the presence of non-perfused and hypoxic retinal areas that induce a pronounced upregulation of VEGF-A. Proliferative diabetic retinopathy (PDR) and retinopathy of prematurity (ROP) are paradigmatic examples.

Premature infants are born with an incompletely vascularized retina because physiologic retinal vascularization takes place in the final trimester of gestation. Since this process is guided by a VEGF gradient created under physiologic hypoxia conditions, placing the infant into high oxygen after birth suppresses VEGF expression, arresting retinal vascular growth and inducing regression of nascent vessels which are still highly dependent on VEGF for survival. This vaso-obliteration (VO) phase creates avascular regions in the retina that become hypoxic when the infant is returned to ambient oxygen, leading to VEGF upregulation and disorganized neovascular growth on the retinal surface[65].

Studies performed in oxygen-induced-retinopathy (OIR) animal models (rodents, dogs and cats) have demonstrated that (1) cessation of (physiologic) hypoxia-induced VEGF expression in neuroglial cells, in high oxygen conditions, drove the VO phase of ROP and that (2) VEGF is necessary for neovascular growth when

animals are returned to ambient oxygen[66]. Moreover, they have shown that vessel regression occurred via EC apoptosis due to lack of VEGF signaling, corroborating VEGF's role as a survival factor. Taken together these findings reinforce the concept that VEGF signaling is necessary not only to direct the process of retinal neovascularization but also for retinal vascular maintenance.

A similar scenario occurs in diabetic retinopathy (DR) where metabolic alterations induce chronic damage to the neurovascular unit and may lead to development of pre-retinal neovascularization, the hallmark of proliferative diabetic retinopathy (PDR). The inciting factors of diabetic vascular dysfunction are not yet entirely understood, however development of non-perfused retinal areas and VEGF overexpression are know to be pivotal in facilitating disorganized growth of leaky neovessels along the retinal surface and into the vitreous. The major role played by ischemia (and its associated metabolic insufficiency) in DR progression is further corroborated by the beneficial effects of laser photocoagulation, which prevents appearance (or induces regression) of neovessels by destroying the cellular sources of VEGF in ischemic retinal areas.

Currently there are no rodent models that manifest the late stages of diabetic retinopathy. To circumvent this limitation the OIR mouse has been used in this context as a model of ischemic retinopathy that develops secondary neovascularization and has provided relevant insight into PDR. For example, it has been demonstrated by in situ hybridization that the hypoxia-driven-VEGF-response is mainly and most strongly activated in RGC and INL neurons (possibly amacrine cells)[67], suggesting that therapeutic modulation of these cellular responses could become an effective therapeutic strategy to arrest DR progression.

D. Diabetic retinopathy: State of the Art

D.1. Epidemiology

Diabetic retinopathy (DR) is the leading cause of blindness in working age adults (20 – 65 years) in developed countries and it is estimated to affect 35% of the total diabetic patient population (382 million)[68,69].

Epidemiological studies have shown that after 20 years of diabetes, virtually all type 1 and over 60% of type 2 diabetic patients will develop some form of DR[70,71]. In addition, meta-analysis of large-scale studies have shown that approximately one third of these patients (who develop DR) will progress to its vision-threatening stages (proliferative diabetic retinopathy and diabetic macular edema), requiring treatment.

With the expected rise in prevalence of diabetes worldwide, projected to reach 559 million individuals by 2035, the global healthcare expenditure for treatment of diabetes and its complications is expected to exceed $490 (429€) billion (by 2030)[27].

D.2. Histopathology of Early DR

Early diabetic retinopathy has been associated with the following histopathological findings:

A) Pericyte loss, which is considered the earliest sign of DR and is only observable histologically. It is thought to occur due to hyperglycemia induced inhibition of PDGF-β signaling, which in normal conditions is responsible for recruiting pericytes to the vessel wall.

B) Thickening of the basement membrane (of capillaries and arterioles), which has been attributed to increased production and reduced degradation of extracellular matrix components (ECM; collagen IV, laminin and fibronection).

C) Dilation of retinal capillaries (microaneurysms) results from the combined action of (1) EC dysfunction and loss of vascular auto-regulation; (2) pericyte dropout and (3) loss of vascular tight junctions.

D) Acellular capillaries ('ghost vessels'), which are found in post-mortem diabetic human retinas, usually surrounded by microaneurysms, and have been shown to correspond to previously documented areas of non-perfusion on angiography. These are thought to be the result from EC apoptosis after pericyte loss.[72]
Understanding the precise mechanism that underlie disappearance of these capillaries will be pivotal in creating new therapeutic strategies focused on promoting effective revascularization of retinal ischemic areas

D.3. Pathophysiology[73]

Sustained hyperglycemia is considered the most important risk factor for DR development[27,73], however the mechanism through which it induces pathological retinal changes remains elusive. Despite its importance, the fact that ideal glycemic control is not sufficient to effectively arrest disease progression suggests that other unrecognized, yet important, factors also play a role in inducing development of DR[68].
So far, the most relevant molecular pathways that have been associated with hyperglycemia induced-retinal microangiopathy are: (1) induction of the polyol pathway; (2) activation of protein kinase C (PKC); (3) formation of advanced glycation end products (AGEs); (4) subclinical and chronic inflammation with overexpression of growth factors and inflammatory cytokines along with leukostasis; (5) activation of the renin-angiotensin system; and (6) increased oxidative stress.

D.3.a. Induction of the Polyol Pathway

In diabetes, retinal aldose reductase (AR) metabolizes excess glucose to sorbitol, using NADPH as a cofactor and sorbitol is subsequently converted to fructose.
Detrimental effects to the retinal tissue result from (1) accumulation of sorbitol within the cell, which exerts osmotic damage; (2) reduction of NADPH, which

reduces glutathione synthesis, decreasing antioxidant power; and (3) accumulation of fructose which can be metabolized to strongly glycating agents, producing AGEs.

D.3.b. Activation of PKC

Hyperglycemia increases flux in the glycolysis pathway increasing diacylglycerol (DAG) formation. This in turn leads to overactivation of PKC, which contributes to increased vascular permeability, increased extracellular matrix (ECM) protein synthesis and remodeling, release of pro-angiogenic factors and activation and adhesion of leukocytes to the retinal vasculature.

D.3.c. Formation of AGEs

AGEs constitute a heterogenous group of molecules formed by non-enzymatic glycation of proteins, lipids and nucleic acids.

AGEs exert their damaging effects by (1) forming adducts with proteins (extracellular or transmembrane proteins), which alter their structure and function; and by (2) activating a variety of cell-surface AGE binding receptors (e.g. RAGE, galectin-3 and CD36) and promoting prooxidant and proinflammatory effects.

Epidemiological studies in diabetic patients have shown that serum levels of AGEs correlate with severity of DR and that one of these, N-carboxymethyl-lysine, is increased in retinal neurons and vessels of diabetic patients.[74]

D.3.d. Subclinical and Chronic Inflammation

There is a wide body of literature associating diabetes with systemic and retinal inflammation. In the retina, diabetes induces microglial cell activation with increased production of inflammatory cytokines, reactive oxygen species (ROS), growth factors and metalloproteases (MMPs). Additionally, there is increased expression of adhesion molecules on the retinal vasculature (CD18, ICAM-1), which promote leukostasis and leukocyte migration into the retina.

D.3.e. Activation of the Renin-Angiotensin System

Diabetic patients who develop PDR present higher expression levels of renin, angiotensin converting enzyme I and II and angiotensin receptors.
It has been suggested that the renin-angiotensin system contributes to PKC activation and VEGF overexpression.

D.3.f. Increased Oxidative Stress

Evidence for increased oxidative stress in diabetic retinas has been found in animal models and in human postmortem retinas from diabetic patients, with increased membrane lipid peroxidation and DNA oxidative damage.
Animal studies with diabetic rodent models have shown that oxidative stress induces irreversible retinal pathological changes and contributes to development and progression of DR. Oxidative stress mediated retinal damage may explain the lack of beneficial effects observed when intensive metabolic therapy is instituted late in the course of diabetes[75].

D.4. Clinical Classification

Diabetic retinopathy has been regarded as a vascular disease for decades and this is clearly evident from its clinical classification, which is solely based on the observation of retinal vascular changes on the ocular fundus. These changes start with microaneurysms (small dilations in the retinal capillaries) and progress to exudative phenomena (leading to macular edema), ischemic alterations ('cotton wool spots', which are infarcts of the nerve fiber layer), formation of collaterals (intraretinal microvascular abnormalities - IRMA), dilation of venules (venous beading) and lastly, proliferative changes that affect both the vasculature and retinal fibroblasts.

Based on the presence or absence of abnormal neovascular sites, DR is distinguished into an early non-proliferative phase (*Non-proliferative diabetic retinopathy* - NPDR) and a late proliferative phase (*PDR*). *Diabetic macular edema* (DME), one of the most feared and difficult to treat complications of DR, develops due to progressive blood retinal barrier (BRB) disruption and commonly starts during the NPDR stage.

NPDR is further divided into three stages: mild, moderate and severe.

Mild and moderate stages of *NPDR* are characterized by microaneurysms and intraretinal hemorrhages. Increasing BRB compromise leads to plasma leakage, retinal edema and formation of 'hard exudates' (lipid deposits within the retina that frequently accompany macular edema).

Severe NPDR is diagnosed when there is at least one of the following signs:

a) Intra-retinal hemorrhages in all four quadrants
b) Venous beading in two quadrants
c) Intraretinal microvascular abnormalities in one quadrant

It is estimated that 50% of the patients with severe NPDR will progress to PDR within 1 year[76].

PDR is diagnosed when new vessels grow out of the retinal capillaries on the retinal surface and towards the vitreous.

These new vessels are fragile and often rupture, resulting in vitreous hemorrhages. Additionally, vascular growth over the vitreous interface is accompanied by activation and proliferation of fibroblasts and glial cells, which form epiretinal membranes that can contract and lead to tractional retinal detachments, one of the most dreaded complications of PDR. In severe cases, neovascularization can also be found in the anterior segment, on the surface of the iris ('rubeosis iridis'), where it blocks aqueous humor drainage causing a severe type of glaucoma designated neovascular glaucoma.

D.5. Clinical Features

Patients with mild-to-moderate NPDR have impaired contrast sensitivity and visual field defects that may compromise daily activities such as driving, reading or managing their diabetes. A decline in visual acuity, however, occurs only when the central macula is affected in situations such as vitreous hemorrhage, edema (DME), ischemia, epiretinal membranes or retinal detachments.

Even though vascular changes are given priority for purposes of clinical diagnosis, a growing body of evidence has demonstrated that DR impairs neuronal activity at much earlier stages. Studies in early diabetic patients with no signs of (vascular) DR have shown altered oscillatory potentials (OPs) on the electroretinogram (ERG), impaired vasodilation in response to flicker light stimulation, color vision defects (shared with patients with Parkinson's disease) and impaired corneal reflexes[5,77-79]. Taken together these findings suggest that subtle ERG dysfunction along with mild impairment in contrast sensitivity, color vision or corneal reflexes may constitute important predictive signs of eminent vascular changes in the diabetic retina.

Since diagnosis of DR relies exclusively on identification of vascular changes and compromises in visual acuity occur quite late in the disease process, it is paramount to change the existing clinical approach. Introducing a more integrative perspective that takes into consideration disruption of retinal functional units rather than simple vascular changes will help implement effective screening programs and monitoring strategies to achieve an earlier diagnosis and success in preventing disease progression.

D.6. Risk Factors

Epidemiological studies have elucidated the effects of major and minor pathological conditions on incidence and progression of DR[27,70].

The major risk factors are:

Duration of diabetes
Chronic hyperglycemia
Dyslipidemia
Hypertension

Additional risk factors are:

High body-mass index (BMI)
Low level of physical activity
Insulin resistance
Sleep apnea
Nonalcoholic fatty liver disease
Genetic factors (e.g. mutations in the erythropoietin gene promoter)

Clinical trials such as the DCCT and the UKPDS have unequivocally demonstrated that intensive metabolic control reduces incidence (by 76% - DCCT) and progression (by 54% - DCCT) of DR, with HbA1C levels being the strongest predictive risk factor. Surprisingly the values for HbA1c, blood pressure (BP) and total serum cholesterol account for only 9 – 11% of the risk of retinopathy. The ACCORD study did not show an effect of intensive BP control on progression of DR (but confirmed benefit of intensive metabolic control).
Moreover, intensive metabolic control appears to be especially beneficial if instituted early in diabetes development. During the late stages, it does not bring significant risk reduction and may even become detrimental by favoring more episodes of hypoglycemia. This creates difficulties regarding broad implementation of intensive metabolic control strategies, which along with concerns associated

with the non-physiologic route of insulin administration, justify the low percentage of diabetic patients who achieve ideal metabolic control over an extended period (only 17% of patients in the DCCT trial had HbA1c levels below 7% and, from 2000 to 2006, only 7% of type 2 American diabetic patients concomitantly met all three targets - HbA1c, lipids and BP - according to data from the American diabetes association)[27,68].

These findings underscore the importance of regular and long-term ophthalmological follow-up for diabetic patients and show that further understanding of DR's pathogenesis is crucial to reduce its incidence and improve patient care.

D.7. Therapies and Preventive Strategies

D.7.a. Metabolic Control

Adequate control of classic metabolic parameters remains the centerpiece of DR management. Current recommendations suggest an glycated hemoglobin (HbA1c) target level of 6.5 - 7% as well and systolic blood pressure below 140/85 mmHg[80]. In what concerns blood lipid management, low density lipoprotein (LDL) cholesterol target values must be determined on an individual basis but, more importantly, fenofibrate should be added to statin therapy, whenever possible[68]. This recommendation is based on results from the FIELD trial, where fenofibrate (a peroxisome proliferator-activated receptor alpha, PPAR-alpha, agonist) reduced the risk of progression to PDR by up to 40% in patients with NPDR[81].

D.7.b. Laser Photocoagulation

The benefits achieved with laser photocoagulation are thought to be associated with destruction of ischemic retinal areas and subsequent reduction in production of pro-inflammatory and pro-angiogenic cytokines (e.g. VEGF) by dysfunctional

retinal cells. As a consequence, oxygen and nutrients become increasingly available for healthier retinal areas.

Panretinal photocoagulation (PRP) is used in cases of non-center-involving diabetic macular edema and in PDR, to destroy the peripheral ischemic tissue in an attempt to spare the central retina and visual acuity. Despite its cruent nature, it still constitutes the gold standard of care in preventing DR progression. The Diabetic retinopathy study showed that PRP reduced the risk of severe visual loss by 50% over a 5-year period.[68]

Its side effects, however, cannot be overlooked and include worsening of pre-existing macular edema and impairment of peripheral retinal function and night vision[82].

D.7.c. Anti-VEGF Therapies

VEGF has been the most extensively studied growth factor in DR and it is responsible for some hallmark pathological features such as breakdown of the BRB; increased leukostasis and consequent EC dysfunction; and pathological neovascularization.

Anti-VEGF agents exist in three forms[68]:

- **RNA aptamers**
    - ***Pegaptanib*** (an oligonucleotide that binds VEGF-165 with high-affinity)
- **Monoclonal antibodies against VEGF**
    - ***Bevacizumab*** – a full length humanized monoclonal antibody that blocks all isoforms of VEGF-A.
    - ***Ranibizumab*** - a monoclonal antibody fragment (with enhanced affinity for VEGF-A) that also blocks all isoforms of VEGF-A.
- **Soluble VEGFR-like proteins**
    - ***Aflibercept*** – is a soluble recombinant protein that contains extracellular protein sequences from VEGFR-1 and VEGFR2 fused to an immunoglobulin and behaves like a decoy receptor that blocks all isoforms of VEGF-A and neutralizes them. This format allows for prolonged biological activity and less frequent administrations (every two months rather than monthly).

Currently, the only formal indication for intravitreal injections of anti-VEGF agents in DR is center-involving DME (three initial monthly injections potentially followed by further injections, depending on the patient's response) but their efficacy is not guaranteed. If the condition persists and is no longer improving after two

consecutive injections following the initial 3 month-period, laser photocoagulation must be considered[68].

In PDR, anti-VEGF therapy has been found to very effective in promoting rapid regression of retinal neovascularization, however these effects are transient and PRP remains necessary to allow for more permanent inhibition of neovascular growth[68].

A phase III prospective clinical trial is now comparing prompt PRP with intravitreal ranibizumab and deferred PRP in patients with PDR.

Increasing concerns exist over anti-VEGF agents both at the ocular and at the systemic level. At the ocular level, in cases of PDR, anti-VEGF agents may enhance the fibrotic response and promote retinal tractional detachments while simultaneously inducing the beneficial regression of neovessels. In addition, as VEGF is a trophic factor for neurons and vessels, it has been suggested by animal and epidemiological studies that long-term administration of these therapeutic agents may be involved in promoting atrophy of the choriocapillaris and PR dysfunction[4,62,83-85].

At the systemic level, cardio-vascular events (such as congestive heart failure) and renal injury (especially proteinuria and thrombotic microangiopathy) have been reported following intravitreal anti-VEGF treatment.[2,86,87]

D.7.d. Steroids

Chronic inflammation plays a pathological role in diabetes both systemically and at the retinal level.

Intravitreal steroids, such as triamcinolone, can be used for treating DME and exert their beneficial effect by neutralizing the pro-inflammatory effects of cytokines and chemokines.[68]

D.7.e. Surgical Treatment

Despite the previously mentioned therapeutic strategies, which have greatly contributed to reduce the number of late-stage DR cases, a small number of patients suffering from DME and PDR still needs to undergo vitreo-retinal surgery.
Surgical treatment is indicated for patients with DME and significant vitreo-macular traction and for patients with PDR with persistent non-clearing vitreous hemorrhage and/or traction retinal detachment[68].

D.7.f. Therapies targeting Intracellular Signaling Pathways

The following therapies are currently under development:

D.7.f.i. Protein Kinase C (PKC) inhibitors

Protein kinase C-β activation is part of the common downstream signaling pathway from VEGF and TNF-α, contributing to increased retinal vascular permeability.
Ruboxistaurin is a selective inhibitor of PKC-β that is being evaluated in clinical trials with NPDR and DME patients, with encouraging results in terms of reducing vision loss.[88]

D.7.f.ii. Kallikrein Inhibitors

Intraocular activation of the kallikrein-kinin pathway has been shown to increase retinal vascular permeability in animal models and may aggravate DME in some diabetic patients[89].
A phase I clinical trial to assess safety and tolerability of KVD001 (intravitreal) is in progress in a diabetic patient population with DME[68].

D.7.f.iii. TNF-α and CCL2 (MCP-1) Blocking Agents

TNF-α's detrimental role in DR has been shown by the beneficial effects (improved visual acuity and reduced retinal edema) induced by antagonizing it with infliximab in a double-blind, randomized, placebo-controlled study in patients with DME[90]. Furthermore, animal studies have shown that treating diabetic rodent models with etanercept (a soluble receptor that neutralizes TNF-α) prevents early diabetic retinopathy by reducing vascular permeability, leukostasis and nuclear factor kappa B activation.[91] Animal studies have also implicated TNF-α in promotion of pre-retinal neovascularization[92].

CCL2 is one of the most significantly elevated chemokines in the serum and vitreous of DR patients[93]. It induces leukocyte recruitment and activation, exacerbating the inflammatory response, by acting on its receptor CCR2. An ongoing clinical trial is testing a CCR2/CCR5 antagonist in patients with DME[68].

Diabetic retinopathy is known to compromise function of multiple retinal cell types such as neurons, Mueller glia and EC; however, the mechanism through which individual cell dysfunction contributes to disease development and progression remains unclear. To truly understand cellular contributions, a 'systems' approach' must be used. It is critical to understand (1) how do these cells interact with each other in normal conditions and (2) how do these interactions become disrupted by pathological triggers, such as diabetes.

To gain further insight into DR we must, therefore, focus on the retinal neurovascular crosstalk within the neurovascular unit, rather than on phenotypes of individual retinal cells.

E. The Neurovascular unit (NVU)

Neuronal and glial dysfunction contribute to the development of retinal pathological neovascularization – the Neurovascular Unit Approach

Although the typical approach to retinal diseases associated with pathological neovascularization has been to focus on their vascular component, a growing body of evidence suggests otherwise, as neuronal and glial dysfunction emerge as critical contributors for development and progression of the abnormal vascular phenotype[6,29,40,94]

Neurovascular units composed of extensive astrocyte networks connecting neuronal synapses with the cerebral vasculature, have been extensively characterized in the brain, where they are responsible for coupling neuronal activity and energy requirements with cerebral vascular flow[95]. A deeper understanding of the mechanisms underlying dysfunction within the NVU has been especially valuable in the context of neurodegenerative diseases, such as dementia, Parkinson's and Alzheimer's disease [96,97], where it has started to contribute for development of novel therapies.[98]

E.1. Retinal NVUs

Retinal NVUs have not been as widely explored as brain NVUs and detailed knowledge regarding its biological properties and functional interactions is limited.

However, it is known that retinal NVUs are composed of neurons, macroglia, microglia and retinal vasculature and that all these components act in a coordinated fashion to maintain retinal homeostasis and to ensure that neuronal metabolic needs are met, so that retinal activity can proceed uneventfully[99]. This perfect coordination is achieved through neurovascular coupling, which refers to the ability of retinal vessels to adjust their blood flow in response to changes in local neural activity[100].

E.1.a. Neurovascular units in the RGC layer

There is substantial evidence demonstrating that neurovascular coupling occurs in the RGC layer (or at least in the inner retina) and one of the most paradigmatic examples is the response to flicker light stimulation. Human and animal studies have shown that (1) vascular flow to the retina and optic nerve increases in response to diffuse luminance flicker (light on, light off) thanks to RGC or pericyte-induced vasodilation - 'functional hyperemia response'); and that (2) there is a marked correlation between neuronal activity of RGC, increased metabolism and increased glucose delivery during flicker light stimulation[100-105].

Communication between neuroglial and vascular cells can be mediated by two kinds of signaling molecules: those that act rapidly (e.g. metabolites) and those that exert a prolonged effect (e.g. growth factors). Some of these factors have been extensively studied and include the following: Nitric Oxide (NO); metabolites derived from arachidonic acid metabolism; glutamate; VEGF and neurotrophins (e.g. nerve growth factor and brain derived growth factor)[79,100,106].

Despite considerable lack of knowledge regarding the specific molecular mechanisms responsible for compromise retinal neurovascular crosstalk, there is evidence that disruptions at this level occur in retinal pathological settings and that these can play a critical role in promoting disease development and progression.

E.1.b. Evidence of disrupted Neurovascular Crosstalk in ischemic retinopathies

The early stages of ischemic retinopathies are characterized by microvascular degeneration that produces nonperfused retinal areas where neurons undergo severe hypoxia. Disruption of the functional neurovascular unit in the retina occurs during ischemic retinopathies (e.g diabetic retinopathy), in inadequately perfused areas [79,102,107].

The discrepancy between metabolic demand and supply then leads to a second phase featuring pathological neovascularization, which develops as a frustrated attempt to reinstate a positive energy balance. This second phase is marked by a robust pro-angiogenic response, which leads to abnormal neovascularization

towards the vitreous, paradoxically associated with a prominent failure in revascularization of hypoxic areas.

The misguided neovascular growth has been associated with high concentrations of proangiogenic factors in the vitreous, which attract nascent vessels; however, high levels of proangiogenic factors are also produced by retinal cells and would be expected to retain the growing vessels on the retinal surface. Since this confinement to the retinal surface is not observed, this failure to revascularize hypoxic areas is probably an active process mediated by vasorepulsive factors produced in those regions. [40]

A growing body of evidence suggests that severely hypoxic neurons dramatically change their properties and highly contribute to vascular changes in the course of ischemic retinopathies[94,108,109].

An illustrative example of compromised neurovascular crosstalk in retinopathy comes from Eric Newman and colleagues who have elegantly shown that in the mammalian retina, neurovascular coupling is mediated by glial cells via production of nitric oxide, and that this mechanism is compromised in diabetic retinas, where it reduces the 'functional hyperemia response'[79,107,110].

The physiologic intimate relationships amongst neurons, vasculature and microglial cells their importance for retinal homeostasis, and their sustained cooperation in ischemic retinopathies suggest that pathological retinal phenotypes arise due to disruption of functional interactions within the neurovascular unit (NVU).

A deeper understanding of the mechanisms through which the NVU reacts under stress, and especially of how metabolic dysregulation affects the retinal neurovascular crosstalk, will provide important leads for devising therapeutic strategies focused on improving the metabolic mismatch that characterizes ischemic retinopathies to promote effective reparative angiogenesis in hypoxic retinal areas. These strategies will optimize use of hypoxia-induced proangiogenic resources and will eliminate the state of metabolic insufficiency that drives disease progression.

It remains unknown whether relevant neurovascular coupling also exists and functions in the same fashion at other retinal levels (intermediate and deep retinal plexuses and outer retina), however it is expected that this is the case (with potential differences in terms of signaling factors). This suggests that retinal

diseases, both of the inner and outer retina, may benefit from being approached using this integrative perspective focused on interactions within the NVU.
These issues will be addressed in **Chapter IV-A**.

F. The Role of Metabolic Factors in Retinal Disease

Clinical therapies targeting retinal diseases associated with pathological neovascularization typically act late, and focus on blocking excessive activity of pro-angiogenic growth factors (especially VEGF) to abrogate abnormal vascular growth.
New research findings show that in addition to growth factors, vascular metabolism also regulates angiogenesis and does so at a much earlier time-point during disease development[111,112]. Glycolysis is critical for ATP production in EC and modulation of its key regulatory enzyme, 6-phosphofructo-2-kinase/fructose-2,6-biphosphatase 3 (PFKFB3) regulates EC sprouting. As ECs are activated to migrate, proliferate and acquire a tip cell phenotype, they are also required to double their glycolytic production of ATP (proliferating EC are hyperglycolytic). When PFKBP3 is pharmacologically inhibited in pathological conditions where EC sprouting is reactivated (e.g. neovascularization arising in ischemic retinopathies), there is a partial reduction in EC glycolysis and a reduction in pathological angiogenesis with minimal adverse consequences for the normal vasculature. Since mature quiescent EC are not hyperglycolytic, this strategy appears to be safer for preventing pathological neovascularization than the ones currently in use[111,112].
Similarly to what happens in EC, a tight link between metabolic state and functional phenotype is also observed in macrophages. In these cells, the preferentially used pathway for energy production defines the cell's inflammatory phenotype; M1 macrophages (the more pro-inflammatory type, involved in the first line of defense against noxious agents) are highly dependent on glycolysis, which offers energetic advantages in hypoxic regions. M2 macrophages (involved in tissue repair and wound healing, with a less pro-inflammatory action), on the other hand, rely on oxidative metabolism[113].

It has been shown that intermediates generated during these metabolic processes have the ability to drive macrophages' functional responses. For example, in M1 macrophages, succinate stabilizes HIF-1α, which drives and sustains production of IL-1β, thereby promoting a pro-inflammatory environment.[114]

In ischemic retinopathies, energy producing metabolic pathways are profoundly dysfunctional and the accumulated metabolic intermediates can act as signaling factors that influence disease progression. For example, in the OIR mouse hypoxic retina, the lack of oxygen compromises cellular respiration, which induces subsequent accumulation of succinate. This metabolite can bind and activate GPR91 (a G-protein coupled receptor mainly expressed on RGC), promoting production of VEGF and angiopoietins 1 and 2 and pathological retinal neovascularization. Interestingly, the induction of compensatory angiogenesis via the succinate/GPR91 pathway can occur before HIF stabilization, suggesting that it may act as a more sensitive indicator of retinal damage[115,116].

Another HIF independent pathway inducing VEGF production in the hypoxic retina involves PGC-1α (peroxisome proliferator-activated receptor Y coactivator 1-α). It has been shown that PGC-1alpha is (1) strongly induced in the INL under OIR conditions and that (2) it is required for development of full pathological retinal neovascularization at P17 through enhancement of local VEGF production[117].

In addition, alterations in amino-acid metabolism as well as supplementation of arginine and glutamine have also been shown to affect development of neuro-glial dysfunction and of neovascularization in the OIR model[118].

Identification of specific metabolic perturbations and of their detrimental effects on the retina suggests that restoring functionality in these pathways can potentially reinstate harmonious interactions within the NVU and become a promising, safer and more effective therapeutic strategy to prevent progression of ischemic retinopathies, such as DR. Moreover, diabetes is a metabolic disease and consistently dysregulated systemic metabolites can potentially become novel biomarkers for accurate risk prediction and disease monitoring.

Development of metabolic diseases such as diabetes (especially type 2) depends upon a complex set of interactions between genetic and environmental factors and, as mentioned previously, it is not fully understood why some long-term diabetic patients are protected from developing severe DR. Metabolomics, a technology that allows for comprehensive metabolic analysis, is a powerful tool

that can provide relevant insight into this complexity; this technology measures the entire collection of small molecule metabolites present in biological samples, which constitute the metabolome, and are present in biological samples. Analysis of the metabolome output generates chemical phenotypes that are the net result of genomic, transcriptomic and proteomic interactions[119]. Metabolites are the final downstream products of all the chemical reactions occurring in the biological organism/tissue at a specific point in time, and are generated in metabolic pathways whose activity is modulated by interactions between genetic and environmental influences. Therefore, metabolomics provides a more global and integrated overview of biological status when compared to other "omics" approaches, such as genomics, transcriptomics and proteomics; moreover metabolomics is much more sensitive than the latter technologies and is able to identify both short and long-term physiological and pathological changes in biological samples; these represent major advantages for discovery of new biomarkers and for discerning pathophysiological mechanisms.

The two major platforms for comprehensive investigation of metabolic profiles in biological samples are nuclear magnetic resonance (NMR) spectroscopy and mass spectrometry (MS).

NMR is based on the magnetic properties of the atomic nucleus and identifies metabolites in biological samples by assessing behavior of their NMR active nuclei in a strong magnetic field; this provides information on their structural and chemical properties. Although NMR is widely used for metabolomics because of the non-destructive nature of the analysis, its minimal sample preparation requirements, and its robust and reproducible measurements, this method presents a relatively low sensitivity[120].

MS-metabolomics, on the other hand, is highly sensitive and, when both untargeted and targeted approaches are performed, it enables both the detection of a wide range of metabolites in biological samples (untargeted analysis) and confirmation of those metabolites' identity (by using targeted analysis against an internal standard). Global (untargeted) MS-metabolomics provides a global overview of the metabolome in two different biological states and, based on univariate and multivariate statistical analysis, identifies the metabolites that qualitatively differ between them (i.e., is a qualitative approach); Targeted MS-metabolomics, on the other hand, uses internal standards to precisely identify the

analytes being surveyed and accurately quantifies discrete clusters of related metabolites, thus providing their absolute concentrations (is a quantitative approach, in contrast with global metabolomics)[121,122].

Since the work presented in this dissertation was undertaken to both identify potential new biomarkers and discern new pathophysiological mechanisms in DR, we decided to use liquid chromatography (LC)-MS-metabolomics. Sample preparation for this method is long and is performed according to the following sequence: (1) A high performance liquid chromatography (HPLC) system separates chemicals (in a biological sample) by conventional chromatography on a column (the metabolite binds the column by hydrophobic interactions and is posteriorly eluted off by an even more hydrophobic solvent); (2) The analytes enter the mass detector as they exit the chromatography column, and become ionized; (3) the ions are then separated according to their mass-to-charge (m/z) ratio using an analyzer with an electromagnetic field. This procedure provides mass measurements and generates individual peaks for each of the analytes in the sample; In order to identify the nature of these metabolites, their mass measurement are compared against online databases, such as METLIN[123] and, ideally, tandem mass spectrometry analyses (MS/MS; targeted analysis) using an internal standard are subsequently performed to definitely confirm their identities[120].

Although metabolomic analyses focusing on DR have been performed in the past, the metabolome of human DR remains unknown and this probably reflects the use of less sensitive technologies in these studies, which provided very limited metabolic information [124,125]. The work presented in this dissertation uses highly sensitive MS-metabolomics technology to provide a truly comprehensive metabolic overview of DR (including validation of the metabolite's identity via MS/MS targeted analyses) that could potentially improve diabetic patient care and provide new directions for DR research.

The exciting potential of large-scale metabolomic analyses will be explored in **Chapter IV-B** and **IV-C**.

Chapter II: Aims

The main objective of this work is to provide novel and relevant insights into diabetic retinopathy that can pave the way towards development of targeted and more effective therapies to prevent progression of DR into its devastating late stages.

To achieve this goal, the work presented in this dissertation will focus on:

A) Acquiring further knowledge on functionality of retinal NVUs in physiologic and pathologic conditions, so that development of DR (and of PDR-like features) can be perceived from a more integrated perspective.

B) Gaining a better understanding of the role played by metabolic factors in progression of DR, by performing global mass-spectrometry-based metabolomic anlyses to:

(**1**) Generate a global metabolomic profile of PDR, in order to identify the most dysregulated metabolic pathways in the eye during late-stage disease;

(**2**) Identify circulating metabolites with potentially protective properties against progression of DR. and to exploit their beneficial properties in preventing development of PDR-like features in the OIR mouse model.

Chapter III: Material and Methods

A. Study Approval

The Institutional Review Boards of The Scripps Research Institute (TSRI), Scripps clinic and Tokyo Medical University approved all studies involving human samples that are included in this dissertation. Patient data and samples (vitreous and aqueous humor, and blood) were handled in accordance with the tenets of the Declaration of Helsinki.

All patients provided written informed consent for surgery and for collection of clinical data and biological samples. Patient data collection forms accompanying blood drawing for metabolic studies are presented in the **Appendix**.

B. Clinical Samples

Blood serum, vitreous and aqueous humor samples were used in this work.

a) Blood serum samples* (Total: 22 samples) from:

- Long-term diabetic patients (for at least 15 years); included patients with no clinical signs of diabetic retinopathy (DR) and patients with early clinical signs (mild NPDR); n=12
- Diabetic patients (with any disease duration) with clinically diagnosed proliferative diabetic retinopathy; n=10

b) Vitreous samples* (Total: 171 samples)

- Diabetic patients with PDR; n=17
- Non-diabetic controls undergoing surgery for removal of epiretinal membranes or repair of macular holes; n=40
- Patients with macular holes; n=18
- Patients with retinal detachment; n=51
- Patients with branch vein occlusion; n=7
- Patients with diabetic macular edema; n=14
- Patients with proliferative diabetic retinopathy; n=24

c) Aqueous humor samples (Total: 248 samples)

- Patients with macular holes; n=11
- Patients with retinal detachment; n=52,
- Patients with branch vein occlusion; n=24
- Patients with diabetic macular edema; n=16
- Patients with proliferative diabetic retinopathy; n=11
- Patients with glaucoma (Primary open angle glaucoma and normal tension glaucoma); n=28
- Patients with central vein occlusion; n=8
- Patients with AMD; n=24
- Patients with polypoidal choroidal vasculopathy; n=10
- Patients with retinitis pigmentosa; n=18
- Controls: Patients undergoing cataract surgery, or vitreoretinal surgery for epiretinal membrane peeling; n= 46

d) Paraffin-embedded sections from human eyes (healthy and with age related macular degeneration) obtained from the National Disease Research Interchange (NDRI) tissue bank

C. Collection and Processing of Clinical Samples

C.1. Blood Samples

Blood samples were collected by peripheral venipuncture into SST vacutainer tubes (5ml, BD biosciences # 367986) and incubated in the vertical position for 30 minutes at room temperature (RT). After incubation, the samples were centrifuged at 1200g for 10 minutes at RT and 3 aliquots of 300 ul (of serum) were collected into 1.5 ml Eppendorf tubes. The tubes were labeled with the patient study number and stored at -80^{o} C.

C.2. Vitreous Samples

Vitreous samples were collected during standard pars plana vitrectomy conducted using a 25-gauge 3-port system, under local anesthesia, performed using a high-speed vitreous cutter (2500 cycle/minute). Phacoemulsification and aspiration were performed simultaneously in patients with cataracts, with an acrylic foldable intraocular lens (IOL) placed in the capsular bag.
Undiluted vitreous samples (0.1 to 0.5 ml) were aspirated from the mid-vitreous under standardized conditions, at the beginning of the surgery, transferred to sterile plastic tubes (previously labeled with the patient's study number) and frozen immediately (within 15 seconds) in liquid nitrogen until analysis.

Patient selection criteria for the PDR vitreous MS-metabolomics study

<u>Exclusion criteria</u>

Chronic systemic inflammatory diseases
Idiopathic ophthalmic inflammatory disorders
History of retinal vein occlusion
Diagnosis of age related macular degeneration

Inclusion criteria

Cases

Diabetic patients with **active PDR** ("perfused, multi-branching iridic or pre-retinal capillaries"[126]) or **inactive PDR** ("evidence of fully regressed active proliferation or only non-perfused, gliotic vessels or fibrosis"[126])

Controls

Non-diabetic patients undergoing epiretinal membrane or macular hole surgery

C.3. Aqueous Humor Samples

Aqueous humor samples (0.1 to 0.2 ml) were aspirated from the corneal limbus with a 27-gauge needle attached to a sterile tuberculin syringe, transferred to sterile tubes and frozen immediately in -80 °C until analysis.

D. Animal models

All the experiments involving animals were performed in accordance with the NIH Guide for the Care and Use of Laboratory Animals and approved by the Scripps Research Institute Animal Care Committee.

Mouse lines used in Chapter IV-A (Table 1)

"Knock-out" first conditional alleles (tm1a) for *Pam* (*Pam*$^{tm1a(EUCOMM)Wtsi}$) were obtained from EuMMCR (3 clones A11, D12, and F09).[127] The 'knockout-first' allele (tm1a) contains an IRES:lacZ trapping cassette and a floxed promoter-driven neo cassette inserted into the intron of a gene, disrupting gene function. Crossing with FLP deleter mice (B6N.129S4-*Gt(ROSA)26Sor*$^{tm1(FLP1)Dym}$/J; from The Jackson Labs) converts the 'knockout-first' allele to a conditional allele (tm1c), restoring gene activity. Crossing with Crx-Cre (from Dr. Takahisa Furukawa,

Osaka University)[128] deletes the promoter-driven selection cassette and floxed exon of the tm1a allele to generate a lacZ-tagged allele (tm1b) or deletes the floxed exon of the tm1c allele to generate a frameshift mutation (tm1d), triggering nonsense mediated decay of the deleted transcript. Quality control and expansion of the lines was performed at the Embryonic Stem Cell Core at the University of California at San Diego (UCSD), and blastocyst injections were performed at the Mouse Genetics Core at TSRI. $Crx^{RIP/+}$ mice were generated as described previously.[129]

RCS rats were obtained from Dr. Matthew LaVail, University of California at San Francisco (UCSF).

RD1 (CBA/J), RD10 (B6.CXB1-*Pde6b*^{rd10}/J), RDS (*Prph2*^{Rd2}), VLDLR-/- (B6;129S7-*Vldlr*^{tm1Her}/J), Nrl-/- (B6;129-*Nrl*^{tm1Asw}/J), and $ROSA^{mT/mG}$ (*Gt(ROSA)26Sor*$^{tm4(ACTB-tdTomato,-EGFP)Luo}$/J) mice are all available through the Jackson Labs.

In Vivo Electroporation

After anesthetizing P0 pups on ice, DNA solutions containing open reading frame (ORF) clones for murine *Pam* or DsRed (both utilize the same backbone/enhancer; Origene)[130] were injected into the subretinal space and electric pulses (5 pulses of 50 ms with 950 ms intervals; current 0.08-0.15A) were administered immediately after, through tweezer type electrodes placed on the pup's head, to ensure DNA transfection from the subretinal space to the retina. After the procedure, the pups were warmed up using an electric blanket until they recovered from anesthesia and returned to their mother.

Transgenic mice expressing Cre recombinase under *ptf1a* (*ptf1a-Cre* mice) [131] were mated with *VHL*$^{fl/fl}$ [132], *Hif-1α*$^{fl/fl}$ [133], or *Hif-2α*$^{fl/fl}$ [134], *VEGF*$^{fl/fl}$ [135], Pde6b$^{rd10/rd10}$ rd10, and *Rosa26*$^{iDTR/+}$ (C57BL/6-Gt(ROSA)26Sor$^{tm1(HBEGF)Awai}$/J) [136] mice (Jackson Laboratories). *Ptf1a-Cre* mice were crossed with floxed *VEGF*, *VHL*, *Hif-1α, or Hif-2α* alleles for conditional deletion experiments. Littermate controls were used in all cases. To monitor Cre recombination in *ptf1a-Cre* mice, we mated them with two different reporters: (1) ROSA26tm14(CAG-tdTomato)(Ai14 [137]), for ptf1a-specific nuclear expression; and (2) ROSA

mTomato/mGFP transgenic reporter mice [138], for *Ptf1a*-specific membrane expression. We screened mice in our colony for *retinal degeneration slow* (*rds)*, *rd*1 and *rd*8 mutations. Genotyping was performed by Transnetyx, Inc.

In Vivo Genetic Ablation Studies.

For in vivo genetic ablation studies, ptf1a-Cre mice were crossed with $R26^{iDTR/+}$ mice (C57BL/6 Gt(ROSA)26Sortm1(HBEGFAwai/J) [136], yielding double transgenic ptf1a-Cre; $R16^{iDTR/+}$ (iDTR-positive) mice that selectively expressed iDTR (inducible diphetria toxin receptor) in amacrine and horizontal cells. The iDTR is only expressed after Cre-mediated excision of a transcriptional STOP casette. To achieve the phase-restricted depletion of amacrine and horizontal cells, ptf1a-Cre; $R16^{iDTR/+}$ and control littermates (ptf1a-Cre; $R16^{+/+}$ and $R16^{iDTR/+}$) were injected intraperitoneally for three consecutive days with 25 ng/g DT (Sigma-Aldrich).

Mice used in Chapter IV-B and IV-C

Oxygen induced retinopathy (OIR) mouse model

OIR was induced in C57BL/6 mice according to the protocol by Smith et al [139]. Seven day-old (P7) C57BL/6 mice were placed in 75% oxygen for five days and returned to ambient oxygen up to another five day-period (**Figure 10**). Whole eyes were collected immediately after death at twelve (P12), fourteen (P14) and seventeen (P17) days after birth, frozen directly in liquid nitrogen and stored at -80^{o} C until analysis.

All experiments performed in OIR mice were repeated at least 3 times with a minimum n = 4 mice per experimental group.

Age matched C57/Bl6 mice raised in ambient oxygen (normoxia) were used as non-controls in the work presented in Chapters IV-C and D.

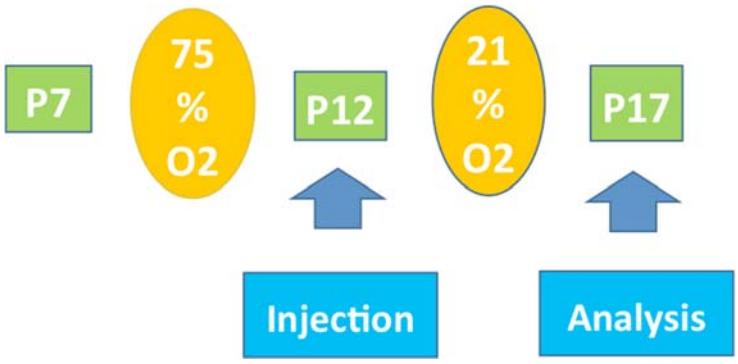

Figure 10 – Experimental protocol for induction of OIR in C57/Bl6 mice

Table 1 – Transgenic mouse lines used

Transgenic Mouse Line	**Publications**	
ptf1a-Cre	Kawaguchi et al, 2002	
VHL$^{floxed/floxed}$	Haase et al, 2001	
Hif-1α$^{floxed/floxed}$	Ryan et al, 2000	
Hif-2α$^{floxed/floxed}$	Gruber et al, 2007	
VEGF$^{floxed/floxed}$	Gerber et al, 1999	
Rosa26$^{iDTR/+}$	Buch et al, 2005	
VMD2-Cre	Le et al, 2008	
VLDLR$^{-/-}$	Chen Y et al, 2009	
RDS	Farrar et al, 1991	
RD10	Chang et al, 2002	
RD1	Chang et al, 2002	
Crx Cre	Nishida et al, 2003	
Nrl$^{-/-}$ mice	Kautzmann et al, 2011	
Crx$^{RIP/+}$	Roger et al, 2014	
Pam$^{a/+}$ mice	Gaier et al, 2014	
Reporter mice		
ROSA26tm14 (CAG-tdTomato)	Madisen et al, 2010	To monitor Cre recombination in *ptf1a-Cre and VMD-2 Cre* lines
ROSA mTomato/mGFP	Muzumdar et al, 2007	

Blood glucose and HbA1c measurements in mice

Blood was collected from the mouse tail vein and measurements of glucose and hemoglobin A_{1C} (HbA_{1C}) were performed using the FreeStyle blood glucose monitoring system (Abbott) and the A1cNow rapid immune-assay (Bayer), respectively.

E. Preparation of Sterile Solutions for Intraocular Injection

NOTE: The solvent most commonly used was sterile Dulbecco's Phosphate Buffered saline with calcium and magnesium (DPBS 1X, catalog# 21-030-CV), hereafter referred to as 'PBS'

Natural abundance (regular) Inosine (Sigma-Aldrich, Catalog # I4125-25G)
Molecular Weight (MW): 268.23 g/mol

- **10 mM**: 0.67g of inosine were added to 250 ml of PBS (Used for intravitreal injections by making a 1:1000 dilution, to achieve a 10 uM concentration)

- **1 M**: 2.68 g of inosine were added to 10 ml of PBS (Used for isotope labeling mass spectrometry based experiments by diluting 1:2 in sterile PBS, to achieve a 500 mM concentration)

^{15}N-labeled Inosine (Cambridge Isotope laboratories; catalog # NLM-4264-PK; 0.01g)
MW: 272.20 g/mol

- **1 M**: 36.7 ul of PBS were added to the vial, which contains 0.01 g (Used for isotope labeling mass spectrometry based experiments by diluting 1:2 in sterile PBS, to achieve a 500 mM concentration)

Natural abundance (regular) Arginine (Sigma-Aldrich, Catalog # A1270000)
MW: 174.20 g/mol

- **500 mM**: 4.35g were added to 50 ml of sterile PBS (Used for isotope labeling mass spectrometry based experiments)

^{15}N-labeled Arginine (Cambridge Isotope laboratories; catalog # NLM-396-PK; 0.01g)
MW: 214.64 g/mol

- **1 M**: 466 ul were added to the vial, which contains 0.1 g (Used for isotope labeling mass spectrometry based experiments by diluting 1:2, to achieve a 500 mM concentration)

F. Intravitreal and Subretinal Injections

Technique

Intravitreal injections

Pups were anesthetized by hypothermia and then placed under the dissecting microscope, where the skin over the eyelid was cut to expose the eye. Intravitreal injections were then performed using a 5 ul Hamilton syringe with a beveled 33 Gauge needle that entered the eye at the margin of the cornea and sclera (limbus), directly into the vitreous. The volume injected was 0.5 ul.[140]

Subretinal injections

After anesthetizing the mice, a sharp 30 G sharp disposable pre-sterilized needle was introduced right below the limbus, at an angle, to create an entry port. Subsequently, a pre-loaded syringe (mounted on a micromanipulator) with a blunt needle was gently inserted through the hole, crossing the vitreous until reaching the retina; at this point, gentle force was applied on the syringe to puncture the retina and deliver its loaded contents into the subretinal space[141]. The volume injected was 0.5 ul in mice and 1 ul in rats.

Substances delivered by intraocular injection

Chapter IV-A

ShH10-GFP virus (specifically transduces Mueller glial cells and astrocytes)

ShH10-GFP virus were generated in Dr Flannery's laboratory (University of California at Berkeley) as previously reported[142] and mouse angiogenin (isoform

1) was inserted into the ShH10 viral vector. The same CMV enhancer was used in both vectors. Genotyping was performed by Transnetyx, Inc.

Recombinant carrier-free human Angiogenin and PAM

These recombinant proteins were obtained from R&D Biosystems and eluted in sterile PBS prior to injection.

Erucamide loaded silicon microparticles - produced in Dr Sailor's laboratory at UCSD, according to the following protocol:

Preparation of Porous Silicon Microparticles: Porous silicon (pSi) films were prepared by anodic electrochemical etch of highly doped, p-type silicon wafers polished on the (100) face (boron-doped, 1.0 mΩ-cm resistivity; obtained from Siltronix Inc., Archamps, France). A Teflon etch cell was used that exposed 8 cm^2 of the Si wafer to 3:1 (v:v) 48% aqueous HF:ethanol electrolyte (obtained from Fisher-Scientific). Samples were etched at a constant current density of 50 mA/cm^2 for 300 sec. The resulting pSi films were removed from the crystalline silicon substrate by application of a current pulse of 30 mA/cm2 for 250 s in a solution of 1:20 (v:v) 48% aqueous HF:ethanol electrolyte. The freestanding pSi films were immersed in ethanol within a glass vial and fractured into microparticles by ultrasonication for 10 min and then washed 3 times with ethanol by centrifugation.

Erucamide Loading into Porous Silicon Microparticles. A 100 mg/mL solution of the pSi particles in ethanol and a 10 mg/mL solution of erucamide in ethanol were prepared and mixed together in a 1:1 (v:v) ratio. The resulting solution was incubated at 37°C for 10 min. Water was then added drop wise to the particle/erucamide solution until diluted 10x. The resulting erucamide-loaded particles were washed with 10% ethanol in water by centrifugation. Thermogravimetric analysis (TGA) in a STA 6000 apparatus (Perkin Elmer) by constant heating from room temperature up to 900°C at 10°/min under a 20 mL/min oxygen flow was used to determine the amount of erucamide loaded in the pSi particles (30 ug drug/mg of particle).

Chapter IV-B and IV-C

Time-points used for injections

Intravitreal injections were performed in OIR mice at P7 and P12.

Solutions injected

Inosine (0.5 ul of a 10 uM or 500 uM solutions, made in sterile PBS)

Arginine (0.5 ul of a 10 uM or 500 uM solutions, made in sterile PBS)

Sterile PBS (Vehicle)

U-^{15}N-Inosine (0.5 ul of a 500 uM solution, made in sterile PBS)

U-^{15}N-arginine (0.5 ul of a solution of a 500 uM solution, made in sterile PBS)

G. Sectioning and Staining

G.1. Preparing cryosections

Method (1)

After sacrificing the animals (by isofluorane inhalation), the eyes were enucleated and the cornea carefully perforated with a sharp needle. The eyes were then fixed for 1 hour in 4% paraformaldehyde (PFA), on ice, and transferred to a 30% sucrose solution overnight at 4^{o} C, in 1.5 ml tubes. The morning after, the eyes were placed in previously labeled molds filled with OCT (Tissue Tek) and immediately frozen on dry ice.

Method (2)

In some of the experiments, in order to reduce background, frozen sections were prepared by immersing the freshly collected eyeballs in OCT and directly freezing them on liquid nitrogen or at -80^{o} C. After sectioning, these slides were fixed in 4% PFA for 10 minutes and then rinsed 3 times with PBS before initiating the staining process.

After obtaining frozen blocks, the eyes were cut into 12 um sections on a Leica CM 1850 cryostat and placed on glass sides (Poly-L-Lysine glass slides from Polysciences, Inc. catalog # 22247)

G.2. Staining Cryosections

General information

All the staining procedures were undertaken inside small humid chambers in order to prevent precocious drying

A volume of 250 ul was used per slide.

To prepare fluorescent stainings of paraffin-embedded sections (NDRI human sections), these were firstly rehydrated by sequential immersion in (1) xylene (2 times; each time for 10 minutes); (2) in 100% ethanol (2 times, for 10 minutes each); (3) in 95% ethanol (for 5 minutes); (4) in 70% ethanol (for 5 minutes) and finally (5) in 50% ethanol (for 5 minutes); after this, they were rinsed with deionized water, rehydrated with wash buffer for 10 minutes and finally stained according to the protocol described below.

Blocking solutions for staining were prepared using donkey or goat serum by combining reagents as indicated in **Table 2**.

Table 2 – Reagents used for preparation of blocking solutions

Blocking solutions	
Bovine serum albumin (BSA)	5% (weight/volume)
Donkey serum or goat serum	10%
Triton 100X	0.01%
PBS	Remaining volume

Staining procedure

Sections were rehydrated with PBS for 5 minutes, then blocked for 1 hour in 10% Donkey serum (DS) or 2% Goat Serum (GS) solution and incubated with primary antibodies (**Table 3**) for 2 hours at room temperature or overnight at 4º C. After this, sections were rinsed with PBS 3 times (3 min each), incubated with Alexa fluor conjugated secondary antibodies (purchased from life technologies; conjugated to fluorophores 488, 594, 567 or 647) for 30 minutes (at a 1:1000 dilution in PBS), rinsed with PBS and finally incubated with DAPI (1:1000 dilution in PBS for 5 minutes). After a final rinse in PBS, the sections were mounted on a glass slide, with a drop of slowfade mounting medium (Life Technologies).

G.3. Preparing vibratome sections

Eyes were enucleated and fixed for 20 min at room temperature (RT) in 4% PFA. Retinas were dissected and further fixed overnight in 4% PFA, at +4ºC. The following morning, the retinas were embedded in 5% agarose and left at room temperature until the agarose solution became solid. Agarose blocks were then sectioned using a Leica VT1000 vibratome to produce 100 micron thick sections.

G.4. Staining vibratome sections

The sections were incubated in blocking solution for 1 hour at RT and then in primary antibody (**Table 3**) solution overnight, at +4ºC. The following morning they were washed in PBS for 4h at room temperature (PBS being changed every hour), incubated with secondary antibodies overnight at +4ºC, in the dark and washed in PBS for 4h. After this, sections were incubated with DAPI (1:1000) for 15 min at RT, washed in PBS for 15 minutes and mounted as previously described.

H. Retinal and RPE-choroid Flatmounting and Immunohistochemistry

H.1. Retinal and Choroid-RPE dissections

Retinal flatmounts

Under the dissecting microscope, the cornea, lens and vitreous were sequentially removed and the sclera/RPE-choroid/retina complex isolated. Four slits, positioned approximately 90º from each other, were cut in the retina/RPE-choroid/sclera complex and the RPE-sclera complex was detached from retina by gently pulling the former and the latter apart with a forceps. After isolating the retina, and before starting the staining procedure, thick remnants of vitreous (still attached to its surface) were removed by gentle cutting with a surgical scissors.

RPE-choroid flatmounts

For choroidal flatmounts, a similar procedure was followed but the RPE-choroid complex was carefully detached from the scleral tissue, after isolating the retina.

Immunohistochemistry

The dissected retinas or RPE-choroids complexes were fixed for 1 hour in 4% PFA on ice and then blocked for 1 hour at RT. Afterwards, samples were incubated with primary antibody (**Table 3**) overnight at +4º C. The next morning they were washed in PBS for 2 hours (changed every hour) and then incubated in the dark with the corresponding secondary antibody (Alexa-fluor conjugated antibodies obtained from Life technologies; 1:200 dilution in PBS) for 2 hours, at room temperature. After this, samples were washed in PBS for 2 hours at room temperature and then mounted as previously described.[140]

Table 3 - Primary antibodies used

Antibody	Company	Catalog #	Host/origin	Dilution
Isolectin GS-IB4 Alexa Fluor 594/488 conjugate	Life technologies	I21411	*Griffonia simplicifolia*	1:200
Iba-1	Wako chemicals	019-19741	Rabbit	1:200
CD11b	AbD Serotec	MCA711G	Rat	1:500
CD31	BD Pharmingen	550274	Rat	1:200
GFAP	Dako	IR524/IS524	Rabbit	1:200
Angiogenin	abcam	AB95389	Rabbit	1:200
PAM	Santa Cruz Biotechnologies	sc-17393	Goat	1:50
Cone Opsin	Millipore	AB5407	Rabbit	1:200
Cone arrestin	Millipore	AB15282	Rabbit	
Rhodopsin	Abcam	AB5417	Mouse	1:100
Collagen IV	Millipore	AB756P	Rabbit	1:200
ZO-1 (FITC conjugated)	Life technologies	339194	Mouse	1:200
Vitronectin	Santa Cruz Biotechnologies	sc-15332	Rabbit	1:100
PAX2	LSBio	LS-C9505	Rabbit	1:200
GFP	Abcam	AB6556	Rabbit	1:100
Calretinin	Swant	7697	Mouse	1:200
Calbindin D-28K	Millipore	AB1778	Rabbit	1:2000
MAP2	Novus biologicals	NB300-213	Chicken	1:200
Glutamine synthetase (GS)	ThermoScientific	PA1-46165	Rabbit	1:200
Glycine transporter 1	Millipore	AB1770	Goat	1:200
Glutamate decarboxylase 65 &67	Millipore	AB1511	Rabbit	1:200
Neurofilament	Developmental Studies Hybridoma Bank	2H3	Mouse	1:500
Synaptophysin	Synaptic systems	101011	Mouse	1:200
Syntaxin (STX1)	Sigma-Aldrich	S0664	Mouse	1:200
Chx10	Exalpha	X1179P	Sheep	1:200
Recoverin	Millipore	AB5585	Rabbit	1:200

I. Imaging on a Confocal Fluorescence Microscope

Imaging was performed on a Zeiss confocal Laser Scanning Microscope (LSM 700 or 710, Zeiss), equipped with 4 objective lenses (5x, 10x, 20x and 40x) and 4 lasers (spanning wavelengths from 405 to 639 nm) using the acquisition software 'ZEN imaging' (Zeiss) and Imaris (Bitplane). All images were obtained with sequential acquisition of the fluorescent channels (usually 488, 567 or 594 and 647 nm) to avoid fluorescence bleed-through.
Image processing was performed using Photoshop CS6 (Adobe), image J and ZEN 2010.

I.1. Quantification of Vascular Density (Retinal Vascular Plexuses)

Three-dimensional reconstructions were generated using ZEN 2010 and Imaris software (Bitplane). To assess the density of the vascular plexus, eight 200X magnification images (four center and four peripheral; 320 × 320 μm fields of view (FOV) per retina) were chosen from each scanned image, and the numbers obtained from each of the eight fields were averaged. Tip cells were scored as GS-lectin positive cells with blind-ended endothelial protrusions that had associated filopodial bursts in areas at the angiogenic front by analyzing high magnification (400x) micrographs. To quantify numbers of filopodia per tip cell, randomly selected high magnification (400X) micrographs images were analyzed. To construct triple-colored images, images were overlaid using Adobe Photoshop CS6.

I.2. Quantification of Retinal Degeneration in RD10 mice

Manual segmentation using the Adobe Photoshop CS6 ruler instrument was used to accurately measure retinal layers. Quantification of degeneration in RD10 mice (injected at P14 and analyzed at P18, P25, and P32) was performed as follows: Eyes were cut in 14μm sections and immunolabeled with recoverin antibodies and DAPI. Retinal thickness values were measured in nine distinct locations from

micrographs in central and peripheral regions in erucamide and empty microparticle injected eyes (n=4). Averages were calculated and plotted using Excel. The experiment was repeated four times. Two-tail students t-tests were used for statistical analyses.

I.3. Quantification of the OIR Phenotype

Quantification of the OIR phenotype on retinal flatmounts was conducted on Adobe Photoshop CS6 (PS CS6) and the corresponding statistical analysis was performed on Microsoft excel, using a previously described protocol[143]

Tiled images of OIR retinal flatmounts stained with the vascular marker GS-lectin were taken under the fluorescent microscope and further processed and analyzed on PS CS6 by following 3 steps: (1) image setup; (2) quantification of tufts; (3) quantification of vaso-obliteration.

Image setup. Resolution was set to 300 ppi and dimensions to 1536x1536 pixels in all images, to achieve a final image size of 5.12 inches^2

Image mode was changed to RGB color; foreground color was set to red (R255, G0, B0) and background color to yellow (R255, G255, B0).

Brightness and contrast were adjusted to enhance differences between vessels and background; and neovascular tufts and normal vessels.

Neovascular tufts quantification. After setting tolerance to 60, tufts were selected in a continuous fashion using the magic wand tool. After selection of all tufts, the area was filled in foreground color (red) manually using the magic wand tool to obtain the corresponding pixel count (revealed under 'histogram').

Quantification of vaso-obliterated (VO) areas. Before starting this step, all tuft areas were deselected. After setting "Feather" to 0, all VO areas were selected with the lasso tool in a continuous fashion, after which they were filled in background color (yellow). The total area of VO was selected using the magic wand tool and the corresponding pixel count (revealed on histogram) was annotated.

Statistical analysis. After inputting the total area of tufts and VO (in pixels) for each individual retina into Excel, a conversion factor (*10.8; based on tile scan

parameters and image resolution) was applied to produce absolute values in square micrometers for each corresponding area.

Mean values regarding area of tufts and area of VO were calculated for each experimental group and plotted on a bar chart. Statistical significant differences between groups were evaluated using Student's *t*-test (paired, two-tailed) and statistical significance was considered when *P*-value < 0.05.

I.4. Microglial cell/Macrophage Quantification on Retinal Cryosections

Retinal cryosections were stained with Iba-1 and DAPI (as previously described) to visualize microglial cells, macrophages and retinal nuclear layers. Quantification was based on to the protocol reported by McVicar et al[144]

For each of the analyzed eyes, eight consecutive sections representing the central and midperipheral (nasal and temporal) retina were selected and the number of Iba-1 positive cells (total and per retinal layer: ONL, OPL, INL, IPL, GCL) was quantified (n=4, per experimental group).

Statistical analysis. Mean cell counts (total and partial, for each retinal layer) were calculated for each experimental group and compared; Student's t-test was used to assess statistical significance.

J. Electron Microscopy Analysis

Tissue preparation: Eye cups formed by the retina and choroid were fixed in 4% PFA and 1.5% glutaraldehyde in 0.1 M cacodylate buffer overnight at 4° C and followed by a rinse in 0.1 M Na cacodylate for 1 hour. Afterwards, the eyecups were postfixed in 1% osmium tetroxide in 0.1 cacodylate buffer for 2 hours followed by washes for 1 hour and dehydration with graded ethanol solutions. Samples were incubated overnight in a 1:2 mix of propylene oxide and Epon/Araldite (Sigma-Aldrich) and embedded in 100% resin. Finally, the blocks were sectioned and used for transmission electron microscopy analysis.

For scanning electron microscopy, lightly fixed retinas (buffered paraformaldehyde) were fixed overnight in 2.5% gluteraldehyde in 0.1M Na cacodylate buffer pH 7.4. Cross sections were prepared with a #11 scalpel blade,

then washed with buffer, postfixed in 1% osmium tetroxide, washed in 0.1M cacodylate buffer, washed with distilled water and then dehydrated in series of graded ethanol. The tissues were then treated with hexamethyldisilazane (HMDS) (Electron Microscopy Sciences, Hatfield PA) as a substitute for critical point drying and dried and mounted onto SEM stubs with carbon tape and then sputter coated with 4nm of Iridium (EMS model 150T S) for examination on a Hitachi S-4800 SEM (Hitachi High Technologies America Inc., Pleasanton CA). A scanning electron microscope (FEI XL30 SEM) was also used to obtain images of the pSi particles (**Figure 1D**). The average particle size (36 ± 14 um) and nominal pore diameter (21 ± 7 nm) were determined from scanning electron microscope (FEI XL30 SEM) images.

K. Enzyme-linked immunosorbent assay (ELISA)

Sample preparation

a) Retinas were dissected on ice, pooled and introduced in 1.5 ml Eppendorf tubes previously loaded with RIPA buffer (sigma Aldrich, catalog # R0278-50ML) and protease inhibitor cocktail (1:100 dilution; Thermo Pierce technologies, catalog # 87785), on ice;

b) Retinas in solution were homogenized, underwent 2 freeze-thaw cycles and were then centrifuged at +4^{o} C at 16000g, for 10 min

c) Supernatants were collected and immediately assayed undiluted or stored at -80^{o} C

ELISA DuoSet kits*(R&D systems)*

Reagents:

Coating buffer: 0.05M $NaHCO_3/Na_2CO_3$

Wash buffer: PBS with 0.05% tween

Blocking/Working buffer: 1% BSA eluted in PBS (50 ml should be made per plate)

Substrate solution: 1ml of TMB (Thermo-pierce; 3,3',5,5'- tetramethylbenzidine) was eluted in DMSO and this was later eluted in 9 ml of citrate buffer (30% sigma Aldrich). Two 2 ul of H_2O_2 were added at the end.

Stop solution: 1M H_2SO_4

Capture antibody

Detection antibody

Streptavidin-HRP (Horseradish peroxidase)

Standards (7 vials; different concentration values depending on the protein being tested)

Assay procedure

Step 1: The plate was coated with capture antibody (100 ul), eluted in coating buffer the night before the experiment, and incubated overnight at room temperature.

Step 2: The plate was washed, blocked for 1 hour at room temperature on a platform shaker, washed again, and incubated for another 2 hours on a platform shaker, at room temperature with standards, samples and working buffer (blank measurements).

After the third wash, the plate was incubated with detection antibody (100 ul/well) for 1 hour at room temperature, washed again and further incubated with streptavidin-Horseradish peroxidase (HRP; 100ul) for 30 minutes, at RT.

After the fourth wash, the plate was incubated with substrate solution (100ul) for 10 to 15 minutes after which stop solution was added. After this, optical densities (OD) were immediately read on a plate reader at 450 nm and at 540 nm (using the Gen5 software, BioTek).

Analysis of the data generated with Gen 5 software was performed on Microsoft Excel and on Graphpad prism software according to the following steps:

1) Obtaining corrected OD values for each well: The optical density (OD) readings made at 540 nm were subtracted from those made at 450 nm. The average OD values for blank wells (negative controls) were then subtracted from the values obtained previously.

2) The OD values (y) obtained for each standard concentration were average and paired with their respective concentration (x). The OD values for the samples were similarly averaged for each duplicate. All the data concerning standards and samples was introduced into Graphpad prism

3) A standard curve was generated on Graphpad prism by reducing the data using a 4-parameter logistic (4-PL) curve-fit, and the concentrations for each sample

were calculated and compared between experimental groups using two-tailed Student's t test.

L. Real Time Polymerase Chain Reaction (qRT-PCR)

In order to perform q-PCR, three steps were undertaken for all the assayed samples

Step 1: RNA extraction (using the miRNAeasy Mini Kit – Qiagen; catalog # 217004)

Dissected and isolated retinas or RPE-choroid samples were added to sterile plastic tubes containing 700 ul of Qiazol lysis reagent, on ice, and the tissues were disrupted and homogeneized using tissuruptor (Qiagen; Catalog# 9001271). The homogenate was then incubated for 5 minutes at room temperature, vigorously mixed with 140 ul of chloroform (shaking the tube for 15 seconds), incubated for 3 minutes at room temperature and centrifuged for 15 min at 12000 g at +4ºC. The upper aqueous phase was then transferred to a new collection tube, carefully avoiding any transfer of interphase, and 525 ul of 100% ethanol were added and thoroughly mixed by pipetting.

700 ul of the sample, including precipitate, were then transferred into a RNAeasy mini column (placed on top of a 2 ml collection) tube and centrifuged at 9000g for 15 s at room temperature with the flow through being discarded. This procedure was repeated for the remainder of the sample.

Afterwards, 700 ul of RWT buffer were added to the RNAeasy Mini column and the tubes were centrifuged at 9000 g for 15 seconds, at room temperature, discarding the flow through.

500 ul of RPE buffer were then added to to RNAeasy Mini column and centrifuged first for 15 seconds and then for 2 minutes at 9000 g, at room temperature.

Finally the RNAeasy mini column was transferred to a new 1.5 ml collection tube and 30 to 50 ul of RNAse free water were added before centrifuging for 1 minute at 9000 g to elute. RNA content was measured using the Nanodrop Spectrophotometer ND-1000 and accompanying software (ND 1000 v 3.3.0) by

placing 1 ul of sample on the device. An RNA yield of 30 ug per sample was considered the minimum acceptable amount and all samples fulfilling this requirement were processed immediately or stored at -80ºC until the second step.

Step 2: <u>Conversion of RNA to cDNA</u> (QuantiTect reverse Transcription Kit, Qiagen; Catalog # 205310)

The RNA samples, quantiscript reverse transcriptase, gDNA wipeout buffer, quantiscript RT buffer, RT primer mix and RNAse free water were thawed on ice. These solutions were then vortexed, briefly spun down and kept on ice for the remainder of the procedure.

The gDNA elimination reaction was set up by mixing 2 ul of gDNA wipeout buffer with the previously calculated amounts of template RNA (aiming at 0.5 ug of RNA per tube) and RNAse free water to make up a total volume of 14 ul. Samples were incubated for 2 min at 42 ºC (using the the Biorad C1000 thermal cycler) and then placed on ice. For the *reverse transcription reaction*, mastermix was prepared on ice (mixing 1 ul of Reverse transcriptase (RT) mix, 4 ul of RT buffer and 1 ul of RT primer mix per reaction) and added to the 14 ul of template RNA for a total volume of 20 ul per tube. Tubes were then incubated for 15 minutes at 42ºC (for the actual reverse transcription) followed by 3 minutes at 95ºC (to inactivate the reverse transcriptase) on the Biorad C1000 thermal cycler and, after this, placed immediately on ice and stored at – 20ºC (the assumed concentration of cDNA per tube is 25 ng/ul, the equivalent to 0.5 ug of RNA in 20 ul)

Step 3: **Relative quantification of gene expression**

cDNA samples were thawed on ice and individual reactions were set up on 96 well plates for PCR (Taqman) by mixing 10 ul of Taqman universal mastermix (no AmpErase UNG), 1 ul of the Taqman gene expression assay (probe; **Table 4**), 8 ul of RNAse free water and 1 ul of cDNA (total volume of 20 ul per reaction). PCR Reactions were run in triplicate using β-actin or 18S as endogenous controls.

Prepared PCR plates were then sealed, briefly spun down and assayed in the 7900HT Real-Time PCR system (Taqman) using the standard protocol† included in the SDS 2.4 software. Expression levels of VEGF isoforms 120; 164 and 188 (**Table 5**) were analyzed using a QuantiTect SYBR Green PCR Kit (Qiagen) and the CFX96 Touch Real-Time PCR Detection System (BIO-RAD).

The results generated by SDS 2.4 were then analyzed on Excel to assess compare differences in gene expression between experimental conditions. Corrected average values of gene expression were calculated and compared between experimental groups. Statistical significance was determined by two-tailed Student's t-tests, with p-values < 0.05 considered statistically significant.

† The standard protocol includes two stages: (1) Hold: – 95^{o} C for 10 minutes; 2) Cycle: – 95^{o} C for 15 seconds and 60^{o} C for 1 hour.

Table 4 – Probes used for RT-PCR

Taqman PCR probes/Array	Company	Catalog #
MCP-1	Life technologies	Mm00441242_m1
TNF-alpha	Life technologies	Mm00443258_m1
VEGF-A	Life technologies	Mm01281449_m1
VEGF-164	Qiagen	Refer to next table, please
VEGF-120	Qiagen	
VEGF-188	Qiagen	
iNOS	Life technologies	Mm00440502_m1
Arginase-1	Life technologies	Mm00475988_m1
Arginase 2	Life technologies	Mm00477592_m1
Pam	Life technologies	Mm01293044_m1
RT^2 Profiler for Mouse Angiogenesis	Qiagen	PAMM-024
RT^2 Profiler for Mouse hypoxia signaling pathway	Qiagen	PAMM-032

Table 5 - VEGF isoform primer sequences (described by Zhang et al[145])

VEGF isoforms primer sequences	
Vegf $_{120}$	
Sense	5′-CCC ACG ACA GAA GGA GAG CAG AAG T-3′
Antisense	5′-TTG GCT TGT CAC ATT TTT CTG GCT T-3′
Vegfa$_{164}$	
Sense	5′-CCC ACG ACA GAA GGA GAG CAG AAG T-3′
Antisense	5′-CAA GGC TCA CAG TGA TTT TCT TGG C-3′
Vegfa$_{188}$	
Sense	5′-CCC ACG ACA GAA GGA GAG CAG AAG T-3′
Antisense	5′-AAC AAG GCT CAC AGT GAA CGC T-3′

M. In Situ Hybridization (ISH)

Kit used: ViewRNA ISH Tissue 2-Plex Assay (Affymetrix Inc.); probe: VEGF (catalog # SB-13465)

This technique involves two steps:

1) Sample preparation and target probe set hybridization

2) Signal amplification and detection

Sample preparation and target probe set hybridization

Mice eyes were harvested and immediately transferred to 4% RNAse free PFA and fixed for 8 hours, at +4° C.

After fixation, eyes were transferred into a 30% sucrose solution (also prepared with RNAse free water) and left overnight at +4° C. The following morning, eyes were embedded in OCT and frozen. Twelve-micron sections were cut (as previously described) onto superfrost plus microscope slides, being carefully placed within the margins (drawn on the slides), as recommended by the manufacturer. Slides were then fixed overnight on a rack placed into a staining dish filled with chilled 10% NBF (made by mixing 178 ml of 1x PBS and 22 ml of 37% formaldehyde, on ice);

Buffers, reagents and equipment were set up in the following fashion:

The hybridization system was set to 40°C and humidified
The following solutions were prepared: 2 L of 1X PBS, using 10x PBS; 200 ml of 50% ethanol; 200 ml of 70% ethanol and 4 L of wash buffer (adding 3 L of RNAse free water, 36 ml of wash comp 1, 10 ml of wash comp 2 and RNAse free water for the remaining volume); 200 ml of storage buffer (adding 60 ml of wash comp 2 and 140 ml of RNAse free water)
The probe set was thawed and then placed on ice
10 ml of 1x PBS and Probe set diluent were prewarmed to 40° C

The following morning, slides were washed twice in PBS for 1 minute with frequent agitation and the tissue was sequentially dehydrated by introducing the rack of slides into 50%, 70% and 100% ethanol for 10 min each, at RT, without agitation. After this, the excess 100% ethanol was drained on paper towels and the rack was transferred to a 60° C dry incubator for 60 minutes (“baking” the slides).
After baking the slides, a barrier was drawn around the tissue sections with a hydrophobic barrier pen and allowed to dry for 20-30 min.
After preparing the working protease solution, 400 ul were added onto the tissue section on each slide and these were incubated in the hybridization system at 40° C. After this, slides were washed twice on a rack (in 1XPBS for 1 min with

agitation) and fixed for 5 minutes in 10% NBF at RT, under a fume hood. Another two washes were performed with frequent agitation (as previously described).
After preparing the working probe set solution, 400 ul of were added to each slide and the slides were incubated at 40^{o} C for 2 h in the hybridization system.
After hybridization with the probe sets, slides were washed three times with vigorous agitation and stored in a covered staining dish, at RT in 200 ml of storage buffer.

Signal amplification and detection

The following day, sections were washed twice in fresh wash buffer at RT for 2 min with vigorous agitation, and incubated with the following seven solutions, in the hybridization system:

1) Preamplifier Mix QT, for 25 min at 40^{o} C
2) Amplifier Mix QT for 15 minutes at 40^{o} C
3) Label probe-6 AP solution for 15 minutes, at 40^{o} C
4) Fast blue substrate for 30 minutes, in the dark, at RT
5) AP stop QT for 30 minutes, in the dark, at RT
6) Working label probe-AP solution, for 15 minutes, at 40^{o} C
7) AP enhancer solution, for 5 minutes, at RT and, after decanting it, with fast red substrate for 30 min, at 40^{o} C

In between these hybridization steps, slides were washed again three times in fresh wash buffer for 2 minutes each, at RT, with vigorous and constant agitation.
After the last hybridization step, slides were counterstained with Gill's hematoxylin (200 ml) for 5-10 seconds at RT, washed 3 times with RNAse free water, incubated with 0.01% ammonium hydroxide for 10 seconds, washed again as before in RNAse free water and stained with DAPI for 1 minute. After a final rinse with RNAse free water, the slides were let air dry in the dark for approximately 20 minutes and then mounted using DAKO ultramount mounting medium.
Images of the ISH sections were finally taken using the Confocal Laser Scanning Microscope (LSM 700, Zeiss).

N. TUNEL Staining

Before starting the Terminal deoxynucleotidyl transferase dUTP nick end labeling (TUNEL) assay (Roche Diagnostics, catalog # 11684795910), a 0.1% TritonX 100 in a 0.1% Sodium Citrate permeabilization solution was prepared (495 ml of PBS + 2.5 ml of Triton + 2.5 g of sodium citrate).

Frozen sections (previously fixed for 1 hour in PFA 4%) were washed in PBS for 30 minutes, incubated with permeabilization solution for 2 minutes on ice (about 100 uL per slide) and rinsed twice with PBS afterwards. After this, slides were incubated with 50 uL of the TUNEL mixture (prepared by mixing the label solution with the enzyme solution immediately before use) for 60 min at 37ºC in a humidified chamber in light protected conditions. Two slides were incubated with DNAse I recombinant (3U/ml in 50mM Tris-HCl 1mg/ml BSA) for 10 minutes at room temperature and then incubated with TUNEL mixture in the same way as the experimental slides (positive control); and 2 slides were incubated with label solution only for 60 min at 37ºC in the dark (negative controls).

After the 60 minute incubation period, all sections were brought back to room temperature, rinsed with PBS (3 times) and mounted with DAPI mounting medium (Vectashield).

The slides were then directly analyzed under the Confocal Laser Scanning Microscope (LSM 700, Zeiss) and imaged in the blue and green channels. (Excitation length 450 - 500 nm and detection range 515 – 565 nm).

Quantification of TUNEL positive cells in the retina (using a previously described protocol[146])

From each of the eyes analyzed, five random sections were selected. The midperipheral nasal and temporal retinas were imaged and the number of TUNEL positive cells in the ONL was quantified and related to the correspondent measured retinal area, with Image J. The number of TUNEL positive cells per square millimeter is shown (Chapter IV-A).

O. Chick Chorioallantoic Membrane Assays

For the work presented in Chapter IV-A, a previously described protocol for *In vivo* Chick Chorioallantoic Membrane (CAM) assays was used [147]

Fertilized eggs containing chick embryos were preincubated for 8 days at 37.5° C in conditions of 85% humidity. After creating a hole over the air sac and subsequently identifying the vascular zone, a 1x1 cm window was opened in the shell to expose the CAM.

Sterilized filter paper disks were impregnated with: VEGF, basic FGF, Erucamide (loaded into 100µm microparticles, was mixed with collagen and sandwiched between two grids) or vehicle (PBS) and applied to the CAM surface.

The window was sealed with clear tape and the eggs were incubated for another 48 hours. After this period, embryos were perfused with DiI to label the vasculature and the onplants were imaged using a confocal microscope. The percentage of vascularization was calculated (by assessing and comparing the number of vascular branching points) and plotted.

P. Experiments assessing Retinal Oxidative Metabolism

For assessing retinal oxidative metabolism we used a Seahorse® Flux analyzer

P.1. Retinal Oxygen Consumption Rate (OCR) Determination

Whole retinas were isolated from OIR P14 mice 48 h after inosine or PBS control injection. Whole retinas were dissected, placed in assay media (DMEM, D5030 Sigma, supplemented with 12 mM glucose (Sigma), 2 mM pyruvate (Gibco), 10 mM HEPES (Gibco) and 2 mM glutamine (Gibco), pH 7.4). Biopsy punches (1 mm) were collected from the “central” region adjacent to the optic nerve, or from the “peripheral” region near the retinal edge. Oxygen consumption rates were determined using a Seahorse XFe96 Flux Analyzer© (Seahorse Biosciences, Massachusetts USA). The highest and lowest OCR measurements from the final 4

- 6 readings from the basal and drug treatments were removed and the remaining OCR readings were averaged. All central punches or peripheral punches from each retina were averaged to yield n = 1 per mouse retina. Basal oxygen consumption rates (OCR) were calculated by taking the initial OCR and subtracting the non-mitochondrial OCR ("RAA rate"; determined in the presence of 2 mM Rotenone (Sigma) and 2 mM Antimycin A (Sigma). Maximal OCR was calculated by subtracting the non-mitochondrial OCR from the OCR in the presence of 0.75 uM FCCP (Carbonyl cyanide-*4*-(trifluoromethoxy)phenylhydrazone, Sigma). The percentage of mitochondrial uncoupling was determined by using the OCR in the presence of 2 mM oligomycin (Sigma) minus the non-mitochondrial (RAA rate) divided by the basal OCR times 100%. Percentage coupling was 100% minus the percentage uncoupled OCR.

Basal OCR = initial rate – RAA rate

Maximal OCR = FCCP rate – RAA rate

Percentage coupling = [(Basal OCR – (oligomycin rate – RAA rate)/basal OCR]*100%

Q. Ocular *In vivo* Imaging

For the following procedures, mice were anesthetized by intraperitoneal injection of 15 mg/kg ketamine and 7 mg/kg xylazine, and their pupils dilated with phenylephrine hydrochloride (Ophthalmic solution 2.5% Bausch & Lomb, NDC 24208-740-06) immediately before imaging.

Q.1. Micron III

Fundus images were taken using the *Micron III system (Phoenix Research Laboratories)* by covering the cornea with "artificial tears" gel, placing the mouse on a moving platform and approaching the micron camera until it came in contact with the eye. To obtain pictures of different retinal areas, the platform was rotated and swiveled until the area of interest could be identified and focused.

Q.2. Spectral Domain-Optical Coherence Tomography (SD-OCT)

Morphological evaluation of retinal layers in vivo was performed with *Bioptigen* (an SD-OCT, Envisu instrument) by placing the mouse on a platform similar to the one described previously. Averaged SD-OCT scans were then exported to Photoshop CS6 (Adobe Systems Inc.) to perform quantitative analyses. Using the PS CS6 built-in ruler, manual segmentation was performed to accurately measure retinal layer thickness (ganglion cell layer (GCL)/IPL, INL). Differences in retinal layer thickness between experimental groups and controls were plotted in ± 15mm increments (up to ± 60mm), from the optic nerve head.

To perform indocyanine green (IG) angiography, IG was injected intraperitoneally (50 ug/g of body weight) at the time of anesthesia (15 mg/kg of ketamine and 7mg/kg of xylazine) and sequential retinal fundus pictures were recorded using the Spectralis Heidelberg Retinal Angiograph (Heidelberg Engineering).

Q.3. Evaluation of Visual Acuity

Visual acuity was assessed in mice based on their optokinetic responses with the OptoMotry system (Cerebral Mechanics Inc.). This device, which consists of an elevated platform (where the animal stands) surrounded by a virtual rotating cylinder with a striped pattern (vertical black and white stripes), measures visuomotor behavior in light conditions by assessing the number of smooth pursuits of the head elicited by the rotating stimulus. The mouse's visual acuity is calculated in accordance to the number of effective pursuit movements of the head (i.e., a tracking movement concordant with the velocity and direction of the stimulus) produced by the rotating stimulus, which are detected by the software.

Q.4. Ganzfeld Electroretinography (ERG)

Mice were dark-adapted overnight before the experiments, and anesthetized under a dim red light by intraperitoneal injection of 15mg/kg ketamine and 7 mg/kg xylazine the morning after. Silver needle electrodes served as a reference

(forehead) and ground (tail). Full-field ERGs were recorded from the corneal surface of each eye after pupil dilation (with 2.5% phenylephrine and 1% tropicamide) with active contact lens electrodes (Mayo, Inazawa, Japan). A computerized system with an electronically controlled Ganzfeld dome was used (Espion E2 with Colordome; Diagnosys). In dark-adapted conditions (scotopic), rod and mixed cone/rod responses to a series of white flashes of increasing intensities (1×10^{-5} to 50 cd·s/m^2) were recorded. In light-adapted conditions (photopic), with a 30 cd/m^2 background, cone responses to 1-Hz (0.63 to 20 cd·s/m^2) and 30-Hz (3.98, 10, and 20 cd·s/m^2) flicker stimuli were recorded. All ERG responses were filtered at 0.3-500 Hz, and signal averaging was applied.

R. Mass spectrometry-based Experiments

R.1. Sample Extraction for Mass Spectrometry-based Metabolomics

Acetone (400 □l) was added to 1.5 ml glass high recovery vials (Agilent Technologies, Santa Clara, CA, USA) containing 100 □l of human vitreous or blood and these were vortexed for 30 s. The samples were then placed in liquid nitrogen for 1 min, thawed for 5 min and sonicated for 15 min. This cycle was repeated 2 more times before the samples were stored overnight at -20ºC. After storage, the samples were centrifuged for 15 min at 13,000 rpm at 4ºC in 1.5 ml microcentrifuge tubes. The supernatant was transferred to 1.5 ml glass vials and stored at -20ºC until later use. The pellet was resuspended in 400 □l methanol/water (80:20 v/v), vortexed for 30 s, sonicated for 15 min and the supernatant pooled with the supernatants previously collected. The samples were stored at -20ºC for 1 h, centrifuged for 15 min at 13,000 rpm, 4ºC, and the supernatants dried in a speedvac. All samples were resuspended in 100 □l acetonitrile:methanol: isopropanol (40:40:10), sonicated for 20 min, centrifuged for 15 min at 13,000 rpm, 4ºC, and transferred to autosampler vials for storage at -80ºC until use.

For the analysis of the mouse model, whole eyes were taken (two per sample) and homogenized in 400 □l methanol/water (80:20 v/v) with 1 mm glass beads (Biospec, Bartlesville, OK, USA) in 1.5 ml glass vials. A minilys homogenizer (Bertin Technologies, Montigny le bretonneux, France) was used for 30 s at 3000 rpm. The samples were sonicated for 15 min and stored overnight at -20ºC. The samples were centrifuged at 13,000 rpm for 15 min at 4ºC. The supernatant was transferred to 1.5 ml glass vials and stored at -20ºC until later use. The pellet was resuspended in 600 □l acetone and homogenized again for 10s, and stored at -20ºC overnight. The samples were centrifuged at 13,000 rpm for 15 min at 4ºC and the supernatant pooled with previously retained supernatant. The samples were dried down in a speedvac and resuspended in 80 □l acetonitrile/water (50/50 v/v), sonicated for 5 min, centrifuged for 15 min at 13,000 rpm, 4ºC, and transferred to autosampler vials for storage at -80ºC until use. To note, two different resuspension solvent mixtures were used for the different eye tissues to allow for optimal recovery of both hydrophobic and hydrophilic metabolites.

R.2. Global Metabolomic Analysis

Analyses were performed using a high performance liquid chromatography (HPLC) system (1200 series, Agilent Technologies) coupled to a 6538 UHD quadrupole time-of-flight (Q-TOF) mass spectrometer (Agilent Technologies). Samples were injected (8 □l) onto either a Zorbax C18, 5 µm, 150 mm × 0.5 mm I.D. column (Agilent Technologies) for reversed phase liquid chromatography (RPLC) analysis, or a Luna Aminopropyl, 3 µm, 150 mm × 1.0 mm I.D. column (Phenomenex) for hydrophilic interaction liquid chromatography (HILIC) analysis. The standard mobile phase for RPLC was A = 0.1% formic acid in water and B = 0.1% formic acid in acetonitrile in electrospray ionization (ESI) positive mode. For HILIC the mobile phase was A = 20 mM ammonium acetate and 20 mM ammonium hydroxide in 95% water and B = 95% acetonitrile in ESI negative mode. The linear gradient elution from 100 % B (0–5 min) to 100 % A (50–55min) was applied in HILIC at a flow rate of 50 µL/min and from 100 % A (0–5 min) to

100% B (50–55min) in RPLC at a flow rate of 20 µL/min. A 10 min post-run was applied for HILIC, to insure column re-equilibration and maintain reproducibility.
ESI source conditions were set as followings: gas temperature 325 °C, drying gas 5 L/min, nebulizer 15 psi, fragmentor 120 V, skimmer 65 V, and capillary voltage 4000 V or −4000V in ESI positive or ESI negative modes, respectively. The instrument was set to acquire over the *m/z* range 60–1000, with the MS acquisition rate of 2.4 spectra/s. For the MS/MS of selected precursors the default isolation width was set as medium (4 Da), with a MS acquisition rate at 2.63 spectra/s and MS/MS acquisition at 2.63 spectra/s. The collision energy was fixed at 20 eV.
LC/MS data were processed using XCMS Online [148]. Unpaired parametric tests were carried out. Features were listed in a feature list table and as an interactive cloud plot, containing their integrated intensities (extracted ion chromatographic peak areas) observed fold changes across the two sample groups, and *p*-values for each sample [149]. The default XCMS parameter set for HPLC-UHD-QTOFMS was used with tolerance for database search set to 30 ppm. Integration of METLIN to XCMS Online allowed for putative identification of metabolites. Identifications were then made by comparing retention times and tandem MS fragmentation patterns to the sample and a standard compound (purchased from Sigma Aldrich, St Louis, MO). **Tandem MS experiments** were carried out with the collision energy set to 20 eV and caused the fragmentation of the metabolites into a number of fragments specific for the metabolite. This fragmentation pattern combined with the retention time comparison to a standard allows for accurate identification. The full datasets are available as public shares on XCMS Online.
Metabolite identified as dysregulated through global metabolomics are considered for targeted studies if they meet the following criteria: fold change over or = to 2; p value below 0.01 and minimum abundance (MS intensity) of 10.000.

R.3. Targeted Metabolomic Analysis

Samples (8 □L) were injected onto a Luna Aminopropyl column or Zorbax C18 using the same LC conditions as described for the global analysis. Selected reaction monitoring triple quadrupole mass spectrometry (Agilent 6410 QqQ-MS)

were used with quantifier and qualifier transitions for each metabolite as seen in **Table 6**. ESI source conditions were set as followings: gas temperature 325 °C, drying gas 5 L/min, nebulizer 15 psi, fragmentor 120 V, skimmer 65 V, and capillary voltage 4000 V or −4000V in ESI positive or ESI negative modes, respectively. The instrument was set to acquire over the *m/z* range 60–1000, with the MS acquisition rate of 1.67 spectra/s. For the MS/MS of selected precursors the default isolation width was set as medium (4 Da), with a MS acquisition rate at 1.67 spectra/s and MS/MS acquisition at 1.67 spectra/s. The collision energy was fixed at 20 eV.

Table 6 - List of metabolites targeted by multiple reaction monitoring

Standard Compound	ESI Mode	Precursor Ion	Quantifier Ion	Fragmentor Voltage (V)	Collision Energy (V)	Qualifier Ion	Fragmentor Voltage (V)	Collision Energy (V)
Oleoylcarnitine	Positive	426.4	85	137	27	57	137	63
Myristoylcarnitine	Positive	372.3	85	137	27	57	137	47
Decanoylcarnitine	Positive	316.2	85	14	19	57	14	47
Octanoylcarnitine	Positive	288.2	85	17	19	57	17	39
Hexanoylcarnitine	Positive	260.2	85	137	43	60	137	15
Propionylcarnitine	Positive	218.1	85	131	15	158.9	131	7
Acetylcarnitine	Positive	204.1	85	131	15	43	131	47
Acetyl-CoA	Positive	810	303	135	28			
Adenosine	Positive	268.1	136	131	15	118.9	131	47
Citrulline	Positive	176.1	158.9	98	7	70	98	23
Methionine	Positive	150	104	77	7	56.1	77	31
Lysine	Positive	147	130.1	77	7	84.1	77	15
Proline	Positive	116	70.1	86	15	43.1	86	43
ATP	Negative	506	158.9	156	30	79	156	75
PRPP	Negative	388.9	291	95	6	176.9	95	14
IMP	Negative	347	135.1	109	26	92.1	109	54
AMP	Negative	346	134	127	34	79	127	70
Inosine	Negative	267	135	129	17	108	129	37
Ribose-5-phosphate	Negative	229	139	89	6	97	89	6
Pantothenate	Negative	218	146.1	61	10	88	61	8
Citrate	Negative	191	111	77	6	87	77	14
Arginine	Negative	173.1	156.1	61	4	131.1	61	10
Cis-	Negat	173	129	76	4	85	76	8

Aconitate	ive							
Aminoadipate	Negative	160.1	142	70	8	116	70	10
Allantoin	Negative	157	114	70	9	97	70	9
Xanthine	Negative	151	108	114	13	42.1	114	25
Glutamate	Negative	146	128.1	80	6	102	80	2
Glutamine	Negative	145.1	127.1	83	6	109.1	83	10
□-ketoglutarate	Negative	145	101	40	5	57	40	5
Hypoxanthine	Negative	135	92	111	13	65	111	29
Malate	Negative	133	115	50	10	71	50	10
Oxaloacetate	Negative	131	87	55	7			
Succinate	Negative	117	73	62	9			
Fumarate	Negative	115	71	60	5			
Lactate	Negative	89	43.2	55	12			
Pyruvate	Negative	87	43	55	3			

ESI; Electrospray Ionization

R.4. Global Isotope Metabolomic Analysis

^{15}N-labeled arginine (500 mM, L-arginine: HCL $^{15}N_4$, 98%) (Cambridge Isotopes Laboratories) in PBS and natural abundance arginine (500 mM, L-arginine >98%, A5006; Sigma Aldrich, St. Louis, MO) in PBS were injected in P17 eyes from the OIR model (n=5 per experimental group) or from age matched C57/bl6 mice raised in normoxia (NOX; n=3 per experimental group). Whole eyes were collected 10 min later for analysis. For controls, OIR (n=5) and NOX P17 (n=3) mice were injected with PBS only. The eye samples were prepared for global metabolic analysis as stated above. The data was processed using X^{13}CMS as previously described [150]. Parameters were as follows: isotopeMassDiff=0.99703, RTwindow=30, ppm=25, massOfLabeledAtom=14.003, noiseCutoff=8000, alpha=0.05. Isotopomers were identified using the isoMETLIN database [123].

The same approach was followed for analysis of OIR and NOX mice eyes intravitreally injected with ^{15}N-labelled inosine (500 mM, Inosine $^{15}N_4$, 95%+; Cambridge Isotope Laboratories), natural abundance inosine (500 mM; Sigma) and PBS but injections were performed at P12.

S. Statistical Analysis

Chapter IV-A.

Photoreceptors generate erucamide for maintenance of the retinal vasculature: LC−MS data from the retina extract were processed using the bioinformatics analysis software XCMS Online (https://xcmsonline.scripps.edu/). XCMS Online is an updated, web-based version of XCMS having the function of peak (feature) picking, alignment and retention time correction, differential profiling, and statistical analysis. XCMS Online allows users to predefine parameter settings for optimal feature detection. Results are viewed online in an interactive, customizable table showing statistics, chromatograms, with putative METLIN identities. All results and images are available for download. MS/MS spectra were manually processed by extracting ion chromatograms Qualitative Analysis of MassHunter Workstation (Agilent Technologies), pNLC and BPC extraction were performed using the MassHunter. Modified Thompson Tau tests were used to identify outliers. Students paired two-tailed t-tests were used to compare averages and calculate significance between experimental conditions. Data were plotted as boxplots using Excel, the boxes label the upper and lower 25% quartiles, the white line marks the median, and the capped lines mark maximum and minimum values in the samples. Scatter plots were prepared in Excel (Microsoft).

Neurovascular crosstalk between interneurons and capillaries is required for vision: Comparison between the average variables of the two different 2 experimental groups was performed using two-tailed Student's t-test. P-values <0.05 were considered statistically significant.

Chapter IV-B and IV-C

Statistical analysis of the metabolomic data was performed by XCMS (employing a two-sample Welch's t-test with unequal variances).

In vivo global isotope metabolomics implicates the arginase pathway in ischemic retinopathy*:* Mann Whitney test was used to compare non-diabetic control to PDR samples. Two-tailed unpaired or paired (depending on the experimental design) Student's t-tests were used to compare mean values between the two experimental groups (OIR mice and controls raised in normoxia) using Excel and Graphpad Prism. P-values <0.05 were considered statistically significant.

Inosine adjusts retinal metabolism in hypoxic conditions and protects against development of late-stage diabetic retinopathy*:* Pearson correlations were calculated to assess the relationships between the different clinical variables. Two-tailed Student's *t*-tests (paired or unpaired, depending on the experimental design) were used to analyze the OIR mouse data (inosine versus vehicle injections) and p-values <0.05 were considered statistically significant.

Chapter IV: Results

A. Retinal neurovascular crosstalk: A novel Role for Retinal Neurons

Rationale for conducting these studies

- Neurovascular units (NVUs) have been extensively studied and well characterized in the brain and their dysfunction has been implicated in pathological conditions such as Alzheimer's and Parkinson's disease[96,151].
- In the retina, however, knowledge regarding NVU functioning is scarce and, so far, the only reported NVUs are in the RGC layer[152]. This is surprising because the retina is one of the most metabolically demanding tissues due to its high neuronal activity (especially that of photoreceptors) and NVUs play a crucial role in regulating blood flow for functionally dynamic retinal neuronal networks.
- Based on the anatomical localization of amacrine and horizontal cells in the retina, with their axons and dendrites running parallel to the primary retinal vasculature, it is possible that additional NVUs exist at this level
- It is surprising that PRs are the most numerous and energy demanding cells in the retina and yet they appear to rely solely on the RPE to maintain their primary blood supply, the choriocapillaris.
- Attenuation of the vasculature is a common feature of many severe retinal neurodegenerative diseases and there is proof-of-concept evidence to suggest that stabilization of the vasculature can slow retinal degeneration[153]. This beneficial effect can potentially be a result of efficient repair of diseased NVUs, by stabilizing retinal neurovascular crosstalk.
- Gaining further knowledge on formation and functionality of retinal NVUs in physiological conditions, and on what induces their dysfunction in contexts of retinal disease may inform future therapies designed to halt neurodegeneration and prevent development of pathological neovascularization.

My contribution

My clinical background in ophthalmology along with my special interest in DR allowed me to work in tandem with Dr Westenskow and Dr Usui (the lead authors of these projects) to provide insights that helped correlate their findings in mice with those seen in human DR and similar retinopathies, and their potential for development of novel therapeutics.

Additionally, I performed immunohistochemistry, PCR and in vivo micron imaging for these projects along with experiments to explore the consequences of intravitreal angiogenin injections on development of retinal pathology (due to space constraints and a choice to focus on the choroid in the manuscript, this data was not included but is presented in appendix A); I also analyzed, interpreted and discussed results with the lead authors of these projects and critically read and reviewed the manuscripts.

Furthermore, I contributed and was a co-author in posters and presentations regarding the findings described in this chapter for the annual meetings of 'The Association for Vision Research and Ophthalmology".

I gained increasing interest in retinal NVUs by working on these projects under the guidance of their brilliant lead researchers, Dr Peter Westenskow and Dr Yoshihiko Usui, Through them I learned basic concepts regarding composition and functionality of retinal NVUs, and explored their role in animal models of retinal neurodegeneration and pathological neovascularization. This knowledge was paramount for developing my own projects, as it broadened my perspective on DR and reshaped my own concept of the disease. There is strong evidence to suggest that DR results from disrupted cellular interactions within the NVU potentially generated by a state of metabolic insufficiency in the diabetic retina.

A.1. Photoreceptors generate Erucamide for maintenance of the retinal vasculature

Background and significance

The activities of neurons are dynamic and energetically expensive, thus requiring flexible and effective blood supplies. Neurons, glia, endothelial cells, and other cell-types are known to function within neurovascular units to regulate local blood flow. Unraveling of neurovascular units in the central nervous system is associated with a host of diseases including stroke, Parkinson's disease, Alzheimer's disease, amyotrophic lateral sclerosis, cerebral palsy, migraines, and mood disorders[151,154]. Therapeutic strategies to reestablish neurovascular units through delivery of proangiogenic factors (VEGF) are being actively explored[151,155].

The retina is one of the most metabolically demanding tissues in the human body, and vascular attenuation is characteristic of multiple retinal degenerations. The most energetically expensive cells in the retina are photoreceptors, however vascular repair strategies for photoreceptor maintenance in the face of metabolic stress have not been actively explored. Retinal vasculo- and neurodegenerative diseases, such as diabetic retinopathy (DR) and age related macular degeneration (AMD) are generally treated after the diseases have advanced to late stages, and treatments are either destructive (laser photocoagulation) or involve targeting vascular endothelial growth factor (VEGF) or its receptors to prevent or slow neovascularization.

Vascular deficits and neurodegeneration are associated with vision loss. Recent studies suggest that attenuation of the retinal vasculature is a shared feature of the most commonly occurring retinal diseases and that the severity of the vascular impairments are correlated with the degree of vision loss[156-166]. Diminished metabolic supply induces hypoxia in the other cellular components of the neurovascular units; this can promote pathological angiogenesis and progression of retinal diseases to their most severe forms (neovascular AMD and proliferative

DR)[163,164]. Therefore, vasculotrophic approaches to normalize retinal neurovascular units may be a very useful therapeutic approach for treating a host of retinal degenerations.

In order to effectively exploit vasculotrophic-based therapies, we need a better understanding of how neurovascular units are constructed and maintained, and what metabolic derangements can lead to their disruptions. Metabolism in the retina is unique based on the following properties: (1) the retina is populated predominately by some of the most metabolically demanding cells in the human body, the photoreceptors; (2) there is very little evidence that photoreceptors function in neurovascular units, but rather that they rely strictly on neighboring retinal pigment epithelium (RPE) cells for metabolic sensing and VEGF-mediated vascular maintenance[167,168]; and (3) even the resting state of the retina is extremely energetically demanding.

To meet these unique needs the vascular networks in the retina are architecturally optimized in species-specific manners. In humans and mice, the retina is nourished through a 10:1 ratio of extra- and intraretinal blood flow[169]. The extraretinal choriocapillaris is an impressive fenestrated vascular bed with perfusion rates that are as high as anywhere in the body[170]. RPE cells form a barrier between the choriocapillaris and photoreceptors in the outer nuclear layer of the retina. Highly efficient neuronal circuits connect primary photoreceptors with several classes of interneurons in the inner nuclear layer[171]. Three interconnected intraretinal vascular plexus layers support these circuits.

Based on the extreme metabolic demands of photoreceptors,[172] and the exquisite sensitivity of the choriocapillaris to changes in RPE-mediated vascular support,[167,168] it is surprising that photoreceptors have not adapted to directly regulate local blood flow like other highly metabolically demanding neurons in the retina and central nervous system.[40,154,173,174]

The focus of this study is to identify novel factors that could correct metabolic disorders of neurovascular units and thereby promote neurotrophism in the retina. If we possessed a deeper understanding of the metabolic “fingerprint” of retinal degeneration, we might be able to develop rational and effective therapies to prevent the metabolic derangements that promote photoreceptor atrophy.

To accomplish this we employed high-resolution global mass spectrometry-based metabolomics to catalog the metabolites dysregulated during retinal degeneration. Dysregulated features were identified using our data processing technology (XCMS)[175] combined with an expansive database that we developed (METLIN).[176] One family of endogenous signaling molecules, the fatty acid amides,[177-179] emerged as one of the most severely dysregulated class of metabolites in degenerating retinas.

Results

Ocular Erucamide levels are lower in rodent models of retinal degeneration and enhancing them induces neuroprotective effects

Work conducted over the last twenty years has provided compelling evidence that fatty acid amides serve as a new class of endogenous signaling molecules[178]. Signaling fatty acid amides may be grouped into two classes, the fatty acid ethanolamides, of which anandamide (C22:4, n-6; $C_{24}H_{41}NO_2$) is the prototypical member, and the fatty acid primary amides. The endogenous fatty acid primary amides[180] emerged as candidate signaling molecules with the discovery that oleamide (18:1, n-9; $C_{18}H_{35}NO$), which exerts a fundamental role in regulating sleep[177,179].

Data from our metabolomic analyses revealed that erucamide (22:1, n-9; $C_{22}H_{43}NO$), a fatty acid amide whose functions are not completely understood,[181-183] was one of the most abundant metabolites in wild-type rat eyes, and dramatically attenuated in a rat model of photoreceptor atrophy (**Figure 11A&B**). Erucamide availability also correlated with the degree of retinal degeneration in several other rodent models of photoreceptor loss (**Figure 11C** and **Figure 12C**; also see **Table 7**), suggesting it might be important for photoreceptor maintenance.

To determine if replacing lost erucamide can slow or prevent retinal degeneration, we injected 250ng (referred to throughout as a “neurotrophic dose”) in the subretinal space of dystrophic mice (RD10) at postnatal day 14 (P14; stage concurrent with the onset of retinal degeneration). The delivery of erucamide in the eye is not trivial due to its hydrophobic properties. To circumvent aqueous lipid

insolubility issues and to potentially prolong its delivery, we used inert silicon-based microparticles with nanoscale mesopores (nominal pore size, 20nm) as delivery agents.[184] A significant increase in the number of surviving rows of photoreceptors was observed at P32 (based on recoverin labeling of cryosectioned eyes) in an eye subretinally injected with erucamide-loaded microparticles compared with the contralateral uninjected control eye (12.4±2.1 vs 1.8±0.7 ($p<0.001$); **Figure 11D**). Furthermore, erucamide abrogated the most significant photoreceptor atrophy of RD10 mice, which occurs between P18 and P25 stages (**Figure 11E**; erucamide vs. vehicle $p=9.57e^{-7}$, erucamide vs. uninjected $p=3.57e^{-7}$).

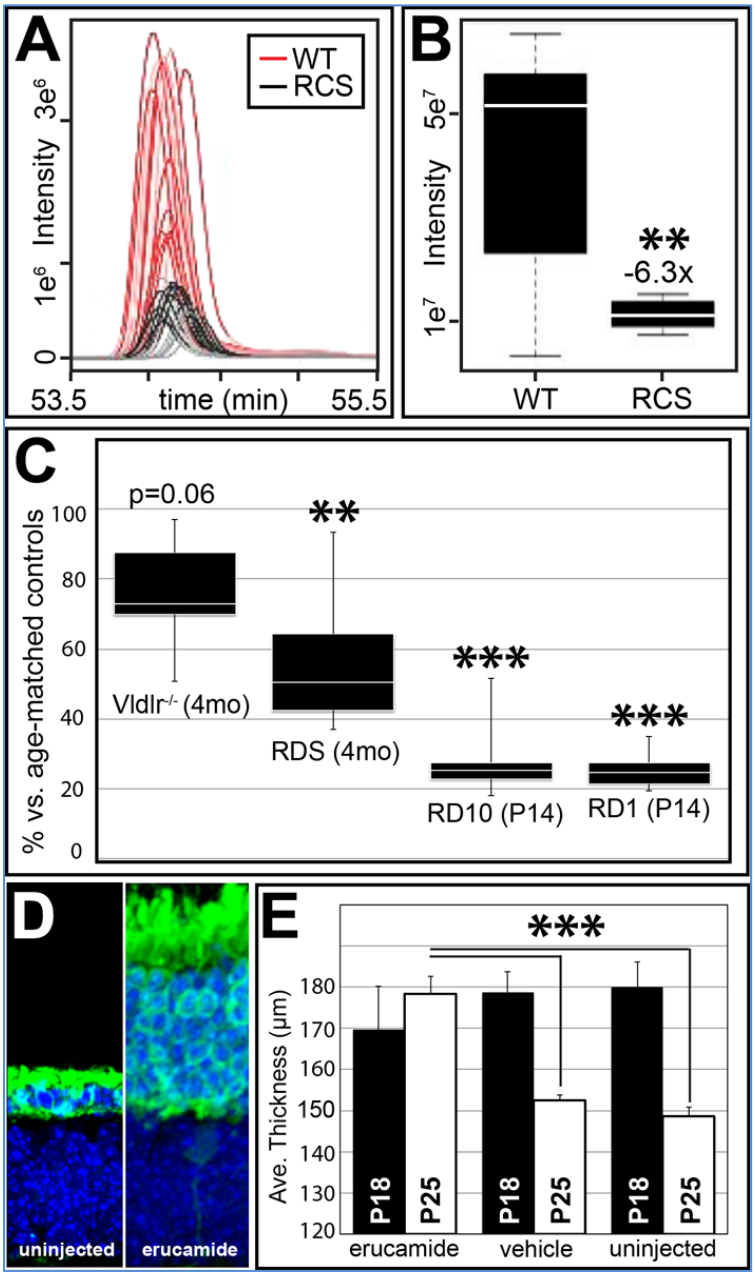

Figure 11 - Erucamide is neurotrophic.(A&B) Erucamide is highly dysregulated in one-year-old RCS eyes (n=10; p=0.002). (C). Erucamide levels are attenuated in multiple types of retinal degeneration (See SI Table 1 for a description of the transgenic lines). Vldlr-/- 76.0% ± 0.1 (p=0.06), RDS 58.1% ± 0.1 (p=0.01), RD10 28.4% ± 0.1 (p=0.0003), RD1 25.5% ± 0.02 (p=0.0001). For all n=6. (D) Retinas from a P32 RD10 mouse (injected at P14). Photoreceptors were immunolabeled green (recoverin). Effects of erucamide injections quantified in (E) (n=5; experiment repeated three times). Erucamide P18 vs erucamide P25, p=0.76; erucamide P25 vs. vehicle P25, p=9.57 x 10-7; erucamide P25 vs uninjected P25, p=3.57 x 10-7. Error bars=max and min values in B & C, SEM in E. *<0.05, **<0.01, ***<0.001

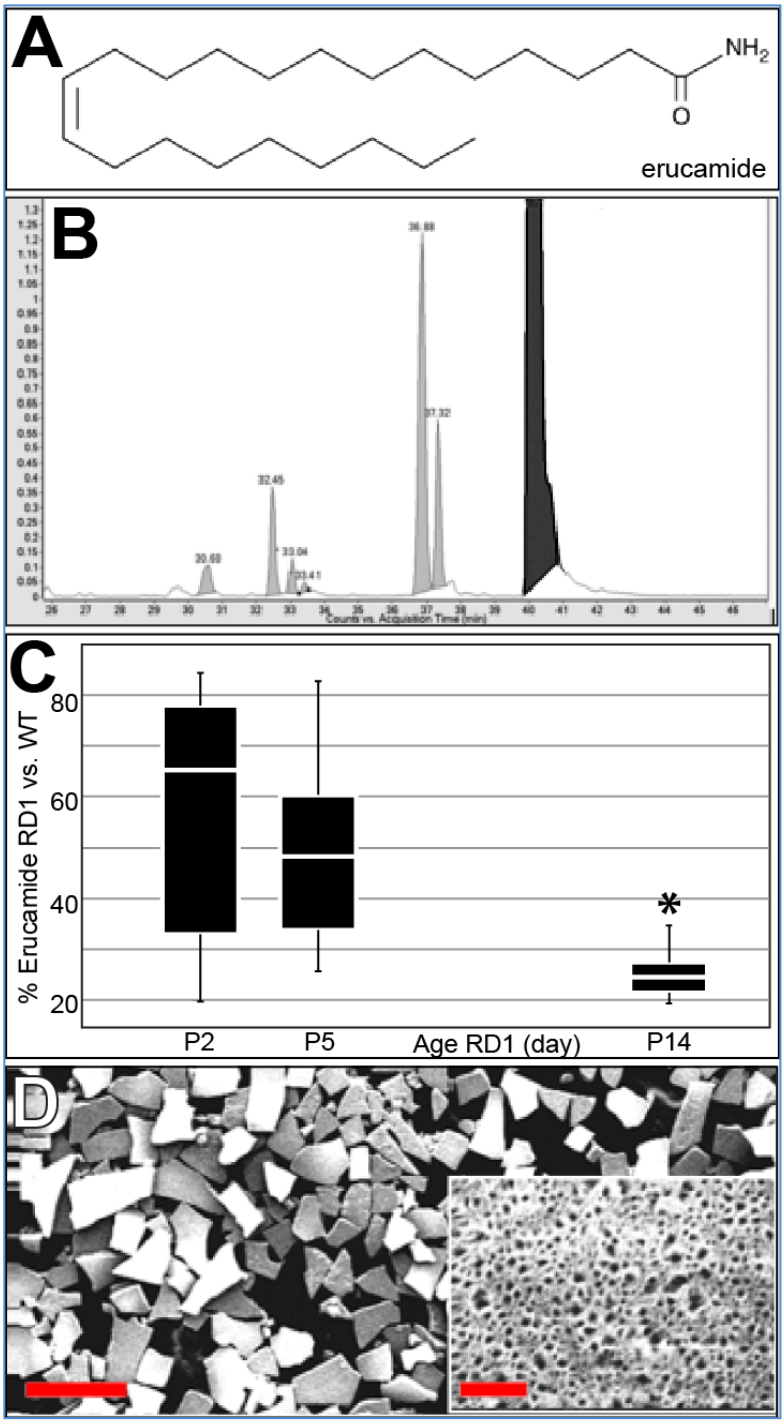

Figure 12 – Erucamide is abundant and dysregulated during retinal degeneration. (A) Chemical structure. (B) Erucamide and other metabolites detected using mass spectrometry (black peak is erucamide). (C) Erucamide availability decreases during retinal degeneration in RD1 mice (n=6; P2 vs P14 p=0.03). Error bars=max and min values. (D) Scanning electron micrograph of microparticles (high magnification image in inset). Scale bars =100μm and 100nm (inset). *<0.05

Table 7 – Rodent models used in this study

Transgenic rodent lines used in this study (alphabetic order)			
Line	**Photoreceptor Phenotype**	**Vascular phenotype**	**References**
Crx-Cre; Pam $^{fl/fl}$	Cone dysfunction	Attenuation	This study
Crx $^{RIP/+}$	Immature cone like PRs	Attenuation	This study and [129]
Nrl $^{-/-}$	Cone-only retina; (sparse & short outer segments). Incomplete degeneration	Excessive permeability, attenuation in late stages	[185] [186]
Pam $^{-/-}$	Not examined; embryonic lethal	Severe vascular defects and edema	[187]
RCS	Slow progressive degeneration	Attenuation	[162]
RD10 & RD1	Rapid degeneration	Attenuation	[153,188,189]
RDS	No rod outer segments, unusual cone outer segments	Attenuation	This study and [190]
Vldlr $^{-/-}$	Mild and variable cone loss	Pronounced vascular defects	[16]

PAM is synthesized in cone outer segments and its dysregulation closely correlates with loss of Erucamide

The enzyme responsible for the amidation step that converts N-erucyl-glycine to erucamide is unknown, but a strong candidate is peptidylglycine alpha-amidating monoxygenase (PAM).[191] Here, we show that enhanced levels of Erucamide, and other fatty acid amides, were generated in eyes injected with recombinant PAM (**Figure 13A&B**). PAM is expressed in developing and adult photoreceptor outer segments (**Figure 13C-G** and **Figure 14A**) of multiple species including human (**Figure 13H**), mouse (**Figure 13I**), rat (**Figure 13J**), and zebrafish (**Figure 13K**), suggesting that its function in the sensory retina may be evolutionarily conserved. PAM expression is also perturbed in mice with photoreceptor outer segment defects. In cone-dominant *Nrl$^{-/-}$* mice with short and sparse outer segments,[185,186] PAM is detected along the RPE/photoreceptor border and in rosettes in the degenerating outer nuclear layer (**Figure 13L**). In *Crx$^{RIP/+}$* mice that

lack outer segments[129], PAM is detected in a solid stripe in the short inner segments of photoreceptors (**Figure 13M**).

Similar to erucamide, PAM expression is also downregulated during retinal degeneration. In healthy human subjects PAM is robustly expressed in photoreceptor outer segments (**Figure 13N-O**; black arrows). In the retina from a 93-year-old patient with atrophic AMD, PAM expression is barely detectable in the atrophic area (**Figure 13P** and **Figure 14B&C**; asterisk). Using a rat model, we demonstrate that the loss of PAM during retinal degeneration is progressive. We detected seemingly normal levels of PAM in three-week-old RCS rats prior to retinal degeneration (**Figure 13Q**), but by seven weeks levels gradually drop and continue to fall over time (**Figure 13R-T**). The expression of PAM in the outer segments of multiple species, and dysregulation during retinal degeneration suggests it may be important for photoreceptor function and/or homeostasis.

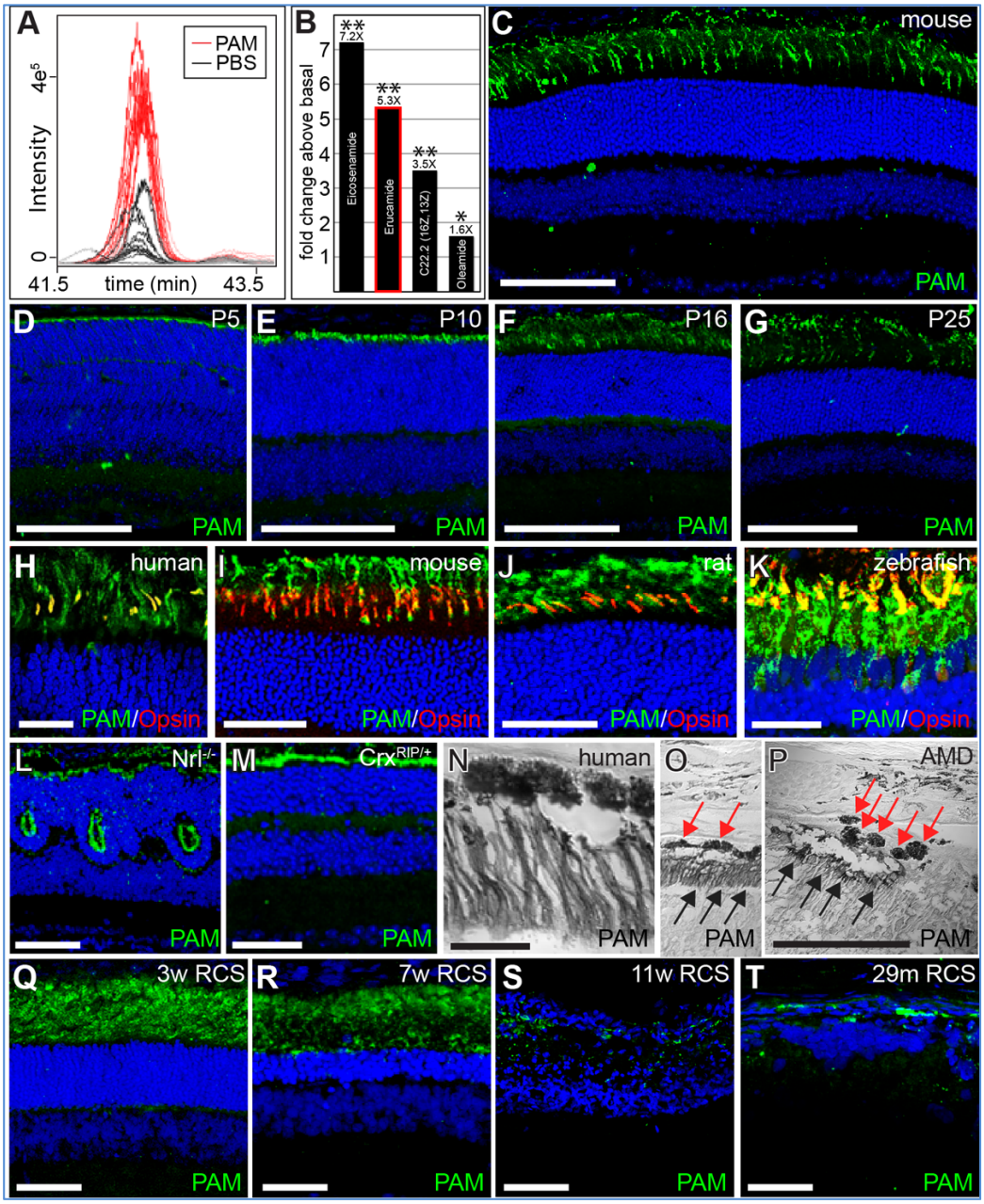

Figure 13 - PAM generates erucamide and is expressed in photoreceptors.(A&B). Potentiated erucamide levels in PAM-injected adult mouse retinas (n=10). Eicosenamide, p=1.8 x 10-8; erucamide, p=1.0 x 10-15; C22.2, p=1.2 x 10-8; Oleamide, p=0.02. (C) Whole retinal image of adult murine retina immunolabeled with PAM. (D-G). PAM is upregulated in immature murine outer segments of photoreceptor cells during postnatal development. (H-K). PAM co-localization with red/green opsin in multiple species (all adults). (L&M). PAM in mice with photoreceptor defects. (N) High magnification image of PAM in adult human photoreceptor outer segments (DAB stained/DIC overlay). PAM dysregulation in an AMD patient; O=unaffected periphery, P=AMD lesion. Black arrows=PAM, red arrows=RPE cells (see also SI Fig 2A&B). (Q-T) Progressive loss of PAM in RCS rats. Scale bars=100μm in A,D- G,H,I,M-P, 50μm in D-F, 25μm in G, 10μm in J. *<0.05, **<0.01

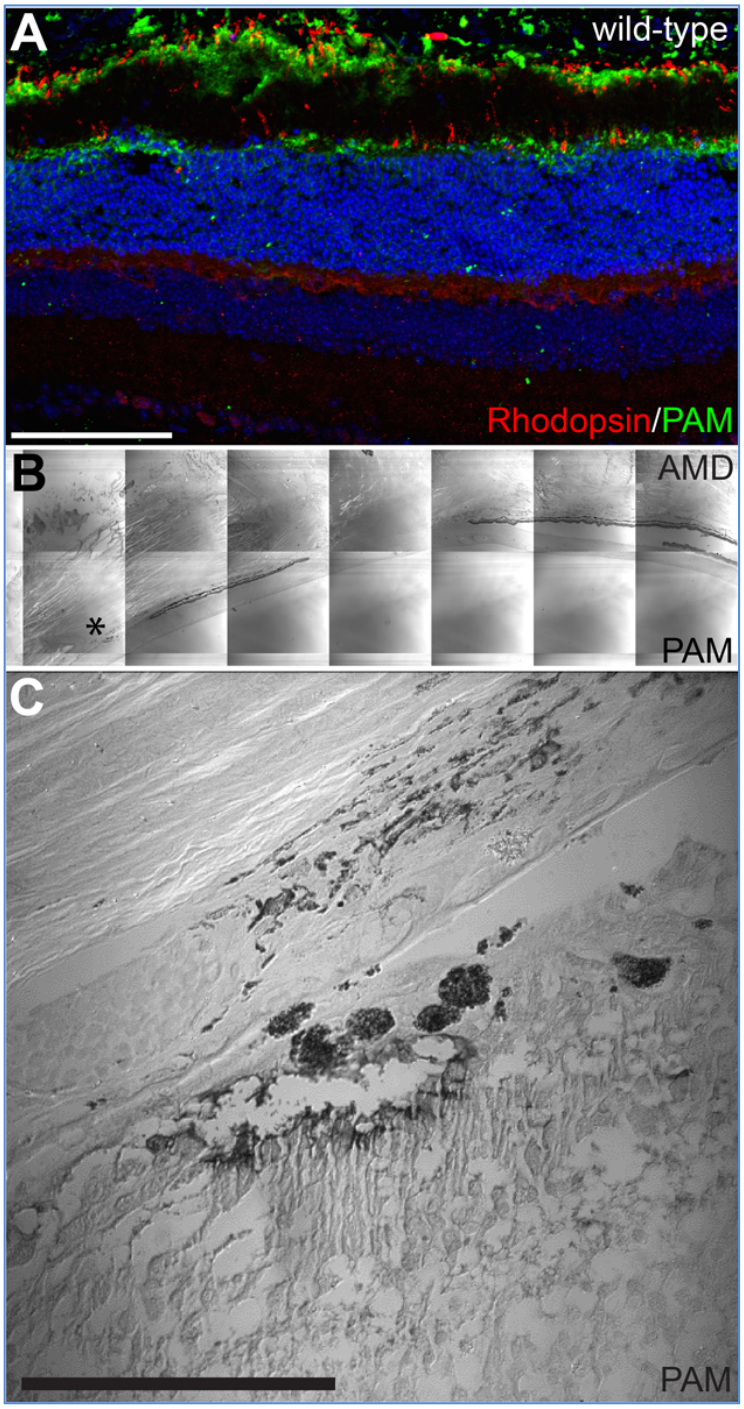

Figure 14 – PAM is expressed in rod outer segments and is dysregulated in human disease. (A) Adult murine retina co-stained with rhodopsin and PAM. (B&C). Toluidine blue stained section from an AMD patient eye. Asterisk marks the affected region. (C) Enlargement of the affected area. Scale bars=100μm.

PAM activity is essential for retinal vascular maintenance and cone photoreceptor health

To further explore the importance of PAM for retinal function, we generated a floxed *Pam* mouse line and crossed it with *Crx-Cre* for genetic ablation studies (**Figure 16A-C**). We measured visual acuity and observed significant deficits in two-month-old mutants compared with littermate controls (**Figure 15A**). We also used electroretinography to compare light responsiveness in the two mouse lines, and observed significant deficits in cone-driven pathways in two-month-old mutants (**Figure 15B; Figure 17A&B**). We also examined the integrity of the retinal vasculature using histology (**Figure 15C-F**), and observed severe attenuation in the choriocapillaris. Vascular attenuation was also observed in $Pam^{+/-}$, $Crx^{RIP/+}$, and RDS mice (**Figure 17D-I**), collectively demonstrating that PAM is critical for regulating angiogenesis in the retina, and its dysregulation induces severe functional defects.

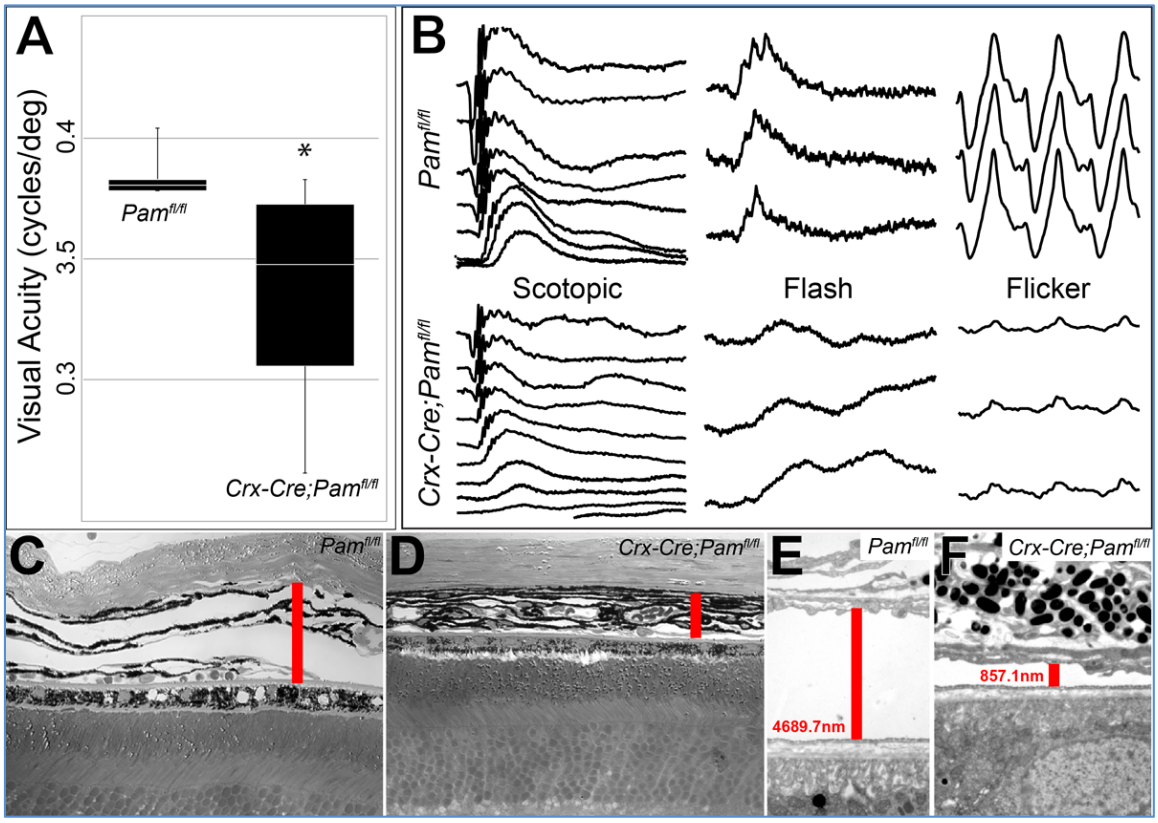

Figure 15 - Conditional loss of *Pam* in photoreceptor precursors induces photoreceptor and choriocapillaris defects. (A) Visual acuity measurements (n=6, p=0.04; error bars=max and min values; *<0.05). (B) Electroretinograms of rod (scotopic) and cone (photopic flash and flicker) light responses (n=6-10; quantification in Fig. 17). (C&D). Toluidine Blue stained retinas in plastic sections (Scale bars=50µm in C, 25µm in (D). (E&F) Electron micrographs with measurements of choriocapillaris thickness.

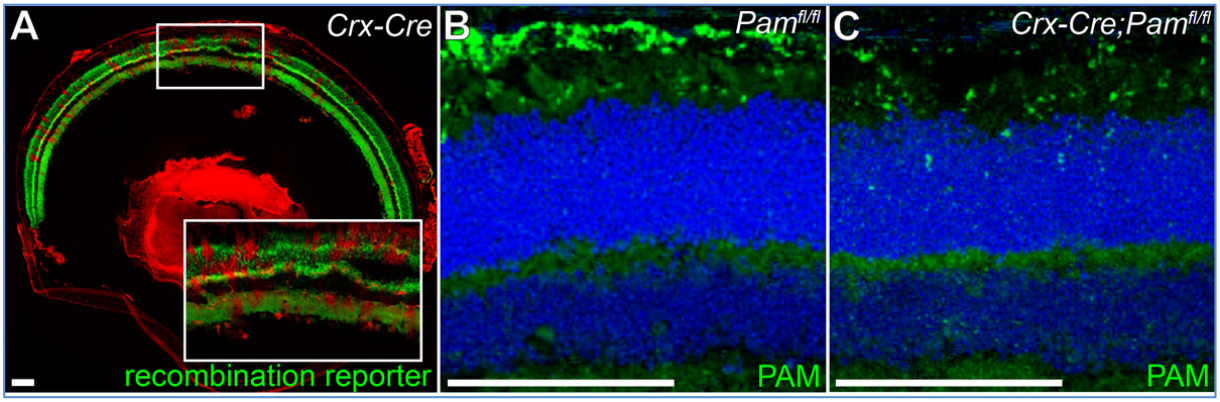

Figure 16 – PAM is deleted in photoreceptors using *Crx-Cre*. (A) *Crx-Cre;ROSAmT/mG* retina. ROSAmT/mG is a dual-color Cre reporter; cell membranes are red prior to Cre recombinase exposure, green fluorescence is activated in cells after Cre recombination. (B&C) IHC for PAM in *Crx-Cre;Pamfl/fl* and *Pamfl/fl* retinas. Scale bars=100µm.

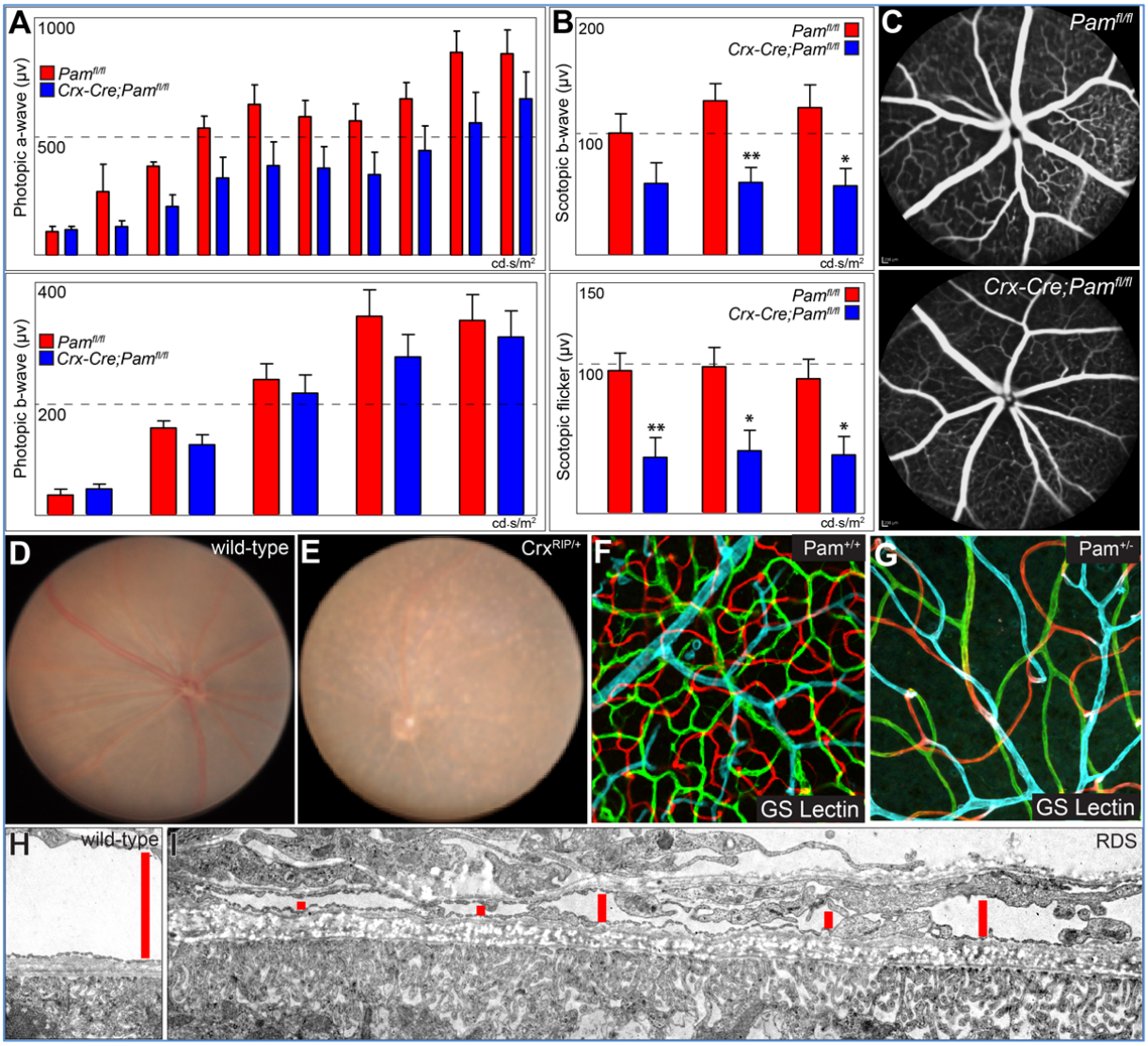

Figure 17 – Functional and vascular defects in *Pam* deficient mice. (A&B) Quantification of electroretinography experiments in two-month-old *Crx-Cre;Pamfl/fl* mutants. (C) Angiography of superficial plexus reveals no gross defects in two- month-old *Pam* mutants. (D&E) Attenuation of the retinal vasculature in *CrxRIP/+* mice (Pam is reduced 89.8%+0.3 according to RNAseq data). (F&G) Intraretinal vascular attenuation in six-month-old *Pam+/-* mutants. (superficial plexus=blue, intermediate plexus=green, deep plexus=red). (H&I) Choriocapillaris attenuation in wild-type and RDS mice. *<0.05, **<0.01.

PAM produces Erucamide and induces ocular neovascularization

Enhancing PAM activity also elicits vascular effects. Either transgenic overexpression of *Pam* in wild-type mice using *in vivo* electroporation or subretinal injections of recombinant PAM result in rapid neovascularization (**Figure 18A-C**). Since PAM can generate erucamide, we compared the effects of overexpressing PAM to those of injecting erucamide. Similar to PAM, subretinal injections of 2.5µg

of erucamide (referred to throughout as a “neovascular dose”) induce choroidal neovascularization three days post injection as evidenced by hemorrhages in fundus images (**Figure 18D**; long arrows), fibrosis (**Figure 18D**; arrowhead), indocyanine green pooling in angiograms (**Figure 18E**), deficits in the RPE/choroid layers using optical coherence tomography (OCT; **Figure 18F**) and histology **Figure 18G-I**). Erucamide also induces hyperangiogenesis of the intraretinal vasculature (**Figure 19**).

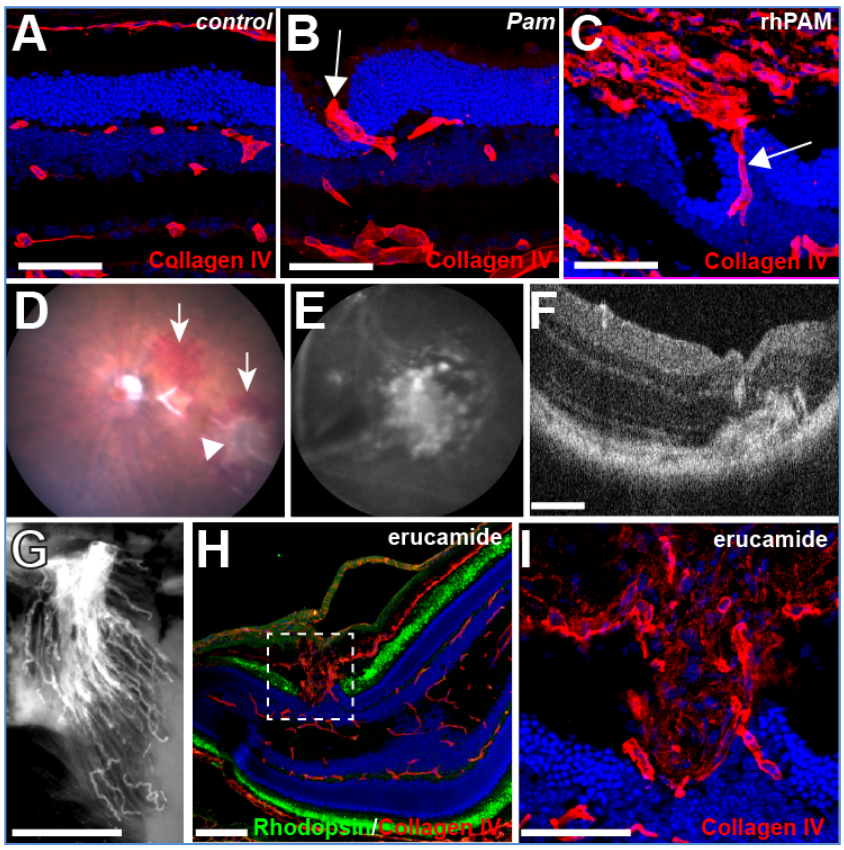

Figure 18 - Both PAM and erucamide potentiation induce profound neovascularization. (A&B) *Pam* or control constructs were electroporated *in vivo* (performed at P0, analyzed by immunolabeled blood vessels with Collagen IV at P24; n=10). (C) Vasculature after recombinant human PAM subretinal injections. (D-I) Effects of subretinal erucamide injections (three days post injection): (D) fundus images, (E) angiography (F) OCT (G), GS Lectin labeled RPE/choroid flat mounts (H, and high mag in I), immunohistochemistry. Scale bars=100μm.

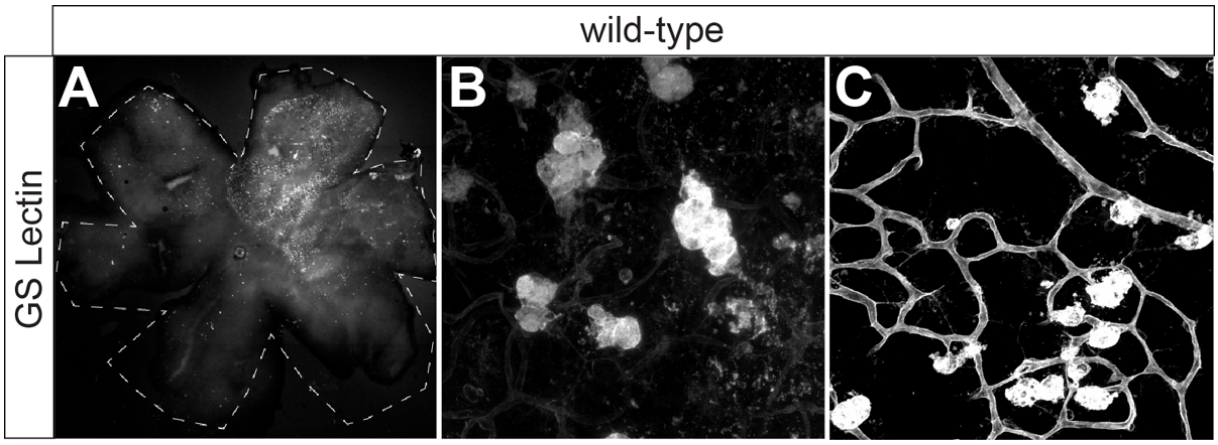

Figure 19 – Neovascularization from the intraretinal vasculature is observed 3 days post erucamide injection. (A) Retinal flat-mounts labeled with GS Lectin (white dots are angiomas) (B) High magnification of the GS Lectin-positive angiomas. (C) Microaneurysms, characteristic of proliferative diabetic retinopathy, in the superficial plexus of erucamide-injected animals.

High doses of erucamide exert potent proangiogenic effects in vitro and in vivo

Finally, we demonstrated that erucamide's angiogenic potential is higher than other pro-angiogenic factors, bFGF and VEGF, using chick chorioallantoic membrane (CAM) assays (**Figure 20A)**. Erucamide also significantly increased neovascularization in oxygen-induced retinopathy mice (**Figure 20B)**. To identify putative mediators of this potent angiogenic response, we performed gene profiling from retinas of mice injected with neovascular doses of erucamide. Of the 84 angiogenesis-related genes analyzed, only the gene, angiogenin, was upregulated (**Figure 20C**). In the retina, erucamide injections induced angiogenin upregulation in the processes of Mueller glia and astrocytes (**Figure 20D&E**). To evaluate the effects of angiogenin levels potentiation, subretinal injections of an angiogenin-overexpressing AAV virus that specifically transduces Mueller Glia and astrocytes[192], or subretinal injections of recombinant human protein were performed. Both techniques induced profound choroidal neovascularization three days post injection (**Figure 20F-I**).

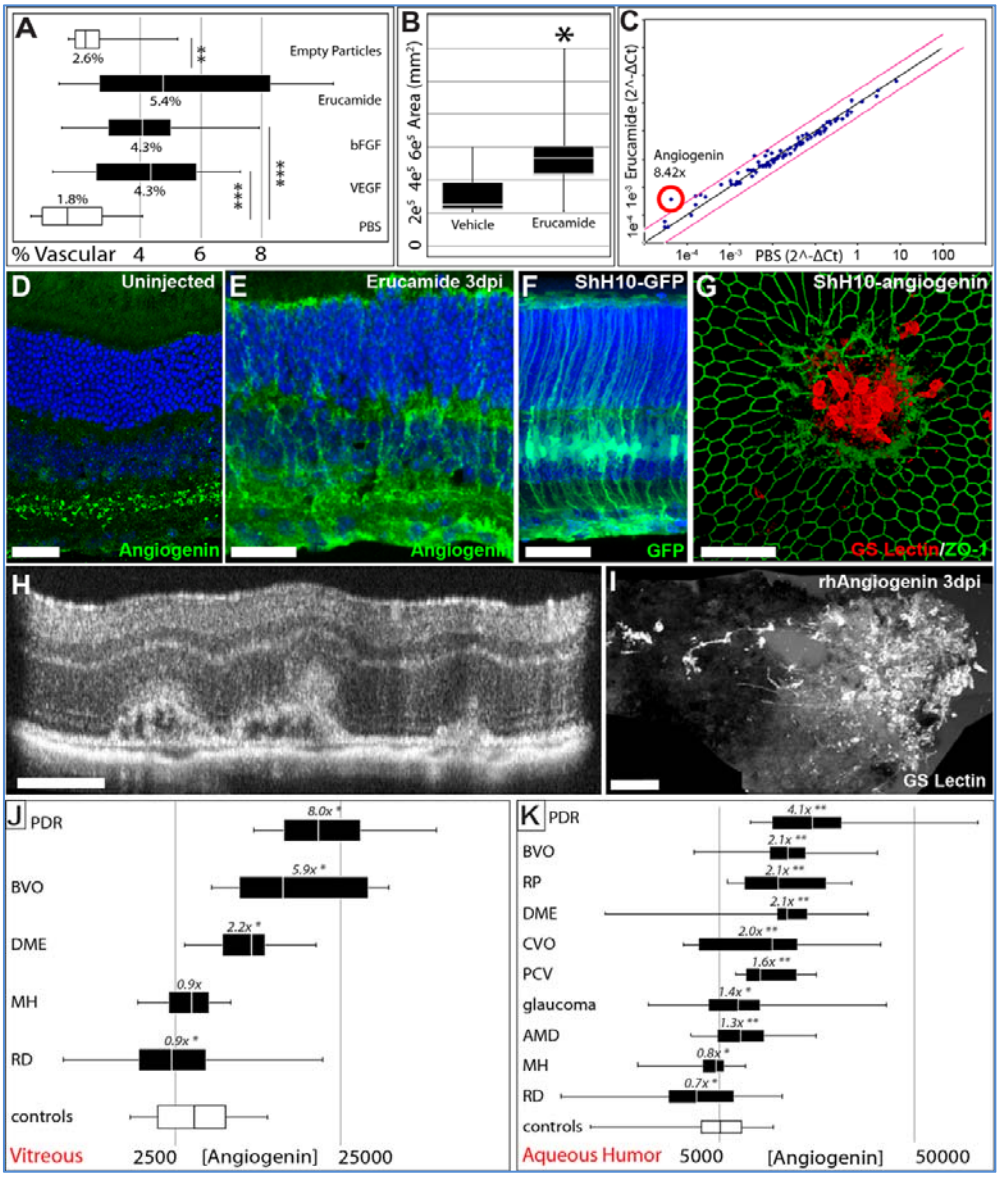

Figure 20 - Erucamide is potently pro-angiogenic and activates Angiogenin in Muller glia. (A) CAM assays with 5.0µg/µl erucamide (vehicle vs erucamide p=0.006; bFGF vs PBS p=0.0001; VEGF vs PBS p=0.00006; n=19-25) (B). Erucamide increases the area of neovascularization in OIR mice (1.9 fold; n=23; representative plot shown from three experiments). (C) PCR array for angiogenesis-related genes (erucamide vs vehicle injected retinas; p=0.07). (D&E) Immunolabeling for angiogenin in erucamide injected adult eyes. (F) ShH10-GFP viruses transduce Muller glia in P24 mice. (G) ShH10-angiogenin induces choroidal neovascularization in adult mice. ZO- 1 marks borders of RPE cells. (H&I) 1µg recombinant human angiogenin also induces choroidal neovascularization in adult mice. (H) OCT (I). RPE/choroid flat mount. (J&K) Multi-plex ELISAs from cytokine-profiling in human vitreous (J) and aqueous humor samples (K) Abbreviations: PDR=proliferative diabetic retinopathy, BVO=branch vein occlusion, DME=diabetic macular edema, MH=macular hole, RD=retinal detachment, CVO=central vein occlusion, PCV=polypoidal choroidal vasculopathy. Controls =cataracts or epiretinal membranes. See methods for more details. Error bars=max and min values. Scale bars=50µm *<0.05, **<0.01, ***<0.001

Erucamide's vasculo and neurotrophic effects may be mediated by Angiogenin

Angiogenin upregulation was detected in multiple mouse lines with retinal degeneration (**Figure 21**). Angiogenin was also significantly upregulated in the vitreous of human subjects with diabetic macular edema (DME), branch vein occlusions (BVO), and proliferative diabetic retinopathy (PDR; **Figure 20J**), and in human aqueous humor samples from patients with multiple retinal diseases of varying etiology, including AMD, glaucoma, polypoidal choroidal vasculopathy, central vein occlusion, DME, BVO, Retinitis Pigmentosa, and PDR (**Figure 20K**). Angiogenin exerts neurotrophic influences in both ALS and Parkinson's disease[193-196] and has been detected in human glial cells and in the choriocapillaris[193,195,197,198]. Since erucamide levels drop during retinal degeneration, photoreceptor-derived erucamide may be just one of several factors that can mediate angiogenin-based stress responses that counteract vascular or neuronal stress.

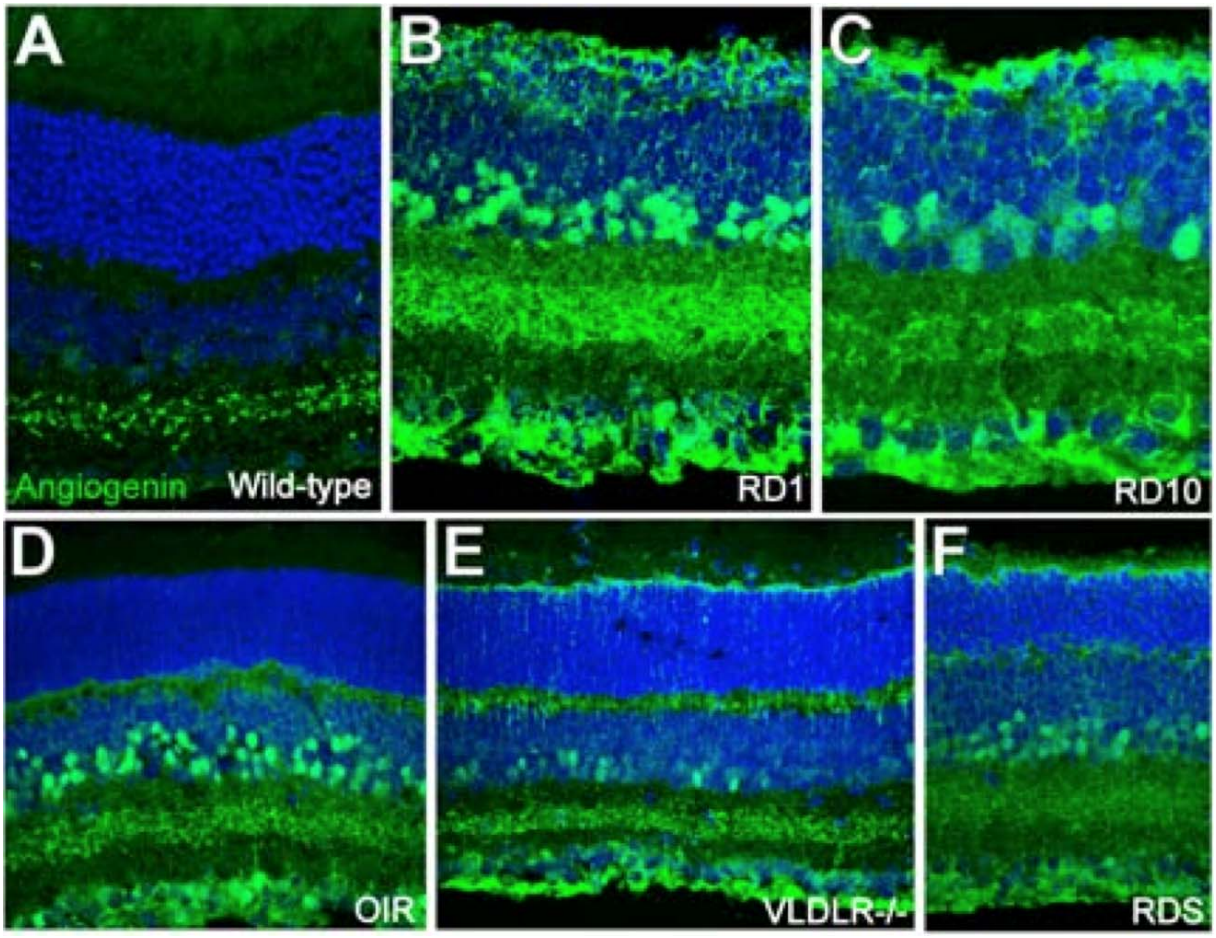

Figure 21 - Angiogenin expression in wild-type and diseased retinas. **A**. In wild

type adult mouse eyes, angiogenin is weakly expressed by cells in the inner nuclear layer. **B-F**. During retinal degeneration, angiogenin is strongly upregulated in processes of Mueller glia and astrocytes. Upregulation of angiogenin is also seen in nuclei of cells in the INL

Discussion

Our data suggest that photoreceptors, Mueller glia, and the choriocapillaris act as a unique neurovascular unit that spans the entire retina. Neuro-vasculo-glial crosstalk is critical in the central nervous system but specific factors that regulate this activity are not widely known. At the center of this unit is erucamide, a potently proangiogenic factor that is one of the most abundant metabolites in wild type eyes, and one of the most dysregulated during retinal degeneration. The expression of the enzyme that generates erucamide, PAM, in photoreceptors from multiple animal species suggests that its function there is evolutionarily conserved. Experimental reintroduction of erucamide significantly slows photoreceptor atrophy, and our data suggest that this may occur because PAM and erucamide exert potent vasculotrophic effects on the intraretinal vasculature and the choriocapillaris. In support of this concept, choriocapillaris thickness is reduced by as much as 50% in human subjects with atrophic AMD and Retinitis Pigmentosa in areas immediately adjacent to regions of photoreceptor loss[156-160]. Furthermore, conditional loss of *Pam* results in severe choriocapillaris attenuation and photoreceptor dysfunction in mice.

Finally, the action of erucamide is mediated, at least in part, through the vasculotrophic protein angiogenin that is detected in human choriocapillaris,[197] in murine Mueller glia, and in the vitreous of human subjects with various vascular and neurodegenerative disorders. Erucamide may function similarly in multiple organ systems since PAM is broadly expressed in the trans-Golgi network and in secretory granules of neural and endocrine tissues[199,200].

Collectively, these findings reveal a novel function of photoreceptors, generating erucamide to maintain the integrity of the choriocapillaris. The ability of neurons to function in neurovascular units to fine-tune local blood flow is becoming widely appreciated, and neurovascular coupling defects are characteristic of Parkinson's disease, Alzheimer's disease, amyotrophic lateral sclerosis, mood disorders,

cerebral palsy, and migraines.[151,154] Therapeutic strategies to repair diseased neurovascular units in the central nervous system to prevent disease progression may represent general and effective approaches, and are being actively explored[151,155]. Retinal diseases with vascular and neurodegenerative components such as DR and AMD are generally treated after the diseases have advanced to late stages, and treatments are either destructive (laser coagulation) or employ drugs targeting VEGF to prevent or slow neovascularization. Intervening early to prevent vascular attenuation and hypoxia by repairing diseased vasculature may be an effective alternative strategy for treating multiple retinal degenerations.

These collected observations provide valuable insight into neurovascular unit physiology, and may inform future therapeutic approaches for treating retinal diseases as well as other neurodegenerative diseases.

A.2. Neurovascular Crosstalk between Interneurons and Capillaries is required for Vision

Background and significance

Neurovascular units consist of varying combinations of neurons, glia, pericytes, and extracellular matrix that interact, and are intimately associated with, endothelial cells to regulate local blood supply. The importance of the neurovascular unit for maintaining local functionality and homeostasis in the CNS has recently received increased attention, since defects in neurovascular units are associated with a variety of CNS diseases, including stroke, Alzheimer's disease, Parkinson's disease, amyotrophic lateral sclerosis, cerebral palsy, migraines, and mood disorders[151,154]. Therefore, learning how neurovascular units are established and maintained may be crucial for understanding the basis of a host of neurodegenerative diseases and developing novel therapeutic strategies for treating them.

The retina is an excellent model system for studying neurovascular interactions in the CNS since formation of the retinal vasculature and neurons occurs in well characterized, consistent, and reproducible temporal and spatial patterns. In

addition, retinal neurovascular units can be directly visualized and assessed functionally using highly sensitive imaging modalities.[39,40] Neuronal and vascular networks in the sensory retina are organized in a highly stratified and functional architecture, although the full extent of their integration is not completely understood. Phototransduction, the process of generating electrical signals from captured photons, occurs in rod and cone photoreceptor cells in the outer retina. Bipolar cells in the inner nuclear layer (INL) transmit the visual signals from the photoreceptors to the retinal ganglion cells, which send the integrated signal to the visual cortex. The INL also contains laterally interconnecting amacrine and horizontal cells that localize at opposite margins of the INL and form homotypic and heterotypic connections within the outer and inner plexiform layers (OPL and IPL), respectively. Horizontal cells provide inhibitory feedback for cone-driven pathways, and amacrine cells have diverse physiologies and exhibit multifaceted connectivity throughout the IPL that allows them to pre-process and integrate visual signals and interpose temporal cues. In this study we demonstrate a novel function for these retinal interneurons: promoting photoreceptor homeostasis through maintenance of the vasculature.

The vascular networks in the retina are architecturally optimized, albeit in a species-specific manner, to sustain the extreme metabolic demands of retinal neurons, in particular, the photoreceptors. In primates and mice, the intraretinal vasculature consists of three interconnected parallel vascular plexus layers that run through the plexiform layers of the retina. In mice, the retinal vasculature forms as endothelial cells migrate from the optic nerve onto the retinal surface at birth and progress radially to form the superficial (or inner) plexus [39]. Around postnatal day 7 (P7), sprouting vessels descend and advance into the OPL where they establish the deep plexus. At P11-12 stages, sprouting vessels from the deep plexus ascend into the IPL and ramify to form the intermediate plexus. The proangiogenic stimuli that direct formation of the intermediate and deep (or outer) plexus layers are not completely understood, and are likely distinct[49]. It has been suggested that oxygen and nutrient insufficiencies, induced as retinal neurons are born and mature, activate hypoxic responses via von Hippel-Lindau (VHL)/Hypoxia-inducible factor (HIF) signaling pathways that drive the expression of pro-angiogenic factors including VEGF and EPO[201,202]. This concept is supported by two key pieces of evidence: (1) the conditional deletion of *Hif-1α* -

which is detectable at high levels in the developing retina, in virtually all cells of the murine peripheral retina - prevents formation of the intermediate plexus [49,53,201]; and (2) while VEGF is transiently expressed throughout the INL, intraocular injections of high doses of VEGF antagonists partially inhibit formation of the intraretinal vasculature[203,204]. While there is a clear role for VHL/HIF and VEGF in regulating intermediate plexus development, the cells in the INL that are responsible for regulating these factors have not been identified.

We observed extensive interactions between horizontal cells and capillaries of the deep plexus, and between amacrine cells with the intermediate vascular plexus in wild-type adult mice. Thus, both cell-types are ideally localized to serve as metabolic and oxygen sensors in the retina, to activate angiogenesis during development through VHL/HIF/VEGF signaling, and to provide structural and trophic support to the vasculature, and perhaps even to prevent pathological neurovascular remodeling. These functions may be critical, since destabilized vascular networks in the retina are associated with dramatic visual defects[161] There is growing evidence that blood vessels and proangiogenic mitogens contribute to the pathogenesis of multiple neurological diseases[54,151]. Therefore, it is important to understand the mechanisms of neurovascular cross talk and vascular maintenance in the retina.

In this study we utilized conditional gene deletion and cell ablation approaches to demonstrate in vivo that amacrine and horizontal cells can regulate local blood supply and thereby promote photoreceptor homeostasis. We demonstrate that the key source of VEGF-A in the INL to regulate intermediate plexus development likely comes from the amacrine cells, and gain- or loss-of function of VEGF in amacrine cells induces pronounced defects in visual function and rod- and cone-driven signaling. These observations may have broad applicability for neurovascular-unit physiology in the CNS and may also inform future therapies that target the neurovascular unit to treat not only blindness, but also a host of debilitating neurodegenerative and neurological diseases.

Results

Amacrine and horizontal cells form neurovascular units with capillaries in the intraretinal plexuses

The retinal neuronal and vascular networks are depicted in **Figure 22A; Figure 23**. P23 retinas were probed with specific markers for amacrine and horizontal cells (calbindin) and for endothelial cells (CD31) to identify putative neurovascular units. Immunohistochemistry analyses revealed that amacrine cell and horizontal cell dendrites appear to interact with CD31-positive intraretinal capillaries in the intermediate and deep plexuses in the IPL and OPL (**Figure 22B**).

To confirm the immunofluorescence findings, and since calbindin labels only a small percentage of amacrine cells, we utilized Cre/loxP transgenic-based approaches - with pancreas-specific transcription factor 1a-*Cre (Ptf1a-Cre*) mice - to genetically label amacrine and horizontal cells in the retina, and not bipolar cells or Müller glia (*Ptf1a-Cre R26*$^{tdTomato/+}$ and *Ptf1a-Cre R26*$^{GFP/+}$) (**Figure 22C**; **Figure 24A-E**) [138,205]. We combined genetic labeling and immunofluorescence techniques to confirm that Cre-recombination occurs in amacrine cells by probing P23 *Ptf1a-Cre R26*$^{tdTomato/+}$ retinas with amacrine cell–specific antibodies (**Figure 24B–D**). Then we performed immunohistochemistry on P23 *ptf1a-Cre;R26*$^{tdTomato/+}$ retinas with antibodies that recognize the intermediate form of neurofilament (NF-M), a marker for ganglion, amacrine, and horizontal cell axons [206], or Microtubule-associated protein 2 (MAP-2), a marker for neuronal dendrites. Using this approach, we were able to more clearly visualize the extent of colocalization of the amacrine and horizontal cell arbors, and the vasculature in the IPL (**Figure 22D-F** and **H**; **Figure 24D–F**) and in the OPL (**Figure 22D, G, and I; Figure 24D and F**). Based on the findings that amacrine and horizontal cells interact extensively with the intraretinal capillaries, we hypothesized that amacrine and horizontal cells form neurovascular units in the 2 plexiform layers.

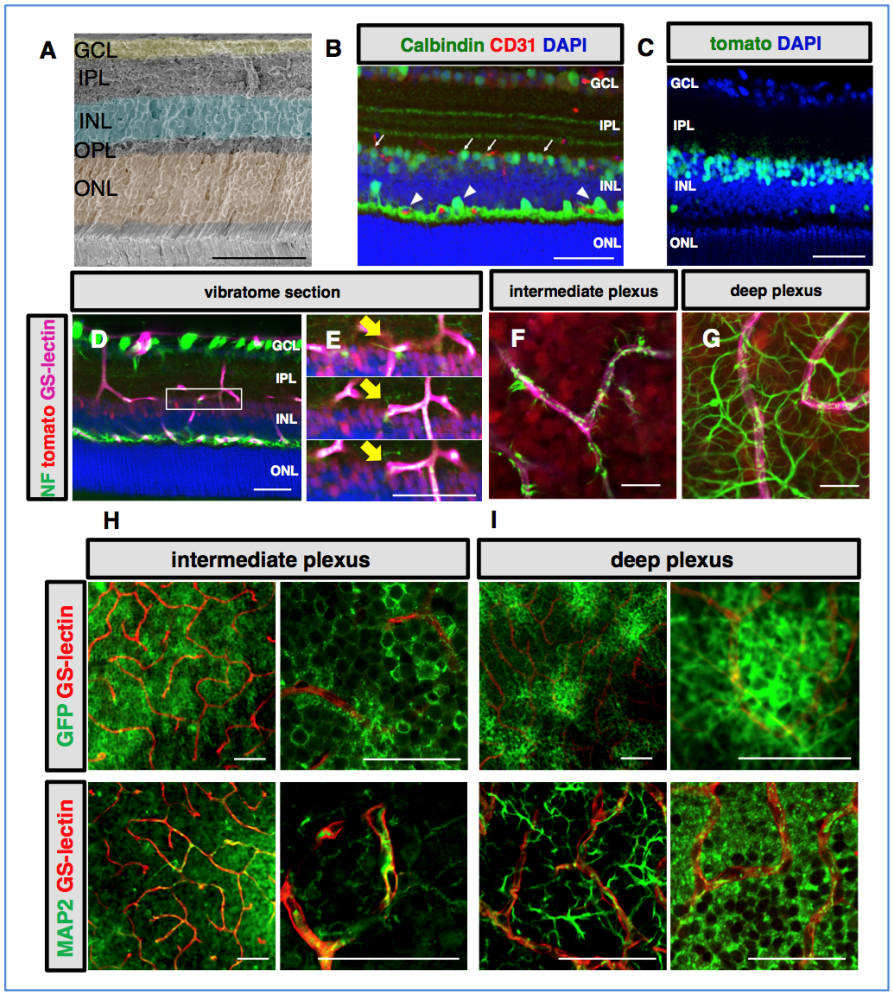

Figure 22 - Amacrine and horizontal cells form neurovascular units with the intraretinal capillaries. (A) Pseudo-colored cross-section of an adult murine retina. (B) Immunohistochemistry was used to identify putative neurovascular units between amacrine cells (arrows) or horizontal cells (arrowheads) with the vasculature using anti-calbindin (green), and anti-CD31 (red), and DAPI (blue) in wild-type retinal cryosections at P23. (C) Cre recombination reporters labels amacrine and horizontal cell nuclei in P23 *ptf1a-Cre;R26*$^{tdTomato/+}$ mice (tomato signal was psuedo-colored green). (D-I) Amacrine (D-F) and horizontal cell (D and G) neurites (NF-M labeled; green), associate with the intraretinal vasculature (GS-Lectin; cyan) as seen in thick cut (100µm) sections (Amacrine/horizontal nuclei=red) (E) Adjacent optical slices from the region of interest boxed in (D); arrows in mark co-localization. (F and G) Flat-mounted P23 *ptf1a-Cre;R26*$^{tdTomato/+}$ retinas co-labeled with anti-neurofilament and GS-lectin (endothelial cell marker). (H and I) Amacrine cell neurites are decorated with GFP in *ptf1a-Cre;R26*^{GFP} *mice, and can be observed in close* proximity to GS-Lectin positive endothelial cells. Immunofluorescence for MAP2 in whole-mount retinas at P23 also reveals colocalization of amacrine and horizontal cell neurites with the intraretinal vasculature. Scale bars: 50 µm (A, B, C, D, E, H, and I); 20 µm (F and G). GCL, ganglion cell layer; IPL, inner plexiform layer; INL, inner nuclear layer; OPL, outer plexiform layer; ONL, outer nuclear layer.

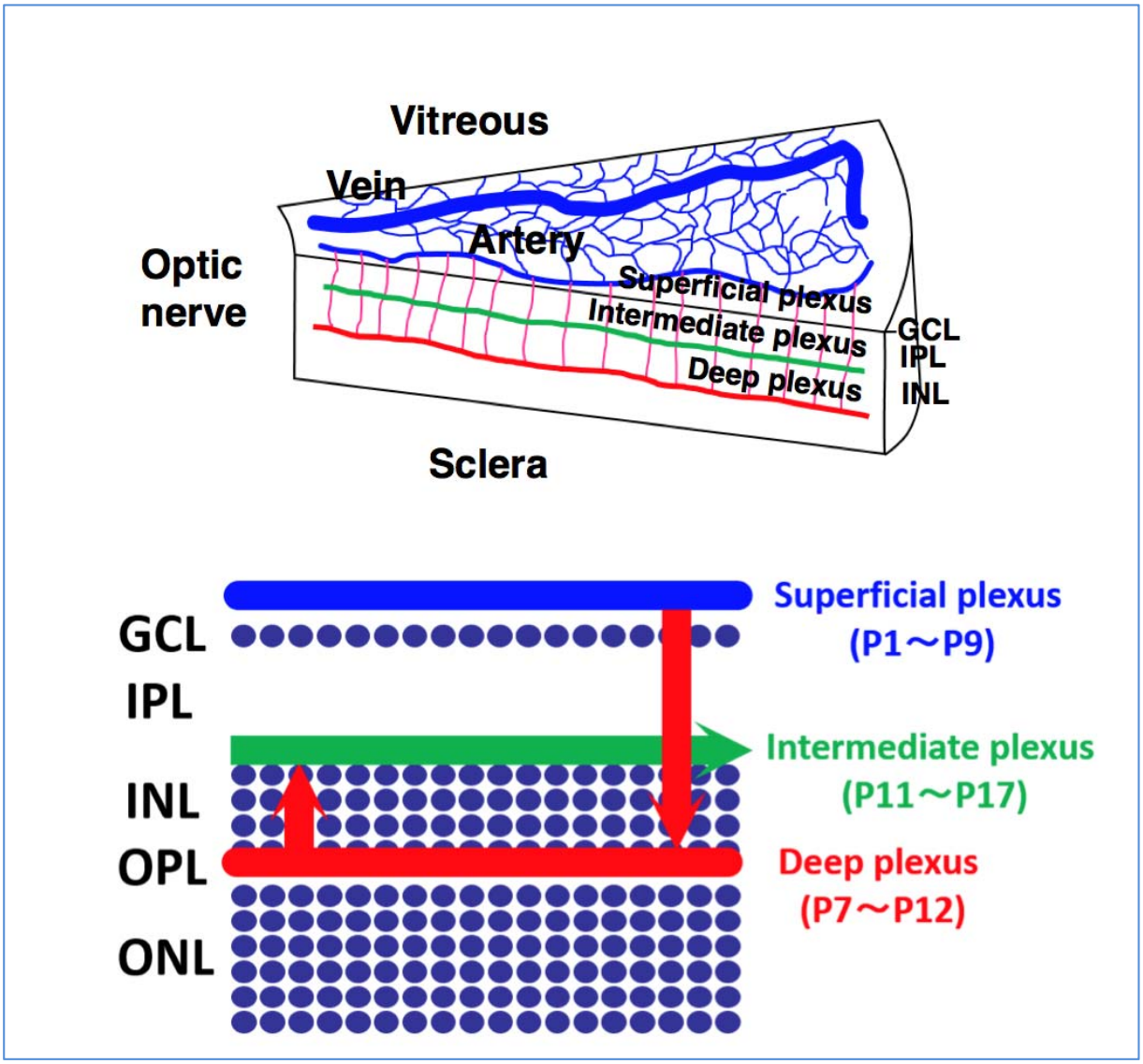

Figure 23 - Schematic diagram illustrating development of the vascular networks in the murine retina. The retinal vasculature forms as endothelial cells migrate from the optic nerve onto the retinal surface at birth and progress radially to form the superficial (or inner) plexus. Around postnatal day 7 (P7), sprouting vessels descend and advance into the OPL where they establish the deep plexus. At P11-12 stages, sprouting vessels from the deep plexus ascend into the IPL and ramify to form the intermediate plexus. GCL, ganglion cell layer; IPL, inner plexiform layer; INL, inner nuclear layer; OPL, outer plexiform layer; ONL, outer nuclear layer.

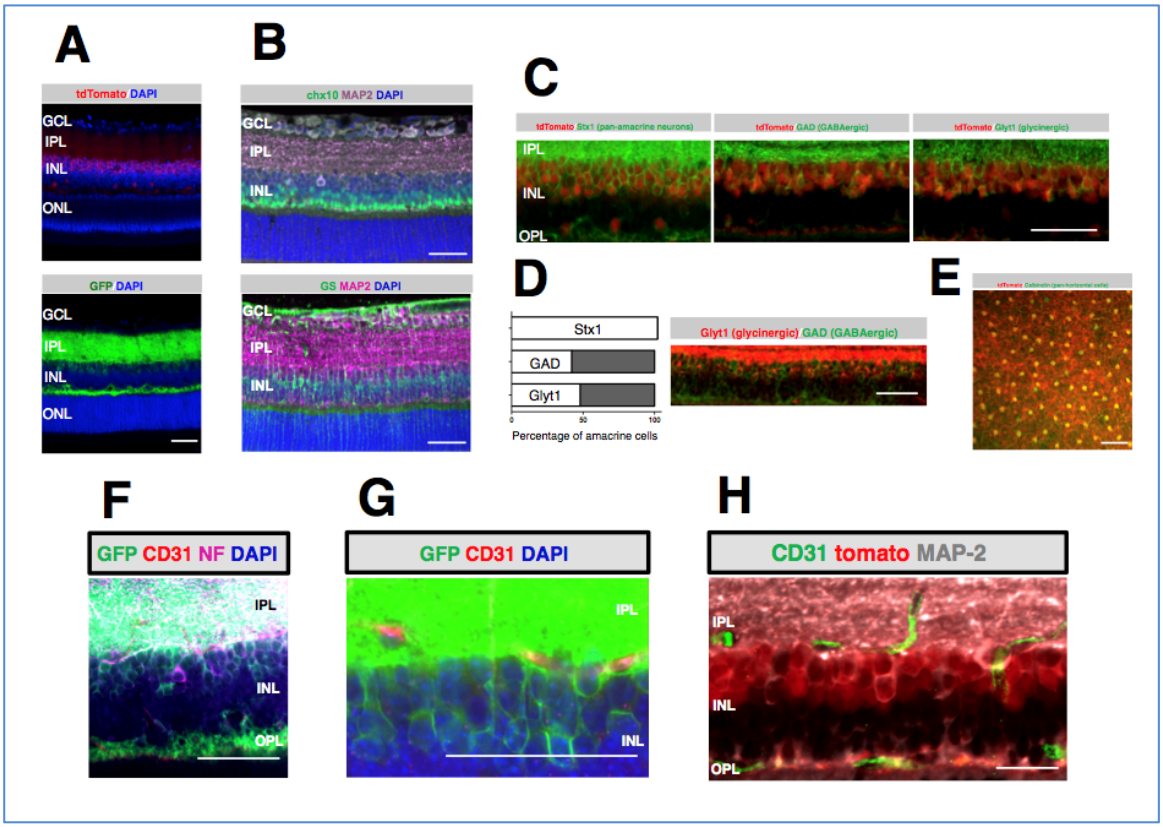

Figure 24 - Putative neurovascular units in the INL. (A) Whole retinal sections from mice harboring two Cre-recombination reporters and *ptf1a-Cre*. (B) IHC for bipolar (Chx10; top panel) and Mueller glia (glutamine synthetase (GS); bottom panel) is shown to highlight that their locations in the INL are distinct from amacrine cells. (C) Cre-mediated recombination occurs in amacrine cells in the inner margin of the INL and colocalizes with a pan-amacrine cell marker, Syntaxin 1 (Stx1), a GABAergic amacrine cell marker (GAD), and glycinergic amacrine cell marker (Glyt1) in cryosectioned retinas. (D) The percentage of Cre-positive amacrine cells that colocalized with amacrine cell subtypes was determined by counting cells in cryosectioned retinas (≥250 cells were counted for each cell type). (E) Colocalization of Cre-mediated recombination (td-Tomato) with calbindin positive horizontal cells at P23. (F and G) IHC on thick cut sections on *ptf1a-Cre;R26GFP/+* mice with NF-M (F) and CD31 (G). (H) Immunofluorescence for anti- MAP-2 and anti-CD31 in cryosections from P23 *ptf1a-Cre*; R26*tdTomato/+* retinas. Scale bar: 50 µm (A-G); 20 µm (H). GCL, ganglion cell layer; IPL, inner plexiform layer; INL, inner nuclear layer; OPL, outer plexiform layer; ONL, outer nuclear layer.

Amacrine and horizontal cell-derived VEGF is essential for neurovascular unit formation in the IPL

We first confirmed that the proangiogenic cytokine *Vegfa* is highly and broadly expressed in the INL at P12 when the intraretinal vasculature is developing (**Figure 25A**). To determine the contribution of amacrine and horizontal cell-derived VEGF, we first combined floxed *Vegfa* [135] and *ptf1a-Cre* alleles in transgenic mice and analyzed the vascular phenotype. While the deletion of *Vegfa* from amacrine and horizontal cells substantially reduced *Vegfa* transcript levels in the INL (**Figure 25A**), no noticeable effect was observed in the developing superficial (**Figure 26A**) or deep plexus layers in P23 staged mice (**Figure 25B&C**). However, the conditional deletion of *Vegfa* results in severe attenuation of the intermediate plexus (**Figure 25B**; bottom row; green). In order to better understand the mechanism of vascular attenuation in the *Vegfa* mutants, we quantified endothelial cell sprouting events during key timepoints of intraretinal angiogenesis. The defect is not due to vertical vascular sprouting defects from the superficial plexus or deep plexus or incomplete vascularization of the deep plexus (**Figure 26C-F; Figure 26B&C**). There were, however, significant differences in the number of branching events, tip cells, and filopodia on the tip cells of the sprouting vessels once they change direction and begin expanding within the intermediate plexiform layer (**Figure 25G-J**). Therefore, *Vegfa* inhibition in amacrine and horizontal cells inhibits endothelial cell sprouting in the IPL and prevents normal vascularization (**Figure 25K**).

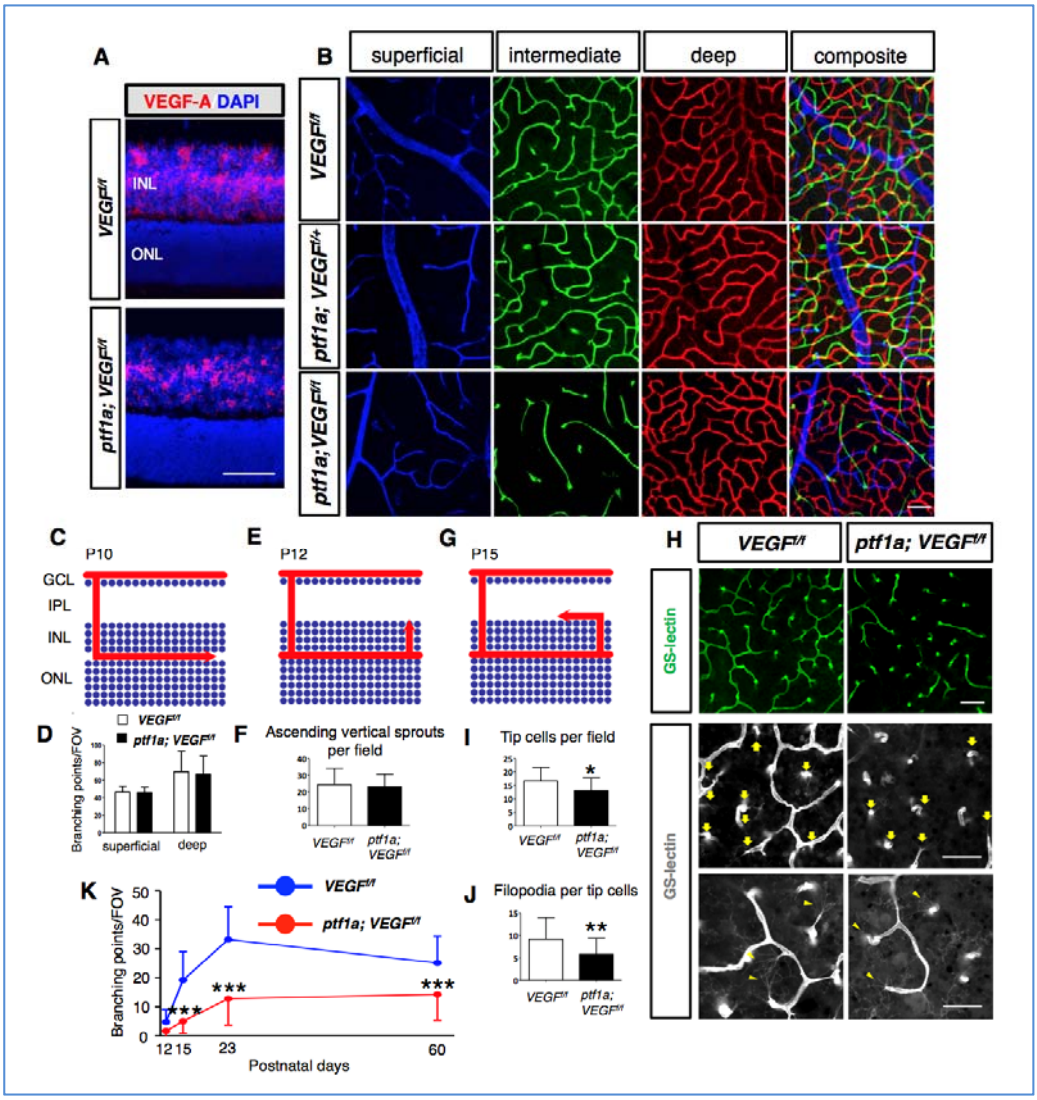

Figure 25 - *Vegfa* deletion in amacrine and horizontal cells severely impairs intraretinal vasculature development. (A) *in situ* hybridization was performed on P12 *VEGF*$^{f/f}$ or *ptf1a-Cre*; *VEGF*$^{f/f}$ cryosectioned retinas with a *Vegfa* probe (counterstained with DAPI). (B) The intermediate plexus (green) is severely attenuated in P23 *ptf1a-Cre*; *VEGF*$^{f/f}$ compared with controls. (C) Schematic of deep plexus development in a P10 staged mouse. (D) The number of branching events in the superficial and deep plexuses of P10 *VEGF*$^{f/f}$ or *ptf1a-Cre*; *VEGF*$^{f/f}$ retinas were counted and plotted (n = 4). (E) Schematic of vertical sprouting events from the deep plexus in P12 retinas. (F) There are no differences in the numbers of ascending vertical sprouts of *ptf1a-Cre*; *VEGF*$^{f/f}$ in flat-mounted retinas compared with controls (*VEGF*$^{f/f}$) (n = 4). (G) Schematic of intermediate plexus development at P15. (H-J) GS-lectin positive laterally expanding sprouts are fewer in number in P15 *ptf1a-Cre*; *VEGF*$^{f/f}$ mice due to a reduced number of tip cells (I; arrows) and filopodia (J; arrowheads) (n = 4-5). (K) Quantification of the number of branching points in the intermediate plexus were counted, quantified, and plotted at P12, 15, 23, and 60 (n = 4-6). *P<0.05, **P<0.01, ***P<0.001; 2-tailed Student's t tests. Error bars indicate mean ± SD. Scale bars: 50 μm (A, B, and H); 40 μm (I and J). GCL, ganglion cell layer; IPL, inner plexiform layer; INL, inner nuclear layer; ONL, outer nuclear layer.

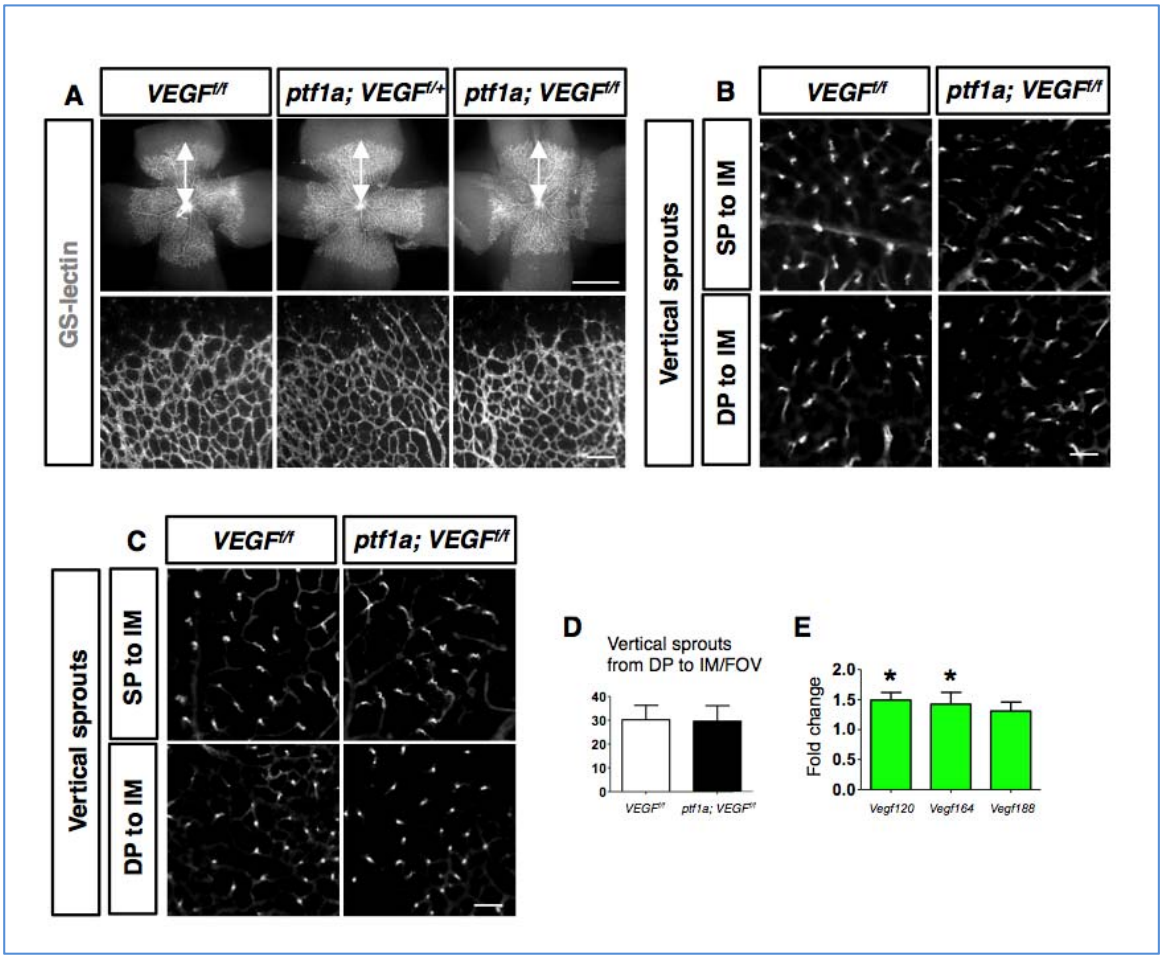

Figure 26 - The retinal vasculature of the superficial and deep plexuses are unaffected by *Vegfa* deletion in amacrine and horizontal cells. (A) Normal vascularization (bidirectional arrows) is observed in GS-lectin-positive P6 *ptf1a-Cre*; *VEGF*f/f retinas and controls (*VEGF*f/f (no Cre), *ptf1a-Cre*; *VEGF*f/ +). (B-D) Whole-mount staining in *VEGF*f/f or *ptf1a-Cre*; *VEGF*f/f retinas at P12 (B) or P15 (C and D), reveals no differences in the number of vertical sprouts descending through the IPL from the superficial plexus or ascending through the INL from the deep plexus (*n* = 4). Scale bar: 1 mm (A; upper panels); 100 µm (A; lower panels); 50 µm (B and C). (E) qPCR analysis showed that soluble VEGF120 and VEGF164 were the most abundant *Vegf* isoforms expressed in *ptf1a-Cre*; *VEGF*f/f mice at P15 (*n* = 4). SP; superficial plexus, IM; intermediate plexus, DP; deep plexus.

Vegfa gain-of-function in amacrine and horizontal cells induces massive neovascularization in the INL and IPL

We also performed gain-of-function assays for VEGF in amacrine and horizontal cells by crossing *ptf1a-Cre* mice with floxed *Vhl* mice to induce pseudo-hypoxia. Sprouting blood vessels in the *Vhl* mutants became diverted from their normal paths and stopped in the INL rather than continuing to the OPL. As a result, an abnormally dense and multi-stratified capillary network formed in the intermediate plexiform layer at the expense of the superficial and, in particular the deep plexus layer (**Figure 27A-E**). Abnormal vessels persisted as long as 20 months, although some vascular pruning occurred and the number of branching points decreased with age. The mechanism leading to this neovascular phenotype can most likely be explained by an upregulation of non-diffusible VEGF from pseudo-hypoxic amacrine and horizontal cells. Quantitative real-time polymerase chain reaction (PCR) experiments in *Vhl* mutants revealed an upregulation of all three VEGF isoforms, with the greatest change seen in the non-diffusible isoform ($VEGF_{188}$) that strongly binds the extracellular matrix (**Figure 27F**). However, in P15 *ptf1a-Cre; VEGF$^{f/f}$* mice soluble VEGF120 is the dominant and most abundant isoform, followed by VEGF164 (P=0.021646 for VEGF120, P=0.04667 for VEGF164, P=0.059891 for VEGF188; **Figure 26E)**. This could indicate that membrane-bound rather than soluble VEGF is more important for intermediate plexus development (or that neighboring neurons upregulate soluble VEGF to compensate for the genetic depletion). Collectively, these results indicate that VHL is required for regulating HIFs and the expression of specific VEGF isoforms at proper levels for retinal vascular patterning and maintenance.

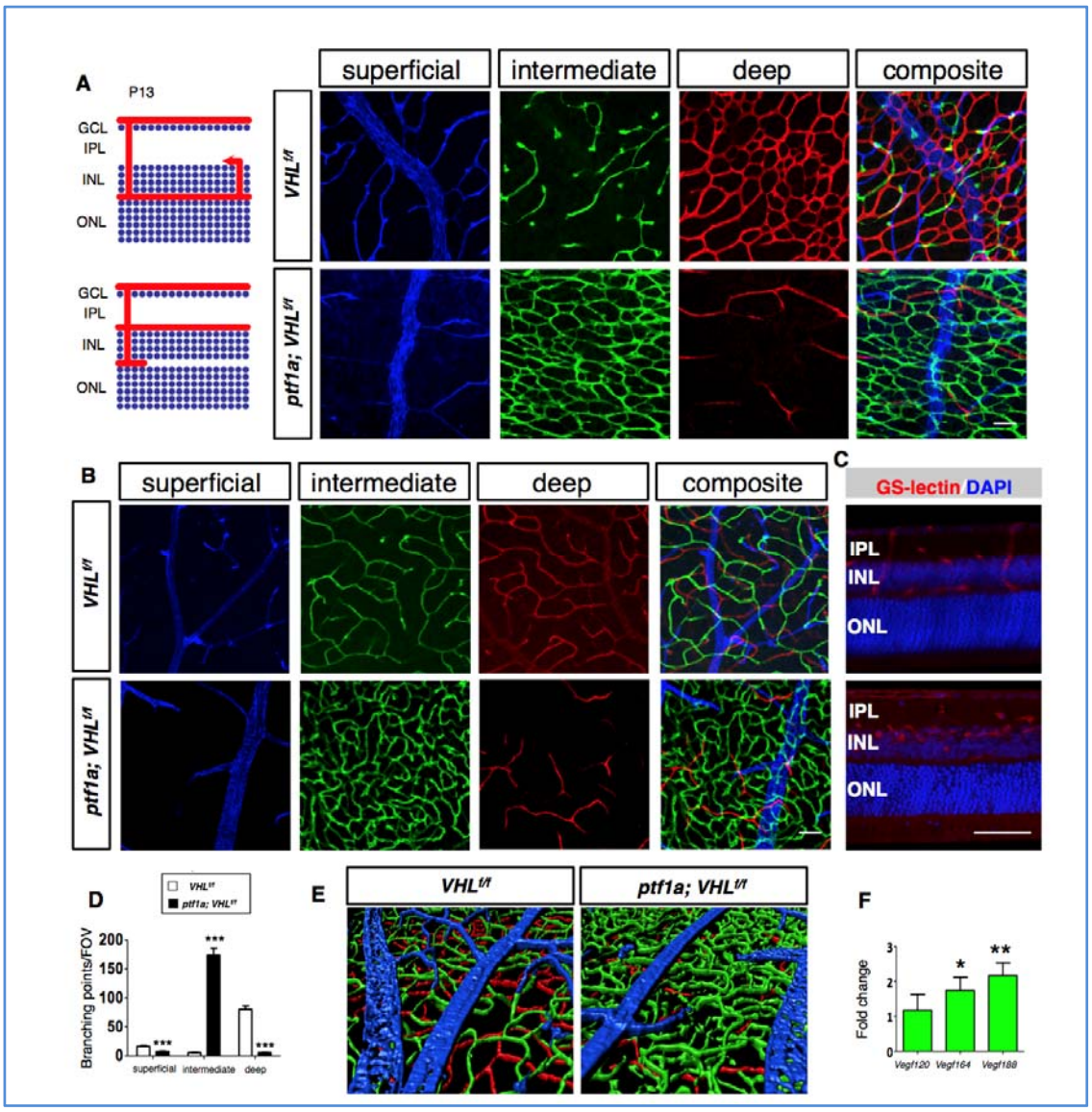

Figure 27 - VHL deletion in amacrine and horizontal cells induces formation of a dense and convoluted intermediate plexus at the expense of the deep plexus. (A&B) Schematic of angiogenesis in *VHL*$^{f/f}$ (control) or *ptf1a-Cre*; *VHL*$^{f/f}$ retinas at P13. Note dramatic alterations in the intermediate plexus (green) and deep plexus (red) at P13 (A) and P23 (B) in flat-mounted retinas. (C) 100µm sections from P23 *ptf1a-Cre*; *VHL*$^{f/f}$ mice were stained with GS-Lectin to highlight the extent of the neovascularization in the VHL mutants. (D) The number of branching events in P13 *VHL*$^{f/f}$ or *ptf1a-Cre*; *VHL*$^{f/f}$ retinas was plotted (n = 4). (E) 3D reconstruction of three retinal plexuses in P23 *ptf1a-Cre*; *VHL*$^{f/f}$ retina (superficial: blue; intermediate: green; and deep plexus: red) highlighted the abnormally dense intermediate plexus. (F) qPCR analyses revealed that non-diffusible $VEGF_{188}$ was the most abundant isoform expressed in *ptf1a-Cre*; *VHL*$^{f/f}$ mice at P15 (n = 4). *P<0.05, **P<0.01. ***P<0.001; 2-tailed Student's t tests. Error bars indicate mean ± SD. Scale bars: 50 µm (A-C). GCL, ganglion cell layer; IPL, inner plexiform layer; INL, inner nuclear layer; ONL, outer nuclear layer.

HIF-1α/VEGF signaling is required in the IPL for development of functional neurovascular units

Since others have shown that the conditional deletion of *Hif-1α* in all retinal cells prevents formation of the intermediate plexus[49], we set out to determine if the deletion of *Hif-1α* exclusively in amacrine and horizontal cells was sufficient to phenocopy the effect. Indeed, the deletion of *Hif-1α* in amacrine and horizontal cells (*ptf1a-Cre; VHL$^{f/+}$; Hif-1α$^{f/f}$*) phenocopies the intermediate plexus defects seen in both *Hif-1α* or *Vegfa* mutants at P12 (**Figure 28A&B**) and P23 (**Figure 29A&B; H**). Conversely, mice lacking both copies of HIF-2α (*ptf1a-Cre; VHL$^{f/+}$; Hif-2α$^{f/f}$*) appear normal (**Figure 29C; I; Figure 28C**). *Vhl* is haplosufficient but, when both copies are deleted, *Hif-1α* and *Hif-2α* become dominantly stabilized and *Vegfa* is overexpressed. The deletion of *Hif-1α* and both *Vhl* alleles (*ptf1a-Cre;VHL$^{f/f}$;Hif-1α$^{f/f}$*), but not *Hif-2α* and *Vhl* (*ptf1a-Cre; VHL$^{f/f}$; Hif-2α$^{f/f}$*), prevented the formation of the unusually dense capillary bed seen in *Vhl* mutants (**Figure 29D-G, and J-L; Figure 28D-G**). These genetic perturbations all result in spatial changes in *Vegfa* expression (**Figure 28H-J**), and collectively suggest that carefully regulated VHL/HIF-1α signaling is imperative for development of neurovascular units in the intermediate plexus.

To determine whether the neovascularization in the intermediate plexus is regulated by HIF-mediated VEGF activation, we generated *ptf1a-Cre;VHL$^{f/f}$;VEGF$^{f/f}$* mice. Interestingly, despite observing a clear reduction in *Vegfa* expression using in situ hybridization, no obvious differences were observed in the vascular density of the intermediate plexus at P12 and P23 in *ptf1a-Cre;VHL$^{f/f}$;VEGF$^{f/f}$* and control littermates (*VHL$^{f/f}$;VEGF$^{f/f}$*) (**Figure 29G, L; Figure 28G, K**). Gene-profiling experiments in *ptf1a-Cre;VHL$^{f/f}$;VEGF$^{f/f}$* and *VHL$^{f/f}$;VEGF$^{f/f}$* mice revealed that other proangiogenic factors are upregulated in the mutants (**Figure 29M; 28L**). These data suggest that other angiogenic factors can contribute to patterning of the intermediate plexus.

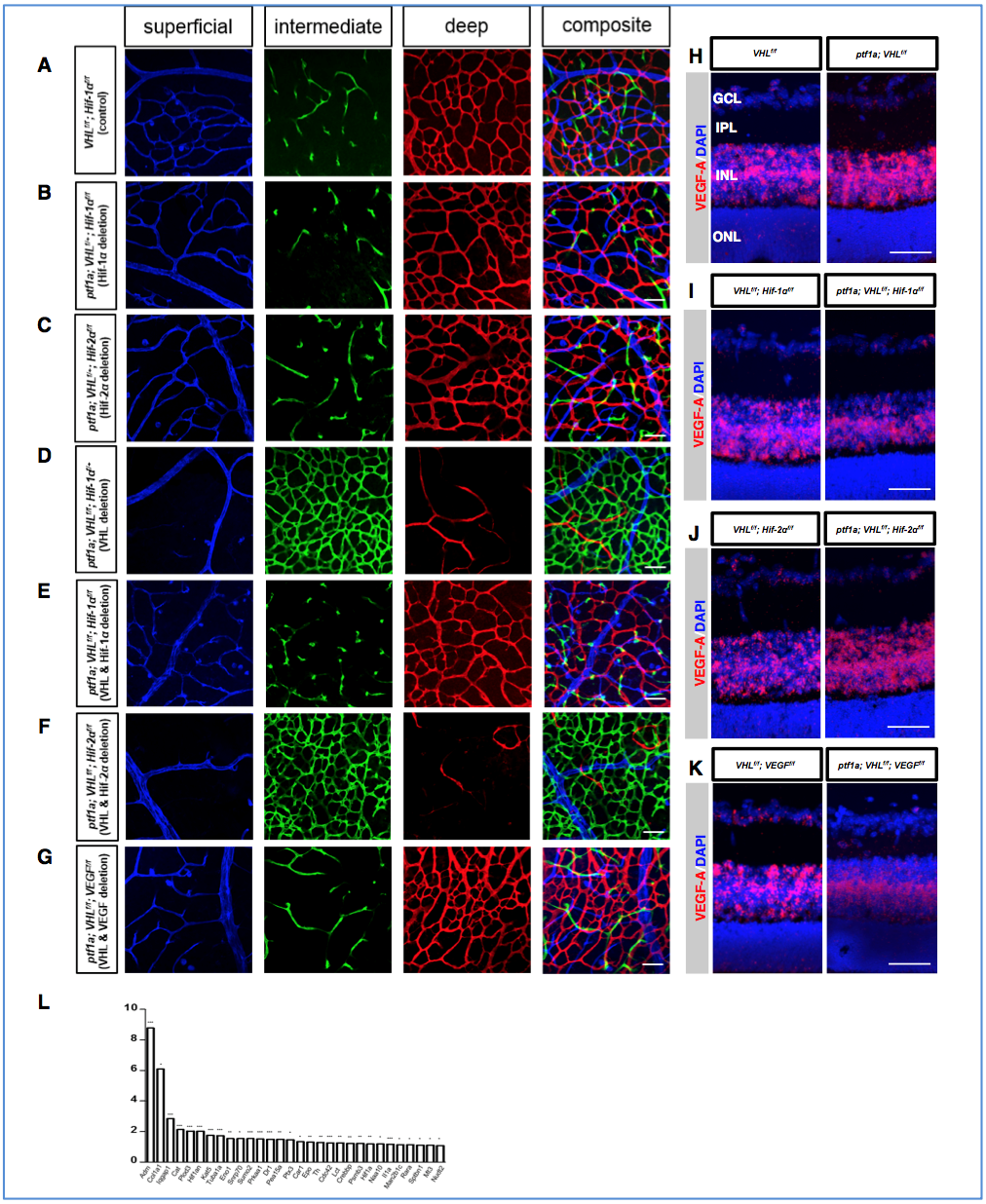

Figure 28 - Early angiogenesis events (P12) are regulated by VHL/HIF-1α/VEGF signaling. (A-F) Combinatorial conditional knock-out strategies were employed to show that the loss of HIF-1α (B) but not HIF-2α (C) in amacrine and horizontal cells interferes with intermediate plexus development in haplosufficient Vhl +/- mutants compared with controls (A). (D-F) Homozygous deletion of *Vhl* and *Hif-1α* (E) prevents the neovascularization observed in *Vhl* mutants, but deletion of HIF-2α elicits no effect (F) compared with controls (D). (G) Homozygous deletion of *Vhl* and *Vegfa* also rescues the *Vhl* phenotype. (H) *In situ* hybridization for *Vegfa* in *Vhl* mutants and controls. (I) *In situ* hybridization for *Vegfa* in double *Vhl/ Hif-1α* mutants and controls. (J) *In situ* hybridization for *Vegfa* in double *Vhl/ Hif-2α* mutants and controls. (K) *In situ* hybridization for *Vegfa* in double *Vhl/ Vegfa* mutants and controls. (L) Relative mRNA expression values from qPCR gene-profiling analysis of 84 hypoxia signaling related genes in *ptf1a-Cre*; *VHL*f/f; *VEGF*f/f retinas at P12 compared with controls (harboring floxed alleles but no Cre); upregulated genes are plotted (n = 4). *P<0.05, **P<0.01. ***P<0.001; Scale bars: 50 μm (A-K).

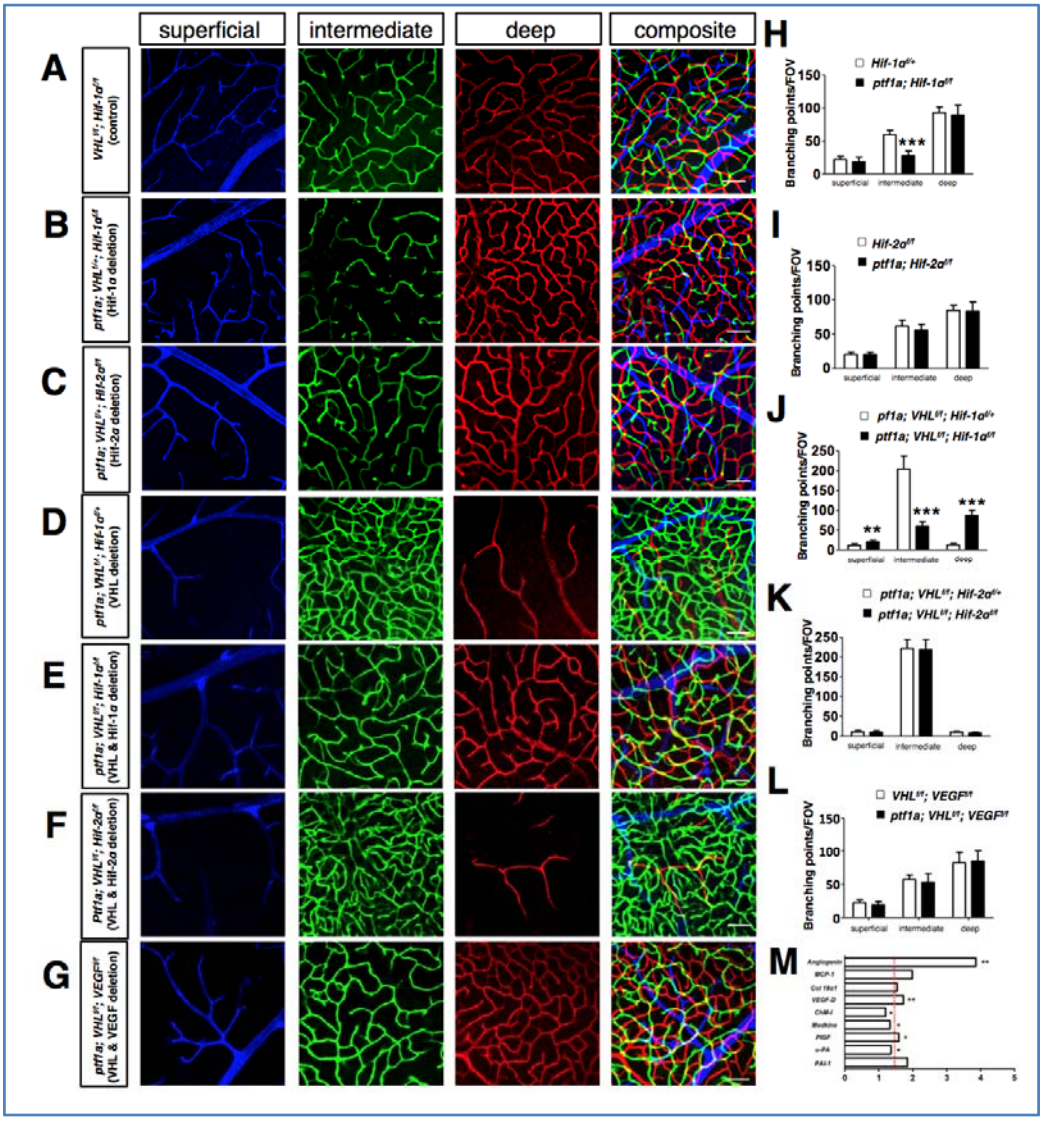

Figure 29 - VHL/HIF-1α/VEGF signaling regulates angiogenesis in the intermediate plexus. (A-F) Combinatorial conditional knock-out strategies were employed to show that the loss of HIF-1α (B; quantified in H) but not HIF-2α (C; quantified in I) in amacrine and horizontal cells interferes with intermediate plexus development in haplosufficient P23 $Vhl^{+/-}$ mutants compared with controls (A). (D-F) Homozygous deletion of P23 *Vhl* and *Hif-1α* (E) prevents the neovascularization observed in *Vhl* mutants (D; quantified in J), but deletion of *Hif-2α* elicits no effect (F; quantified in K) compared with controls (D). (G) Homozygous deletion of *Vhl* and *Vegfa* also rescues the *Vhl* neovascular phenotype. (All assays were performed in P23 staged mice; *n* = 4-6). (M) Relative mRNA expression values from qPCR gene-profiling analysis of 84 angiogenesis-related genes in *ptf1a-Cre*; $VHL^{f/f}$; $VEGF^{f/f}$ retinas at P12 compared with controls (harboring floxed alleles but no Cre); upregulated genes (P<0.05 or > 1.5 fold-change) are plotted (*n* = 4).**P<0.01. ***P<0.001; 2-tailed Student's *t* tests. Error bars indicate mean ± SD. Scale bars: 50 μm (A-G).

Genetic ablation of amacrine and horizontal cells phenocopies the effects of *Vegfa* deletion

To confirm that amacrine and horizontal cells can regulate development of the

intraretinal vasculature, we performed genetic techniques designed to selectively ablate both cell types. This was accomplished by crossing *ptf1a-Cre* mice with a mouse strain in which the human diphtheria toxin receptor (iDTR) is knocked into the ROSA26 locus (*R26*^{iDTR}) (**Figure 30A**). Using this technique, inducible and selective genetic ablation of 82.4% of amacrine cells (89.3±17.8/0.1mm^2 in controls vs. 15.7±4.9/0.1mm^2 in mutants) and 87.9% of horizontal cells (4.5±1.1/0.1mm^2 in controls vs. 0.5±0.5/0.1mm^2 in mutants) and a prominent decrease in synaptic density in the IPL occurs 10 days after diphtheria toxin (DT) administration (**Figure 31A-E**). The reduction in the number of amacrine cells induced profound attenuation of the intermediate plexus, but not of the superficial or deep plexuses compared with controls **Figure 31F&G**). The same phenomenon was observed when amacrine or horizontal cells were ablated starting at P6, before formation of the deep plexus **Figure 30B-G**). We also induced ablation in adult mice and examined the vasculature 3 months after DT administration. In adult mice we observed a significant decrease in vascular density in the intermediate plexus, but not in the superficial or deep plexuses indicating a role for vascular maintenance, not just development **Figure 31H&I**). We also recorded light responsiveness (a- and b-waves) in DT-treated *ptf1a-Cre*; *R26*$^{iDTR/+}$ and *ptf1a-Cre*; *R26*$^{+/+}$ mice. Functional analyses using full-field electroretinography (ERG) revealed a significant reduction in the b waves (negative ERG) of *ptf1a-Cre*; *R26*$^{iDTR/+}$ mice (**Figure 30H**) collectively indicating that amacrine cells are required for both development and maintenance of the intermediate plexus, and for propagation of the rod- and cone-driven pathways in adult stages.

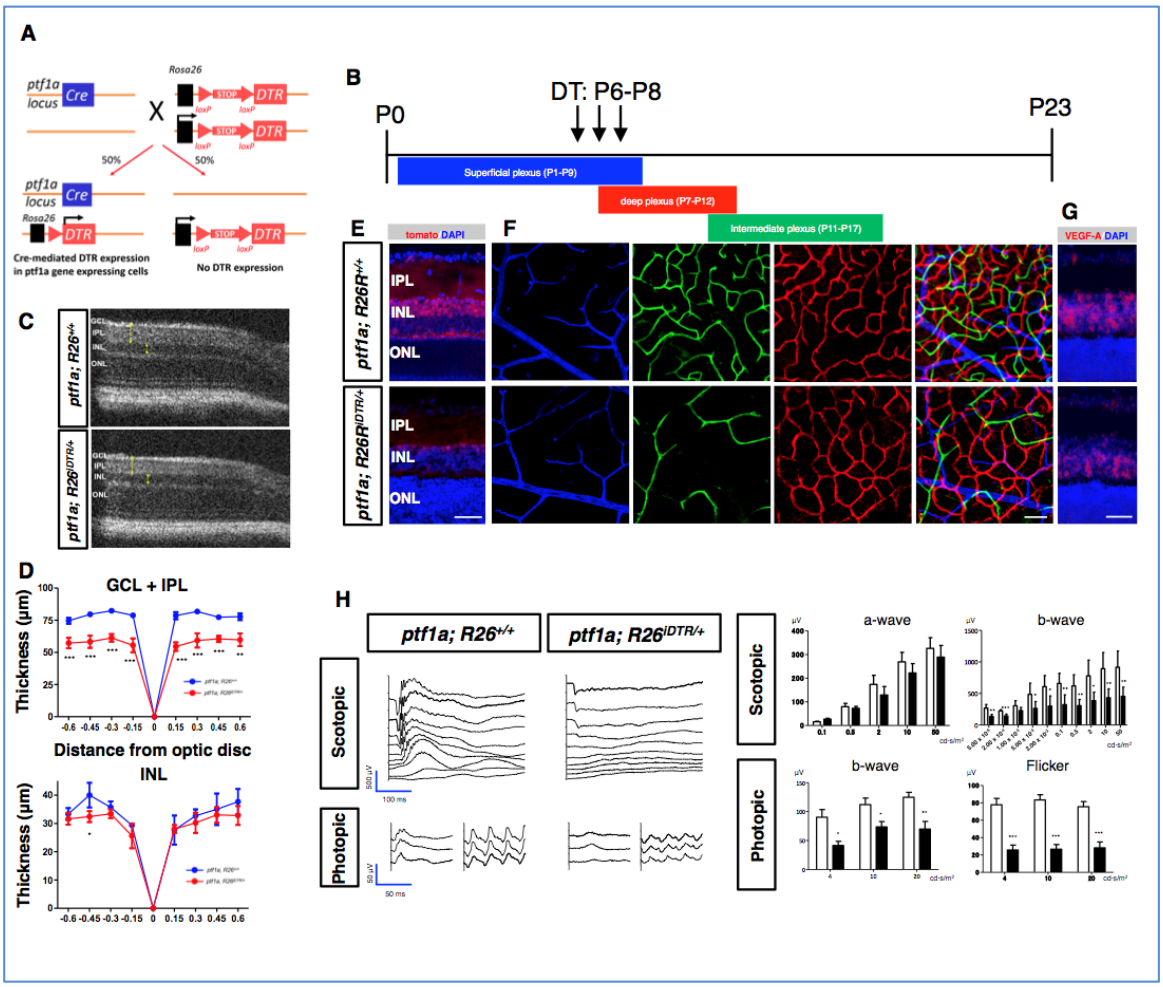

Figure 30 - The genetic ablation of amacrine and horizontal cells in mice results in attenuation of the intermediate plexus and negatively affects visual function. (A) Schematic of the experimental design for the genetic depletion of amacrine and horizontal cells in *ptf1a-Cre*; *R26i*DTR/+ mice. (B) DT was injected daily from P6-8. (C and D) Thinning of the GCL/IPL and INL is observed in vivo using SD-OCT (C), and quantified (D) in P23 *ptf1a-Cre*; *R26+/+* and *ptf1a-Cre*; *R26i*DTR/+ mice (*n* = 6). (E) IHC from P23 DT- treated *ptf1a-Cre*; *R26*iDTR/+:tdTomato/+ and *ptf1a-Cre*; *R26+/+*: tdTomato/+ mice after DT treatment at P6-8 reveal a loss of the majority of amacrine and horizontal cells. (F) DT injections from P6-8 in P23 *ptf1a-Cre*; *R26+/+* and *ptf1a-Cre*; *R26*iDTR/+ staged mice induced attenuation of the intermediate plexus. (G) *in situ* hybridization was performed on P12 *ptf1a-Cre*; *R26+/+* or *ptf1a-Cre*; *R26*iDTR/+ retinas with a *Vegfa* probe and counterstained with DAPI. (H) Full-field ERGs performed on *ptf1a-Cre*; *R26*iDTR/+ mice 3 months after DT treatment at P30-32 revealed reduced b waves and gross defects in cone-driven pathways (*n* = 5-6). **P*<0.05. ***P*<0.01. ****P*<0.001; 2- tailed Student's *t* tests. Error bars indicate mean ± SD. Scale bar: 50 µm (F, G); 40 µm (E). GCL, ganglion cell layer; IPL, inner plexiform layer; INL, inner nuclear layer; ONL, outer nuclear layer.

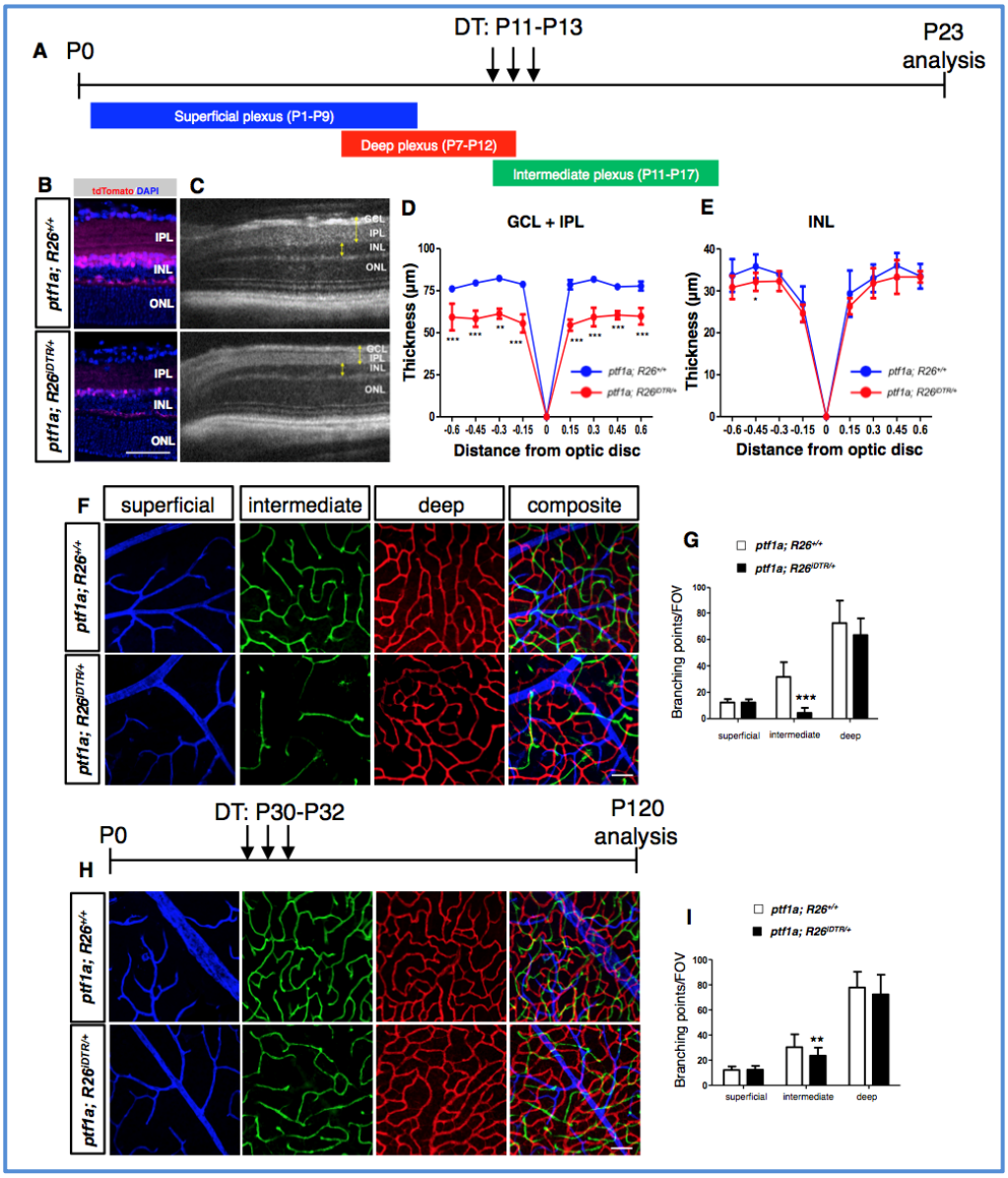

Figure 31 - Genetic ablation of amacrine and horizontal cells phenocopies the defects in the intermediate plexus observed in HIF-1α and VEGFa mutants. (A) DT was injected daily at the time-points indicated. (B-E) The reduced number of cells post-ablation was examined by comparing cryosectioned retinas from P23 *ptf1a-Cre*; *R26*$^{iDTR/+:tdTomato/+}$ and P23 *ptf1a-Cre*; *R26*$^{+/+:tdTomato/+}$ mice after injecting DT (B), and by measuring the thickness of the GCL/IPL and INL (C; yellow brackets) from images captured in vivo using SD-OCT (D&E) (*n* = 4-6). (F&G) An attenuated intermediate plexus is observed (F; green) and quantified (G) in P23 *ptf1a-Cre*; *R26*$^{iDTR/+}$ mice (*n* = 6). (H and I) An attenuated intermediate plexus is also seen when amacrine and horizontal cells are ablated well after intermediate plexus development (H; quantified in I), suggesting that amacrine cells are required for development and maintenance of the intermediate plexus (*n* = 4). ***P*<0.01. ****P*<0.001; 2-tailed Student's *t* tests. Error bars indicate mean ± SD. Scale bar: 50 µm (B,F&H). DT, diphtheria toxin; GCL, ganglion cell layer; IPL, inner plexiform layer; INL, inner nuclear layer; ONL, outer nuclear layer.

Intermediate plexus abnormalities are associated with loss of visual acuity

To determine the importance of neurovascular units in the IPL for visual function,

ERGs were performed on the *Vegfa* or *Vhl* mutants to measure the integrity of the photoreceptors (negative a-wave) and of the second- and third-order neurons (positive b-wave) in either dark adapted (scotopic) or light adapted (photopic) animals. Significant reductions of both scotopic (rod-driven) and photopic (cone-driven) responses (**Figure 37A**), and prominently reduced optokinetic reflexes were observed in *ptf1a-Cre*; *VEGF*$^{f/f}$ mice (**Figure 32**).

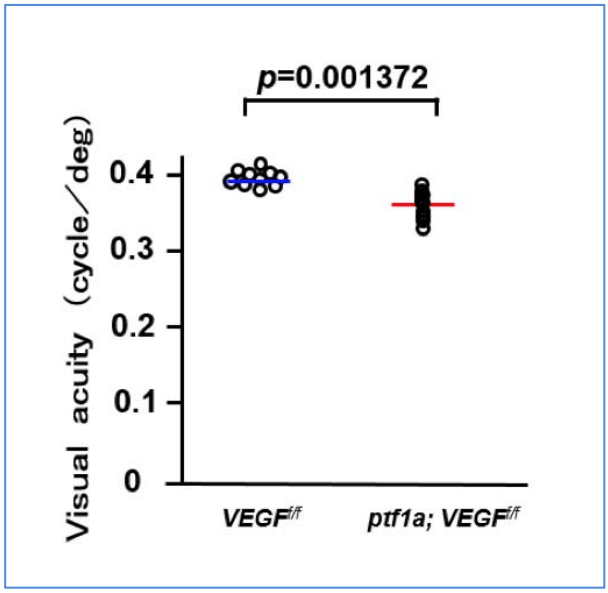

Figure 32 - Visual acuity in ptf1a-Cre; *VEGF* knockout mice is significantly impaired. Optokinetic reflexes were measured in *VEGF*f/f or *ptf1a-Cre*; *VEGF*f/f mice and significant defects were observed in 3 month old mice (*n* = 10).

Significant reductions in scotopic (rod-driven) responses were also detected in *ptf1a-Cre*; *VHL*$^{f/f}$ mice (**Figure 37B**). Importantly, neither manipulation induced neurovascular uncoupling in the INL (**Figure 33)**.

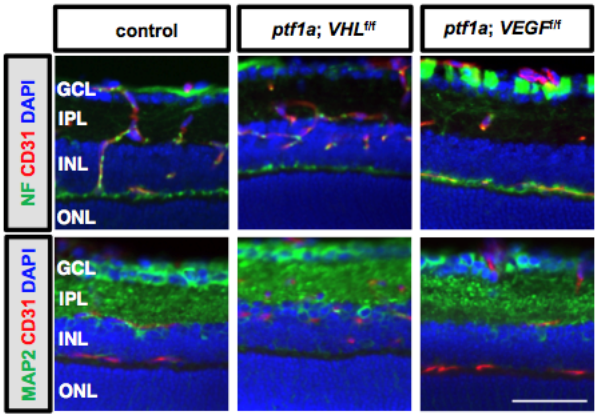

Figure 33 - Neurovascular units with the amacrine and horizontal cells and intraretinal capillaries in ptf1a-Cre; VEGF knockout and ptf1a-Cre; VHL knockout mice. Fluorescent immunostaining for anti neurofilament (NF) or anti-MAP2 with CD31 in retinal cryosections from P23 *ptf1a-Cre*; *VHL*f/f mice or *ptf1a-Cre*; *VEGF*f/f mice. The nuclei of cells were counterstained with DAPI (blue). Scale bar: 50 µm. GCL, ganglion cell layer; IPL, inner plexiform layer; INL, inner nuclear layer; OPL, outer plexiform layer; ONL, outer nuclear layer.

TUNEL assays, basic ultrastructural examinations, blood tests, weight measurements, and immunohistochemistry in longitudinally monitored mutant mice show no obvious evidence of increased cell death, neuronal development/synaptic densities, or changes to the diabetic status of the mutants (since *ptf1a-Cre* is active in the pancreas (**Figures 34; 35 and 36**). Collectively, these results suggest that either attenuated or potentiated amacrine and horizontal cell-derived VEGF expression disrupts vision.

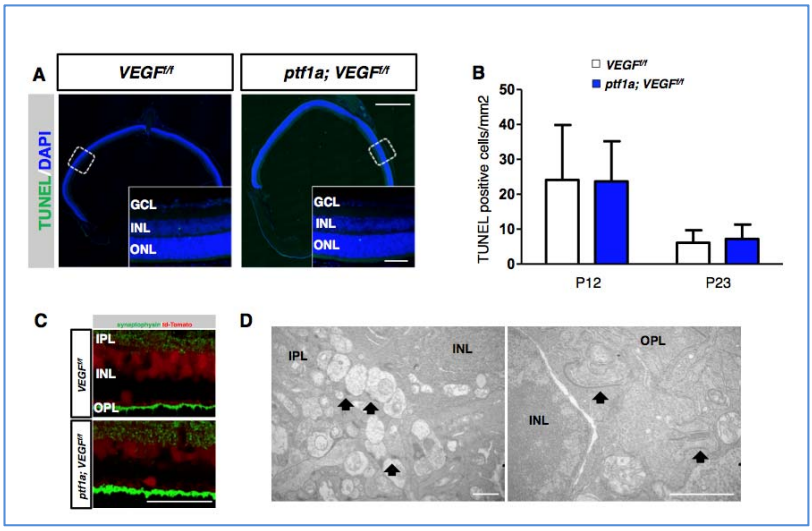

Figure 34 - No evidence of heightened neurodegeneration or abnormal synaptogenesis was observed in *ptf1a-Cre*; *VEGF*f/f mice. (A) TUNEL staining of P12 *ptf1a- Cre*; *VEGF*f/f retinas and controls. Scale bars: 500 µm (A; upper right); 50 µm (A; lower right). (B) Quantification from (A) at P12 or P23 (*n* = 4). (C) The expression pattern of synaptophysin is unremarkable in P15 *ptf1a-Cre*; *VEGF*f/f ;R26*tdTomato/+* retinas. (D) Transmission electron micrograph showing normal synaptic ultrastructure (arrows) and synaptic vesicles in P23 *ptf1a- Cre*; *VEGF*f/f retinas. Scale bars: 1 µm. GCL, ganglion cell layer; IPL, inner plexiform layer; INL, inner nuclear layer; ONL, outer nuclear layer; OPL, outer plexiform layer.

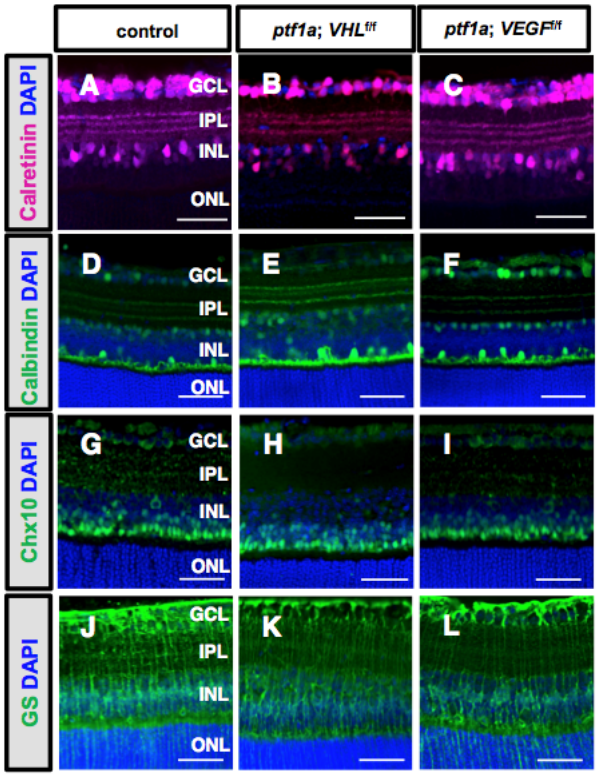

Figure 35 - No differences in the topographies of interneurons and Mueller glia are observed in ptf1a-Cre VEGF knockout and ptf1a-Cre; VHL knockout mice. (A- L) Cryosections from 23-day-old *ptf1a-Cre*; *VEGF*f/f and *ptf1a-Cre*; *VHL*f/f mice and controls were stained for calretinin (A-C), calbindin (D-F), chx10 (G-I), and glycogen synthase (GS) (J-L). The nuclei of cells were counterstained with DAPI (blue). Scale bar: 50 µm in A-L GCL, ganglion cell layer; IPL, inner plexiform layer; INL, inner nuclear layer; ONL, outer nuclear layer

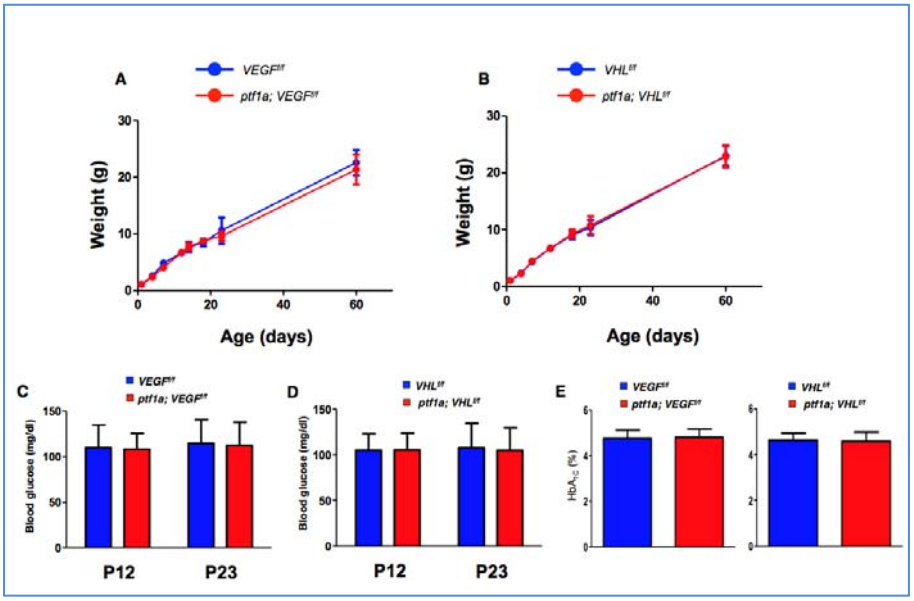

Figure 36 - Normal weight, blood glucose, and HbA1c levels in VEGF and VHL mutant mice. (A, B) Body weights in both groups were comparable. (*n* = 9-10). (C, D) Blood glucose was measured at P12 and P23 of *ptf1a-Cre*; *VEGF*f/f mice and *ptf1a-Cre*; *VHL*f/f mice. (*n* = 10 each). (E) HbA1C levels in 4 month-old *ptf1a- Cre*; *VEGF*f/f and 6 month-old *ptf1a-Cre*; *VHL*f/f mice. (*n* = 8 each).

Finally, *Ptf1a-Cre*; *VEGF*$^{f/f}$ mice were crossed with a *retinal degeneration 10* (rd10) mouse line (*Pde6b*$^{rd10/rd10}$), which is a widely used model of photoreceptor atrophy. To quantify the degree of photoreceptor degeneration in rd10 mice with attenuated intermediate plexuses, we measured the thickness of the outer nuclear layer (ONL) in histological sections and performed terminal deoxynucleotidyl transferase dUTP nick end labeling (TUNEL) staining. At the earliest time point of retinal degeneration, P21, the number of TUNEL positive cells was significantly increased (**Figure 37C&D**) and ONL thickness was significantly thinner at six positions in the retina of *ptf1a-Cre*; *VEGF*$^{f/f}$; *Pde6b*$^{rd10/rd10}$ mice compared with controls (*VEGF*$^{f/f}$; *Pde6b*$^{rd10/rd10}$ and *ptf1a-Cre*; *VEGF*$^{f/f}$; *Pde6b*$^{rd10/+}$ mice) (**Figure 37E)**, indicating that degeneration is accelerated in mice with impaired intermediate plexuses. These findings highlight a critical and novel role for amacrine cells, promoting photoreceptor homeostasis and function through vascular maintenance of the intermediate plexus.

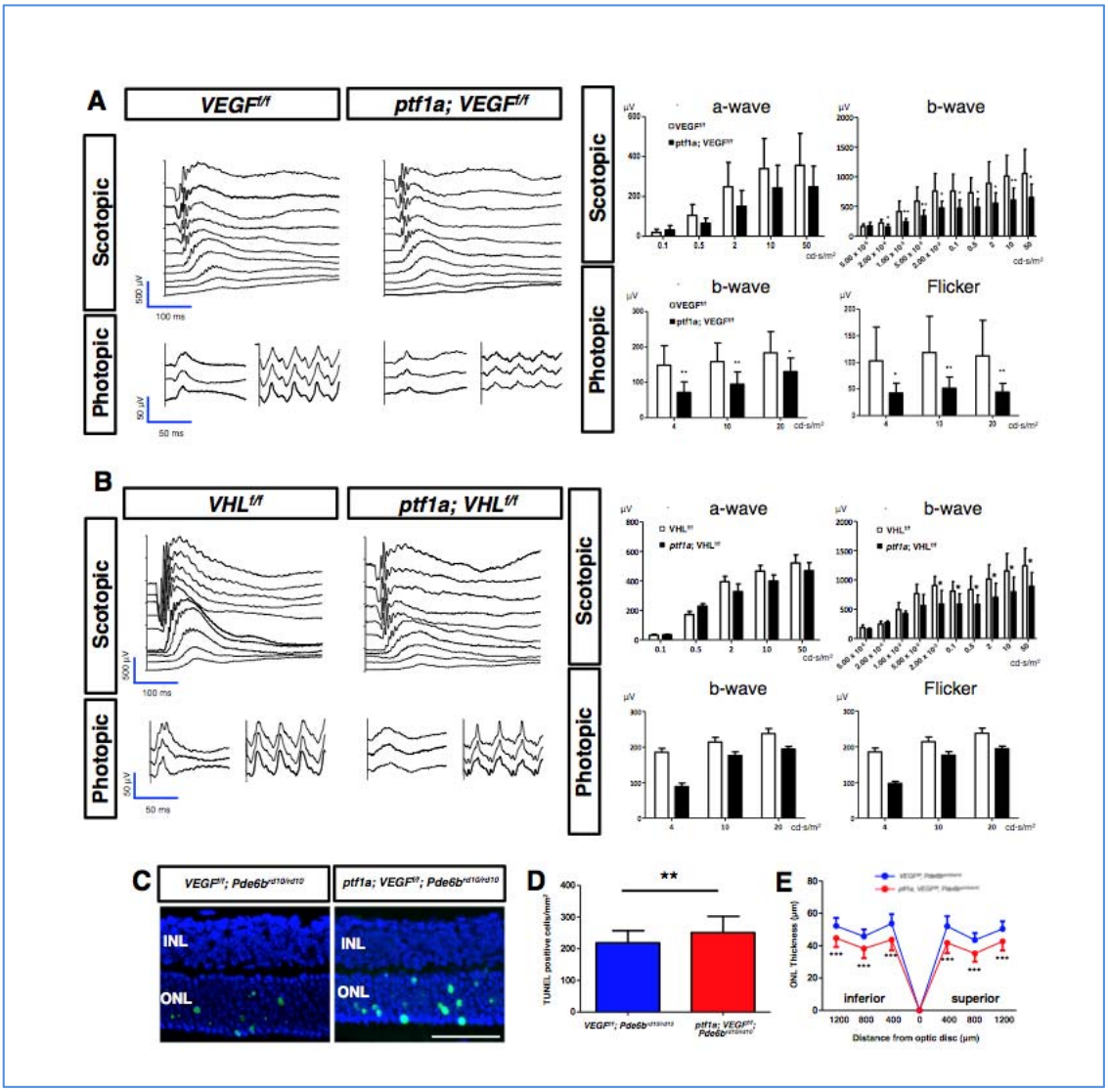

Figure 37 - Intermediate plexus abnormalities are associated with visual dysfunction. (A) Full-field ERGs in two-month-old *ptf1a-Cre*; *VEGF*$^{f/f}$ mice reveal significant defects in both rod- and cone-driven pathways (*n* = 8-10). (B) Full-field ERGs performed on two-month-old *ptf1a-Cre*; *VHL*$^{f/f}$ mice reveal that the rod-driven pathways are significantly impaired (*n* = 6). (C-E) Photoreceptor atrophy is accelerated in a mouse model of spontaneous retinal degeneration (rd10 mice) with impaired intermediate plexuses, based on TUNEL staining in the ONL (C; green, quantified in D), and reduced ONL thickness values (E) in P21 *ptf1a-Cre*; *VEGF*$^{f/f}$; *Pde6b*$^{rd10/rd10}$ mice and controls (*VEGF*$^{f/f}$; *Pde6b*$^{rd10/rd10}$; n = 6 each). **P*<0.05, ***P*<0.01, ****P*<0.001; 2-tailed Student's *t* tests. Error bars indicate mean ± SD. Scale bar: 50 µm. INL, inner nuclear layer; ONL, outer nuclear layer.

Discussion

There is mounting evidence that retinal neurons, including ganglion cells and photoreceptors, act as oxygen and nutrient sensors that can drive and regulate angiogenesis; ganglion cells can even act as rheostats to fine tune VEGF availability [39,40,173]. However, the roles of other neurons to facilitate growth and maintenance of the deep retinal vascular layers are incompletely understood. Oxygen consumption increases at distinct time points during development as neurons are born and mature. This results in localized zones of hypoxia in the developing retina. In P15 staged rats (just prior to eye opening), the intermediate vascular plexiform layer is underdeveloped and oxygen consumption is very low in the inner retina [207]. During these stages of mouse development, HIF-1α levels are very high in the retina [53,201] and VEGF is broadly, albeit transiently, detectable throughout the INL [208]. Earlier reports suggested that Mueller glia were the primary source of VEGF in the inner retina [208], however conditional deletion of *Vegfa* in Mueller glia cells did not affect the vasculature [209]. In this study we used genetic ablation strategies to show that amacrine cell-derived VEGF (perhaps more specifically $VEGF_{188}$) is essential for regulating intermediate plexus development (although other factors including adrenomedullin, angiogenin, or EPO may also contribute). This conclusion is based on the observation that interactions between amacrine cells and the capillaries are extensive, and that *Vegfa* loss- and gain-of-function assays using *ptf1a-Cre* result in attenuation or neovascularization of the intermediate plexus (at the expense of the deep plexus).
The onset of hypoxia and intermediate plexus formation in the INL correlates well temporally with the timing of synaptogenesis and the maturation of amacrine cells. At P10-P12 stages in mice (a few days prior to eye opening) when the intermediate plexus forms, all of the key events of synaptogenesis have been initiated. Amacrine cells are properly sublaminated, but are still actively remodeling their lateral connections to form mature circuits. This occurs as the amacrine cells disassemble their immature cholinergic networks and generate mature ionotropic glutamate-based synapses. As the density and size of the IPL increases and the metabolic demands change, HIF-1α/VEGF signaling in amacrine cells drives angiogenesis from the deep plexus. Perturbations to VEGF signaling through ptf1a-Cre-induced *Vhl* deletion results in a highly convoluted and unusually dense

intermediate plexus since the sprouting vessels from the deep plexus are attracted to a temporally inappropriate, ectopically localized, VEGF gradient.

We report here a novel function for amacrine cells, generating VEGF for vascular maintenance, photoreceptor homeostasis, and visual function. Amacrine and horizontal cells were previously thought to be required only for pre-processing and integrating visual stimuli. Our findings demonstrate that dysregulated *Vegfa* expression in amacrine and horizontal cells causes retinal microvascular deficits that diminish retinal blood flow, reduce oxygen nutrient availability, and ultimately induce loss of visual acuity. Additionally, we have observed that photoreceptor atrophy occurred earlier and faster in two animal models of human retinal degeneration, one of which was presented in this paper, after deleting *Vegfa* in amacrine cells. Finally, it has been reported that in an animal model of diabetic retinopathy, VEGF inhibition markedly increased amacrine cell apoptosis [210]. These findings not only demonstrate the importance of amacrine cells, but also add to a growing body of evidence that chronic VEGF antagonism in the eye, the preferred therapeutic strategy for treating neovascular age-related macular degeneration, could elicit concerning off-target effects leading to visual dysfunction [4,62,168].

This work also shows that the attenuation of the intermediate and deep vascular plexuses negatively affects retinal physiology. This concept is supported by recent evidence suggesting that neuronal dysfunction and neurodegeneration are tightly correlated with microvascular dysfunction. Microvascular dysfunction and breakdown of the blood-retinal barrier in the retina are characteristic of retinal neurodegenerative disorders such as retinitis pigmentosa and diabetic retinopathy [161,211-213]. IPL thinning and retinal amacrine neuronal dysfunction are observed in diabetic patients [213,214]. Attenuation of the intraretinal vasculature is also highly correlated with progression of vision loss in retinitis pigmentosa [161], and our data strongly suggests that amacrine cell loss or dysfunction and ensuing intermediate plexus attenuation can accelerate photoreceptor atrophy in a murine model of the disease. Furthermore, pre-clinical experiments in rodent models of retinal degeneration have provided proof-of-concept evidence that stabilization of the intraretinal vasculature can retard photoreceptor atrophy [153]. Finally, in humans, efforts to rebuild or repair defective neurovascular units are

being actively explored to prevent or slow neurodegeneration [151]; studies like this one may inform those therapeutic strategies.

In summary, we have described a role for retinal lateral interneurons, providing critical neurotrophic support through vascular maintenance of the intermediate plexus. Learning how to therapeutically control VHL/HIF-1α/VEGF signaling in amacrine cells may represent a therapeutic intervention for treating degenerative conditions that lead to vision loss.

Main conclusions

Aspects reported in this chapter that shed new light onto DR research

- Although it has been widely suggested that PRs play a critical role in promoting DR progression[100,215-217], DR research has been focusing mainly on the inner retina, where structural changes can be more clearly identified.
- Diabetes is known to compromise amacrine cell function[218,219] - which is expressed by ERG deficits - before vascular changes become evident in the diabetic retina. These new findings suggest that diabetes-induced amacrine cell dysfunction may be contributing to microvascular degeneration with consequent neurodegeneration and a compensatory neuronal response (in an attempt to restore neuronal nourishment) that favors development of pathological neovascularization.
- Therefore, pathological retinal features in DR may not result from amacrine-cell dysfunction *per se* but rather from a disruption in neurovascular crosstalk between these neurons and the vasculature, as neurons seem to play an active role in maintaining the latter in a healthy state.
- This works identifies NVUs in locations where they had never been described before, namely in the IPL and OPL. These NVUs are composed by amacrine cells, horizontal cells and their respective retinal vascular plexus layer (intermediate and deep). Additionally, it reveals a critical role for amacrine cells and their HIF-1α/VEGF-A response in (1) retinal vascular development; and (2) vascular maintenance of the intermediate plexus (in the adult retina), which is essential for ensuring adequate visual function.

- This chapter also identifies a new angiogenic pathway in the retina, and describes NVUs in the outer retina along with an active role for PRs in retinal neurovascular crosstalk; it shows that cone photoreceptors are able to produce factors to maintain retinal vasculature in a healthy state, therefore ensuring their own nourishment and adequate functionality of the outer retina (neuroprotection).

- Implications for DR management:

    - These findings suggest that therapies for DR must be implemented **early in the disease** process **to stabilize crosstalk within the NVU**, for example, by enhancing photoreceptor or amacrine cell production of endogenous, protective factors that maintain a healthy vasculature, which in turn ensures adequate nourishment of retinal neurons. Acting early to reinforce endogenous processes and to restore harmonious interactions within the NVU (rather than late using destructive and indiscriminate therapeutic procedures) could determine better retinal and visual outcomes in patients with DR.
    - The strongest dysregulation in angiogenin levels was observed in PDR and DME patients. For now the meaning of these alterations remains unclear, however further work assessing if enhancement of angiogenin levels early in the disease process, or their blockade at late stages could improve the characteristic pathological changes seen in human DR would be of interest.

B. The Metabolic Landscape of Proliferative Diabetic Retinopathy

Rationale for conducting this study

- PDR, the late stage of DR, is a leading cause of blindness in adults below the age of 65 in industrialized countries
- Current therapies for DR are not ideal because they are unable to prevent progression into PDR in a sustainable fashion in every diabetic patient, and also because they present concerning adverse effects:

  A) Laser photocoagulation is effective in preventing development of PDR but only in approximately 50% of cases; it is, however, a destructive procedure that kills peripheral retinal cells in order to maintain those responsible for central vision.
  B) Intravitreal injections of anti-VEGF agents produce remarkable neovascular regression in eyes affected with PDR but these effects are only temporary, thus requiring repeated injections to maintain such results; furthermore, these agents may enhance local neurodegeneration, as VEGF is also a neurotrophic factor, and induce adverse cardiovascular and renal events.

- There are no specific biomarkers to accurately monitor risk of developing PDR (the only currently validated biomarker to predict risk of developing diabetic complications is HbA1c; however, adequate glycemic control is not clearly correlated with protection, as described in the next chapters).
- For all of the above, identification of novel druggable targets and biomarkers is crucial to effectively prevent disease progression into late, irreversible stages
- Since metabolites have been shown to mediate retinal neurovascular crosstalk, disrupted interactions within the NVU are expected to be expressed as local metabolic dysregulation.

- Attaining a global overview of metabolic dysregulation in PDR will provide important cues regarding the most affected biochemical pathways, revealing potential therapeutic targets and metabolic biomarkers

➢ L.P.P. designed the research plan, prepared the animals, performed intraocular injections (assisted by EA) and eyeball extractions, analyzed the clinical data and organized both the scientific and clinical data for the manuscript; the LC/MS experiments and MS data analysis were performed in collaboration with Prof. Siuzdak's laboratory at TSRI, by C.H.J, L.T and H.P.B.

B.1. In vivo global Isotope Metabolomic Analysis implicates the Arginine-to-Proline Pathway in Ischemic Retinopathy

Background and significance

Diabetic retinopathy (DR) is the leading cause of vision loss in adults aged 20 to 65 years [27] and meta-analyses of large-scale studies have shown that this diabetic complication is quite common, as approximately one third of the diabetic population will develop DR to some extent, and approximately one third of those (or 10% of the whole diabetic population) will progress to its vision-threatening stages - PDR and diabetic macular edema (DME)[1,69]. Prevention strategies focusing on early screening and optimization of metabolic control have been implemented, and have moderately improved the outlook for patients in many countries. Nevertheless they have proved to be insufficient on their own to fully, and efficiently, arrest DR progression towards late stage disease[68]. Proliferative diabetic retinopathy (PDR), the most advanced stage of DR, is especially concerning. It is commonly associated with diabetic macular edema (DME), the main cause of vision impairment in diabetic patients[27]), and can lead to vitreous hemorrhage and tractional retinal detachment, which constitute important causes of blindness in diabetic patients [220]. In addition, the current therapeutic strategies (laser photocoagulation and anti-VEGF intraocular injections) are untargeted, act late, and are not able to curtail disease progression in a sustainable and effective manner for every patient. Moreover, concerns regarding safety issues with anti-VEGF agents have been raised at the ocular (choroidal vasculature and photoreceptors) and systemic levels (renal and cardiovascular effects) [2,83,221].

Incomplete understanding of the pathophysiology of DR is exacerbated by the absence of an *in vivo* diabetic rodent model that fully recapitulates the disease. As rodent models of diabetes do not spontaneously develop pre-retinal neovascularization, the oxygen-induced-retinopathy (OIR) mouse model is frequently used in studies of neovascular retinal disease such as PDR [54,222]. The OIR model resembles retinopathy of prematurity (ROP) by developing regions

of vascular obliteration and pathological neovascularization after a five-day exposure to a hyperoxic environment, which arrests physiologic retinal vascular development. These retinal findings resemble those seen in human PDR.

Metabolites are the biological products of genomic and proteomic perturbations, and also result from environmental (e.g., diet, disease) and microbial influences. Metabolomic analysis is the unbiased survey of all metabolites within a sample, and can thus reveal biologically relevant changes within a system. Previous metabolomic studies performed in pre-diabetic and type 2 diabetic patients revealed that amino-acid and lipid concentration changes can be used as biomarkers for identifying patients at risk, and also for monitoring disease progression and therapeutic efficacy [223]. Indeed, unraveling major metabolic changes in the vitreous of PDR patients has the potential to reveal novel targets for the development of more effective therapeutic strategies to treat patients with diabetic eye disease. Our global (untargeted) and highly sensitive targeted mass spectrometry (MS)-based metabolomic workflows allow for a comprehensive coverage of the metabolome [224]. Furthermore, novel technologies such as stable isotope global metabolomics enable the incorporation of a labeled metabolite to be tracked in an unbiased manner through metabolic pathways [225]. Although reproducibility is a concern in metabolomics, especially when translation into the clinic is being considered, the high number of clinical and mouse samples available in our study has allowed for multiple opportunities for validation, enhancing the robustness and reliability of the data.

In this study, a global and highly sensitive mass-spectrometry (MS)-based approach was used to generate and validate a metabolomic profile of (1) human vitreous samples from two separate patient sample sets (controls and patients with PDR); and (2) eyes from a rodent model of ischemic retinopathy that shares characteristics with PDR (the OIR model). Furthermore, isotopic global metabolomic analysis carried out here for the first time *in vivo*, in the eye, revealed a role for the arginine-to-proline pathway in OIR. Simultaneously, we reiterated the validity of the OIR mouse model for therapeutic studies regarding PDR by demonstrating shared metabolic dysregulation with the human disease, despite differences in the pathological trigger. An overview of our metabolomic workflow can be seen in **Figure 38.** These novel metabolic findings will pave the way

towards identification of new disease biomarkers, discovery of new druggable targets and development of more effective therapeutic algorithms.

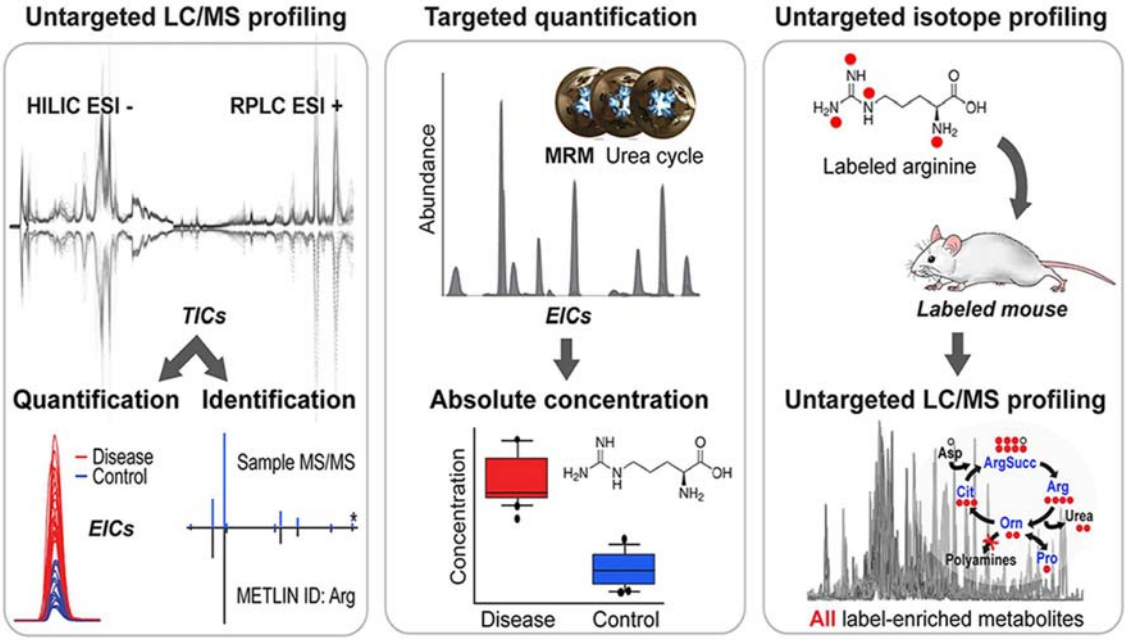

Figure 38 - Metabolomic workflow. Samples initially undergo untargeted quadrupole time-of-flight mass spectrometry (QTOF-MS) metabolomics by hydrophilic interaction and reversed-phase liquid chromatography (HILIC and RPLC) to obtain a comprehensive coverage of the metabolome. Metabolites are identified using the statistical software XCMS Online and the METLIN database. Tandem MS is carried out to verify the metabolite identification. The metabolites of interest are further validated through multiple reaction monitoring by triple quadrupole (QqQ)-MS with authentic standards, and absolute concentrations obtained. Isotopes of metabolites correlated to pathogenesis are introduced into the model system and their transformation observed by global metabolomics. The role of these metabolites in metabolic pathways can thus be elucidated.

Results

Global metabolomics revealed a clear distinction between PDR and control vitreous human samples

Global metabolomic analysis by RPLC-MS (Reverse-Phase Liquid Chromatography) and HILIC-MS (Hydrophilic Interaction Liquid Chromatography) provided a comprehensive coverage of the non-polar and polar metabolome, respectively. The analyses performed on the first set of human vitreous samples revealed clear dysregulation (meaning differential regulation) between vitreous samples from non-diabetic controls (n=10) and patients with PDR (n=7). The general metabolic dysregulation between the two patient groups can be seen on **Figure 39** and **Figure 40**.

RPLC-MS analysis revealed 106 features that were significantly dysregulated ($p<0.01$, fold change >2) from a total of 3117 aligned features (**Figure 41A**). Of these features, a number were adducts and fragment ions. A q-value threshold of <0.05 was used to remove any p-values (up to a 95 % confidence) that could have been false positives. The metabolites that were positively identified by tandem MS with comparison to authentic standards included the following metabolites, which were upregulated in PDR samples: octanoylcarnitine (fold change 5.4, p=0.005, q=0.01) and propionylcarnitine (fold change 2.1, p=0.007, q=0.02). Other carnitines mined for in the feature tables that had higher p-values than 0.01 were similarly dysregulated hexanoylcarnitine (fold change 5.2, p=0.012, q=0.01), acetylcarnitine (fold change 1.5, p=0.012, q=0.02), palmitoylcarnitine (fold change 3.8, p=0.038, q=0.04) and elaidic/vaccenylcarnitine (fold change 4.9, p=0.035, q=0.04). HILIC-MS analysis revealed 61 dysregulated features from a total of 1910 total aligned features (**Figure 41B)**. The features that were positively identified and upregulated in the PDR samples included allantoin (fold change 4.0, p=0.006, q=0.03), glutamate (fold change 3.2, p=0.0002, q=0.008), lysine (fold change 1.7, p=0.004, q=0.03), and arginine (fold change 2.1, p=0.005, q=0.03). A second sample set of non-diabetic controls (n=16) and PDR (n=10) samples was obtained, which allowed us to observe the specificity of the metabolites. The RPLC-MS metabolomic analysis did not show dysregulation to the acylcarnitines and only revealed 30 dysregulated features, from a total of 6834 aligned features,

this low number of dysregulated features (0.4%) shows that with a p-value threshold of 0.01 these are most likely random. Humans have high interindividual variation, and carnitine metabolism in particular, is dependent on diet and other factors; and perturbations in carnitine metabolism have low specificity as they are identified in a wide spectrum of diseases; therefore it was not surprising to see these results in the 2nd set of patient samples. However the HILIC-MS analysis showed 129 dysregulated features from a total of 7827 aligned features and again revealed an upregulation to allantoin (fold change 1.9, p=0.001, q=0.007), glutamate (fold change 2.8, p=0.0001, q=0.02), lysine (fold change 2.1, p=0.001, q=0.02), and arginine (fold change 1.6, p=0.002, q=0.04) in patient PDR samples. In this 2nd set of samples HILIC-MS also showed a number of metabolites downregulated in the PDR samples, N-acetylaspartate (fold change 2.3, p=0.0006, q=0.02), iditol (fold change 2.0, p=0.002, q=0.03), glycerate (fold change 1.8, p=0.002, q=0.04) and N-acetylglutamate (fold change 1.8, p=0.0004, q=0.02). These metabolites were confirmed through tandem MS to standards. In addition, these downregulated metabolites were mined for in the feature table from the first set of samples but they were not dysregulated.

Having two sets of human samples from non-diabetic controls and patients with PDR has been invaluable to show the specificity of these biomarkers to this disease. Some metabolites were perturbed in both, while some were specific to just one set.

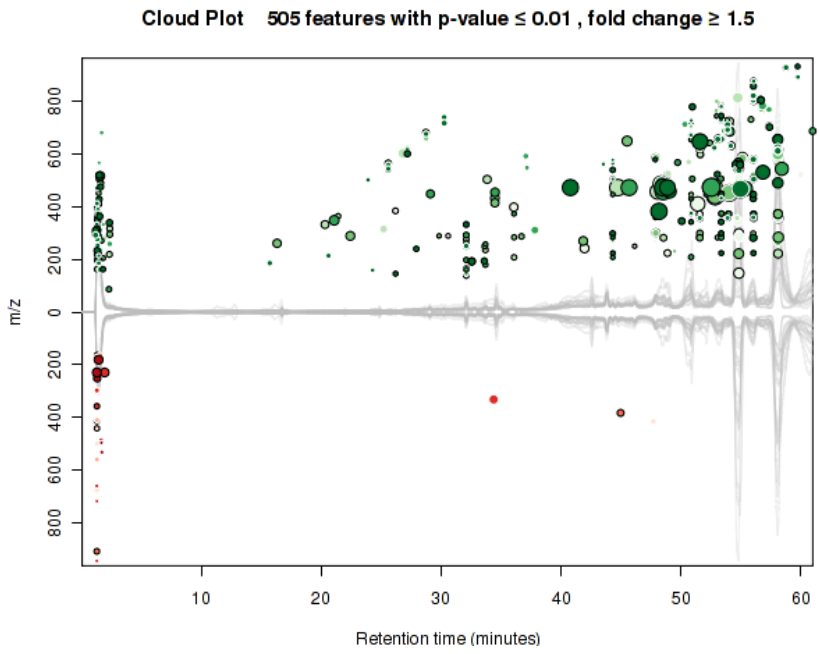

Figure 39 – Global liquid chromatography quadrupole time-of-flight mass spectrometry (LC-QTOFMS) metabolomics. Cloud plots generated by XCMS Online representing all dysregulated features between control and PDR samples (two-tailed Mann-Whitney test; p value $\leq$ 0.01; fold change $\geq$ 1.5). Green dots represent upregulated metabolites and red dots represent downregulated metabolites in PDR samples.

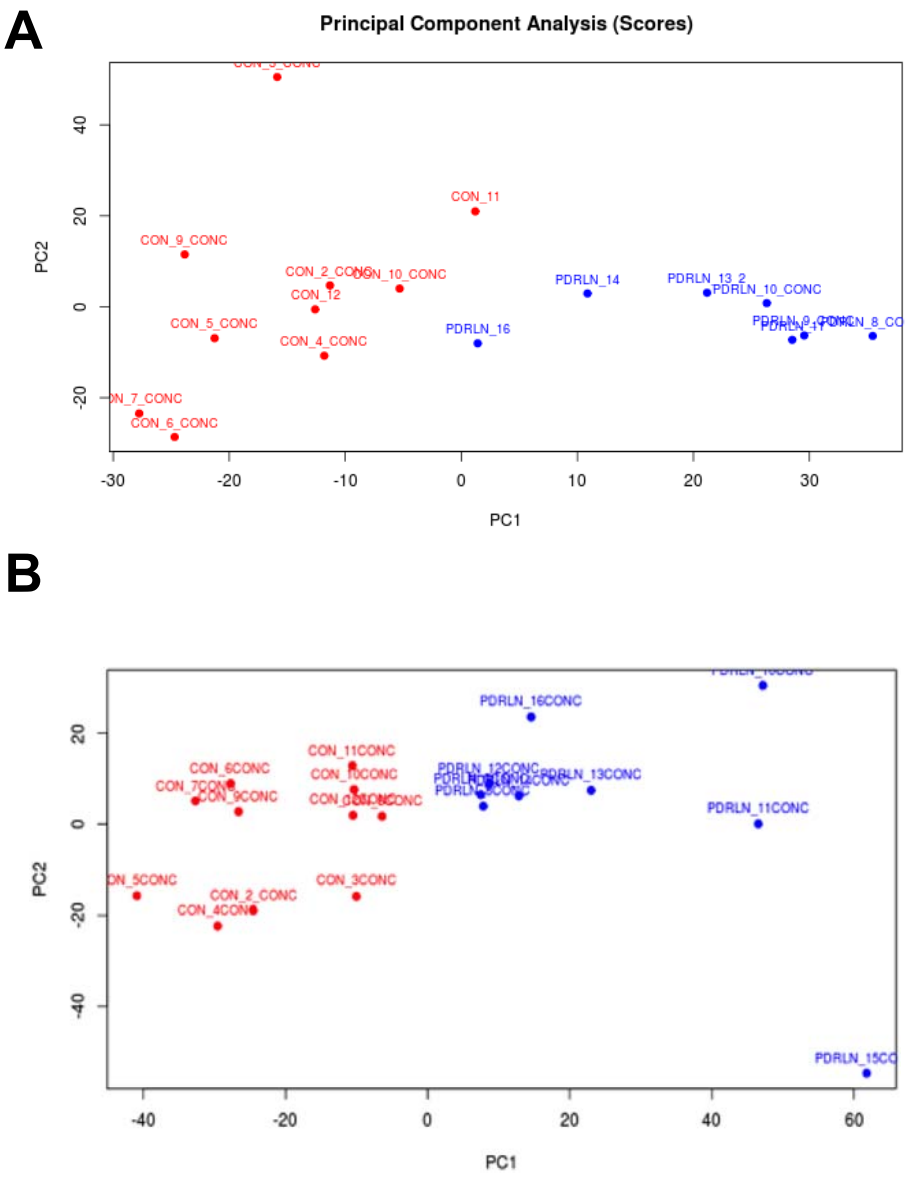

Figure 40 - Principal component analysis (PCA) reveals a clear demarcation between vitreous samples from PDR patients (blue) and non-diabetic controls (red); (A) First set of human vitreous samples; (B) Second set of human vitreous samples.

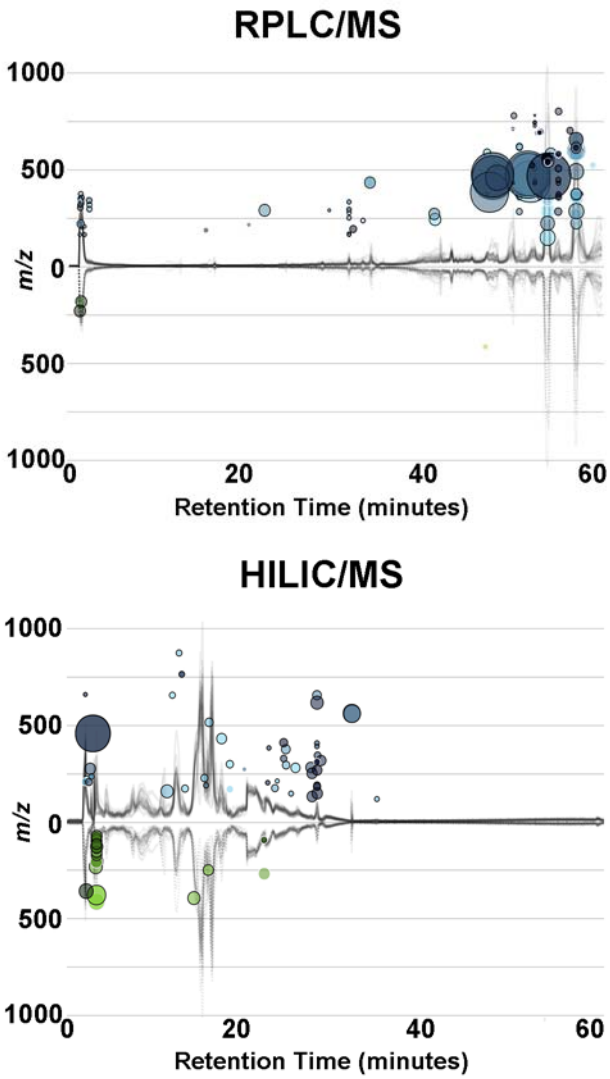

Figure 41 - Global liquid chromatography quadrupole time-of-flight mass spectrometry (LC-QTOFMS) metabolomics. Cloud plots generated by XCMS Online showing dysregulated features between control (n=27) and PDR (n= 17) samples (two-tailed Mann-Whitney test) for (A) RPLC-MS analysis and (B) HILIC-MS analysis. Total ion chromatograms (TICs) for each sample can be seen on the plot; features whose intensity are increased in PDR vitreous are shown on the upper part of the plot as blue circles and features whose intensity decreases are shown on the bottom part of the plot as green circles. Larger and brighter circles (features) correspond to larger fold changes and lower *p*-values respectively.

Untargeted metabolomics by QTOF-MS can reveal thousands of features, many novel to the disease, however specificity can be more challenging with human sample analysis due to interindividual variation providing lower p-values. In addition, QTOF-MS analysis is not as quantitative as targeted triple quadrupole (QqQ)-MS analysis due to coeluting ions and detector saturation, and when fold

changes are subtle (in the range of 1-2.5) it is difficult to assess specificity. Thus, we next sought to validate our findings using targeted analysis to quantify the concentrations of these metabolites. As well as targeting the metabolites dysregulated in both sample sets, we expanded the targeted analysis to include metabolites from related metabolic pathways, to determine the biological relevance of our findings. These pathways included those related to acylcarnitine and amino acid metabolism (aconitate, fumarate, succinate, glutamine, pantothenate, proline, citrate), nitrogen disposal (citrulline, ornithine) and purine metabolism-related oxidative stress (AMP, ATP, adenosine, inosine, IMP, hypoxanthine, xanthine). Targeted analysis was thus carried out using authentic standards to obtain accurate fold changes of the metabolites in the extracted samples. It was confirmed that arginine and allantoin, metabolites seen in both sets of samples were upregulated in PDR, however lysine and glutamate were not changed. Many of the metabolites targeted were below the limit of detection in the samples, but an upregulation in octanoylcarnitine could also be confirmed in both sample sets, and further dysregulation was seen in proline, citrulline, methionine and ornithine along with decanoylcarnitine, which were all significantly upregulated in the samples from PDR patients **Figure 42A**. The most prominent metabolic perturbations, however, pertained to arginine-to-proline metabolism and suggested a preferential activity in pathways leading to proline production (namely the arginase pathway). A summary of the targeted analysis for both sets of human samples can be seen in **Table 8.**

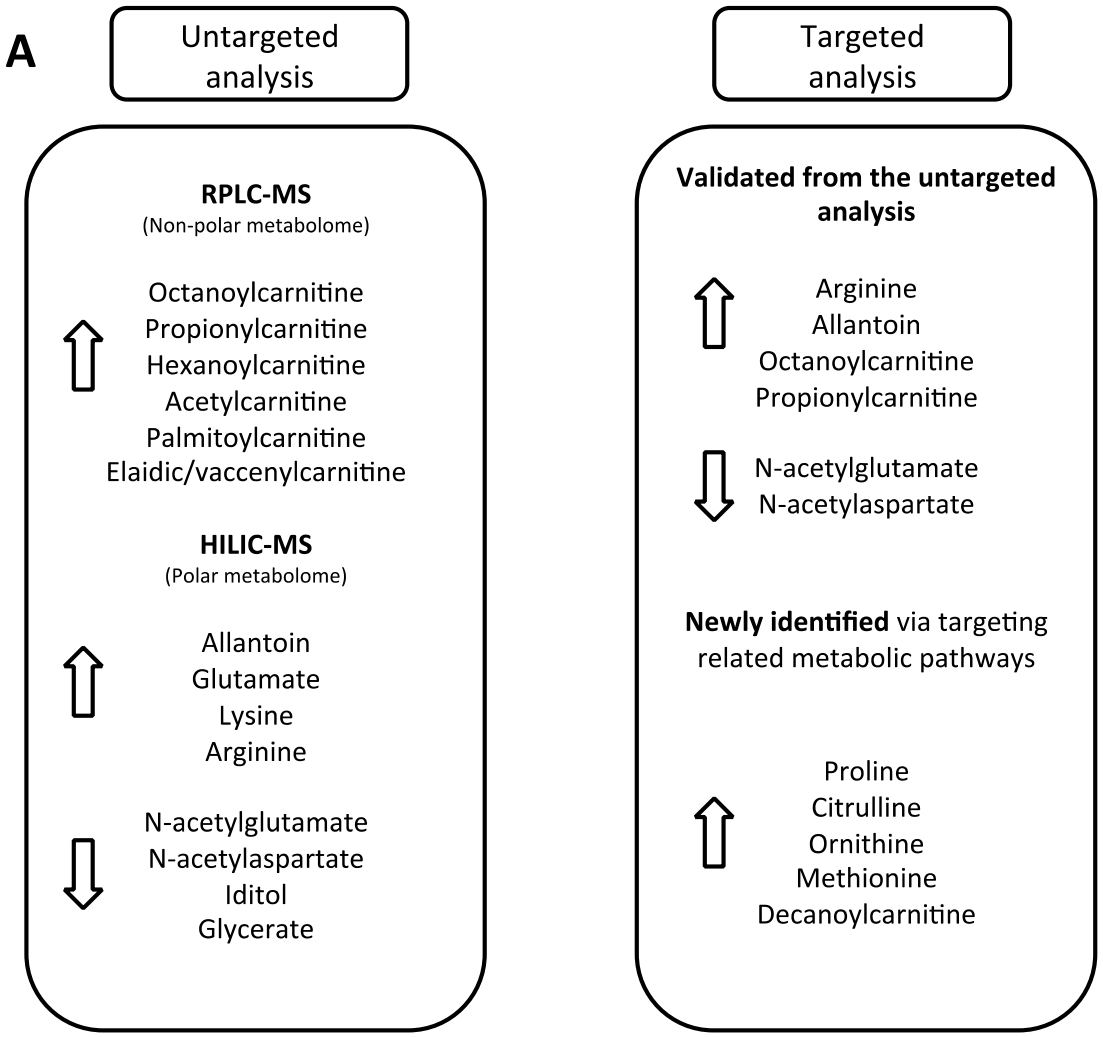
A
Untargeted analysis
RPLC-MS
(Non-polar metabolome)
Octanoylcarnitine
Propionylcarnitine
Hexanoylcarnitine
Acetylcarnitine
Palmitoylcarnitine
Elaidic/vaccenylcarnitine
HILIC-MS
(Polar metabolome)
Allantoin
Glutamate
Lysine
Arginine
N-acetylglutamate
N-acetylaspartate
Iditol
Glycerate
Targeted analysis
Validated from the untargeted analysis
Arginine
Allantoin
Octanoylcarnitine
Propionylcarnitine
N-acetylglutamate
N-acetylaspartate
Newly identified via targeting related metabolic pathways
Proline
Citrulline
Ornithine
Methionine
Decanoylcarnitine

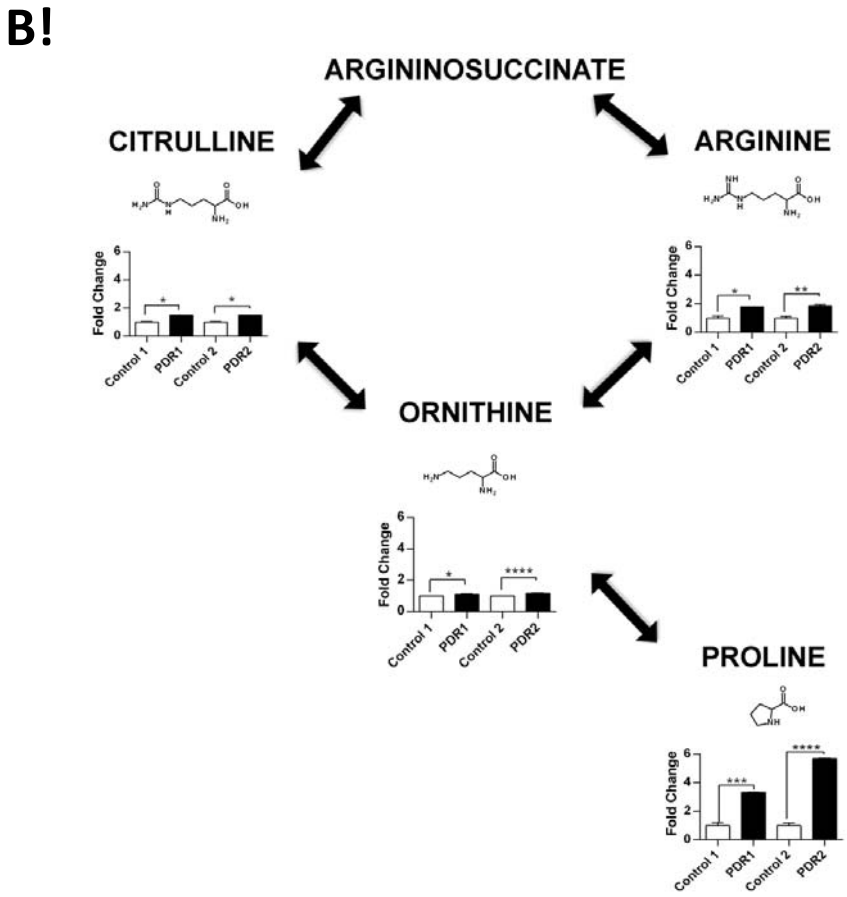

Figure 42- Significant metabolic perturbations identified in human PDR vitreous samples. (A) A summary of the metabolic perturbations identified during global and targeted metabolomic analyses on vitreous human samples from diabetic patients with PDR and non-diabetic controls; These analyses confirmed upreregulation of arginine, allantoin, proline, citrulline, ornithine, methionine, octanoylcarnitine and decanoylcarnitine in PDR samples (for fold changes and p-values please see table 8); (B) The arginine-to-proline pathway shows the highest number of metabolic perturbations in this disease. Fold changes of each metabolite in PDR samples are shown compared to control * = p≤0.05, ** = p≤0.01, *** = p≤0.001,****= p≤0.0001; error bars represent standard deviation

Table 8 – Dysregulated metabolites confirmed by targeted MS analysis in two sets of vitreous samples from PDR patients, and in OIR mouse eyes at P17.

	Human PDR				OIR P17 mouse	
	First set		Second set		OIR	
Metabolite	**Fold change**	**p-value**	**Fold change**	**p-value**	**Fold change**	**p-value**
+Methionine	1.7	0.0387	3.0	0.0002	1.1	0.6436
+Allantoin	2.5	0.0003	1.7	0.0081	1.4	0.2349
+Decanoylcarnitine	1.7	0.0028	1.4	0.0054	Below limit of detection	
+*Arginine	1.8	0.0387	1.9	0.0081	2.2	0.0109
+*Proline	3.3	0.0003	5.7	<0.0001	5.0	0.0002
+*Citrulline	1.5	0.0201	1.5	0.0211	2.0	0.0003
+*Ornithine	1.1	0.0346	1.2	<0.0001	1.3	0.0084
+*Octanoylcarnitine	2.2	0.0200	1.7	0.0005	3.0	0.0004
*Lysine	1.3	0.0573	1.1	0.2383	1.5	0.0024
*Succinate	1.4	0.6180	1.3	0.8580	-1.6	0.0226
*Pantothenate	Below limit of detection				1.7	0.0175
*AMP	Below limit of detection				-1.4	0.0477
*Hypoxanthine	1.4	0.0573	1.4	0.2542	-3.4	<0.0001
*Xanthine	Below limit of detection				-1.9	0.0017
*Inosine	Below limit of detection				-2.8	<0.0001
*+Propionylcarnitine	5.4	0.005	Below limit of detection		86.4	0.0480
*Acetylcarnitine	Below limit of detection				2.0	<0.0001

+ Statistically significant dysregulation in human PDR
* Statistically significant dysregulation in the OIR mouse

Clinical characteristics of the patients with PDR

In order to provide clinical context to the metabolic perturbations observed in PDR, the 17 diabetic study subjects (1:8=M:F ratio) underwent comprehensive clinical evaluation (medical and ophthalmological history, and laboratory work-up). This information is present in **Table 9** and **Table 10**.

All study subjects were type 2 diabetics for an average of 26 years and their average HbA1c values were 7.52%. Their best-corrected visual acuity (BCVA) ranged from hand motion (HM) to 0.6 (20/33); intraocular pressure (IOP) ranged from 7 mmHg to 24 mmHg. Fifty-three percent (53%) of the patients had developed PDR despite laser photocoagulation, which had been complete in 89% of the cases. Regarding diabetes-related systemic complications (reported on the patients' clinical files), 41% did not have any complications other than DR, 12% had isolated diabetic nephropathy, 18% had isolated diabetic neuropathy and 29% had both nephropathy and neuropathy.

Table 9 – General clinical features of the patients with PDR

Age/gender	DM	DM duration	HbA1c	Ins vs OAD	BP	Cr serum	eGFR	LDL	BMI
54 F	2	10 y	10.3	1,2	113/72	1.19	52	136	17.7
67 F	2	15 y	9.2	1,2	152/70	0.78	79	N/A	21.5
51 M	2	2 y	10.9	1,2	126/90	0.77	105	N/A	31
69 M	2	24 y	6.9	1,2	148/80	0.97	79	104	22
42 F	2	8 y	6.8	1,2	110/64	0.58	114	N/A	26.1
42 F	2	8 y	6.8	1,2	127/75	0.58	114	N/A	26.1
61 M	2	6Y	6.2	2	180/80	1.48	50	N/A	23
75 M	2	2 y	7.6	2	114/58	0.69	93	N/A	23.6
62 M	2	24 y	6.7	1	148/93	0.82	95	181	30.8
61 M	2	20 y	6.6	2	143/83	0.71	101	N/A	25.9
40 M	2	20 y	5.3	1	140/81	1.82	45	101	29.9
65 F	2	9 y	7.5	2	186/86	2.65	18	165	27.9
48 M	2	15 y	9.1	1	105/61	1.1	79	N/A	24.9
35 M	2	10 y	8.5	1	157/107	0.83	114	139	21.2
65 F	2	10 y	6.8	2	152/55	0.56	98	N/A	24.9
68 M	2	24 y	5.7	1	171/76	2.82	22	101	23
58 M	2	15 y	6.9	2	105/61	0.71	103	81	24.9

DM = diabetes mellitus; DM duration: y = years; HbA1c = glycated hemoglobin (optimal value < 6.5 -7%); Ins = insulin; OAD = oral antidiabetics (1 = insulin; 2 = oral anti-diabetics); BP = blood pressure (mmHg; optimal BP for diabetics <130/80 mmHg); Cr serum (mg/dl) = serum creatinine (reference values: 0.5 – 1.5 (males); 0.6 – 1.2 (females)); eGFR = estimated glomerular filtration rate in ml/min/1.73m^2 (CKD-EPI equation 2009; stage 1: >90 with evidence of kidney damage; stage 2: 60-90; stage 3: 30-60; stage 4: 15-30; stage 5: <15); LDL = serum low density lipoprotein levels (mg/dl; optimal for diabetics <70 mg/dl); BMI = body mass index (kg/m^2): underweight< 18.5; normal 18.5 – 24.99; overweight >25; obese > 30; N/A = not available.

Table 10 – Ophthalmological characteristics of the patients with PDR

Age/gender	BCVA	PC	IOP mmHg	Anti-VEGF	IO CS	Other DM complications
54 F	HM	Complete	10	2	2	DNP, DN
67 F	0.02	Complete	13	2	2	DN
51 M	HM	Complete	15	2	2	DN
69 M	0.03	Complete	20	2	2	DNP, DN
42 F	0.04	0	24	2	2	0
42 F	0.03	0	18	2	2	0
61 M	HM	Complete	16	2	2	DN
75 M	0.5	0	14	2	2	0
62 M	0.2	0	14	2	2	DNP
61 M	0.6	Complete	11	2	2	0
40 M	0.03	Complete	10.7	2	2	DNP, DN
65 F	0.07	0	16	2	2	0
48 M	0.4	0	15	2	2	DNP
35 M	HM	0	15	2	2	DNP, DN
65 F	0.08	Partial	11	2	2	0
68 M	0.04	0	10	2	2	DNP, DN
58 M	HM	Complete	7	2	2	0

BCVA – best corrected visual acuity (Range: light perception < HM (hand motion) < counting fingers < clinical optotypes on a chart); PC – photocoagulation (complete, parcial, 0 = none); IOP - intraocular pressure (reference values: 10 – 20 mmHg); Anti-VEGF = Prior Anti-VEGF treatment (1 = yes; 2 = no); IO CS = previous administration of intraocular steroids (1 = yes; 2 = no); DN - diabetic nephropathy; DNP - diabetic neuropathy.

The OIR mouse mimics human PDR metabolic dysregulation

Since the OIR mouse model spontaneously develops several pathological retinal features that are also observed in PDR, (e.g., retinal ischemia, pre-retinal neovascularization and profound neurodegeneration), global and targeted metabolomic analyses were performed on ocular samples from these mice to identify and validate their metabolic profile at the time of maximal pre-retinal neovascularization (17 days of age, P17). We compared whole eyes extracted from OIR mice and from ge-matched controls raised in ambient oxygen and found that metabolites involved in the arginine pathway/urea cycle (arginine, proline, citrulline and ornithine) and in beta-oxidation (octanoylcarnitine) were similarly dysregulated to what had been observed in clinical samples from PDR patients (**Table 8**).

In the OIR mouse model methionine and allantoin were not dysregulated, but lysine, pantothenate and succinate were increased, when compared to controls. Furthermore, a downregulation in several metabolites involved in purine metabolism pathways was also identified in the OIR model, with dysregulated levels of adenosine monophosphate (AMP), inosine, hypoxanthine and xanthine.

To further understand how these metabolic alterations develop over the hypoxic period (from P12 until P17) in the OIR mouse, global metabolomic analyses were carried out on ocular samples collected at P12, P14 and P17. They were compared to those of age-matched controls raised in ambient oxygen (normoxia - NOX).

Pantothenate was increased with fold changes of 1.6 ($p=0.0154$, $q=0.3746$, at P12) and 2.0 ($p=0.009$, $q=0.1909$, at P14). Proline, arginine and lysine were increased from P14 onwards with fold changes of 3.1 ($p=0.0000009$, $q=0.0006$), 2.3 ($p=0.0164$, $q=0.2356$), and 2.7 ($p=0.0017$, $q=0.1175$), respectively, while at P17 they were increased 3.1 ($p=0.0049$, $q=0.1537$), 3.1 ($p=0.009$, $q=0.1596$) and 2.1 ($p=0.0398$, $q=0.1764$) respectively (the q-values are out of the ideal threshold of 0.05, however the p-values are very low and indicate a trend for these metabolites).

Arginine metabolism and ammonia detoxification are similarly dysregulated in human PDR and in the OIR mouse.

Pathway enrichment analysis was performed for the metabolites dysregulated in the OIR mouse and human PDR samples using the MetaboAnalyst program [226]. The analysis revealed that arginine metabolism and ammonia detoxification (urea cycle) were two of the most perturbed pathways in both species for the conditions under study, being dysregulated to a similar magnitude (**Figure 43**). This adds to a growing body of evidence suggesting that Mueller glial cell metabolism is particularly compromised in diabetic retinopathy and that this disrupts neurovascular crosstalk within the retina, thus promoting disease progression [227,228].

Fatty acid oxidation was also disturbed both in the OIR mouse and in human PDR as a result of dysregulated acylcarnitines; however, the fatty acid oxidation pathway was not sufficiently enriched in the pathway enrichment analyst for human PDR due to an incomplete reference metabolite dataset for this pathway. In the OIR mouse eye, there was an additional compromise in purine metabolism revealed by a significant downregulation of AMP, inosine, hypoxanthine and xanthine.

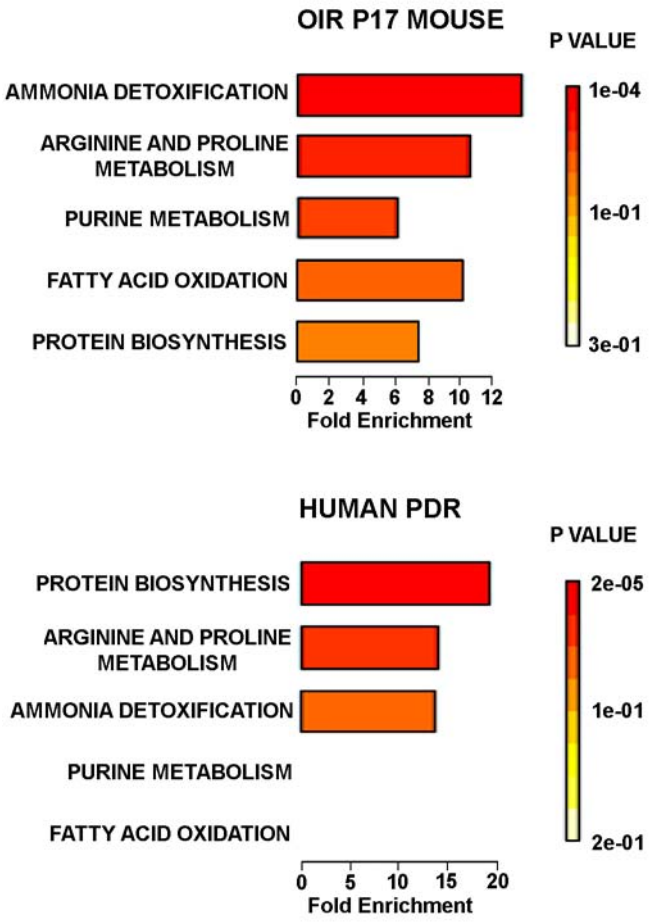

Figure 43 - Metabolite Set Enrichment Analysis. Arginine metabolism and urea cycle (ammonia disposal) pathways are the most significantly affected both in (*A*) Human PDR (4 dysregulated features out of 26 (4/26), False discovery rate (FDR) p value = 0.00353; and 3/20, FDR = 0.0249, respectively) and in the (*B*) OIR P17 mouse (4/26, FDR=0.0184; and 4/20, FDR = 0.0126).

Arginine is metabolized to proline and argininosuccinate in the OIR mouse eye.

Ornithine, proline and citrulline, which are dysregulated in the OIR mouse eye at P17, can be generated from arginine *via* the arginase or the nitric oxide synthase (NOS) pathway. Overexpression and excessive activity of the arginase pathway in the diabetic rodent retina has been implicated in vascular endothelial cell dysfunction, *via* reduced activity in the NOS pathway[229]. This is concomitant with increased peroxynitrite formation, increased formation of polyamines and proline, which induce cellular proliferation and fibrosis[229]. Arginase overactivity has also been described in the OIR model, where it contributes to hyperoxia-

induced retinal neurodegeneration, *via* upregulation of polyamine synthesis, and retinal microvascular dropout *via* increased oxidative stress [230,231].

To gain further insight into arginine metabolism in the OIR eye and better understand the observed metabolic dysregulation, global isotope metabolomic studies were performed *in vivo*, in the OIR mouse model. This is the first time this type of study has been performed *in vivo* in the eye. U-^{15}N-arginine, natural-abundance arginine and vehicle (PBS) were injected intravitreally, and the metabolites analyzed by global MS analyses ten minutes post-injection. Both pairwise and multigroup analyses were used to compare vehicle, U-^{15}N-arginine and natural-abundance arginine OIR P17 extracts by X^{13}CMS [225]. It was seen that U-^{15}N-arginine (*m/z* 179.1055 $[M+H]^+$) was converted into U-^{15}N-argininosuccinate (*m/z* 293.1044 $[M-H]^-$), U-^{15}N-ornithine (*m/z* 133.0772 $[M-H]^-$), and U-^{15}N-proline (m/z 117.0682 $[M+H]^+$), suggesting predominant activity in the arginase-to-proline pathway. Tandem MS can be seen for natural abundance and U-^{15}-metabolite for proline and argininosuccinate on **Figure 44** Mass isotopomer distributions (MIDs) can be seen for these metabolites on **Figure 45**. We also saw production of another potential isotopomer of argininosuccinate with *m/z* 294.1214 $[M+H]^+$. This isotopomer was not seen in negative mode. At present the identification of this metabolite is not known as the abundance was below the limit of detection for tandem MS. Polyamine synthesis was not dysregulated following arginine injections, suggesting that in OIR conditions, at P17, proline plays a more relevant role for generation of the retinal pathological phenotype **Figure 45**. Beyond promoting production of the extracellular matrix component collagen, proline can also be metabolized by proline oxidase to generate: (1) ATP, which can help sustain endothelial cell proliferation; (2) or reactive oxygen species that may contribute to further retinal damage [232]. Citrulline, another key metabolite in arginine metabolism could not be identified following U-^{15}N-arginine injection. This could be due to very low abundance or fast conversion through this intermediate. Given that U-^{15}N-argininosuccinate was identified it is possible that it was produced directly from arginine [233]; for argininosuccinate to be formed from citrulline, only two of its nitrogen atoms would be ^{15}N-labeled, and two would be natural abundance ^{14}N atoms having come from aspartate and carbamoyl phosphate.

In order to determine whether the metabolism of arginine was different in control mice housed in normoxia (NOX) conditions, we similarly injected U-^{15}N-arginine, natural-abundance arginine and vehicle (PBS) intravitreally, and analyzed the metabolites by global mass spectrometry analyses ten minutes post-injection. We observed the appearance of U-^{15}N-arginine, U-^{15}N argininosuccinate, U-^{15}N-ornithine and U-^{15}N-proline, and **Figure 45** shows the MIDs for these isotopomers. It is clear that in the OIR model U-^{15}N-arginine has a larger conversion to U-^{15}N-proline 9.8 %, compared to 1.0 % in the NOX model **Table 11**. This shows that arginine is metabolized to proline to a larger extent in the OIR mouse compared to the control NOX mice. In the NOX model there is a larger conversion to U-^{15}N-ornithine (37.8 % compared to 6.1 % in the OIR model). Due to limitations in experimental design (the experiments performed provide a snapshot at 10 minutes post injections and do not allow for a longitudinal evaluation of metabolic conversions), the fate of newly produced U-^{15}N-ornithine could not be further identified; however, future studies using flux analysis and follow-up of a larger number of mice over the span of a year will provide further information on metabolic conversions and dosage optimization.

Table 11 – Percentage of U-^{15}N-metabolite produced from U-^{15}N-arginine

	NOX	OIR
U-^{15}N-Arginine	58.8%	78.65%
U-^{15}N-Proline	1.03%	9.8%
U-^{15}N-Ornithine	37.8%	6.1%
U-^{15}N-Argininosuccinate	2.3%	5.4%

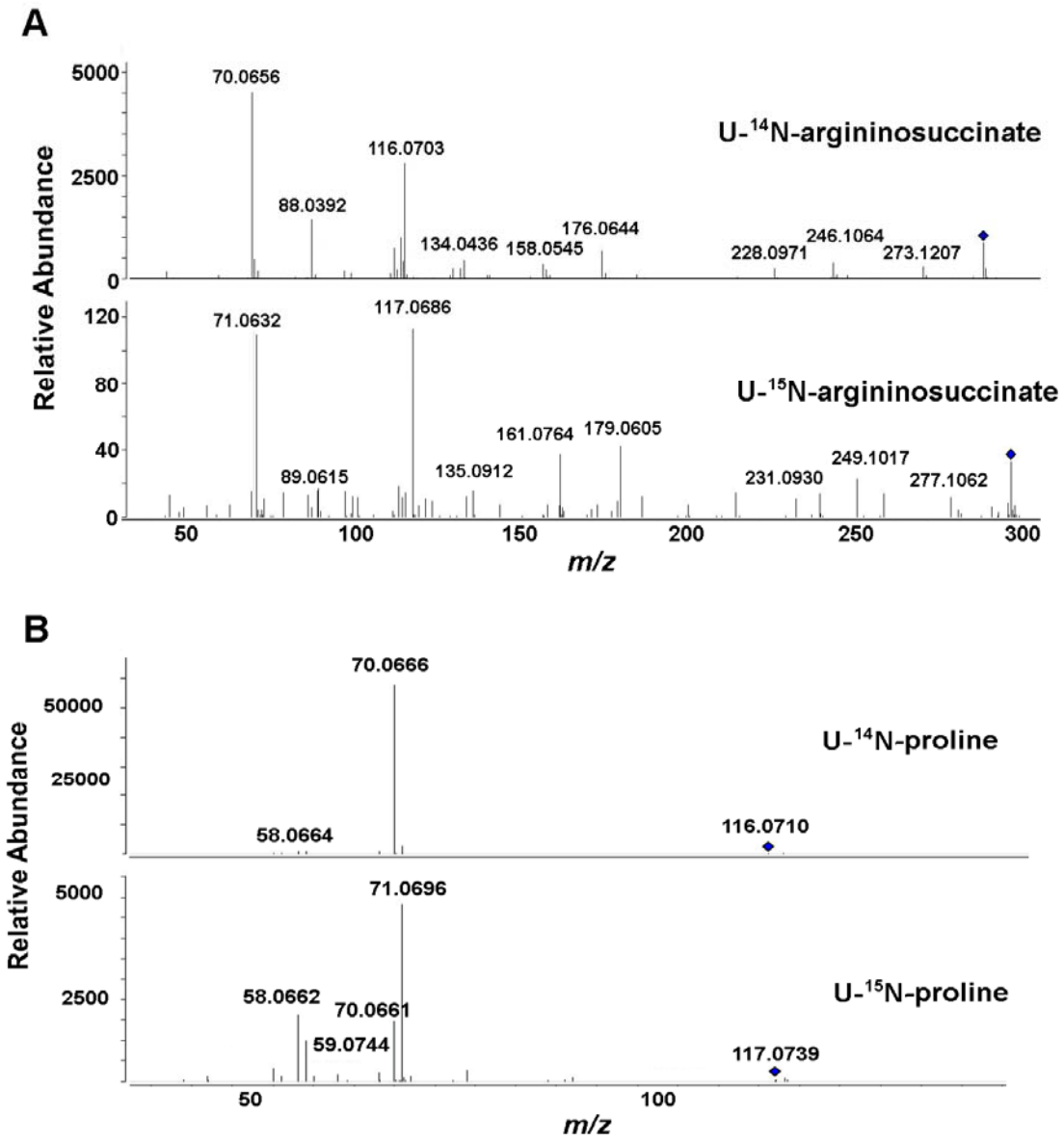

Figure 44 - Global stable isotope analyses with U-15N-arginine. (A) Tandem MS of natural abundance and U-15N-argininosuccinate and (B) natural abundance and U-15N proline.

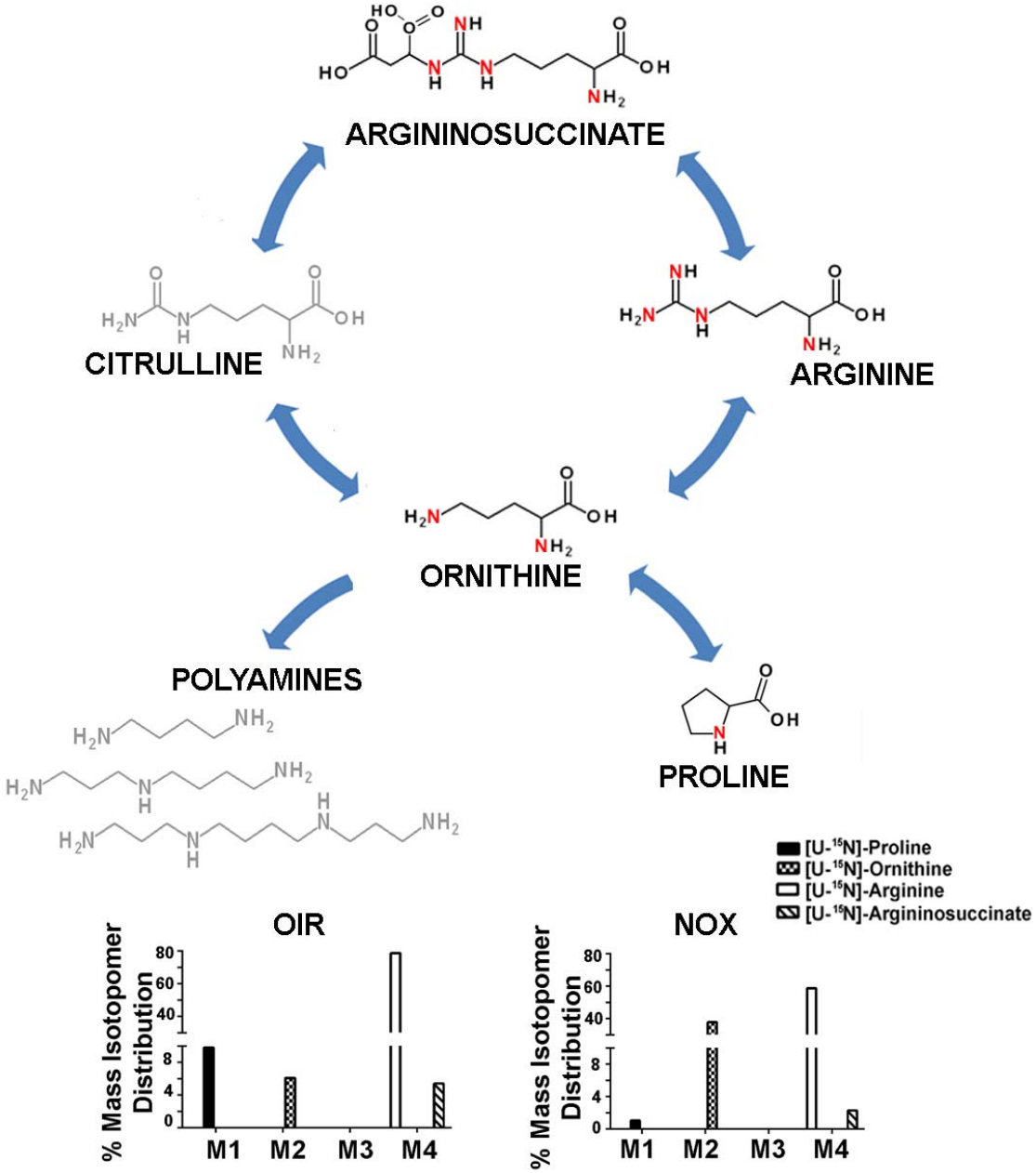

Figure 45 - Argininosuccinate, ornithine and proline are increased 10 minutes after intravitreal injection of U-^{15}N-arginine. Metabolites in gray were not detected. Mass isotopomer distributions (MID) corrected for natural stable-isotope abundance in oxygen induced retinopathy (OIR) and normoxia (NOX) mice.

Discussion

A better understanding of the pathophysiological processes occurring in PDR is necessary for improving patient care and for developing new and effective therapeutic strategies. Diabetes is a metabolic disease, an attribute that is highly amenable to MS-based metabolomic analysis. Here we were able to identify metabolic dysregulation in the vitreous humor of patients with PDR, which was further validated in a second set of patient samples. Furthermore we were able to observe similar metabolic perturbations in the eye of the OIR mouse model, which allowed us to then use novel global isotope metabolomics and pathway mapping tools to investigate the metabolic pathway changes that occurred.

One of the most prominently dysregulated pathways in PDR was arginine-to-proline metabolism, which has been widely studied in other diabetic tissues as well as in diabetic rodent models that recapitulate the early stages of DR [229,231,234]. Arginine and metabolites from the urea cycle also predominated in the eye extracts from the OIR mouse model. Two different pathways in the retina can metabolize arginine: the arginase pathway that produces ornithine and urea, and the NOS pathway, which generates citrulline and NO. Current knowledge suggests that the pathological features observed in diabetic rodent model retinas are caused by overactivity of the arginase II enzyme. This causes a shortage of arginine for the NOS pathway, resulting in lower availability of NO, endothelial cell dysfunction, and, consequently, impaired vasodilation[234]. It also causes NOS uncoupling with subsequently increased production of oxygen and nitrogen reactive species that contribute to further retinal damage[234]. Studies in the OIR model have also reiterated the detrimental effect of arginase II in the retina showing that transgenic models with a global genetic deletion of this enzyme are partially protected against development of hyperoxia-induced vascular obliteration and, thus, present reduced levels of preretinal neovascularization[235]. This beneficial effect has been attributed to normalization of NOS activity with consequent reduced production of reactive oxygen and nitrogen species, and higher NO availability.[235]

In vitreous samples from PDR patients, simultaneous upregulation of metabolites involved in both the arginase and the NOS pathway was observed (arginine, ornithine, proline and citrulline) but proline dysregulation was clearly the most

pronounced feature. This suggests that investigating the causes and mechanisms that lead to over-activity in the arginine-to-proline pathway in the diabetic eye may provide important clues for better understanding the pathophysiology of DR.

A similar metabolomic landscape was identified in the eye of the OIR mouse model at P17, further suggesting preferential activity in the arginine-to-proline pathway. The aim of our global isotope metabolomic analysis was thus to determine which pathways predominate (and to what extent) for arginine metabolism in the OIR mouse model, which could lead to a hypothesis regarding human PDR. The analysis revealed that proline, argininosuccinate and ornithine were formed after U-^{15}N-arginine injection, further validating the hypothesis that the arginase-to-proline pathway predominates over the NOS pathway.

Methionine metabolism was also compromised in PDR, which is in accordance with previous studies revealing high plasma levels of methionine in streptozotocin dosed rats [236] which inversely correlated with plasma insulin levels. Moreover, methionine plasma levels increased with exogenous insulin administration and progressively decreased after cessation of therapy, revealing its potential as a therapeutic biomarker. The concomitant upregulation of various amino acids in the vitreous of human PDR patients suggests a compromise in the metabolic capacity of the retina, pointing to a potential metabolic overload in Mueller cells, and raises concerns about potential amino acid toxicity and indiscriminate use of amino acid supplements by diabetic patients. Since the retina does not express all the enzymes involved in the urea cycle, it relies on Mueller glia for amino acid metabolism and ammonia disposal [237]. These cells play a very important supportive role in the retina and their proper functioning is crucial for maintenance of local neuronal and vascular health. It has been shown that local accumulation of ammonia in the retina, in hepatic retinopathy, results in ammonia-induced Mueller cell swelling [237,238], which leads to neuronal defects. Studies assessing extreme retinal remodeling in the context of retinal degeneration induced by light damage have also shown that arginine metabolism is profoundly affected and that it is temporally associated with evident phenotypic changes in Mueller glia [239]. Furthermore, the retina is a highly metabolically active tissue that strongly relies upon its local energy stores of creatine and phosphocreatine for adequate functioning [228]. Creatine is produced by Mueller glia from methionine and arginine [240]. Dysfunctional Mueller glia may therefore deplete essential energy

stores in the retina further contributing to development of neurodegeneration and pathological vascular changes. A study focusing on supplementation of S-adenosyl-methionine in the context of reduced retinal creatine stores has suggested that this procedure can exert neuroprotective effects [241]. These findings and the results presented here therefore suggest that a severe impairment in metabolic activity of Mueller glia can strongly contribute to the profound retinal neurodegeneration and neovascularization seen in patients with PDR.

A defect in lipid metabolism, more precisely in mitochondrial fatty acid oxidation, was also identified in the first set of PDR samples, being expressed as a significant upregulation of octanoyl carnitine, propionylcarnitine and decanoyl carnitine. These acylcarnitines have been shown to be increased in the serum of pre-diabetic patients and are considered a marker for insulin resistance and a risk factor for disease progression [242]. Further studies assessing the association between serum, urine and vitreous levels of acylcarnitines may reveal important and consistent correlations among the different types of biological samples, which can lay the foundations for discovery of novel biomarkers for risk stratification and therapeutic efficacy monitoring in DR patients. However further validation and assessment of acylcarnitines as robust biomarkers is warranted, as they have been observed in many metabolomic studies in very diverse pathologies, such as cancer, Alzheimer's disease and obesity-associated inflammation [243-245].

Previous clinical studies have shown that purine metabolism is affected in patients with diabetic retinopathy [246] and that progressive serum uric acid levels associate with DR of increasing severity [247]. In humans, allantoin is the primary and stable oxidation product of uric acid and is therefore considered a sensitive biomarker for oxidative stress [248], which has been widely implicated in the pathophysiology of DR [249]. Our study corroborates the current notion that oxidative stress plays an important role in PDR and suggests that the association between increasing serum uric acid levels and increasing severity of DR reported in the literature may be related to production of allantoin in the eye.

Although the presence of metabolic dysfunction has been widely explored in other tissues in diabetic conditions, little is known about what happens in the eye in PDR. In this study we have generated a global metabolomic profile for PDR from

patient vitreous samples and revealed novel metabolic perturbations, characterized by prominent impairments in amino acid and acylcarnitine metabolism. In addition, these results were validated in a second set of patient samples. Analogous analyses in the OIR mouse showed that this model shares not only retinal pathological features with human PDR but also important disturbances in metabolic pathways, further investigated by novel *in vivo* global isotope metabolomics. The pronounced increase in proline in both PDR patients and the OIR model, and the predominance of the arginase-to-proline pathway in the OIR mouse eye suggest a severe impairment in retinal metabolic activity, and especially that of Mueller glia. Finally, the ability of the OIR mouse to recapitulate the PDR metabolic phenotype shows its value and promise as an appropriate model. This model can be used for the discovery of novel druggable targets and the development of alternative therapeutic strategies that, when successful, can be implemented in the clinic to greatly improve patient care. These findings provide new directions for research in PDR and will pave the way towards implementation of additional disease monitoring strategies to include metabolic biomarkers of disease progression and of therapeutic response.

Main conclusions

- Metabolic dysregulation in PDR mainly affects amino acid metabolism and ammonia detoxification pathways followed by purine metabolism related oxidative stress and acylcarnitine metabolism
- Arginine-to-proline metabolism is the most dysregulated metabolic pathway in human PDR and this feature is shared with the OIR mouse, a model that recapitulates retinal pathological features resembling those of human PDR
- An over-activity of the arginase pathway in the eye leads to (1) increased production of proline and (2) potentially reduced activity in the NOS pathway, with consequent reductions in NO availability (simplified representation **Figure 46**). Even though NO's role in ischemic retinopathies is controversial, this metabolite is important for maintenance of adequate endothelial function and vasodilation, and acts as a modulator of retinal neurovascular crosstalk[100]; therefore, lower availability of NO at critical time-points and/or sites along with increased proline levels may significantly compromise interactions within the NVU, generating 'danger signals' that activate detrimental responses in retinal cells.
- The profound perturbations in arginine metabolism and ammonia detoxification pathways observed both in PDR and in OIR suggest that Mueller cell dysfunction, potentially induced by metabolic overload, can play a role in development of retinal pathological features.
- In OIR eyes, levels of inosine, hypoxanthine and xanthine are lower than in controls, suggesting that lower production or increased metabolism of these purine metabolites may promote development and progression of ischemic retinopathy in this model.

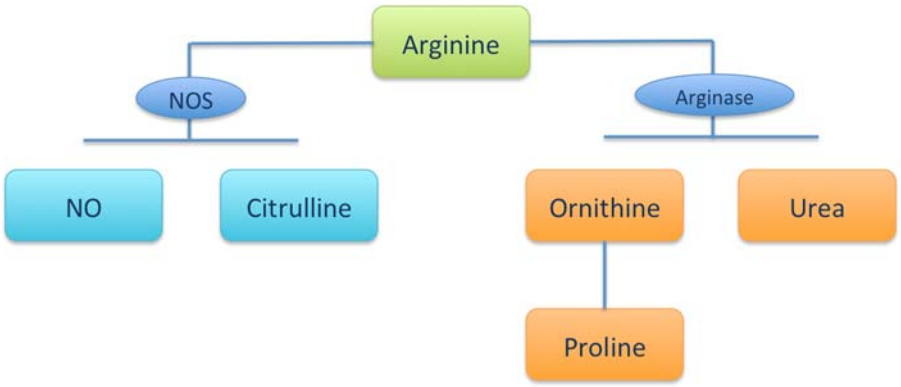

Figure 46 – Simplified representation of arginine metabolism focusing on its two main pathways: Nitric oxide synthase (NOS), which produces NO and citrulline; and Arginase, which generates urea and ornithine that is later converted to proline.

C. Protective Metabolic Factors in Diabetic Retinopathy

Rationale for conducting this work

- There are no specific and reliable biomarkers to assess risk of development or progression of DR or to monitor response to therapy
- Prevention strategies, based on metabolic control, are unable to consistently and efficiently avoid disease development and progression
- Available therapeutic strategies are “non-selective” (even though anti-VEGF agents are a specifically targeted therapy, VEGF also has beneficial neurotrophic functions in the retina; therefore non-selective VEGF inhibitions induces detrimental consequences), act late and are only able to prevent further vision loss, i.e., they cannot reverse or improve what has been lost during earlier DR stages
- Developing targeted therapies that can act at earlier DR stages to reverse the initial pathological changes (before these can elicit detrimental and uncontrollable retinal pathological responses) is, therefore, the ideal strategy to prevent progression and DR-induced vision loss.
- Even though there are no available strategies to effectively arrest DR at its early stages or to prevent its development, there is a subset of diabetic patients who are endogenously protected from developing severe DR complications, despite long-term disease (diabetes for at least 15 years)
- Identifying specific metabolic responses in this subset of protected patients can potentially provide new and meaningful information for discovery of novel drugs and biomarkers

➢ All experiments presented in this chapter were performed by L.P.P.; The experimental results illustrated in Figs. 51, 58 and 59; and 61, 62 and 63 were obtained in collaboration with YU, MG and CHJ, respectively.

C.1. Inosine slows retinal metabolism in hypoxic conditions and prevents development of the most severe features of diabetic retinopathy

Background and significance

Diabetic retinopathy (DR) is the leading cause of blindness in industrialized nations in adults under the age of 65 and recent epidemiological studies estimate that it will affect 191 million people worldwide by the year 2030.[69]

DR is classified as non-proliferative (NPDR) or proliferative DR (PDR) depending on the severity of vascular changes, and PDR, the late-stage disease, is frequently associated with severe vision loss due to retinal edema, vitreous hemorrhage and retinal tractional detachment[250]

Retinal vascular changes have classically been given the most relevance in DR and remain the mainstay of diagnostic classification and treatment orientation; however, neurodegenerative changes, reflected by abnormal electroretinographic oscillatory potentials[5] and reduced flicker-light induced vasodilation responses[251], occur much earlier in diabetic patient retinas, and have even been reported in the pre-diabetic state[252].[253]. Since retinal neurovascular units (NVUs) regulate local blood supply to ensure that the metabolic needs of retinal neurons are met, the events previously described in diabetic retinas suggest that compromises in the retinal neurovascular crosstalk may be contributing and eventually driving DR progression[254]. This concept is supported by studies showing that an impaired light-evoked retinal vasodilation response is associated with abnormal nitric oxide (NO) signaling between Mueller cells and the retinal vasculature; and that the vasodilatory response is significantly improved by inhibiting inducible nitric oxide synthase (iNOS)[110,227].

Currently, there are no reliable strategies to effectively prevent DR in every case, and no validated specific biomarkers to predict risk of progression. Maintaining adequate glycemic, lipid and blood pressure control has been advocated as the best strategy to prevent and arrest DR progression, however studies have shown that up to 20% of long-term diabetic patients (with diabetes over 30 years) still

develop late-stage disease - proliferative diabetic retinopathy (PDR) – despite ideal metabolic control. [27,68]

Existing therapeutic strategies for management of DR (e.g., laser photocoagulation and anti-vascular endothelial growth factor (VEGF) agents) act late and are ineffective at arresting disease progression in a sustainable fashion in every patient. Moreover, anti-VEGF agents may further exacerbate disease at the retinal, and systemic (renal and cardiovascular) levels[27,221,255-257].

Laser photocoagulation, the preferred therapeutic approach in DR, reduces risk of severe vision loss by 50%[250,258], by eliminating peripheral hypoxic retinal neurons and thereby reducing retinal metabolic demand. This suggests that metabolic supply and demand mismatches are involved in pathogenesis of DR. Developing non-destructive approaches to prevent damage to or stabilize interactions within the NVU in the retina may represent a more efficient therapy.

Unfortunately, retinal metabolism and neurovascular interactions in the retina are understudied, especially in the context of diabetic retinopathy. A deeper understanding of these topics may explain why up to 50% of patients with type 1 diabetes and about 10% of those of type 2 are expected to develop PDR after 15 years of diabetes, and why there is a small subset of patients who appear to be protected from developing severe diabetic complications (or from developing them at all[259]) despite long-term disease[259]. In fact, duration of diabetes is the single most important risk factor for development of DR[27] and it is expected that the latter will develop, to some extent, in nearly all type 1 and in over 60% of type 2 diabetic patients after 20 years of disease[70,71]. The previously mentioned “protected” diabetic patients provide an opportunity to identify protective factors and to further understand DR pathophysiology.

Furthermore, diabetes is characterized by profound metabolic dysfunction, which severely compromises cellular energy production; and, the retina is one of the most metabolically demanding tissues in the body due to its constant photoreceptor activity[260,261]. This dangerous association suggests that individual differences in metabolic activity within the diabetic patient population may be associated with protection against development and progression of DR.

Global and highly sensitive mass-spectrometry (MS) metabolomic approaches are currently available and constitute the ideal tool to study potential metabolic differences between subjects[262,263]. These techniques generate

comprehensive and reliable metabolic profiles that are able to clearly differentiate groups of patients otherwise indistinguishable from one another.[264,265] Additionally, they can provide metabolic cues that can help achieve a deeper understanding of disease pathophysiology and pave the way towards discovery of novel disease biomarkers and therapeutic targets.

In this study, we hypothesized that protection against development of severe DR in long-term-diabetic patients could be related to individual metabolic idiosyncrasies. To test this hypothesis, we performed global metabolomic analysis on blood serum to compare the metabolomic landscape of two groups of patients on opposite ends of the disease spectrum: long-term diabetics without PDR ("protected" group) and diabetic patients with PDR regardless of disease duration ("unprotected group).

We selected a candidate purine metabolite, inosine, based on its reported neuroprotective and immunomodulatory properties[266] and further tested its effects on (1) retinal aerobic metabolism using the novel Seahorse technology, and (2) retinal phenotype in the oxygen-induced retinopathy mouse (OIR), a rodent model that develops areas of retinal ischemia and pre-retinal neovascularization resembling those observed in human PDR. Inosine intravitreal injections prevented pathological pre-retinal neovascularization by slowing basal aerobic retinal metabolism in vaso-obliterated areas and enhancing their revascularization. Inosine can thus become an advantageous alternative to laser photocoagulation therapy because it similarly reduces retinal metabolic demand to better match supply and to effectively arrest disease progression, but in a non-destructive fashion

Results

Glycemic control and disease duration cannot accurately predict risk of DR progression

Although glycemic control is the cornerstore of diabetes care and considered one of the most critical approaches to prevent development of diabetic complications[80], it is becoming increasingly clear that maintaining classic metabolic parameters under control alone is insufficient to prevent development of diabetic complications and, in some cases, may even be dispensable.[68,267] In addition, duration of diabetes is considered one of the strongest predictors for development and progression of DR[268].

In order to assess the role of demographic and clinical parameters in protection against PDR in our study population, we compared the "*protected" group* (n=12; patients who did not develop PDR despite long-term diabetes), to the *non-protected group* (n=10; patients who developed PDR regardless of diabetes duration. The detailed clinical characteristics are described in **Table 12**.

Both groups showed similar characteristics: (1) type of diabetes: 50% type 1 and 50% type 2; (2) gender distribution: M/F=1/3 in "protected" patients and M/F=1/3.3 in non-protected patients; **Figure 47A** and (3) profile of comorbidities (**Figure 47B**); Patient age, however, was higher in the "protected" group (66.08±3.7 versus 51.50±3.4; p=0.01; **Figure 47C**). Furthermore, there were no significant differences between groups regarding duration of diabetes (34±5.4 versus 26±4.4; p>0.05; **Figure 47D**) or common metabolic parameters such as, serum levels of glycated hemoglobin (HbA1c; 7.3±0.45 versus 7.46±0.27; p>0.05; **Figure 47E**) or body mass index (BMI; 27.7±1.8 versus 27.52±1.0; p>0.05; **Figure 47F**).

The clinical characteristics of our study cohort reinforce the notion that (1) adequate glycemic and/or BMI control alone is insufficient to prevent PDR (**Figure 47E-F**), and is not an absolute requirement for protection (some "protected" patients showed unfavorable metabolic characteristics (**Table 12**); and that (2) longer diabetes duration does not necessarily correlate with higher likelihood of progression to late-stage disease.

Table 12 - Clinical characteristics of the study cohort

DR stage	Age Gender	Ethnicity	Type of DM	Duration of DM (years)	HbA1c (%/mmol/mol)	Comorbidities	BMI (kg/m^2)	Oral AD	Insulin	Inosine levels (Abundance)
Mild NPDR	77 F	Caucasian	2	19	6.9 (52)	HTN; HL	25.2	From diagnosis	Last 4 yrs	70800.870
Mild NPDR	47 M	Caucasian	1	37	7.1 (54)	HTN; HL	23.1	0	37 yrs	7987.723
No DR	62 M	Caucasian	1	45	9.1 (76)	HTN; HL; DN	24	0	45 yrs	12764.910
No DR	39 M	Caucasian	1	27	5.9 (41)	0	23	0	27 yrs	45000.380
Mild NPDR	73 M	Caucasian	2	30	7.5 (58)	HTN; HL; CVD	37.7	From diagnosis	Last 3 yrs	11713.880
Mild NPDR	61 M	Caucasian	1	42	6.2 (44)	HTN	20.4	0	42 yrs	14997.350
Mild NPDR	80 F	Caucasian	2	20	5.9 (41)	HTN; HL	27	20 yrs	0	82825.980
Mild NPDR	75 M	Caucasian	2	18	6.8 (51)	HTN; HL	30.3	From diagnosis	Last 10 yrs	10107.800
Mild NPDR	76 M	Caucasian	1	66	6.6 (49)	HTN; HL	28.3	0	66 yrs	24714.480
No DR	78 F	Caucasian	1	70	6.8 (51)	HTN; HL	23.4	0	70 yrs	11803.950
Mild NPDR	63 M	Caucasian	2	16	7.4 (57)	0	27.9	From diagnosis	Last 9 yrs	9589.691
Mild NPDR	62 F	Hispanic	2	18	11.5 (102)	0	41.6	N/A	Last 8 yrs	77710.520
PDR	50 F	Caucasian	2	3	6.9 (52)	HTN; HL	27.9	3 yrs	0	11671.230
PDR	67 M	Hispanic	2	21	7.1 (54)	HTN; HL;	33.2	21 yrs	0	5000.644

						DN				
PDR	36 F	Caucasian	1	18	7.2 (55)	HTN	24.8	0	18 yrs	15264.540
PDR	41 M	Caucasian	1	33	7.3 (56)	HL	28.3	0	33 yrs	10716.950
PDR	57 M	Asian	2	22	N/A	HTN; HL	29	N/A	Last 20 yrs	7191.215
PDR	59 F	Caucasian	1	45	9.3 (78)	HTN; HL; CVD	22.3	0	45 yrs	11188.700
PDR	41 M	Hispanic	2	25	7.3 (56)	HTN; HL	26.6	25 yrs	Last 12 yrs	4786.110
PDR	62 M	Hispanic	2	14	8.1 (65)	HTN; HL	26.7	N/A	Last yr	8227.129
PDR	42 M	Caucasian	1	29	7.4 (57)	HTN; HL	31.2	0	29 yrs	6615.780
PDR	60 M	Caucasian	1	50	6.5 (48)	0	25.1	0	50 yrs	6477.118

Table 12 (legend)

Mild NPDR = mild non-proliferative diabetic retinopathy; PDR = Proliferative diabetic retinopathy; # patient number as seen in the graph on Fig. 1 C; F = female; M = male; HbA1c = glycated hemoglobin; AD = antidiabetics; HTN = hypertension; HL = hyperlipidemia; CVD = cardiovascular disease; DN = diabetic nephropathy; BMI = Body Mass Index (categories: underweight < 18.5; Normal weight 18.5 – 24.9; Overweight 25 – 29.9; Obesity 30 or greater); Yrs = years; N/A = information not available.

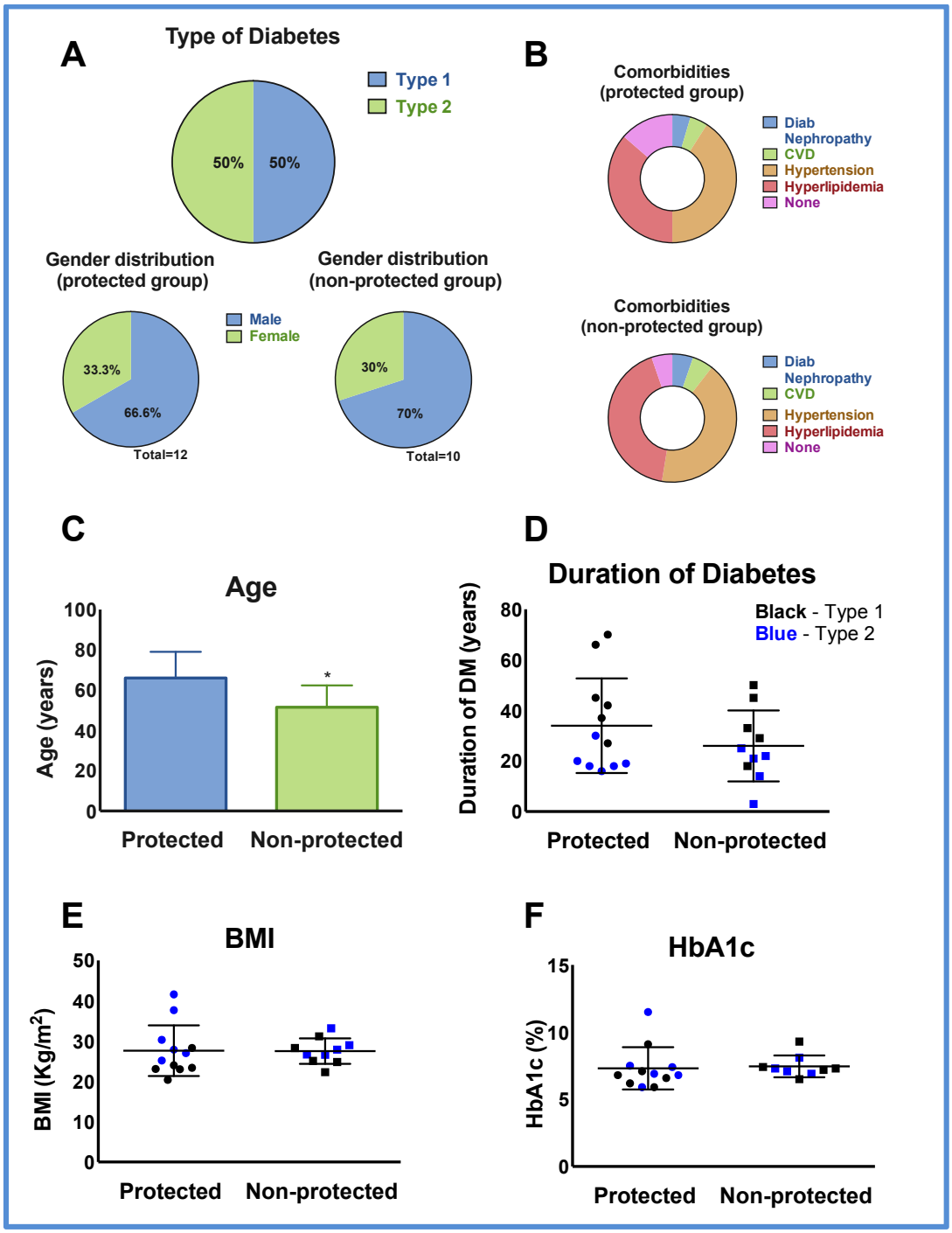

Figure 47 - Characteristics of the study population. (**A**) Type of diabetes, gender distribution and (**B**) comorbidities are similar between protected and non-protected diabetic patients; (**C**) Protected patients are significantly older than non-protected patients (66.08 ± 3.741 versus 51.50 ± 3.436; p=0.0105); (**D**) Duration of diabetes is not significantly different between groups (34±5.4 versus 26±4.4; p>0.05); (**E**) HbA1c levels are not significantly different between groups (7.3±0.45 versus 7.46±0.27; p>0.05); (**F**) BMI is not significantly different between groups (27.7±1.8 versus 27.52±1.0; p>0.05). *p < 0.05; **p< 0.01; values shown represent Mean±SEM.

Increased serum inosine levels may distinguish "protected" from non-protected diabetic patients

In order to identify circulating metabolites potentially associated with protection against development of PDR, highly sensitive, untargeted, MS-based metabolomic analyses were performed on blood serum samples from “protected” and non-protected diabetic patients.

Inosine, a purine nucleoside, was one of the most significantly dysregulated metabolites between groups, demarcating “protected” from non-protected patients (**Figure 48A**). It was significantly increased in the “protected group” (3.63 fold; p=0.02; **Figure 48B**), suggesting a potentially beneficial role in preventing progression of DR.

Serum inosine levels did not correlate with (1) metabolic parameters, such as HbA1c (**Figure 48C**) or BMI **Figure 48D**); (2) patients’ age (**Figure 48E**); or (3) duration of diabetes (**Figure 48F**).

Diabetic patients commonly have higher serum levels of uric acid and are at increased risk of developing episodes of gout[247,269], which can be prevented by using allopurinol.

Allopurinol inhibits xanthine oxidase, an enzyme involved in purine catabolism that catalyzes two successive reactions, hypoxanthine to xanthine and xanthine to uric acid (the relevant metabolic pathways are presented in the appendix). Inhibition of xanthine oxidase leads to accumulation of hypoxanthine, which in turn can be converted back to inosine by a freely reversible reaction catalyzed by purine nucleoside phosphorylase (PNP).

In order to assess if higher inosine serum levels in long-term diabetic patients could be a consequence of allopurinol usage, serum levels of allopurinol, oxypurinol (allopurinol’s active metabolite), hypoxanthine and uric acid were compared between the two groups.

Due to technical limitations (mass-to-charge ratio - *m/z* - within the same range), it was not possible to distinguish between allopurinol and hypoxanthine; and oxypurinol and xanthine. However, there were no significant differences in serum levels for any of the metabolites under study (**Table 13**), suggesting that in our patient cohort protection against PDR and higher inosine levels were not associated with allopurinol usage; Moreover, protection against PDR was not associated with higher uric acid levels, as has been suggested in studies addressing inosine’s beneficial effect in multiple sclerosis[270]

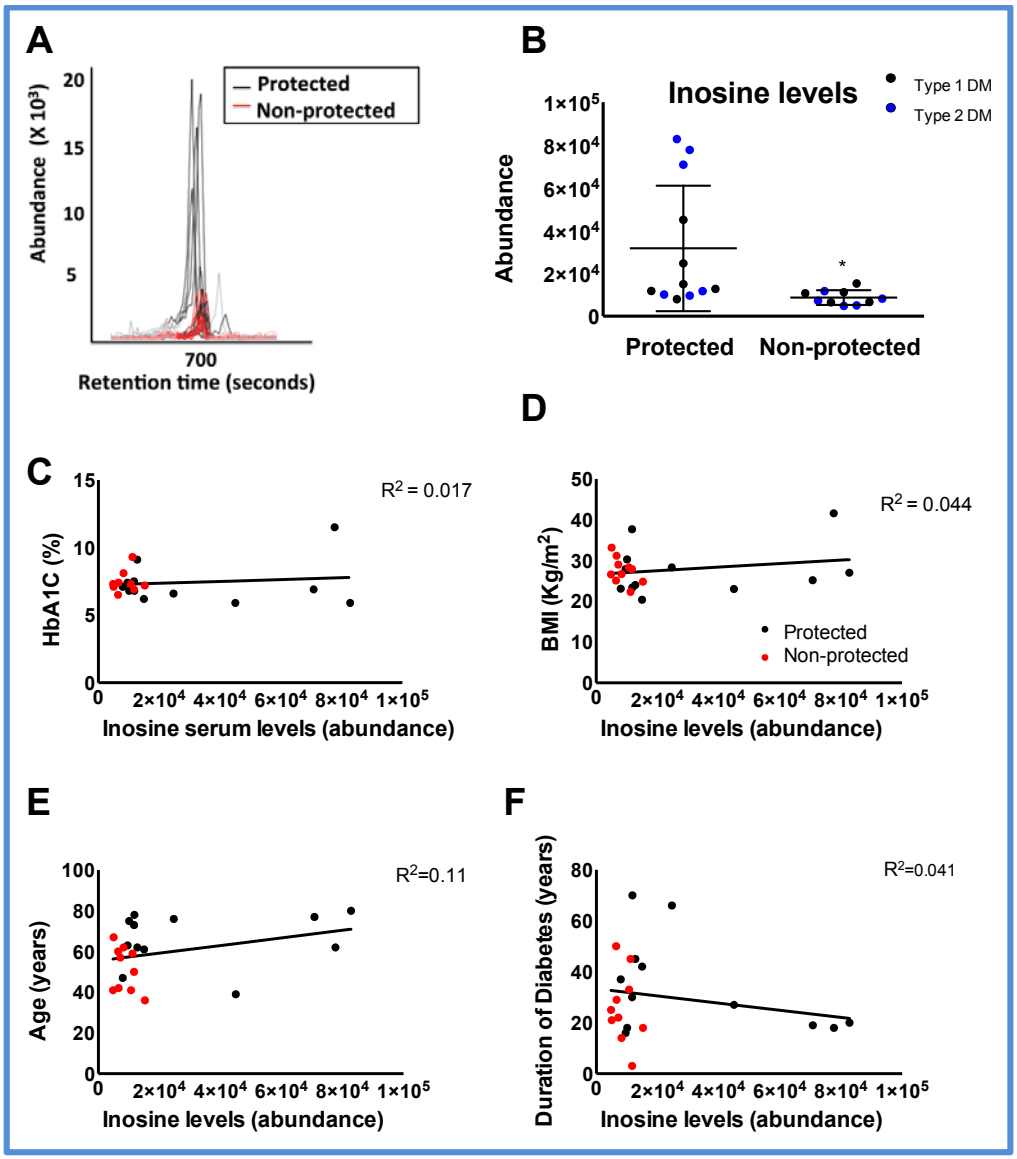

Figure 48 - Inosine serum levels differentiate protected from non-protected patients. (A&B) Metabolomic analyses showed significantly augmented inosine levels in protected diabetic patients (3.6 Fold; p = 0.02); Inosine serum levels do not correlate with (C) HbA1c, (D) BMI levels, (E) age or (F) duration of diabetes. The straight line constitutes the best-fit line obtained by linear correlation analysis; *p < 0.05; **p< 0.01; values shown represent Mean±SEM

Table 13 – Untargeted mass spectrometry-based metabolomics showing putative identification of metabolites that are not significantly changed between "protected" and unprotected patients.

Putative Metabolite Identification*	*m/z*	Mass error (ppm)	Fold change	p-value
Allopurinol/ Hypoxanthine	137.0468 $[M+H]^+$	7 ppm	1.19	0.3
Allopurinol/ Hypoxanthine	137.0317 $[M-H]^-$	3 ppm	2.34	0.2
Oxypurinol/ Xanthine	151.0232 $[M-H]^-$	19 ppm	1.26	0.5
Uric acid	169.0364 $[M+H]^+$	4 ppm	1.02	0.8
Uric acid	167.0258 $[M-H]^-$	28 ppm	1.07	0.6

m/z = mass to charge ratio
ppm = part per million

Inosine promotes intraretinal revascularization of ischemic areas and reduces pathological neovascularization in the OIR mouse

Since there is no diabetic rodent model that spontaneously develops features of PDR, the OIR mouse, a non-diabetic model, is frequently used in this context[222]. The OIR mouse develops PDR-like features, such as areas of retinal ischemia (due to vaso-obliteration) and pathological pre-retinal neovascularization after exposure to a 5-day hyperoxic environment.

Given the correlation between higher serum inosine and protection against PDR in long-term diabetic patients, we performed inosine and vehicle (PBS) intravitreal injections in the OIR mouse and assessed the effects on development of PDR-like retinal features.

Inosine administered both at postnatal day seven (P7) and at P12 significantly prevented development of the typical retinal pathological features at P17 OIR by significantly accelerating revascularization of vaso-obliterated areas, thus dramatically reducing pathological neovascularization (**Figure 49A-B**).

Inosine's beneficial effects observed with P7 injections could not be attributed to reductions in the ischemic area at P12 (**Figure 49C**). This suggests that inosine

does not prevent development of vascular obliteration during hyperoxia but rather exerts its beneficial action during the hypoxic period (from P12 onwards).

In order to assess inosine's safety profile and to rule out potential detrimental effects on physiologic retinal vascular development, we also injected inosine and vehicle at P12 in control mice, raised in ambient oxygen, and analyzed their retinas at P17. There were no significant differences in terms of vascular density or vascular structure between inosine and vehicle injected eyes (**Figure 50**), showing that inosine does not interfere with normal vascular development. Furthermore, we also excluded potential toxic effects on neuroretinal function by performing ERG studies, which showed comparable retinal neuronal activity in inosine and vehicle injected eyes (**Figure 51**).

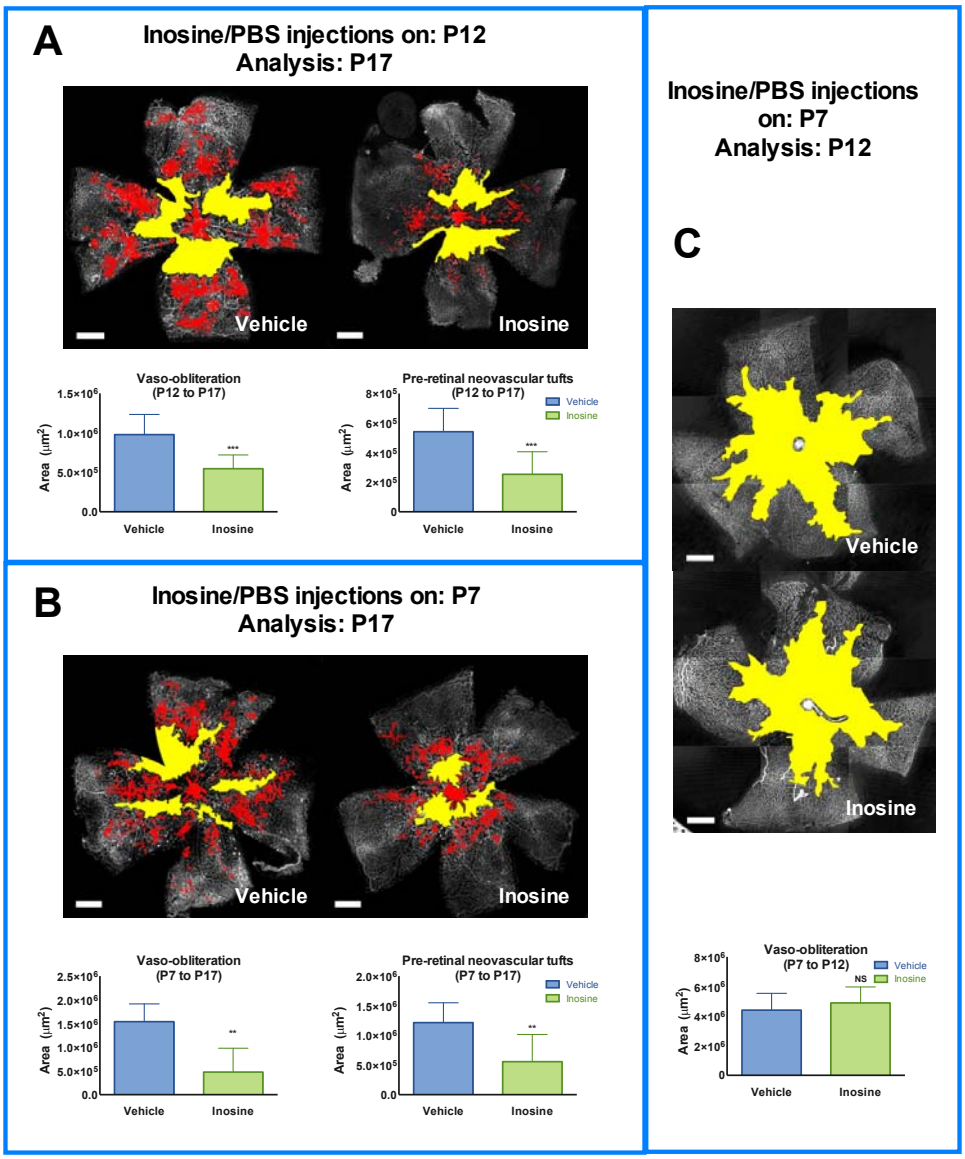

Figure 49 - Inosine promotes revascularization of ischemic retinal areas and reduces development of pathological neovascularization. (A) Inosine injections at P12 significantly reduced vaso-obliteration (depicted in yellow; p=0.0001) and pathological neovascularization at P17 (in red; p=0.0002), when compared to vehicle controls; (B) The same beneficial effect (at P17) was observed when inosine is injected at P7 (p=0.0001 for vaso-obliteration and p=0.001 for neovascularization); (C) Inosine injections at P7 did not prevent development of vaso-obliteration during hyperoxia (p>0.05). Two-tailed Student t-tests; *p<0.05; **p<0.01; ***p<0.001; NS = p>0.05; values shown represent mean±SEM; n=8; Scale bars 500 µm.

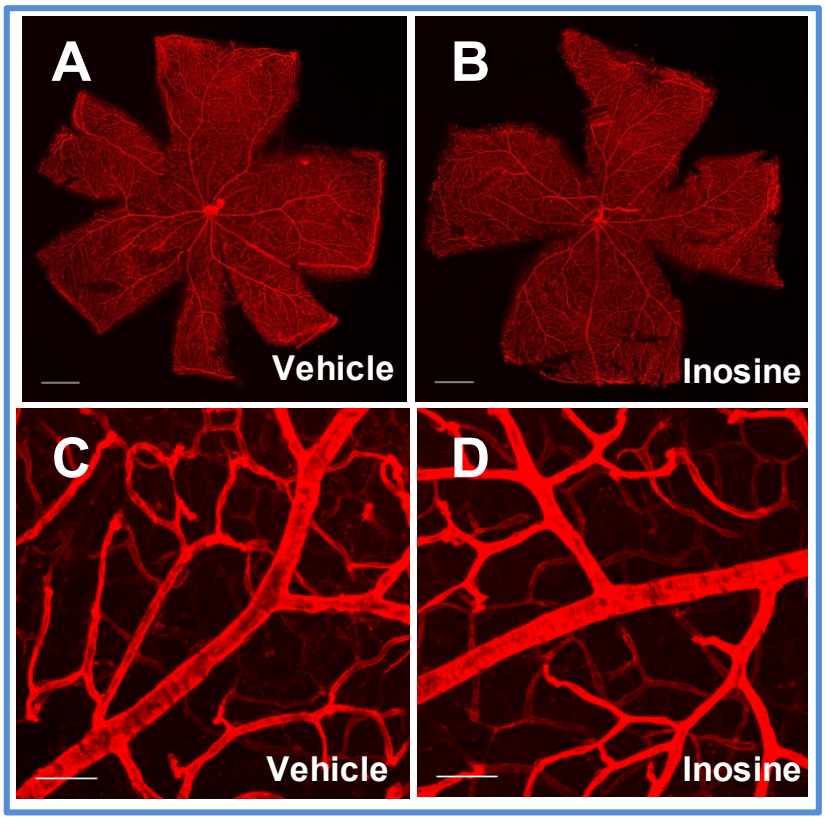

Figure 50 – Inosine injections at P12 do not affect physiologic retinal vascular development in C57/Bl6 P17 pups raised in normoxia. (**A&B**) Retinal flatmounts from vehicle and inosine injected eyes stained with GS-isolectin to highlight the vasculature; (**C&D**) Higher magnification images showing comparable retinal vascular density and structure. Scale bars: 500 µm (**A&B**) and 50 µm (**C&D**).

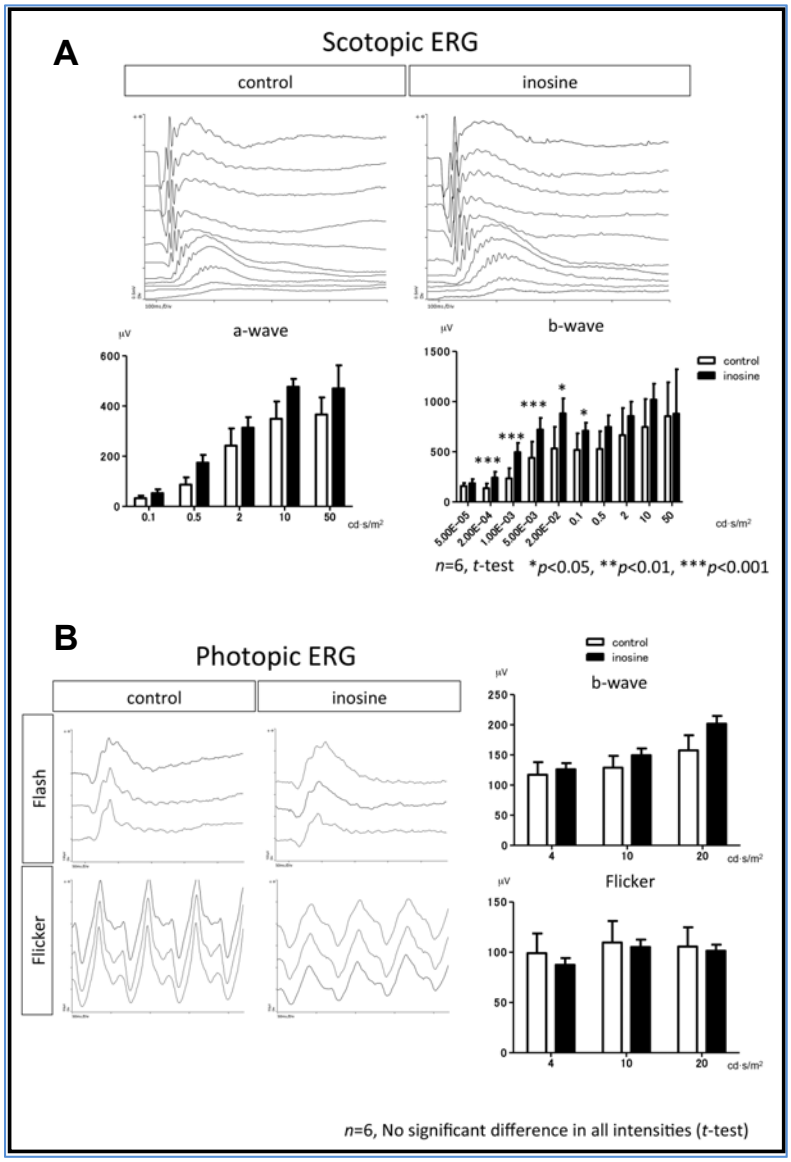

Figure 51 - Intravitreal inosine injections do not compromise retinal functioning in wild-type C56/bl6 adult mice raised in normoxia. Electroretinograms obtained under (**A**) scotopic (low light) and (**B**) photopic (bright light) conditions show similar neuroretinal functionality in inosine and vehicle injected eyes (5 days post injection), thus excluding a potential negative impact on retinal neurons. ERG = electroretinogram. Two-tailed Student's t test; Data represents mean ± SEM.

Inosine moderates the inflammatory response in P17 OIR retinas

Production of chemokine ligand 2 (CCL2 or MCP-1), tumor necrosis factor alpha (TNF-α) and VEGF-A is significantly upregulated in the retina under OIR conditions and these factors play a crucial role in promoting development of the retinal pathological phenotype[6,92,271-273]. Additionally, these also foster progression of diabetic retinopathy[68,93] and are upregulated in the vitreous of PDR patients.

Inosine's role as an immunomodulatory agent has been demonstrated in various animal models of disease, ranging from sepsis to experimental autoimmune encephalomyelitis [266,274]. To assess if inosine was acting through a similar mechanism in the OIR model, gene expression analysis for CCL2, VEGF-A (and its isoforms) and TNF-α were performed on retinal lysates. Twenty-four hours after intravitreal injection, only VEGF-A expression levels were significantly downregulated in retinas from inosine injected eyes when compared to controls (**Figure 52A**); However at the time point of maximal neovascularization (P17) all three factors were found to be moderately and significantly downregulated by inosine injections (**Figure 53A**).

In mice, three functionally distinct VEGF-A isoforms (VEGF-A 120, 164 and 188) can be identified based on their solubility and heparin-binding affinities. It has been suggested that different VEGF isoforms can regulate formation and maintenance of specific retinal vascular plexuses in the mouse retina (**Chapter IV-B**). Knowing that VEGF-A gene expression is downregulated by inosine injections, we next sought to identify if specific isoforms were preferentially affected and to what extent. At P13, only VEGF164 expression levels were significantly downregulated by inosine injections (**Figure 52B**). However at P17, all VEGF-A isoforms were downregulated to a comparable extent, suggesting that inosine does not preferentially regulate expression of any of them at later time-points (**Figure 53B)**.

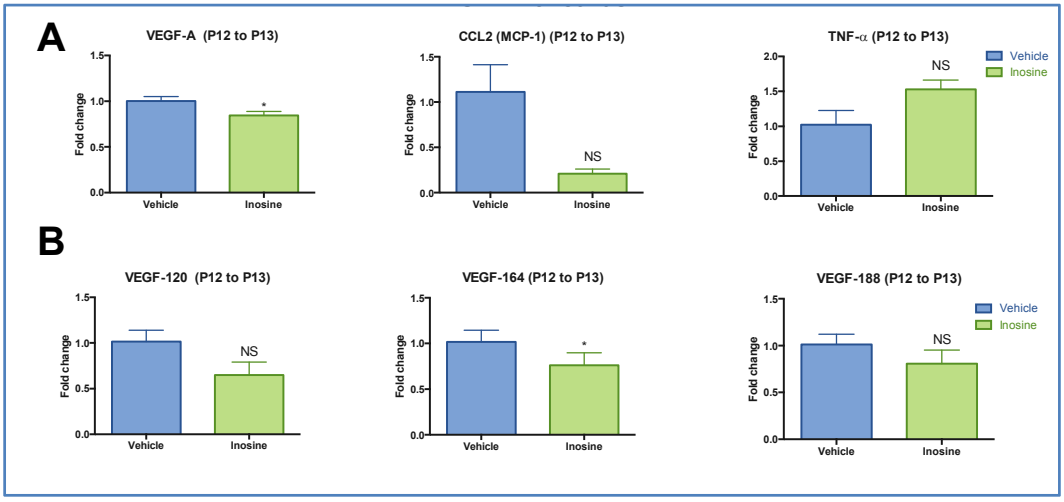

Figure 52 – Effects of inosine injections on gene expression levels of pro-inflammatory and pro-angiogenic factors in OIR P13 retinas. (**A**) Inosine injections at P12 significantly reduce gene expression levels of VEGF-A at 24 hours post-injections, without a significant effect on expression levels of CCL2 or TNF alpha. (**B**) Only VEGF 164 expression is significantly downregulated by inosine injections at 24 hours after injection. (Two tailed Student's t-test; *p<0.05; n=8; values shown represent mean±SEM).

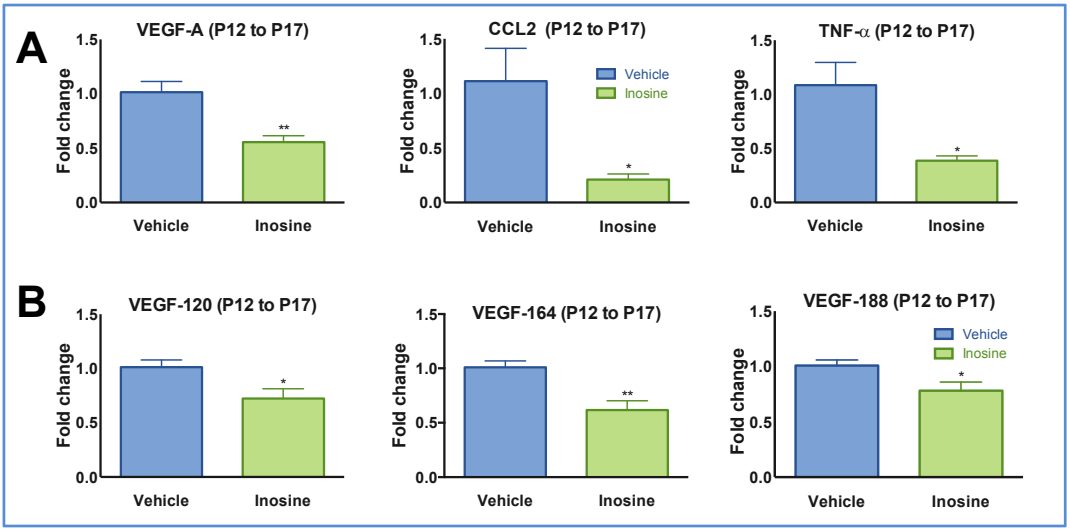

Figure 53 – Effects of inosine injections on gene expression levels of pro-inflammatory and proangiogenic factors Inosine in OIR P17 retinas. (**A**) Inosine injections (P12) significantly reduce gene expression levels of CCL2, TNF-alpha and VEGF-A at P17, in retinal lysates; (**B**) All VEGF isoforms (120, 164 and 188) are downregulated to a similar extent in retinal lysates collected from inosine injected OIR eyes when compared to vehicle injected controls. (Two tailed Student's t-test; *p<0.05; **p<0.01; n=8; values shown represent mean±SEM).

Microglial cells, the resident macrophages of the retina, are the first cells to sense retinal damage, upon which they become activated (maximally at 24h), initiating production of cytokines and acquiring motile properties[18,275]. Concomitantly, circulating macrophages are also attracted and invade the retina, further contributing to the local pro-inflammatory response. There is a growing body of evidence suggesting that the beneficial or detrimental effects determined by microglial cells and macrophages on CNS pathology (e.g. neurodegenerative diseases) may be dependent on the time of activation and migration (early in the disease process versus late)[276,277].

DR is characterized by chronic inflammation and one of the anti-inflammatory drugs that is showing encouraging results in clinical trials[68] is an anti-CCL2 agent, which blocks recruitment of macrophages to the eye.

To evaluate inosine's effect on retinal microglial cells and macrophages *in vivo*, the number and location of Iba1+ cells (a marker for both cell types) on retinal cross-sections was analyzed 24h post-inosine or vehicle injections. Although the total number of Iba1+ cells was unchanged between treated and untreated mice, there were significant differences in cell distribution across the retinal layers. Retinas from inosine injected eyes showed higher numbers of Iba1+ cells in the superficial RGC (**Figure 54**), which is one of the earliest and most profoundly affected by hypoxia in OIR conditions. This could suggest that inosine may be prompting MGC migration to the most severely damaged superficial retinal layers to ensure early removal of debris, thus preventing an exponential pro-inflammatory response and the ensuing retinal damage. A similar phenomenon has been described in the developing retina in mice and zebrafish, where microglial cells phagocytize pyknotic cells produced during neural remodeling, to maintain a 'clean' area that is critical for adequate retinal growth and neurogenesis[278,279].

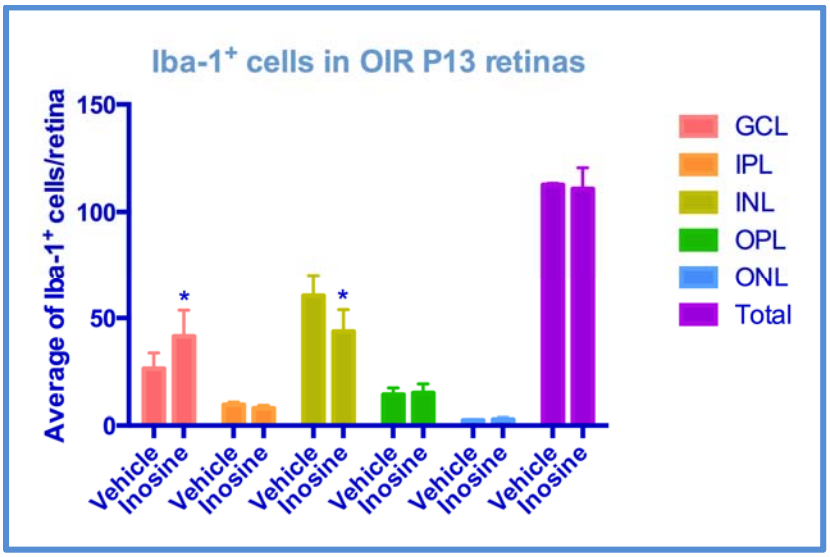

Figure 54 - Inosine promotes early accumulation of macrophages/microglial cells (Iba1+) in the hypoxic RGC layer, in OIR retinas. Average number of Iba-1$^+$ cells in OIR retinas. (Two-tailed Student's t-test; *p<0.05; n=8 per experimental group; values shown represent mean±SEM). RGC = retinal ganglion cell; OIR = oxygen-induced retinopathy.

To further characterize the microglia/macrophage population in inosine and vehicle treated OIR retinas, gene expression levels of macrophage polarization markers, iNOS (inducible nitric oxide synthase; a marker for M1 polarization) and Arginine-1 (Arg-1; a marker for M2 polarization), were assessed in retinal lysates at 24 h (P13) and 5 days post injection (P17). At P13 (24 hours post injection) no significant changes in iNOS or arginase-1 were found between experimental groups (**Figure 55A**). However, at P17, iNOS was found to be significantly downregulated in inosine injected retinas while Arg-1 remained unchanged between inosine and vehicle treated retinas (**Figure 55B**). This finding further supports the possibility that early removal of debris in the most damaged retinal regions (promoted by inosine) may prevent accumulation of material that can favor preferential M1 polarization at later stages (as the pro-inflammatory phenotype M1 is characterized by high iNOS expression levels). Moreover, enhanced iNOS activity and subsequent excessive NO production (by this specific isoform) have been shown to disturb the crosstalk between Mueller cell and the retinal vasculature in early diabetic retinopathy and contribute to reduced flicker-light induced vasodilation.[110]. Collectively these data further suggest that inosine may prevent retinopathy progression by improving cellular interactions within the

NVU, and one of the involved mechanisms may be through preventing M1 polarization and thereby reducing iNOS activity locally to normalize NO signaling.

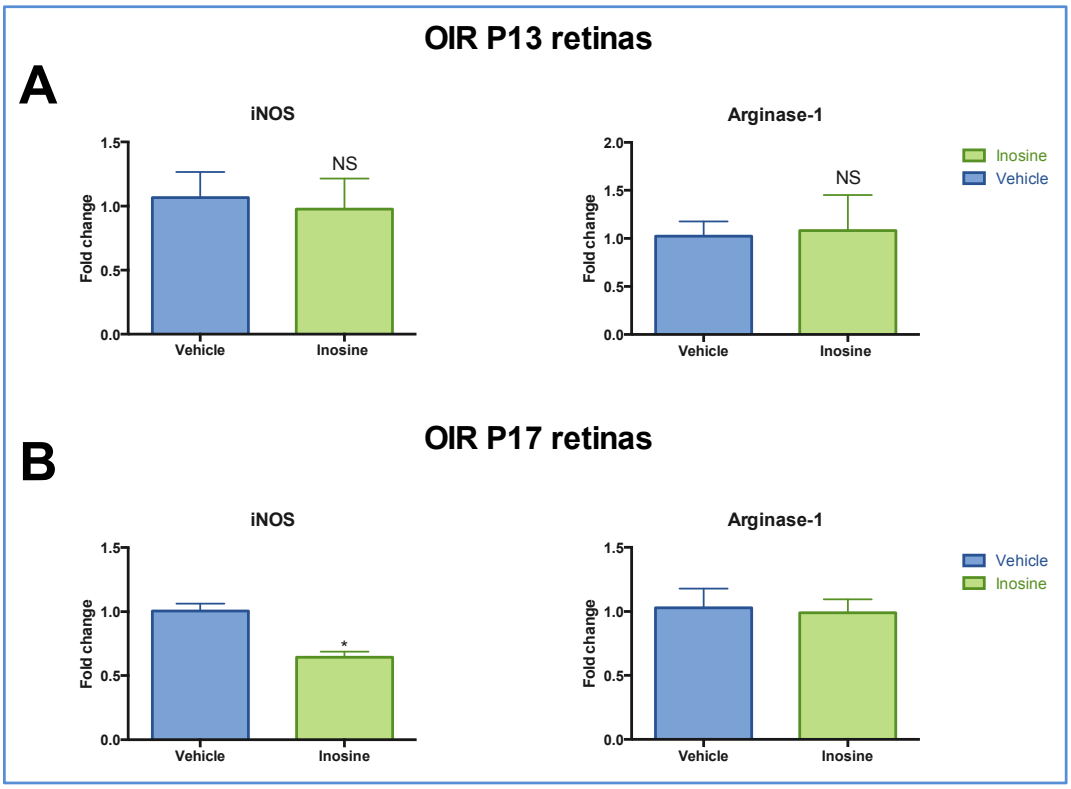

Figure 55 - Gene expression levels of macrophage polarization markers in retinas from inosine and vehicle injected OIR eyes. (A) Differences in macrophage polarization markers are not evident between inosine and vehicle injected eyes at P13 (24 h after injection); (B) Expression levels of M1 macrophage marker iNOS are significantly reduced in retinal lysates from inosine injected eyes while M2 markers are not changed between retinas from treated and untreated OIR eyes. (Two tailed Student's t-test; n=8; values represent mean $\pm$ SEM; * $p<0.05$; NS = no statistical significance).

Inosine reduces basal mitochondrial metabolism in OIR retinas

To better understand the metabolic effects that inosine induces in OIR retinas, concepts regarding retinal metabolism; cellular respiration and oxidative phosphorylation; and seahorse® flux analyzers will be briefly reviewed.

A) Retinal metabolism:

The retina is the most metabolically active tissue in the body per unit weight mainly due to intense photoreceptor (PR) activity both in photopic (light) and scotopic conditions (dark)[22,40,280]. Retinal energy requirements are higher in the dark than in the light and most of its energy supplies are produced via oxidative metabolism (mitochondrial respiration). Even though Mueller cells rely primary on glycolysis for energy production (by converting glucose to lactate), overall retinal metabolism mainly reflects that of retinal neurons[22]. In the rabbit retina (under basal conditions), only 16% of the energy supply is generated through glycolysis, while 84% (in scotopic) or 61% (in photopic conditions) of ATP is produced via mitochondrial respiration, which is evaluated via oxygen consumption rates – OCR[22].

Most of the energy generated in the retina is used for active transport of ions (and especially for ion exchanges carried out by Na^+K^+ATPase, which uses 50% in the dark and 15% in light, of the total ATP pool) that ensure repolarization of plasma membranes for subsequent neuronal reactivation[22].

Given its (1) high metabolic activity, (2) almost exclusive dependence on glucose oxidation and (3) very little reserve (spare) capacity (it utilizes near maximal respiratory capacity even under basal conditions), the retina is particularly vulnerable to even subtle alterations in metabolic supply (e.g., O_2 or nutrient deprivation) and changes in retinal energy metabolism (translated into changes in O_2 consumption rates) constitute one of the earliest and most sensitive indicators of impending retinal cell dysfunction[281,282]. This concept is corroborated by studies in diabetic cats showing that pO_2 levels are reduced even in areas with no evidence of capillary dropout[281].

In conditions of metabolic scarcity, metabolism shifts from oxidative to glycolytic in an attempt to generate enough energy to maintain adequate retinal functioning.

However, this only sustains retinal activity for a short period of time because retinal metabolic requirements remain incredibly high while the ATP yield of glycolysis is low. [283,284].

B) Cellular respiration and oxidative phosphorylation

Aerobic cellular respiration is the process by which biological substrates are oxidized to CO_2 and water in a step-wise fashion, which includes glycolysis, the Krebs cycle and the electron transport chain (ETC), to produce large amounts of ATP. The ETC is a series of consecutive redox reactions carried out by a number of protein complexes located on the inner mitochondrial membrane (IMM). The ETC receives electrons from donors such as NADH and $FADH_2$ that are generated during glycolysis and the Krebs cycle and transfers them successively along the ETC protein complexes in the presence of an inorganic electron acceptor (oxygen); finally, these electrons are incorporated into H_2O. The energy generated by electron flow down the electron transport chain is used to pump protons across the IMM, creating an electrochemical potential across the membrane that drives ATP production via ATP synthase (oxidative phosphorylation). More specifically, when protons move from the inter-membrane space back into the matrix according to their electrochemical gradient, they do it mainly through ATP synthase (complex V), which couples this proton motive force to phosphorylation of ADP into ATP (**Figure 56**). However, the IMM is not completely impermeable to protons and proton leak can occur, in which case the energy produced is not in the form of ATP but in the form of heat.

Oxidative phosphorylation is tightly coupled to the ETC, so if the electron flow decreases, so does oxidative phosphorylation and vice-versa. When ATP synthase is inhibited, by lack of substrate or by a drug, the proton gradient is not dissipated and consequently this proton motive force exceeds the potential energy of moving electrons through the ETC, which is therefore blocked until the H^+ gradient dissipates again.

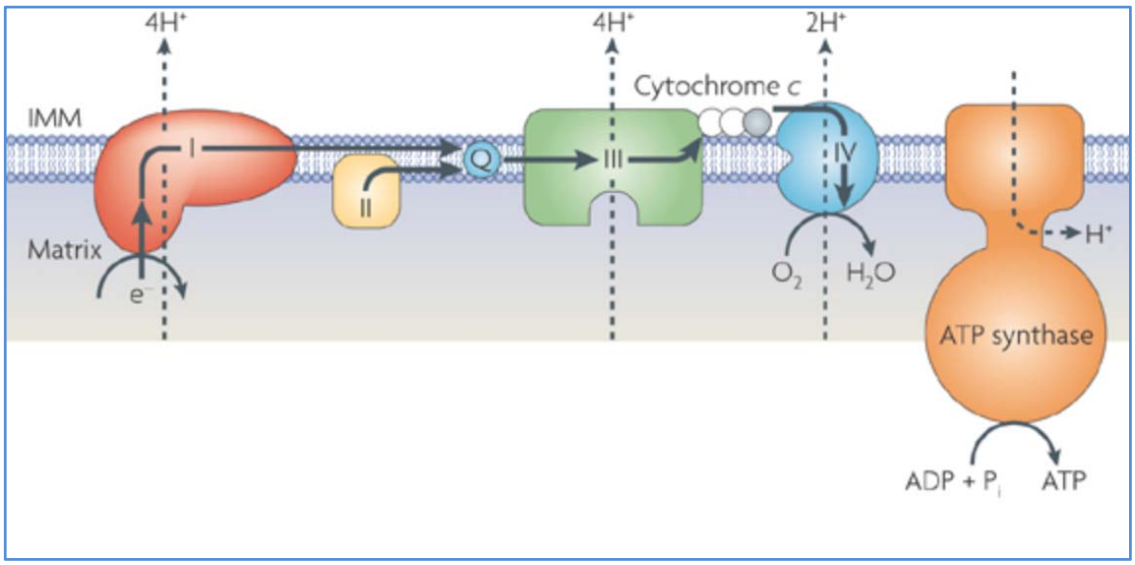

Figure 56 - Electron transport chain (ETC): Complexes I to V transfer electrons successively to produce a proton motive force across the inner mitochondrial membrane (IMM). [285]

Retinal oxygen consumption mainly reflects local mitochondrial respiratory activity, which produces ATP via oxidative phosphorylation (and a smaller portion of energy in the form of heat, when protons leak across the inner mitochondrial membrane). This is the preferred process for energy production (especially in cells such as retinal neurons that are extremely metabolically active) as it generates a high net amount of ATP (29 - 30 in contrast to 2 ATP molecules, during glycolysis).

C) Bioenergetic analyses and the Seahorse Flux analyzer

Mitochondrial respiration in cells and tissues can be evaluated by measuring oxygen depletion in the media surrounding them. With the introduction of Seahorse XF Flux Analyzers this can now be done in a higher throughput manner using multi-well plates. The Seahorse Flux Analyzers create a transient micro-chamber in each well allowing the measurement of oxygen consumption rates (OCR) by assessing rates of oxygen depletion in the extracellular media that surrounds the tissue/cells under study (in our case, retinal punches)[286]. This technology also allows for assessment of different indices of mitochondrial function by sequentially administering a defined set of drugs that block mitochondrial respiration at different levels. These drugs are:

1) **Oligomycin**: this drug blocks ATP synthase and therefore the ETC and oxygen consumption by complex IV (i.e., oxidative phosphorylation). Any respiration occurring in the presence of oligomycin is a result of a proton leak in the IMM. This allows for differentiation between OCR associated with ATP production (coupled respiration) and OCR associated with proton leak (uncoupled respiration).

2) **FCCP (carbonylcyanide-p-trifluoromethoxyphenylhydrazone)**: This drug is an ionophore that permeabilizes the IMM to protons and therefore dissipates the proton gradient, uncoupling the normally dependent relationship between the ETC and ATP synthesis. Without the resistance of the proton gradient, the ETC (terminating in O_2 consumption) proceeds at maximal speed although ATP is not generated (heat is produced instead). The lack of ATP further enhances activity in the ETC in a desperate attempt to increase energy production within the cell. This enhanced activity in the ETC allows for determination of the *maximal respiratory capacity* of cells and tissues, which reflects the overall fitness of the mitochondria (determined by a combination of factors including their number and ETC density), in contrast to the *basal respiration* that reflects a cell's current energy demands.

3) **Rotenone and Antimycin A (RAA)**: These drugs inhibit the electron flow down the electron transport chain by blocking complexes I and III, respectively.

With this set of drugs (1-3), which are administered sequentially during the experiment, the following parameters can be assessed (**Figure 57**):

a. Basal level of oxygen consumption – measured before addition of oligomycin, which is indicative of a cell's current energy demand

b. Amount of oxygen consumption linked to ATP production (i.e., OCR related to oxidative phosphorylation – coupled respiration) – corresponds to the oligomycin-sensitive OCR (the drop seen in OCR after oligomycin addition)

c. Level of non-ATP-linked oxygen consumption that results in heat production (i.e., OCR related to proton leak – uncoupled respiration) – corresponds to the oligomycin-insensitive OCR

d. Maximal respiratory capacity (i.e., the maximal capacity that tissue/cells have to consume oxygen, which occurs when the ETC and ATP synthesis become uncoupled)– corresponds to the OCR measured after FCCP injection

e. Spare capacity (obtained by: maximal capacity – basal rate), which indicates the flexibility that the cell or tissue has to increase ATP production in order to meet increasing metabolic demands.

f. Non-mitochondrial oxygen consumption – corresponds to the OCR measured after rotenone and antimycin A (RAA) administration. Since these drugs inhibit the ETC, no oxygen is further consumed by mitochondrial cytochrome c oxidase. This non-mitochondrial OCR potentially reflects activity of cytosolic oxidase systems

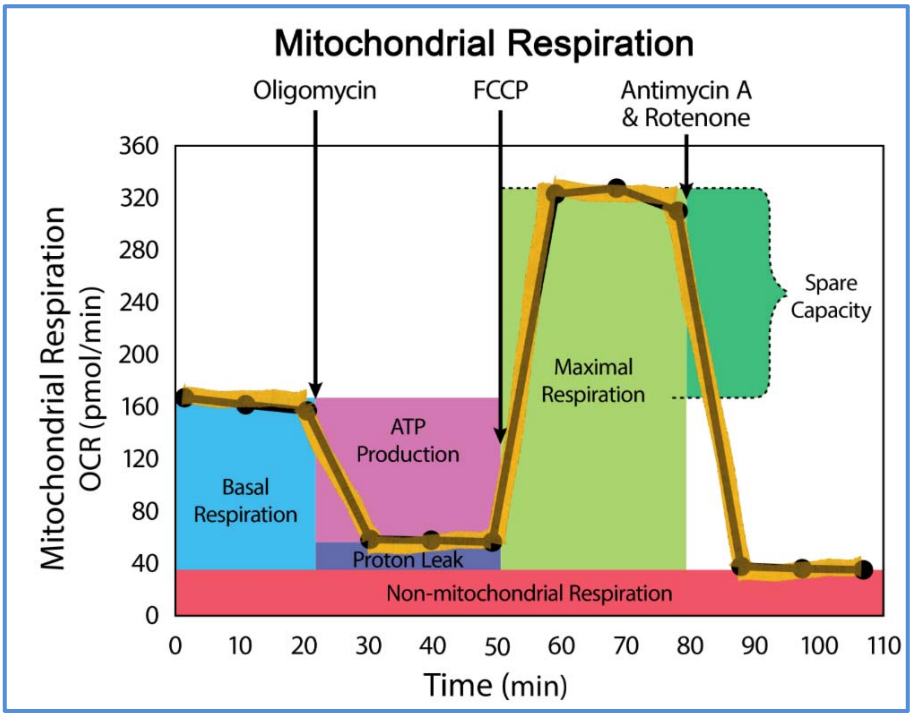

Figure 57– Representative graph depicting the different mitochondrial indexes that can be evaluated with the Seahorse Flux Analyzer using Oligomycin, FCCP, Antimycin A and Rotenone (www.seahorsebio.com)

In non-perfused retinal areas, the striking discrepancy between energy supply and demand causes a state of profound metabolic insufficiency that drives progression of ischemic retinopathies. In order to assess if inosine was affecting retinal

metabolism in OIR conditions, we compared oxygen consumption rates (OCR) in central (vaso-obliterated) and peripheral (vascularized) retinal regions from inosine and vehicle (PBS) OIR injected eyes (**Figure 58 and 59**).

In **central (vaso-obliterated) regions** of inosine treated retinas (Figures 58 and 59):

a) Basal OCR was significantly reduced (by 15%) when compared to controls
b) Maximal respiratory capacity was identical to that of controls
c) There was a trend towards an increase in spare capacity when compared to controls
d) The % of ATP-coupled and the % of uncoupled mitochondrial respiration were not changed when compared to controls.

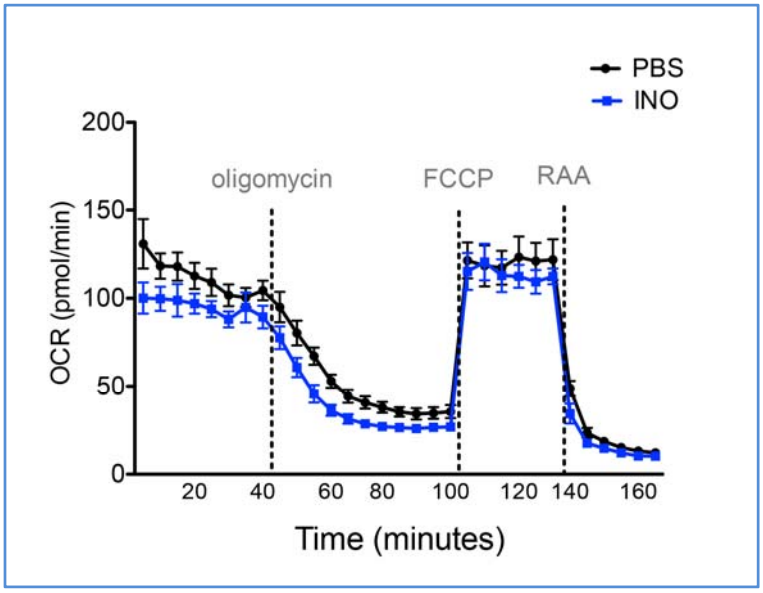

Figure 58 – Inosine reduces basal metabolism in central vaso-obliterated areas of OIR retinas without affecting their maximal respiratory capacity [in comparison to retinas from vehicle (PBS) injected eyes]. RAA = rotenone and antimycin A.

In **peripheral (vascularized) regions**, there were no significant differences in terms of retinal mitochondrial metabolism between inosine and vehicle injected eyes (**Figure 59**).

The fact that inosine only reduces OCR in vaso-obliterated but not in vascularized peripheral retinal regions suggests that it can act selectively in response to local conditions. Woollard and colleagues have described a similar situation in the myocardium after experimental acute coronary artery occlusion where inosine exhibited selective inotropic action (positive or negative) depending on specific tissue locations (hypoxic versus non-hypoxic) [287].

The reduced basal OCR in central, vaso-obliterated regions indicates that the energetic demand of these ischemic areas is reduced when inosine is provided. Given that inosine treatments did not affect maximal respiratory capacity or the percentage of uncoupled mitochondrial respiration, it suggests that neither the retinas' metabolic capacity nor their coupling efficiency were altered (i.e. mitochondrial fitness is not affected) by treatment, and that inosine is functioning primarily through altering the current energetic needs (metabolic demand) of the tissue. This functional yet energetically conservative retinal hypometabolic state can facilitate the revascularization process in ischemic areas, thus preventing pathological neovascularization.

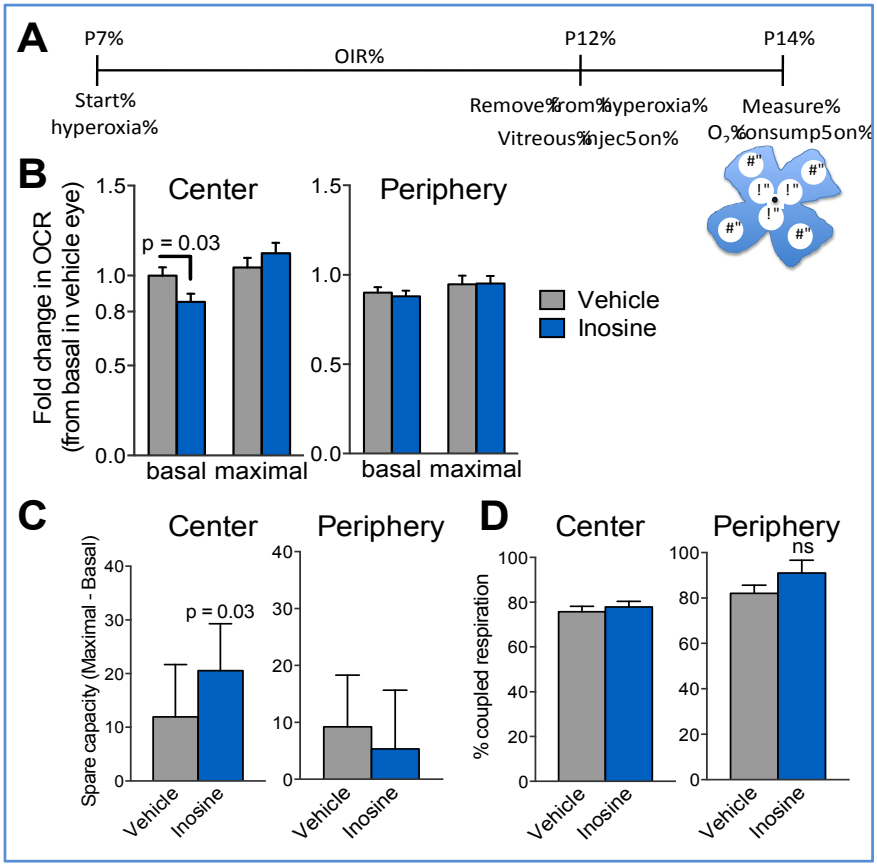

Figure 59 - Inosine slows basal mitochondrial respiration in the central vaso-obliterated areas of retinas from OIR mice. (A) Scheme depicting experimental time course. (B) Normalized oxygen consumption rates (OCR) from retinas punches in absence (basal) or presence of 0.75 uM FCCP (maximal). Data are mean plus SEM (n = 18 mice), p-value calculated with unpaired student's t-test. (C) Spare respiratory oxygen capacity (maximal OCR - basal OCR). Data are mean plus SEM (n = 3 experiments), p-value calculated with paired student's test. (D) Percent mitochondrial coupled respiration calculated from OCR in the presence of oligomycin (2 uM) and basal. Data are the mean plus SEM (n = 18 mice).

Inosine is rapidly converted to inosine-5'-monophosphate (IMP) and uric acid in OIR mice eyes

Metabolomic analyses revealed that eyes from OIR mice show lower levels of inosine, hypoxanthine and xanthine (as mentioned in **Chapter IV-B**) when compared to age matched controls raised in normoxia (NOX) suggesting that lower purine levels in the eye may contribute to development of retinal pathology, under ischemic conditions.[288]

To better characterize inosine metabolism in the OIR mouse eye, we performed *in vivo* global isotope metabolomic analyses using ^{15}N-labeled inosine intravitreal injections (and vehicle injections for controls; **Figure 60**). Shortly after injection (at 10 minutes), ^{15}N-inosine was converted to ^{15}N-hypoxanthine (387.8 fold upregulation in comparison to vehicle injected eyes; $p>0.05$), which was in turn metabolized to ^{15}N-IMP (422.91 fold upregulation; $p=0.01$) and ^{15}N-uric acid (31.36 fold upregulation; $p=0.003$) in the OIR mouse eye (**Figure 61A&B**)**.** General pathways of purine metabolism, including that of inosine, can be seen in presented in the Appendix.

Performing the same analysis in NOX eyes (non diseases eyes) revealed that ^{15}N-inosine was also preferentially converted to ^{15}N-IMP (313 fold upregulation; $p = 0.007$) with milder upregulation of ^{15}N-hypoxanthine (74.1 fold; $p =0.04$) and ^{15}N-uric acid (74 fold; $p=0.0002$; **Figure 61A&C**).

Comparing metabolism of ^{15}N-inosine in OIR and in NOX eyes suggests that the latter are more efficient at metabolizing inosine as they show significantly higher levels of uric acid (2.18 fold; $p=0.006$) along with a tendency towards increased production of IMP (2.24 fold, $p=0.07$) at 10 minutes post-injection (**Figure 62**).

IMP has been shown to play a beneficial role in energy metabolism by being converted to GMP and ATP[289]; and uric acid can potentially exert potent anti-oxidant effects in disease states[290]. These data on inosine's effect on metabolism suggest that increasing inosine ocular levels during hypoxia may contribute to retinal protection by inducing a more balanced metabolic profile in hypoxic retinal cells, through (1) reduction of basal O_2 consumption in vaso-obliterated areas (**Figure 59**), thus generating an energetically conservative hypometabolic state that does not compromise retinal function (**Figure 51**); and through (2) provision of high-energy phosphates and antioxidant power to retinal

cells. Similar phenomena have been suggested for inosine's protection in the ischemic myocardium[287,291-293].

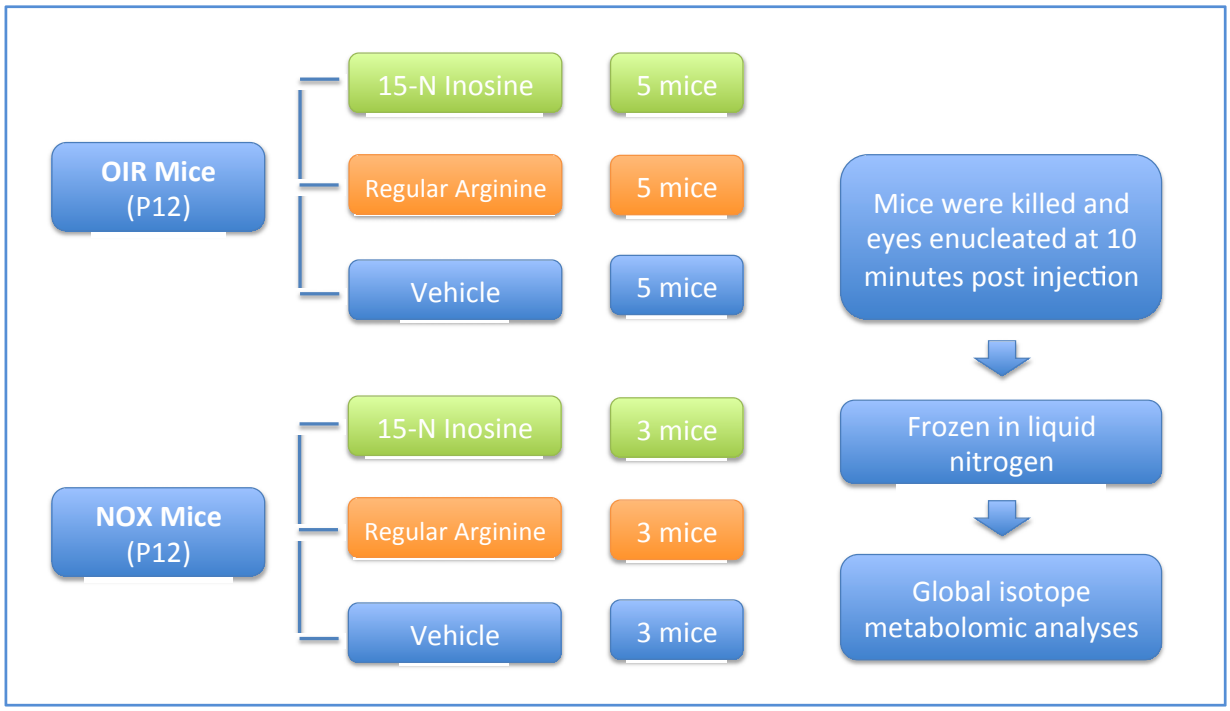

Figure 60- Global isotope experiments with ^{15}N-inosine: experimental design

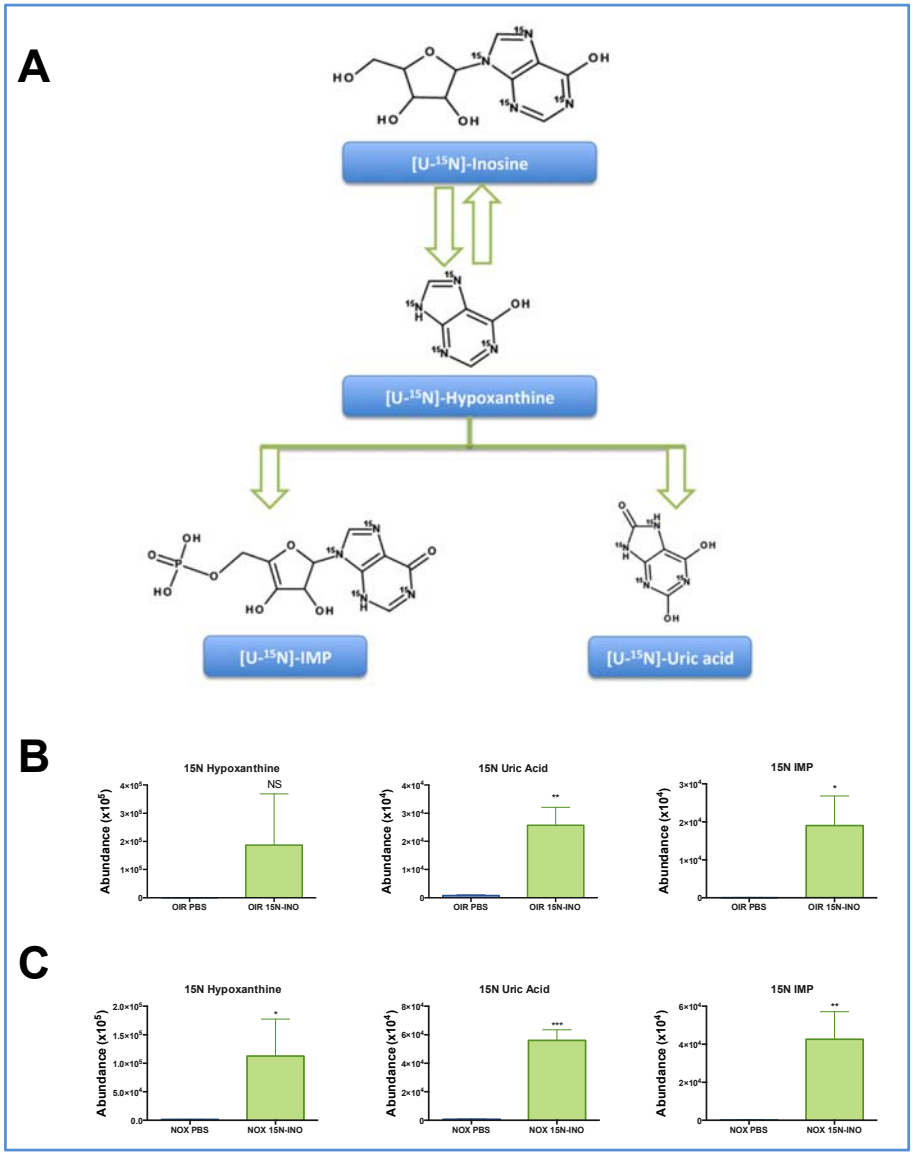

Figure 61 - Global isotope metabolomics with U-^{15N}Inosine (simplified diagram). (A) Ten minutes after intravitreal injection, U-^{15}N-inosine was metabolized to U-^{15}N labeled-hypoxanthine, U-^{15}N labeled-IMP and ^{15}N labeled-uric acid (27.3 fold upregulation over vehicle injected controls; p=0.0009); (B) In OIR eyes, levels of ^{15}N metabolites were upregulated as follows: Hypoxanthine (387.8 fold; p>0.05); Uric acid (31.36 fold; p=0.002); IMP (422.91 fold; p=0.01); (C) In NOX eyes, levels of ^{15}N metabolites were upregulated as follows: Hypoxanthine (74.1 fold; p=0.04); Uric acid (74 fold; p=0.0002); IMP (313 fold; p=0.007). Data analysis: Two-tailed unpaired Students' t-test; Values shown represent mean±SEM; *p<0.05; **p<0.01; ***p<0.001.

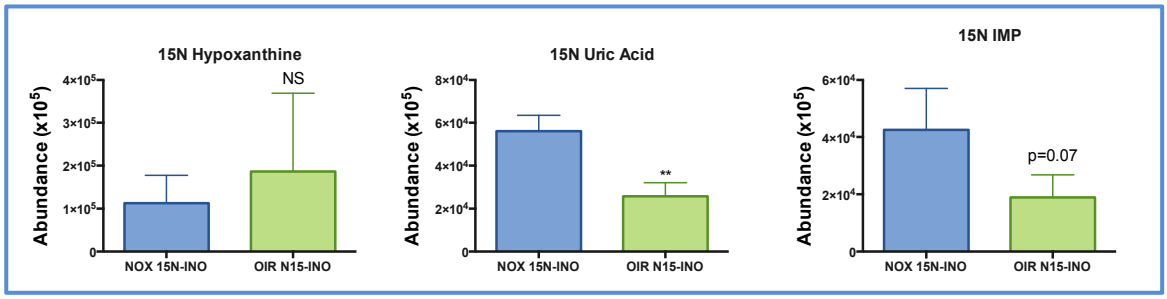

Figure 62 - Metabolism of ^{15}N-inosine to ^{15}N-uric acid is significantly higher in NOX eyes (2.18 fold upregulation; p =0.006) when compared to OIR eyes; ^{15}N-Hypoxanthine and ^{15}N-IMP are not significantly changed between the two conditions. Data analysis: Two-tailed unpaired Students' t-test'; Values shown represent mean±SEM; **p<0.01; NS =non statistically significant.

Due to the rapid metabolism of the ^{15}N-metabolites in the eye, additional experiments using flux analysis (to follow metabolic conversions over time), larger numbers of mice and longer follow-up will be the perfect future approach. These experiments will be important for optimization of the intravitreal dosage, and will ultimately provide comprehensive information on inosine metabolism in the eye.

Inosine down-regulates proline production in the OIR mouse eye

Over-activity in the retinal arginase pathway (of which proline is a downstream product) has been shown to strongly contribute to development of pathological neovascularization in the OIR mouse, and to retinal inflammation in an LPS-induced uveitis model[235,294]. In **Chapter IV-B** we reported that (1) a prominent dysregulation in arginine metabolism exists in the OIR mouse due to preferential activity in the arginase pathway; that (2) proline is one of the earliest metabolites to become dysregulated in the OIR mouse eye when compared to NOX control eyes; and that (3) similar perturbations in arginine metabolism exist in the vitreous of diabetic patients with PDR[288]. These results along with those reported in the literature suggest that arginase over-activity is an important contributor to retinal inflammation and development of the retinal pathological phenotype seen in human DR and in the OIR mouse.

To evaluate potential effects on arginine metabolism, inosine or vehicle were injected at P12 and targeted metabolomic analyses (focusing on products of

arginase metabolism: ornithine, urea and proline) were performed at P17. Proline was significantly downregulated in treated eyes (-1.74 fold; p = 0.041), suggesting that inosine may be reducing activity in the retinal arginase pathway, similarly to what has been reported in other tissues (**Figure 63A&B**). Due to their low concentrations in the OIR mouse eye, it was not possible to accurately compare ornithine and urea levels between vehicle and inosine injected eyes.

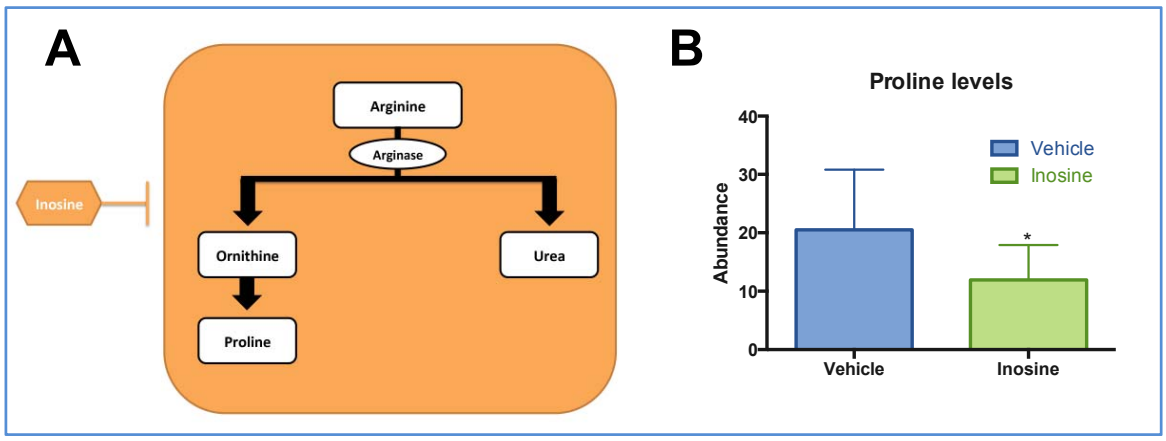

Figure 63– Inosine affects arginine-proline metabolism: (A) Working model for inosine in OIR retinas: Inosine inhibits the arginase pathway to reduce proline production (B) Global metabolomics showed that intravitreal injections of unlabeled (regular) inosine significantly reduce proline levels in OIR P17 retinas (1.74 fold downregulation; p=0.041). (Two tailed, unpaired Student's t-test; *p<0.05; values shown represent mean±SEM; *p<0.05).

To assess if reduced proline production could be associated with decreased retinal arginase levels, we performed gene expression analyses for arginase 1 (see **Figure 55**) and arginase 2 (**Figure 64**) in OIR retinal lysates from inosine vehicle injected eyes at different timepoints. There were no significant differences between experimental groups for neither of the retinal arginase isoforms. This suggests that the inosine-induced reduction in proline levels is not associated with differential transcriptional regulation but must rather occur post-translationally, potentially by a mechanism of competitive antagonism, as reported in other tissues[295,296].

The pathological retinal changes associated with arginase over-activation have been attributed to lack of arginine availability for the alternative NOS pathway, with consequent reduction in NO production and NOS uncoupling with increased nitrosative stress[234]. However, dysregulated proline levels locally may also be

playing an active role in development of the pathological phenotype; It has been shown that L-proline can act as a as a potential endogenous excitotoxin in cultured rat dorsal horn neurons by stimulating Ca^{2+} entry after activation of excitatory amino acid receptors[297]. This suggests that a dysregulation in proline may be further contributing to disrupt the neurovascular crosstalk in the NVU, thus promoting retinopathy progression; inosine, by reducing proline dysregulation, may be stabilizing intercellular communication and preventing disease progression.

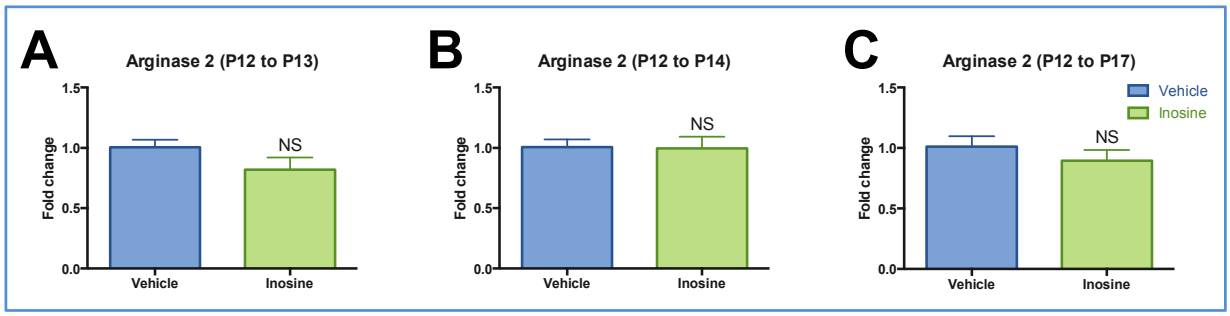

Figure 64 – Arginase 2 expression in OIR retinas from inosine and vehicle injected eyes. No statistically significant differences in gene expression levels were found between experimental groups at 24 h post-injection (A), at 48h post injection (B) or at 5 days post injection (C). (Two tailed Student's t-test; n=4 per experimental condition; values represent mean ± SEM; * $p<0.05$; NS = no statistical significance).

Discussion

Although it has been widely reported that a subset of diabetic patients does not develop severe diabetic complications despite long-term diabetes, the precise factors and mechanisms underlying this protection remain elusive.

Since there is no diabetic rodent model that spontaneously develops the late stages of DR[298], studying this subset of patients provides an excellent opportunity to identify potentially protective factors and to obtain critical information for development of novel biomarkers and more effective therapeutic strategies.

Our metabolomic analyses revealed a distinctive feature in the peripheral blood of some long-term diabetics "protected" from developing PDR, which consisted of significantly higher levels of inosine (in our study, inosine levels were especially upregulated in four of the "protected" patients), an endogenous purine metabolite. This suggests that (1) polymorphisms inducing hyperactivity in enzymes involved

in purine metabolic pathways (and especially in those upregulated under ischemic conditions, such as AMP deaminase[299]) may potentially act as protective factors for DR progression; and that (2) modulation of purine metabolism towards inosine production may be a therapeutic strategy to consider in DR management.

Additionally, circulating levels of inosine could potentially be used as a biomarker for assessment of risk of DR progression. Further studies with larger cohorts will be necessary to assess inosine's relevance as a reliable serum biomarker.

Inosine has been shown to exert neuroprotective[266,300], anti-depressant[301] and immunomodulatory effects[274] in several animal disease models. In humans, inosine's neuroprotective effects are currently being explored in clinical trials for multiple sclerosis and Parkinson's disease.[302,303]

To assess its effect on progression of ischemic retinopathy, inosine was injected intravitreally to the OIR mouse, a non-diabetic model that shares metabolic perturbations at the ocular level[288] (**Chapter IV-B**) and develops retinal pathological features resembling those observed in human PDR[304]. Inosine injections provided significant benefit to the OIR mouse retina by effectively accelerating revascularization of vaso-obliterated areas and secondarily reducing development of pathological neovascularization. Since inosine was unable to significantly prevent development of vaso-obliteration when injected before administration of 75% oxygen, the observed beneficial effects did not occur during the hyperoxic period but rather during hypoxia, which led us to choose the P12 time-point (right after they are removed from the hyperbaric chamber) for further therapeutic injections.

The inosine-induced improvement in the OIR retinal phenotype was associated with an effect on basal metabolism that was observed only in central, vaso-obliterated areas. This effect consisted on a 15% drop in basal mitochondrial metabolism with no associated compromise of maximal respiratory capacity or retinal neuronal function. The metabolic mismatch present in retinal ischemic areas disrupts retinal neurovascular crosstalk in the NVU, thus driving and sustaining progression of retinopathy. Taken together, these results suggest that inosine may be slowing basal mitochondrial metabolism in vaso-obliterated areas, where metabolic supply is scarce, to reduce metabolic demand and thereby increase retinal cell tolerance to hypoxia. In the literature, it has been shown that induction of a similar energetically conservative hypometabolic state allows for (1)

survival of mammals during periods of hibernation and (2) preservation of organs from non-hibernating mammals (e.g. human hearts for transplantation are transported in cold conditions with no blood supply for many hours) during considerable periods of ischemia[305]. Induction of hypometabolic states has also been implicated in life-span extension in *C.elegans* (and potentially in mammals as well), under conditions of caloric restriction[306,307].

Previous *in vitro* studies have shown that loss of mitochondrial spare (reserve) capacity, due to experimentally induced reduction of the maximal respiratory rate, causes cone photoreceptor cell degeneration, thus suggesting that preservation of maximal mitochondrial respiratory function is critical for retinal neuronal health[282]. Inosine did not reduce maximal respiratory capacity or coupling efficiency, which suggests that the observed reduction in basal metabolism is not due to hypofunctional mitochondria (i.e., lower 'mitochondrial fitness') or neuronal cell death (ERG responses in inosine and vehicle eyes were comparable) but rather constitutes an adaptive response to conditions of nutrient scarcity that can potentially be reversed when metabolic supply and energy conditions improve.

Designing future studies to gain further insight into the mechanism through which inosine slows basal mitochondrial metabolism in the retina may provide critical knowledge for development of new targeted therapies for retinal ischemic diseases.

Furthermore, induction of hypometabolic states has been shown to effectively prevent exacerbated inflammatory responses in cases of critical illness and has been proposed as a potential therapy for myocardial ischemia in adults.[308,309] Other mechanisms have also been suggested for inosine's protection of the ischemic myocardium; Inosine has been shown to be able to reduce infarct size and to significantly increase regional myocardial performance in ischemic areas after experimental coronary artery occlusion (in the pig heart, *in situ*) by exerting selective inotropism without any associated increases in metabolic demand [287,310]. This selective beneficial action favoring ischemic areas has been attributed to inosine's ability (1) to act as a potent coronary vasodilator (specifically increasing blood flow to the most hypoxic regions); and (2) to increase anaerobic ATP production by providing glycolytic substrates such as ribose-1-Phosphate, and precursors for purine nucleotide re-synthesis, such as hypoxanthine. [287].

Impaired endothelium-dependent vasodilation is a prominent and generalized feature of diabetes, and therapeutically targeting the vascular endothelium to re-establish normal vascular reactivity and achieve systemic metabolic benefits is a promising therapeutic strategy [311,312]. In DR and other ischemic retinopathies, disrupted neurovascular crosstalk contributes to impaired retinal vascular auto-regulation early on in the disease process. As a consequence, there is reduced compensatory vasodilation to hypoxia and other noxious stimuli, and development of metabolic mismatches[313]. Vasodilation and the consequent improvement in metabolic state can, therefore and by definition, prevent development of pathological neovascularization. Moreover, induction of vasodilation with sildenafil (in the early stages of hypoxia) has been shown to effectively prevent development of pathological neovascularization in the OIR model (by reducing HIF1alpha activation)[314].

Adenosine improves retinal arteriolar vasodilation to hypoxia through activation of A2A receptors, which are prominently expressed at the edge of the developing vasculature in OIR animals. Since inosine can also activate A2A receptors, therapeutically enhancing its levels in the eye may improve hypoxia-induced-vasodilation in the developing vessels at the interface of vascularized and vaso-obliterated regions in OIR retinas. This could increase metabolic supply to hypoxic areas and prevent development of exacerbated pro-inflammatory and pro-angiogenic responses, which would further slow basal mitochondrial metabolism in vaso-obliterated areas. The data showed here supports this hypothesis because inosine injections also induced a moderate reduction in expression levels of VEGF-A (and isoforms), TNF-α and CCL2 (MCP-1), which are known to be critical cytokines for development of retinal pathological neovascularization in the OIR model.

An additional mechanism through which inosine may be improving metabolic supply/demand ratios in the retina is related to its ability to favor a shift from oxidative to anaerobic metabolism, which is less ATP consuming[22]. Previous *in vitro* work has shown that inosine (and other purines) can act as alternative energy sources in conditions of metabolic deprivation[315-318] by providing ribose moieties (glycolytic substrates) and precursors for the purine salvage pathway, that are ultimately used for ATP production. Future studies focusing on accurately assessing glycolytic activity using flux analysis will be valuable to fully understand

inosine's potential in retinal ischemic diseases and potentially in other conditions characterized by metabolic insufficiency.

Results obtained during our *in vivo* global isotope metabolomic studies have also shown that ^{15}N-inosine is rapidly metabolized to ^{15}N-IMP and ^{15}N-uric acid in the OIR mouse eye, and both metabolites may further contribute to inosine's beneficial net effect. IMP has been shown to exert anti-inflammatory effects in remote lung injury, following hindlimb ischemia[319,320] and it may potentially enhance cell energy production by being converted to GMP and ATP[289]. Regarding uric acid, it can be protective by providing strong local anti-oxidant defense.

Alternatively, or as a complement to acting as an alternative energy source, inosine may also be protective by acting as a non-competitive inhibitor of retinal arginase[295,296], an enzyme that has been shown by our group and others to be overactive in the retina under OIR conditions[234] and in diabetic rodent models with early retinal features of DR[229]. Arginase 2 has been shown to be required for: (1) development of ischemic retinopathy changes in the OIR model[235]; (2) development of early DR retinal changes[229] in rodent models; and (3) development of LPS-induced retinal inflammation[294]. These findings may also have implications for human DR since in **Chapter IV-B** it is shown that, in human PDR, the most profound metabolic dysregulation in the vitreous occurs in the arginine-to-proline pathway, which suggests preferential activation of arginase.

Taken together, our results and those reported in the literature suggest that inosine may beneficially affect metabolism at three different levels, all of which may contribute to the inosine-mediated retinal protection seen in the OIR mouse retina and potentially in human DR. These three levels are:

(1) Serving as an alternative metabolic fuel for energy production;
(2) Improving the metabolic state of retinal vaso-obliterated areas by slowing basal mitochondrial metabolism (reducing demand), thus improving the crosstalk within the NVU and preventing exacerbated and deleterious pro-inflammatory and pro-angiogenic responses;
(3) Reducing proline production in the retina, potentially by inhibiting arginase by competitive antagonism.[295,296]

In this study, we show that inosine (1) is upregulated in diabetic patients who develop minimal, if any, changes of DR and that (2) it significantly prevents development of pathological pre-retinal neovascularization (resembling that seen in PDR) in the OIR mouse. A metabolic mechanism may be promoting these beneficial effects and ensuring more efficient energy management in ischemic retinal cells, by slowing basal aerobic metabolism, and thus reducing the metabolic mismatch that destabilizes cellular interactions in the NVU. This global improvement in retinal cell metabolism and NVU crosstalk may prevent development of exaggerated retinal pro-inflammatory responses, thereby breaking the vicious cycle that sustains progression of ischemic retinopathies. These events may explain the retinal protection seen in OIR retinas after inosine injections and in ”protected” long-term diabetic patients with high serum inosine levels.

Judging from the significant benefits observed in the OIR mouse and from its protective effects in human patients with multiple sclerosis, inosine could prevent some of the early disruptive events in NVU pathophysiology that drive progression of DR, and therefore potentially become a promising therapeutic to arrest DR progression at its early stages.

The currently preferred therapeutic approach in DR, laser photocoagulation, is destructive and prevents disease progression by reducing metabolic demand through ablation of peripheral retinal neurons; in this work we show that inosine can similarly and effectively prevent progression of ischemic retinopathy by selectively reducing retinal metabolic demand in a non-destructive fashion,

As such, inosine (alone or in combination) could become a more effective, early acting and safer therapeutic strategy for DR than the ones currently used in the clinic, which act late and present concerning off-target effects.

Main conclusions

- Differentially regulated serum inosine levels may distinguish protected long-term diabetic patients from those who develop late-stage disease (PDR)
- Inosine may become a biomarker to assess risk of progression of DR
- Inosine also holds promise as a therapeutic agent for the early stages of DR, as studies in the OIR mouse show that it significantly prevents

development of retinal PDR-like retinal features by slowing basal metabolism (without inducing neuronal cell death), thereby reducing metabolic demand in a non-destructive fashion. These effects are expected to stabilize cellular interactions within the NVU, thus preventing progression of DR. Moreover, inosine also downregulates proline levels in the eye, which become significantly upregulated under pathological conditions (in human PDR and in OIR).

- Inosine also exhibits immunomodulatory properties in the retina that may result from the improved metabolic state in the ischemic retina and its associated beneficial effects on retinal neurovascular crosstalk (a stabilized neurovascular crosstalk can potentially prevent development of excessive pro-inflammatory responses and therefore progression of retinal disease).

D. Inadequate Metabolic Control and Development of DR: A Case Study

Rationale for conducting this study

- It has been suggested that patients with Wolfram syndrome (WS), a rare neurodegenerative disorder characterized by simultaneous presence of optic atrophy and diabetes mellitus, are relatively protected from developing diabetic retinopathy[321]
- The main mechanisms suggested for this protection are the following: (1) better glycemic control (when compared to age-matched type 1 diabetic patients); and (2) lower retinal metabolic demand, as a consequence of profound RGC death due to optic nerve atrophy (although PRs have the highest metabolic rate in the retina, RGC also significantly contribute to the overall metabolic demand of this tissue).
- Here, we report a case of Wolfram syndrome in a 16-year-old male patient who presented with progressive optic atrophy and a severe form of diabetes since diagnosis at the age of 6, with challenging glycemic control despite intensive therapy; although metabolic control was inadequate, the patient did not develop any diabetic complications during the 10-years of follow-up.
- To further investigate potential causes for this metabolic idiosyncrasy, we performed genetic analyses that revealed a novel combination of homozygous mutations as the cause of the syndrome in this family. The identified genotype included a novel mutation in the Wolfram syndrome type 1 gene (*WFS1*) along with a previously described one, which had initially been associated with low frequency sensorineural hearing loss (LFSNHL).

➢ The work presented in this chapter was performed by LPP

D.1. A challenging form of non-autoimmune insulin-dependent diabetes in a Wolfram syndrome patient with a novel sequence variant

Background and significance

Wolfram syndrome (WS) is a rare multisystem neurodegenerative disorder of autosomal recessive origin that minimally requires the presence of two diagnostic criteria, insulin-dependent diabetes mellitus (of non autoimmune origin) and progressive optic nerve atrophy [322]. WS is also referred to as DIDMOAD, an acronym for its most common clinical presentation that includes: diabetes insipidus (DI), diabetes mellitus (DM), optic atrophy (OA) and deafness (D)[323].

Even through diabetes mellitus and optic atrophy are the earliest and most common manifestations of WS, neurological and genito-urinary tract complications, which usually develop at later disease stages, are especially concerning, as they constitute the leading causes of morbidity and mortality in the patient population.[323,324]. WS is classified into type 1 or type 2, according to the genetic mutation that determines the pathological phenotype.

WS type 1 is caused by mutations in the *WFS1* (Wolfram syndrome type 1) gene and is responsible for approximately 90% of the WS cases worldwide; Incidence is variable depending on geographic location, with reported estimates of 1/700.000 in the UK and 1/100.000 in South America [325]. Even though mutations of exon 8 of the *WFS1* gene (NM_006005; chromosome 4p16.1) cause the majority of WS type 1 cases, this syndrome is characterized by significant genetic heterogeneity, which contributes to a non-linear genotype-phenotype correlation [326,327].

The *WFS1* gene encodes wolframin, a transmembrane protein localized to the endoplasmic reticulum (ER) that is involved in membrane trafficking, secretion, processing and regulation of ER calcium homeostasis, therefore being critical for preventing ER stress signaling[328] Wolframin is ubiquitously expressed but its highest levels are found in pancreatic beta cells, cardiomyocytes and specific neurons[329]. It has been shown that deletion of the *WFS1* gene in rodents leads to progressive pancreatic beta cell loss due to increased ER stress, along with impaired insulin secretion and higher incidence of diabetes[330-332]. In humans,

various genetic studies have also shown a strong association between *WFS1* gene variants and increased risk of type 2 diabetes[333-335]. The existence of *WFS1* variants with different severities, with inactivating or non-inactivating properties, and the way in which these interact to induce and modulate phenotypic expression of progressive pathological features remains unclear.
In this study we identify a novel *WFS1* missense sequence variant in a WS patient and describe its associated progressive clinical picture (over a 10-year follow-up period) in a 16-yr old patient who developed an especially challenging form of insulin-dependent diabetes at the age of 6.

Case report

A 6-year-old male patient with a history of mild learning disabilities was referred to our hospital for polyuria and polydipsia and diagnosed with insulin dependent diabetes, which rapidly proved to be particularly challenging in terms of metabolic control with fasting blood glucose levels ranging from 203 to 431 g/dl, despite intensive therapy with different therapeutic regimens (**Table 14**).
Further investigation of the disease excluded autoimmune causes (both Islet Cell Cytoplasmic Autoantibodies, ICCA, and Glutamic Acid Decarboxylase Autoantibodies, GADA, were negative) and revealed the following HLA haplotype: HLA-A*02, *24; HLA-B*07, * 08; HLA-C*04, * 07; DRB1*03, * 13; DQB1*02, * 06.
His learning disabilities and general pediatric exam suggested a potential visual impairment, which prompted an evaluation by ophthalmology. At age 6, the patient presented with best-corrected visual acuity (BCVA) of 6/20 (3/10), bilateral optic nerve head palor (**Figure 65A**) and no other retinal abnormalities. The presence of bilateral optic atrophy associated with non-auto immune diabetes suggested a clinical diagnosis of Wolfram Syndrome (WS).

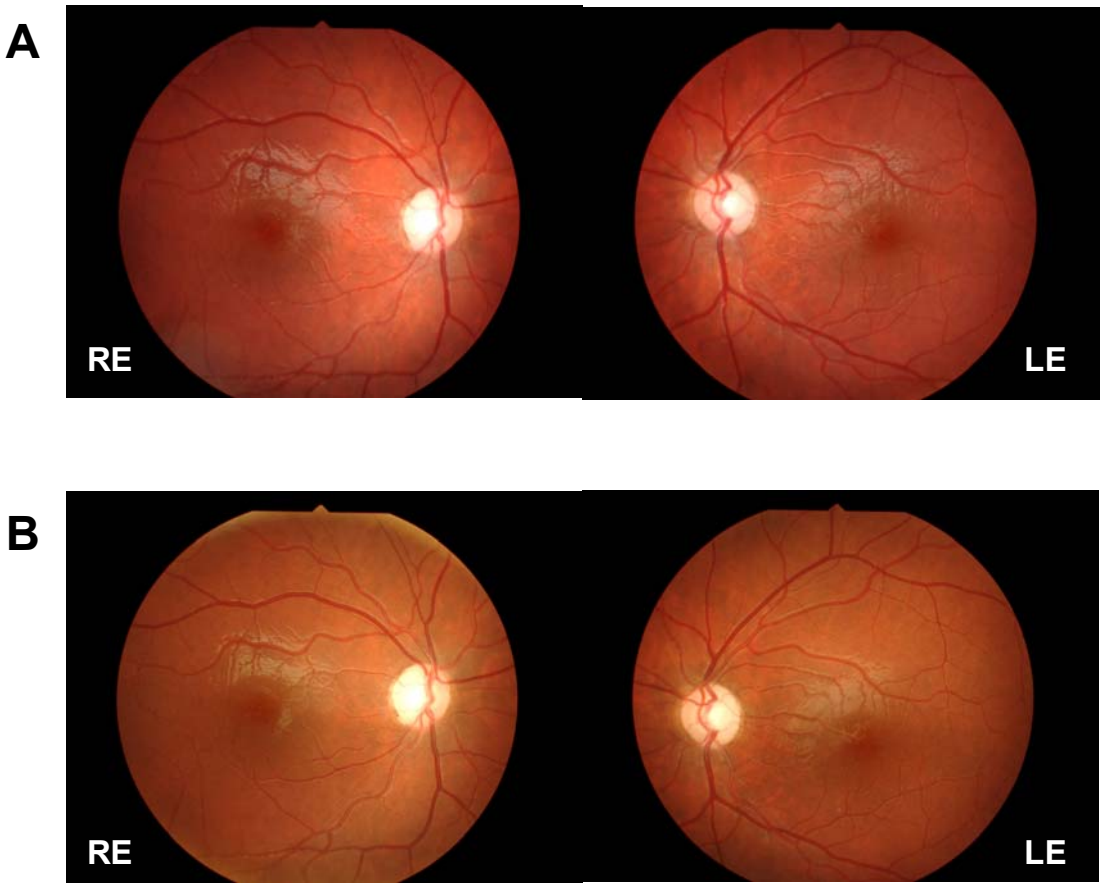

Figure 65 - Retinographies at age 10 (A) and 16 (B), showing severe optic atrophy with no retinal changes suggestive of diabetic retinopathy. RE = right eye; LE = left eye

At age 8, nocturnal enuresis became frequent and ultrasonography suggested neurogenic bladder. A deteriorated performance at school was also noted due to problems in speaking (immature speech and difficulties in articulation and phonological processes), reading and interpreting, leading to his failing to pass to the next school year. His intelligence quotient (IQ) was evaluated twice with the Wechsler Intelligence Scale for Children (WISC-III) and determined to be 64 at age 8 and 59 at age 11 (an IQ between 50 and 69 is considered "borderline mental functioning" in this testing conditions). The patient currently attends the 9th grade (at age 16).

At age 16, the patient had incomplete pubertal development with testicular atrophy associated with increased FSH levels, normal LH and normal total testosterone levels (**Table 14**). His height and weight were 1.65 m (5.41 ft; percentile P 10-25) and 64.5 kg (142.2 lbs; P 50-75), respectively. Regarding his metabolic status, abdominal lipodystrophy was evident and glycemic control remained highly

inadequate (HbA1c 8.8 - 9%) under treatment with a 1.5 U/kg daily dose of insulin. His insulin sensitivity factor was 20g/dl and his insulin/carbohydrates ratio was 5G. Blood pressure was 119/63 mmHg.

Table 14 - Evolution of analytical parameters in our patient

	Age 16	Age 14	Age 13	Age 6	Reference values
Fasting blood glucose (mg/dl)	183	272	198	352	70-105
Urea (mg/dl)	25	42	32	51	16.7-45.4
Creatinine (mg/dl)	0.8	0.9	0.7	0.5	0.7-1.3
Uric acid (mg/dl)	4.4	5.6	5.2	N/A	3.5-7.2
Total cholesterol (mg/dl)	130	142	133	N/A	< 200
HDL (mg/dl)	36	47	45	N/A	> 60
LDL (mg/dl)	85	82	72	N/A	< 100
Triglycerides (mg/dl)	44	63	79	N/A	< 150
TSH (uUI/ml)	2.54	2.33	2.09	4.52	0.35 -5.50
Free T4 (ng/dl)	1.12	1.24	1.07	1.36	0.89-1.76
Cortisol (ug/dl)	19.8	15.7	14.1	19.1	3.7 – 19.4
Insulin (uU/ml)	19.5	N/A	N/A	N/A	2.6-24.9
C peptide (ng/ml)	0.3	N/A	N/A	N/A	1.1 – 4.4
LH (mUI/ml)	6.20	7.92	3.88	N/A	1.14 – 8.75
FSH (mUI/ml)	22.24	31.95	16.09	N/A	1.37 – 8.75
Estradiol (pg/ml)	19	N/A	N/A	N/A	0
Total testosterone (ng/dL)	402	410	377	N/A	166-811
Glucose (urine) mg/dl	1000	N/A	N/A	N/A	0
Glomerular filtration rate (MDRD-4) ml/min	137.06	N/A	N/A	N/A	> 60

During the 10 years of follow-up, the patient underwent periodic multidisciplinary assessments; inadequate metabolic control was observed throughout these evaluations with HbA1c ranging from 8.6 to 9% despite multiple attempts with different therapeutic combinations and nutritional strategies.

Ophthalmological assessments revealed a progressive deterioration in BCVA [from 6/20 (3/10), at age 6, to 6/125 (1/20), at age 16] associated with continued atrophy of the optic disc (**Figure 65B**) and significant functional impairment in visual field (Goldmann) and electrophysiological testing. Visual evoked potentials (VEP), an electrophysiological test that measures conductance of electrical impulse from the optic nerve to the brain, were significantly impaired showing increased latency and decreased amplitude of the P100 wave, especially in the left eye. However, no associated changes were noted in the full field ERG. These findings are suggestive of a significant and isolated defect at the level of the optic nerve.

The patient also underwent two audiometry exams at age 10 and 12 that were normal for all hearing frequencies (**Figure 66**). He did not develop any symptoms suggestive of diabetes insipidus or diabetic vascular complications, such as diabetic retinopathy, nephropathy or neuropathy. His thyroid function and cortisol values were within the normal range of values (**Table 14**)

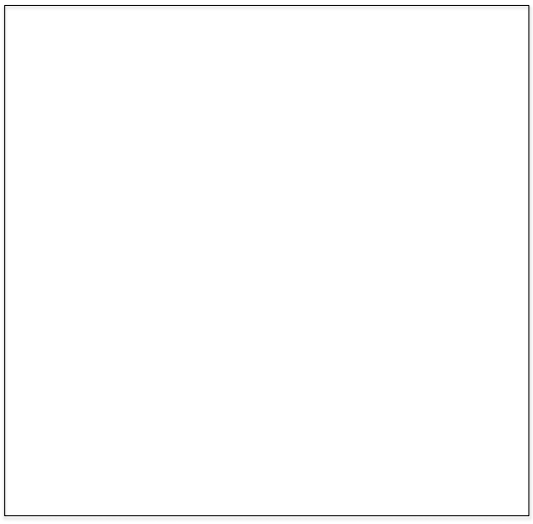

Figure 66 – Audiograms of the patients at age (A) 10 and (B) 12.

Genetic analyses identified two sequence variants in homozygosity in the *WFS1* gene of our patient, who is the second child of a self-reportedly couple. The

presence of non-consanguinity, however, could not be accurately determined because the father and the family members from the older generation refused to undergo genetic testing.
The sequence variants identified were the following:

(1) A novel missense variant **c1066T>C** (pSer356Pro), in exon 8;
(2) A previously described variant **c482G>A** (pArg161Gln), in exon 5, initially associated with low frequency sensorineural hearing loss (LFSNHL)[336] and later described in the 1000 Genomes Project[337] and interpreted as benign by Shearer et al[338].

His mother and his 19-year-old sister were heterozygous for the same sequence variants in the *WFS1* gene, while the 11-year-old brother did not present any variations (**Figure 67**).
These findings highly suggest that (1) both sequence variants must be located on the same chromosome (haplotype) and that (2) the presence of the two haplotypes in homozygosity is the cause for Wolfram syndrome in this family.

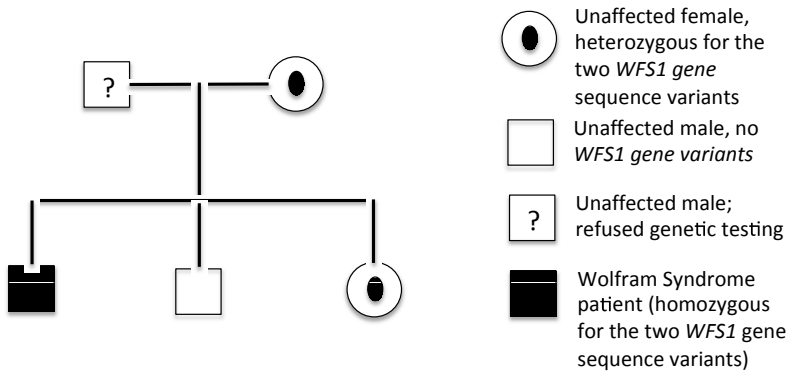

Figure 67 - Segregation of the *WFS1* gene variants (c1066T>C and c482G>A) in the nuclear family of the patient.

Discussion

Wolfram syndrome, also known as DIADMOAD, is a rare autosomal recessive neurodegenerative disease that typically includes clinical features of insulin-dependent diabetes, diabetes insipidus, optic nerve atrophy and deafness that progress during the patient's lifetime[323]. The minimum diagnostic criteria are the presence of diabetes mellitus and optic nerve atrophy, which usually develop during the first decade[339].

The patient in this study came to our attention clinically due to a diagnosis of insulin dependent diabetes at the age of 6, which was later found to be non-autoimmune. This finding is quite unusual as 70-80 % of the type 1 Diabetes cases are initially positive for ICCA and GADA antibodies [340]. The diabetes in the patient was very challenging to manage and despite multiple therapeutic strategies, HbA1c levels were always above the desired values. He also presented prominent learning disabilities that were partly due to his visual impairment.

The presence of insulin dependent diabetes with peculiar features, such as non-autoimmune diabetes and difficult metabolic control, associated with visual impairment, or very significant learning disabilities, which may be masking a profound visual disorder, should prompt the clinician to consider Wolfram syndrome as a possible diagnosis. These patients need to be evaluated and managed by a multidisciplinary team to maximize their quality of life. Support and knowledge about the condition must be provided to their families, including information about prognosis; the mortality rate is very high with 60% of the patients dying by the age of 35[341].

After establishing a clinical diagnosis of WS from the simultaneous presence of non-autoimmune diabetes mellitus and optic nerve atrophy, genetic testing was offered to our patient and his family. Two sequence variants were identified in homozygosity in the *WFS1* gene (exons 5 and 8):

The novel variation c1066T>C (pSer356Pro) is a missense variant predicted to be: pathogenic by MutationTaster and PolyPhen-2; and likely benign by PROVEAN and SIFT. Mutations in the vicinity codons (350 and 361) have been described in association with Wolfram syndrome. Since this is a highly conserved residue, except in drosophila, and family segregation is compatible, we interpret this variant as likely pathogenic.

The other sequence variant (c482G>A) has initially been reported to confer a 50% risk of developing autosomal dominant non-syndromic low-frequency hearing loss and has later been described in association with Wolfram syndrome[336,338]. Interestingly, our patient did not present any evidence of hearing impairment over the ten years of follow-up (**Table 15**).

Table 15 - Clinical features present in our patient in comparison to those commonly reported

Clinical features	Typical WFS1 cases	WFS1 our case
Diabetes mellitus	X	X
Optic atrophy	X	X
Sensorineural Hearing Loss	X	
Diabetes insipidus	X	
Neurological disorders	X	X
Genito-urinary tract problems	X	
Hypogonadism	X	X

To facilitate the diagnosis of WS within the type 1 diabetic population, Ehrlich and Fishman suggested in 1986 that certain HLA haplotypes could be of interest, (HLA DR2 had a higher prevalence in WS patients)[341]. Pinelli challenged this notion in 1987, claiming that the higher prevalence of specific HLA subtypes in the WS patient population was more likely a reflection of the genetic heterogeneity of the population from which those cases had arisen[342].

The work by Marshall et al showed that diabetes mellitus and optic nerve atrophy were the most common (94%) and earliest features to develop in young patients

with WS[323].Neurogenic bladder and dilations in the renal outflow tract are common in WS patients in their third decade of life. Our patient developed symptoms of enuresis due to a neurogenic bladder quite early, at the age of 8.

Marshall et al reported that enuresis, nocturia and post-void residual bladder volume were present in 22%, 17% and 45%, respectively, of their young WS patient cohort[323].

Earlier studies have suggested that metabolic control is more easily attained in WS patients when compared to regular type 1 diabetic populations.[343] This was not observed in our patient where glycemic control proved to be incredibly challenging despite multiple attempts of therapeutic plan optimization and confirmed compliance with treatment.

A genetic variant in the *WFS1* human gene has been shown to determine impaired glucagon-like peptide-1-induced insulin secretion[344]; it is possible that the novel *WFS1* sequence variant identified in our patient plays a particularly disruptive role in beta cell functioning, contributing to profound impairment in insulin production, secretion or sensitivity.

Surprisingly, despite 10 years of highly inadequate metabolic control (HbA1c ranging from 8 to 9%) there was no evidence of diabetic retinopathy (DR) or other complications in our patient. Most clinical studies suggest that WS patients are relatively protected from developing diabetic microvascular complications when compared to regular type 1 diabetics, however the cause for this protection remains elusive.[345,346] Diabetes severely reduces metabolic supply to the retina, thereby generating a metabolic mismatch that drives development and progression of diabetic retinopathy (DR)[40]. It is possible that the protection against DR reported in WS patients is associated with premature retinal ganglion cell (RGC) death due to the optic atrophy that develops early on (RGC form the optic nerve) with consequent reduction in retinal metabolic demand. This potentially reduces the metabolic mismatch and leads to a better overall retinal energy status, thus eliminating the pathogenic stimulus that drives development and progression of DR.

Signs of hypogonadism are common in patients with WS and are usually attributed to hypothalamic or pituitary dysfunction[323]. The testicular atrophy and hormonal profile (high FSH with normal LH and testosterone) observed in our patient are consistent with a Sertoli-cell-only syndrome, also known as germinal cell

aphasia[347]. These findings are consistent with animal studies reporting that *WFS1* deficient male mice show impaired fertility with significantly reduced number of spermatogonia and Sertoli cells.[348] As wolframin is involved in calcium homeostasis and in preventing ER stress, Haghighi A et al suggested that mutations in the *WFS1* gene can disrupt ion homeostasis, affecting Sertoli cell development, sperm maturation and function, and ultimately reducing fertility.[349]

Conclusion

In the present study we report a 16 year-old patient with Wolfram syndrome with a therapeutically challenging form of non-autoimmune diabetes associated with a novel sequence variant in the *WFS1* gene.

Over the 10-year follow-up period by a multidisciplinary hospital team, our patient developed: (1) insulin-dependent diabetes that was difficult to control metabolically; (2) a profound visual deficit due to progressive optic nerve atrophy; (3) enuresis associated with neurogenic bladder; and (4) hypogonadism.

Interestingly, and in contrast to what would have been expected from his genotype, he did not develop hearing loss or diabetes insipidus. These findings reinforce the concept that genotype-phenotype correlations are not clear in WS[327] and suggest that functional studies assessing interactions of different sequence variants and/or mutations in the *WFS1* gene may hold the key to a more precise understanding of the pathophysiology of this devastating syndrome.

Chapter V: Discussion, Conclusions and Future Directions

Discussion

Despite the high prevalence of DR worldwide and the devastating visual consequences of its late-stages, reliable biomarkers and early-acting, effective and sustainable therapeutic strategies to arrest disease progression remain to be developed.

As described in **Chapter I**, most research on DR focuses on studying how diabetes damages individual retinal structures (e.g., vessels; neurons; Mueller glia) and disregards the context they live in. This over-simplistic perspective dangerously neglects the diabetes-induced compromise of the global retinal metabolic landscape and the disrupted interactions between the different retinal cell types. In addition, this perspective has contributed to the lack of new knowledge required for development of novel targeted, effective and earlier acting therapies for DR.

The studies performed in this dissertation are intended to advance and improve diabetic eye care, by providing a new perspective on DR that focuses on the NVU and on metabolic interactions that mediate retinal neurovascular crosstalk.

In order to gain better knowledge regarding distribution and functionality of NVUs in normal and diseased retinas, studies in different animal models of retinal disease were undertaken (**Chapter IV-A**), and highly sensitive metabolomic analyses were performed on ocular tissue and blood samples of well-characterized diabetic patients to (1) generate a global picture of the characteristic metabolic landscape of DR and (2) identify distinguishing metabolic perturbations in diabetic patients that may have potential clinical interest (**Chapters IV-B and IV-C**).

Chapter IV-A conclusively demonstrates that NVUs are not restricted to the RGC layer by showing, for the first time, that amacrine cells and PRs function in NVUs in the IPL and outer retina. Additionally, it shows that these neurons actively participate in neurovascular crosstalk and are able to regulate their own metabolic supply (and ensure its adequacy), by producing vasculotrophic factors (e.g., VEGF and erucamide, respectively) that maintain healthy retinal and choroidal vascular beds during adulthood.

PRs have long been suggested to markedly contribute to progression of DR due to their high metabolic needs that further aggravate the energetic state of hypoxia-damaged neurons in regions of retinal ischemia[100,215,217]; however PR dysfunction has long been considered a secondary consequence of primary vascular changes induced by diabetes.

Similarly, loss of amacrine cells and amacrine cell dysfunction have been reported in the diabetic retina, both in patients and in animal models that develop early DR changes, and this has also been considered a passive result of primary vascular changes[218].

Data presented in **Chapter IV-A** challenge the notion that neuronal dysfunction is simply a consequence of vascular changes by showing that dysregulated production of vasculotrophic factors by amacrine cells and PRs (induced by disruptions in neurovascular crosstalk secondary to pathological conditions) leads to abnormal vascular phenotypes in the surrounding retina. This strongly suggests that neuronal dysfunction, along with the subsequently induced disruption of neurovascular crosstalk, can initiate and drive development of retinal vascular changes under pathological conditions (such as DR) that compromise delivery of energy supplies and retinal cell metabolism.

This work also shows that stabilizing retinal neurovascular crosstalk early in the disease process (e.g. administration of erucamide in models of retinal degeneration, before neuronal death starts) is critical and effective for avoiding further disease progression. These findings suggest that potentially more effective therapies for human retinal neurovascular diseases can be developed if a similar approach is followed; better outcomes will be attained if therapeutic strategies aim at restoring functionally effective intercellular communication within retinal NVUs (by reverting metabolic derangements) early in the disease process, before irreversible phenotypic changes take place.

Chapter IV-B identifies the most severely dysregulated metabolic pathways in eyes affected with late-stage diabetic retinopathy (PDR). By expanding knowledge on ocular metabolic dysregulation in PDR, it provides critical information for development of targeted therapies aimed at reinstating homeostasis within the NVU

In PDR eyes, the most perturbed pathways included amino acid metabolism and ammonia detoxification, purine related oxidative stress and acylcarnitine metabolism. Ocular pathways of amino acid metabolism, were the most notoriously dysregulated and, in particular those pertaining to arginine-to-proline metabolism.

Knowing that arginine metabolism is the most severely compromised pathway in PDR sheds new light onto dysfunctional ERG responses to flicker-light stimulation (defective 'functional hyperemia'), which have been reported in patients with diabetic retinopathy[79,350]. This dysfunctional retinal response to flickering light, which consists of insufficient vasodilation in response to light-induced increases in neuronal activity, has been attributed to defective communication between Mueller glia and the vasculature due to inadequate production of NO, which is an important modulator of retinal neurovascular crosstalk[227].

The work presented in this dissertation suggests that arginine metabolism occurs preferentially by activation of the arginase pathway in the OIR model (and that this may also be the case in human PDR) and, as a result, activity in the alternative arginine-metabolizing pathway, the NOS pathway (responsible for NO production), is reduced. This diabetes-induced perturbation in arginine metabolism can potentially restrict NO production in Mueller cells at crucial time-points, being responsible for disruption of the crosstalk between Mueller glia and vasculature and, consequently, for the defective functional hyperemia response observed in diabetic patients.

Work by Robert Marc *et al.* further supports involvement of disrupted Mueller cell arginine metabolism in neuroretinal disease by showing that arginine works as a largely Mueller cell-specific signal that closely follows and reflects alterations in Mueller cell function in conditions of extreme retinal remodelling[239]. In a model of light-induced retinal damage, retinal neuronal death is followed by extreme morphological transformation of Mueller cells and formation of a glial seal, which triggers a pronounced increase in arginine levels (especially near the seal) followed by a subsequent drop once remodeling is complete.[239] Over-activity of the arginase pathway also leads to increased proline production, which may further compromise crosstalk within the NVU, contributing to progression of retinal disease. Moreover, the compromise in ammonia detoxification pathways also identified in PDR ocular samples, can further impair Mueller cell function and

produce retinal damage by inducing metabolic overload in these cells[351]. Taken together, these findings suggest that metabolites generated during arginine metabolism can potentially become valuable metabolic biomarkers for assessing risk of progression of DR and for monitoring response to therapy. In addition, these results also suggest that (1) metabolic overload and a compromise in arginine metabolism in Mueller cells may play a pivotal role in initiating disruption of retinal neurovascular crosstalk; and (2) effective therapies for preventing progression of DR should be able to antagonize, prevent and/or reverse arginase hyper-activity early in the disease process to potentially re-establish homeostatic cellular interactions within the NVU, thus avoiding the development of subsequent pathological retinal responses.

Chapter IV-C identifies a circulating metabolite with potentially protective properties in regard to DR progression in human serum samples, and further explores its therapeutic potential for preventing development of features of ischemic retinopathy in the OIR mouse model.

It is widely known that a subset of diabetic patients does not develop severe diabetic complications despite long-standing diabetes.[352] The cause and mechanisms underlying this protection, however, remain largely unknown and are among the most intriguing questions related to diabetes.

The work presented in this chapter suggests that inosine, an endogenous purine metabolite, may be a factor involved in protection against development of severe DR in long-term diabetic patients through an effect on retinal oxidative metabolism. Studies in the OIR mouse suggest that inosine has therapeutic potential for preventing features of ischemic retinopathy and that this beneficial effect is accomplished by reducing basal metabolic demand in retinal cells to a level that maximizes efficiency of energy usage in conditions of scarce metabolic supply, while preserving adequate retinal functioning.

In the OIR mouse, intravitreal injections of inosine promoted effective intraretinal revascularization of vaso-obliterated (hypoxic) areas and, thus, prevented development of pathological neovascularization by reducing the characteristic metabolic mismatch that exists in these regions. Addressing this mismatch between metabolic supply and demand is critical because it fosters progressive

neuronal damage, disrupts retinal neurovascular crosstalk and exacerbates pro-inflammatory responses.

Formation of new vessels in adulthood only occurs in pathological states, such as PDR; in such circumstances (and according to the plane of growth), two types of vessels can be distinguished in the retina: (1) intraretinal vessels, which are mature, covered by pericytes and smooth muscle cells and do not leak; and (2) preretinal vessels, which grow outside of the retinal plane towards the vitreous, are immature, not covered by mural cells and therefore leaky.

One of the most challenging paradoxes in retinal ischemic diseases such as PDR and Retinopathy of prematurity (ROP) relates to understanding why and how a highly proangiogenic environment promotes misdirected vascular growth towards the vitreous rather than into ischemic areas, which desperately need to be nourished[40].

Identifying factors, such as inosine, that are capable of modulating the retinal microenvironment to ‘re-educate’ vascular growth and promote significantly higher levels of effective intraretinal revascularization of hypoxic areas, provides a promising therapeutic strategy, as it optimizes allocation of proangiogenic resources in the retina and efficiently eliminates areas of retinal metabolic insufficiency, which constitute the driving forces for disease progression.

This inosine-induced retinal protection observed in the OIR mouse was associated with additional metabolic effects that may be beneficial for the overall retinal phenotype: (1) after injection, inosine was rapidly metabolized into hypoxanthine, and later IMP and uric acid, which can potentially improve the retinal energetic and antioxidant cell status, respectively[289,290];(2) inosine treated eyes had lower levels of proline, suggesting that inosine may be inhibiting activity in the ocular arginase pathway to prevent pathological accumulation of proline, as seen in late-stage DR; evidence from the literature supports this possibility as inosine and uric acid have been shown to be able to inhibit arginase in other tissues.[295,296]

By improving the ocular metabolic landscape and impeding continued dysregulation in arginine-to-proline metabolism, inosine can restore healthy metabolic interactions between cells to maintain a regulated neurovascular crosstalk in the retina, stabilizing the NVU. This in turn can prevent activation of neuronal stress responses and their detrimental consequences, such as development of pathological NV, a hallmark of PDR.

These novel findings can potentially contribute to significant improvements in diabetic patient care, by:

Favoring development of new biomarkers

Since (1) inosine production increases under conditions of metabolic insufficiency due to ATP breakdown and (2) patients with higher levels are apparently protected from progressing into PDR, serum measurements of inosine in diabetic patients (who all undergo retinal ischemia but only a few can upregulate inosine production to protective levels) may become a valuable biomarker in assessing risk of progression of DR. Moreover, performing genetic studies in diabetic patients to identify predictably functional polymorphisms in inosine producing pathways and assessing their potential relationship with risk of DR, may reveal novel protection-associated genotypes and shed new light into inosine's role in progression of DR.

Favoring development of novel, more effective therapeutics

Ocular administration of metabolites capable of preventing and/or counteracting local metabolic dysregulation could become an effective targeted strategy to restore retinal neurovascular crosstalk in the early disease stages and, consequently, prevent activation of pathological events, such as extreme neuronal hypoxic damage and exacerbated pro-inflammatory responses that foster further disease progression.

Inosine could become a valuable therapeutic agent for early DR due to its favorable metabolic effects, which can potentially stabilize cellular interactions within the NVU by reducing retinal metabolic demand, thus preventing progression of DR into its catastrophic late-stages.

Conclusions

- **Retinal cells form NVUs across the retina, developing interdependent interactions that are mediated by metabolic factors; these cellular**

interactions become disrupted under disease conditions, promoting development of pathological retinal neovascularization, neuronal degeneration and severe visual dysfunction.

- Regulated metabolic interactions within the NVU play a pivotal role in ensuring retinal homeostasis and proper visual function.

- Retinal neurons function in neurovascular units in the different retinal layers and play an active role in ensuring their own nutrition by directly participating in angiogenesis promoting pathways; retinal neurons (such as amacrine cells and photoreceptors) are actively involved in inducing retinal vascular development during embryogenesis and in maintaining healthy retinal and choroidal vascular beds, in adulthood.

- This neurovascular crosstalk is, at least in part, mediated by metabolites that function as signaling factors whose production is highly regulated in order to guarantee harmonious interdependent cellular interactions within the NVU. Disease (e.g. diabetes) disrupts retinal cell metabolism, thus compromising production of these signaling metabolic factors and destabilizing retinal neurovascular crosstalk, leading to further metabolic dysfunction and development of retinal pathological phenotypes.

- **Highly sensitive MS-based metabolomic analyses identified**

a) The most severely compromised metabolic pathways in PDR eyes
b) A circulating metabolite with potentially protective properties

- Global characterization of the ocular metabolic landscape in PDR revealed severe biochemical perturbations, with the most prominent one being in the arginine-to-proline metabolic pathway (with marked upregulation of proline levels)

- Metabolomic analysis performed in the blood of long-term diabetics who do not develop severe DR revealed the elevated presence of a purine

metabolite, inosine, with potentially protective properties in the context of ischemic retinopathies

- **A novel integrated therapeutic approach to DR is suggested**

  - In order to effectively prevent progression of diabetic retinopathy and other retinal diseases, it is critical to act early to restore homeostatic interactions within the NVU by: (1) administering exogenous metabolic signaling factors to stabilize their local concentrations to physiologic levels; (2) administering drugs that counteract the most prominent biochemical perturbations, such as inhibitors of the arginine-to-proline pathway (e.g. arginase inhibitors).

  - Inosine is a promising therapeutic agent for DR management as it can counteract activity in the arginine-to-proline pathway and potentially exert beneficial effects in both energy and antioxidant retinal status, to stabilize retinal neurovascular crosstalk and prevent development of late-stage pathological retinal features

---

The work presented in this dissertation provides evidence that pathological retinal insults, such as hypoxia and other conditions leading to metabolic insufficiency, induce prominent metabolic dysregulation in retinal cells potentially disrupting retinal neurovascular crosstalk within the NVU. This disrupted communication leads to inadequate provision of energy supplies to highly metabolically demanding neurons, such as photoreceptors, which activate 'neuronal stress responses' culminating in deregulated production of commonly vasculo- and neurotrophic factors, such as erucamide and VEGF. These factors are beneficial when produced in moderate levels under physiologic conditions, however, when produced in massive amounts (as occurs in hypoxia), they promote development of pathological neovascularization, disorganization of the retinal architecture and further neurodegeneration.

Given the close interaction and interdependence among different retinal cell types shown by defects in NV coupling after flickering light stimulation[79], retinal diseases such as DR should not be regarded as resulting from a primary vascular or neuronal defect but, rather, as resulting from disrupted cellular interactions in the neurovascular unit. Accordingly, therapeutic efforts should be directed at restoring the intercellular “symbiotic relationships” that were present before disease onset.

Future directions

The work presented in this dissertation suggests that inosine may have significant potential in treating diabetic retinopathy and, eventually, other ischemic retinal diseases through its direct effect on retinal oxidative metabolism and its secondary effect on arginine-to-proline metabolism.

Further metabolic experiments can provide additional insight regarding inosine's mechanism of action in retinal tissue undergoing ischemia or other pathological conditions characterized by metabolic insufficiency. Such studies can also assist in the development of specific biomarkers to use in the clinic.

To further understand inosine's mechanism of action in the retina under ischemic conditions, the following questions need to be answered:

(A) How does inosine affect aerobic glycolysis and substrate utilization in OIR retinas?

Retinal metabolism is extremely interesting because retinal cells perform not only high levels of oxidative metabolism (i.e., mitochondrial respiration) but also relatively high levels of aerobic glycolysis, in order to meet the extremely demanding metabolic needs of its neuronal cells. [353]. In the work presented here it is shown that inosine is able to induce an energetically conservative "hypometabolic" state to better match up metabolic demand with supply in the ischemic retina. Performing Seahorse analyses on retinas from P17 OIR mice will be interesting in order to assess if there are additional changes in oxidative metabolism after a longer period of hypoxia.

Aerobic glycolysis also plays a relevant role in retinal ATP production, and it is possible that ischemic retinal cells in vaso-obliterated areas are using this pathway to cope with metabolic stress and obtain the additional ATP they need to maintain their basal functioning. It would be of interest to understand what is happening at this level by analyzing lactate production in ischemic area (as this would indicate the level of aerobic glycolysis).

Additionally, inosine may also be inducing a *shift in substrate utilization* (towards alternative fuel sources) by the mitochondria of these ischemic retinal cells, which

would be beneficial in conditions of glucose scarcity. For example, if glucose supply were to become limited due to high utilization for lactate production, retinal cells could adapt to these new conditions by using alternative substrates, such as fatty acids or amino acids, for oxidation; By using alternative energy sources such as glutamine, for example, inosine could be inducing a metabolic substrate switch while reducing mitochondrial metabolism, to overcome the energy deficit present in vaso-obliterated areas.

Performing flux analysis in OIR retinas treated with inosine or vehicle would trace alternative oxidative substrates (e.g., amino acids and fatty acids) and provide accurate information on the 'metabolic fuels' that are being used by ischemic retinal cells to cope with metabolic stress. Differential regulation of substrate utilization has been previously shown in other cell types with drugs such as glitazones[354].

(B) How does inosine induce a hypometabolic state in the hypoxic retina?

Even though hypometabolic states are critical for survival under conditions of extreme environmental stress (e.g. hypothermia, drought, oxygen and/or nutrient deprivation) and are common across the animal kingdom, the mechanisms controlling entry into these energetically conservative states remain largely unknown[355].

One aspect of this dissertation that merits further work is investigation of the molecular events implicated in inosine's induction of hypometabolic states in vaso-obliterated regions of OIR retinas.

It has been shown that activation of the adenosine A1 receptor reduces oxidative metabolism in cells, allowing them to better tolerate noxious stimuli, such as prolonged hypoxia[356]. Inosine has been shown to exert beneficial effects on the CNS through activation of this receptor[357,358].

Especially considering that the dose of inosine provided in our studies (which may be too low to be directly acting as a carbon or energy source), it is conceivable that inosine is inducing its effects on retinal oxidative metabolism through activation of this receptor. To test this hypothesis, treatment with DPCX (an A1 receptor antagonist) can be intraperitoneally injected before inosine or vehicle (intravitreal) injections in OIR mice. If inosine can no longer provide protection

under these circumstances, metabolomic analyses using the Seahorse flux analyzer should be performed to assess the effects of A1 receptor blockade on retinal oxidative metabolism.

(C) Is arginase inhibition required for inosine's beneficial effect?

Studies have shown that arginase over-activity plays a major role in promoting progression of retinal DR changes in diabetic models and in driving pathological neovascularization in the OIR model[230,231,234,359].
Inosine was able to significantly depress proline production (which is a downstream product of the arginase pathway) in the OIR mouse eye and, along with uric acid, has been shown to act as a noncompetitive antagonist to arginase in different tissues[295,296]. To conclusively determine if arginase inhibition is required for inosine's beneficial effect on the ischemic retina, future research studies may use transgenic mice with constitutive arginase expression (in retinal neurons), raise them under OIR conditions and evaluate inosine's potential to prevent progression of retinal pathology.

(D) Does proline dysregulation play an active role in progression of DR?

The work presented in this dissertation shows that proline is one the earliest and most prominently dysregulated metabolites both in human PDR and in the OIR mouse eye. Nevertheless, proline's role in favoring disruption of the neurovascular crosstalk and development of retinal pathological neovascularization remains unclear and it is not known if it is a secondary "player" or an actual signaling factor. In order to evaluate this further, future research could focus on manipulating proline's ocular levels in different models of retinal ischemic diseases to assess how these affect (1) development and progression of pathological features and (2) retinal metabolism (oxidative and glycolytic).

(E) How do variations in NO levels contribute to the generation of PDR-like retinal features?

As a consequence of increased arginase activity in the OIR and DR rodent retina, the alternative arginine-metabolizing pathway, which is catalyzed by NOS and

produces NO, is also expected to be functioning abnormally. In normal retinas, NO can be produced by every retinal cell type and is responsible for regulating hemodynamics and for promoting cell viability[227,359]. NO is also involved in intercellular communication within the NVU, where it acts not only as a simple mediator of neurovascular coupling but rather as a modulator[100,152]; its effects on retinal neurovascular crosstalk and on retinal homeostasis cannot be fully explained by varying overall NO levels, which suggests that its final retinal actions may depend on more subtle aspects, such as its temporospatial distribution in the eye or even the consequences arising from dysfunction of the cell type where its production is more markedly compromised.

In future studies dedicating to understanding the role of NO in OIR, a NO-donor agent, such as nipradilol, can be administered locally and early in the disease process (for example at P7 as well as P12) and its effects on development of the PDR-like phenotype assessed at P14 and P17. To prevent potential increases in formation of reactive nitrogen species due to increased free NO levels, an antioxidant (e.g. gluthathione) could be concomitantly administered.

Nipradilol has shown promising effects in protecting RGC from apoptosis in streptozotocin-induced diabetic rats.[360]

(F) Do IMP and uric acid play a role on retinal neurovascular crosstalk?

This dissertation shows that inosine is metabolized *in vivo* to IMP and uric acid in the OIR mouse eye. It may be that these metabolites also play a role in inosine's protective effects seen in OIR retinas, by acting directly as signaling factors, or indirectly as modulators of cellular communications within the NVU. In order to evaluate these scenarios, modulation of IMP and uric acid levels *in vivo* in the eye (in OIR mice), along with studies using labeled isotopes can be performed in the future.

(G) How does diabetes lead to ocular metabolic dysregulation and how does it destabilize crosstalk within the retinal NVU?

Another important research effort would be to determine the precise mechanisms by which diabetes destabilizes neurovascular crosstalk in the retina. From the

work presented in this dissertation one can suggest that perturbations in arginine metabolism play an important role; however, the mechanism through which this dysregulation destabilizes crosstalk within the NVU remains elusive. In order to achieve a deeper understanding of this event, it will be important to investigate if there is a retinal cell type that instigates the disruption, having the greatest impact on the existing pathological metabolic landscape. One of the most promising candidates is the retinal Mueller glial cell[227,239] and detailed characterization of its metabolome can potentially reveal new mediators of the neurovascular crosstalk, thus shedding new light onto diabetes-induced disruption of neurovascular coupling.

In addition, studying the metabolome and performing Seahorse analysis in parallel to look for hypometabolic states in different cultured retinal cells types treated with inosine or vehicle can potentially identify interesting correlations between production of specific metabolites and effects on mitochondrial metabolism. These studies can pave the way towards development of promising therapeutics to stabilize retinal neurovascular crosstalk.

(H) How do inosine injections impact retinal functionality of ischemic retinas?

In this work, ERG experiments performed on normal mice (raised in normoxia) after intravitreal inosine or vehicle injections showed that inosine is safe and does not compromise retinal function.

Even though performance of functional studies (e.g. ERG; optokinetic reflexes testing) is quite challenging in young OIR mice, assessing the effects of inosine and PBS injections on retinal functioning in other rodent models of neurodegeneration and ischemic retinopathies is still valuable as it can provide insightful information that can be interpreted in light of the accompanying metabolic phenotype (by performing Seahorse analyses at the same time-points).

From a more clinical perspective, it would be valuable to further assess the following issues:

(A) Validate our study results suggesting that elevated inosine levels are significantly associated with "protection" from developing late-stage DR by performing additional studies with larger patient cohorts

(B) What causes higher inosine production in a subset of long-term diabetic patients?
When does systemic upregulation become noticeable?

In the protected diabetic patient cohort analyzed in this work, allopurinol was ruled out as a potential cause for higher inosine levels. Unveiling the cause for higher inosine production in a subset of long-term diabetic patients can potentially provide new biomarkers and new mechanistic information on DR pathophysiology.
It is possible that genetic polymorphisms determine variations in activity of enzymes involved in inosine metabolism should be considered and investigated.
To better understand when inosine dysregulation starts in diabetic patients, it would be interesting to conduct long-term prospective epidemiological studies with serial assessments of serum inosine levels (ideally until most diabetic patients started developing DR changes) in pre-diabetic patients, diabetic patients without evidence of DR and age matched non-diabetic controls.
Since inosine serum levels in healthy populations have not yet been evaluated, it would be helpful to have this type of large-scale studies conducted in parallel, as these would show if factors such as age play a relevant role in promoting differential regulation of inosine levels.

(C) Are arginine, proline and inosine viable biomarkers for assessing risk of DR?

In order to evaluate reliability of these metabolites' levels as predictive and therapeutic biomarkers for DR, clinical studies with large cohorts of diabetic patients suffering from different DR stages will have to be performed. Assessing differences in circulating levels of these metabolites and determining their ratios between distinct patient groups can potentially validate their use for clinical purposes.

(D) Can early administration of vasculotrophic factors prevent progression of DR?

While the initial events that trigger DR and other retinopathies remain to be identified, novel therapeutic opportunities can arise from exploiting the role of early administration of vasculotrophic factors to the retina, as these (1) appear to be significantly reduced early in the retinal (neurodegenerative) disease process and (2) vascular maintenance appears to be key to maintain retinal neuronal health. Administering vasculotrophic factors may seem counterintuitive when one considers that we are using anti-VEGF agents to antagonize pathological neovascularization in late stages of DR; however knowing that these vasculotrophic factors are normally produced by neurons to maintain the surrounding vasculature healthy and to ensure their own adequate nourishment, administration of these factors early on in the disease process could actually be promising because it would avoid states of metabolic insufficiency in retinal neurons and the subsequent detrimental consequences they induce.

Chapter VI: References

1. Yau JW, Rogers SL, Kawasaki R, Lamoureux EL, Kowalski JW, et al. (2012) Global prevalence and major risk factors of diabetic retinopathy. Diabetes Care 35: 556-564.
2. Georgalas I, Papaconstantinou D, Papadopoulos K, Pagoulatos D, Karagiannis D, et al. (2014) Renal Injury Following Intravitreal Anti-VEGF Administration in Diabetic Patients with Proliferative Diabetic Retinopathy and Chronic Kidney Disease- A Possible Side Effect? Curr Drug Saf.
3. Pahor D (1998) Visual field loss after argon laser panretinal photocoagulation in diabetic retinopathy: full- versus mild-scatter coagulation. Int Ophthalmol 22: 313-319.
4. Grunwald JE, Daniel E, Huang J, Ying GS, Maguire MG, et al. (2014) Risk of geographic atrophy in the comparison of age-related macular degeneration treatments trials. Ophthalmology 121: 150-161.
5. Kizawa J, Machida S, Kobayashi T, Gotoh Y, Kurosaka D (2006) Changes of oscillatory potentials and photopic negative response in patients with early diabetic retinopathy. Jpn J Ophthalmol 50: 367-373.
6. Antonetti DA, Klein R, Gardner TW (2012) Diabetic retinopathy. N Engl J Med 366: 1227-1239.
7. Kolb H (1995) The Organization of the Retina and Visual System. In: Kolb H, Fernandez E, Nelson R, editors. Webvision: The Organization of the Retina and Visual System. Salt Lake City (UT): University of Utah Health Sciences Center.
8. Poche RA, Reese BE (2009) Retinal horizontal cells: challenging paradigms of neural development and cancer biology. Development 136: 2141-2151.
9. Yau KW (1994) Phototransduction mechanism in retinal rods and cones. The Friedenwald Lecture. Invest Ophthalmol Vis Sci 35: 9-32.
10. Yau KW, Hardie RC (2009) Phototransduction motifs and variations. Cell 139: 246-264.
11. Heck M, Schadel SA, Maretzki D, Bartl FJ, Ritter E, et al. (2003) Signaling states of rhodopsin. Formation of the storage form, metarhodopsin III, from active metarhodopsin II. J Biol Chem 278: 3162-3169.
12. Bowmaker JK (1998) Evolution of colour vision in vertebrates. Eye (Lond) 12 (Pt 3b): 541-547.
13. Saari JC, Nawrot M, Stenkamp RE, Teller DC, Garwin GG (2009) Release of 11-cis-retinal from cellular retinaldehyde-binding protein by acidic lipids. Mol Vis 15: 844-854.
14. Wang JS, Kefalov VJ (2011) The cone-specific visual cycle. Prog Retin Eye Res 30: 115-128.
15. Wright AF, Chakarova CF, Abd El-Aziz MM, Bhattacharya SS (2010) Photoreceptor degeneration: genetic and mechanistic dissection of a complex trait. Nat Rev Genet 11: 273-284.
16. Dorrell MI, Aguilar E, Jacobson R, Yanes O, Gariano R, et al. (2009) Antioxidant or neurotrophic factor treatment preserves function in a mouse model of neovascularization-associated oxidative stress. J Clin Invest 119: 611-623.
17. Dick AD (2009) Influence of microglia on retinal progenitor cell turnover and cell replacement. Eye (Lond) 23: 1939-1945.
18. Kettenmann H, Hanisch UK, Noda M, Verkhratsky A (2011) Physiology of microglia. Physiol Rev 91: 461-553.

19. Strauss O (2005) The retinal pigment epithelium in visual function. Physiol Rev 85: 845-881.
20. Levin LAAFH (2011) Adler's physiology of the eye. Edingburg: Saunders/Elsevier.
21. Chacon-Camacho OF, Zenteno JC (2015) Review and update on the molecular basis of Leber congenital amaurosis. World J Clin Cases 3: 112-124.
22. Wong-Riley MT (2010) Energy metabolism of the visual system. Eye Brain 2: 99-116.
23. Saint-Geniez M, D'Amore PA (2004) Development and pathology of the hyaloid, choroidal and retinal vasculature. Int J Dev Biol 48: 1045-1058.
24. Marin Garcia PJ, Marin-Castano ME (2014) Angiotensin II-related hypertension and eye diseases. World J Cardiol 6: 968-984.
25. Gardner TW, Antonetti DA, Barber AJ, Lieth E, Tarbell JA (1999) The molecular structure and function of the inner blood-retinal barrier. Penn State Retina Research Group. Doc Ophthalmol 97: 229-237.
26. Dorrell MI, Otani A, Aguilar E, Moreno SK, Friedlander M (2004) Adult bone marrow-derived stem cells use R-cadherin to target sites of neovascularization in the developing retina. Blood 103: 3420-3427.
27. Ding J, Wong TY (2012) Current epidemiology of diabetic retinopathy and diabetic macular edema. Curr Diab Rep 12: 346-354.
28. Potente M, Gerhardt H, Carmeliet P (2011) Basic and Therapeutic Aspects of Angiogenesis. Cell 146: 873-887.
29. Quaegebeur A, Lange C, Carmeliet P (2011) The Neurovascular Link in Health and Disease: Molecular Mechanisms and Therapeutic Implications. Neuron 71: 406-424.
30. Gelfand MV, Hagan N, Tata A, Oh WJ, Lacoste B, et al. (2014) Neuropilin-1 functions as a VEGFR2 co-receptor to guide developmental angiogenesis independent of ligand binding. Elife 3: e03720.
31. Horuk R (1998) Chemokines beyond inflammation. Nature 393: 524-525.
32. Carmeliet P, Tessier-Lavigne M (2005) Common mechanisms of nerve and blood vessel wiring. Nature 436: 193-200.
33. Adams RH, Eichmann A (2010) Axon guidance molecules in vascular patterning. Cold Spring Harb Perspect Biol 2: a001875.
34. London NR, Smith MC, Li DY (2009) Emerging mechanisms of vascular stabilization. J Thromb Haemost 7 Suppl 1: 57-60.
35. Nicoli S, Standley C, Walker P, Hurlstone A, Fogarty KE, et al. (2010) MicroRNA-mediated integration of haemodynamics and Vegf signalling during angiogenesis. Nature 464: 1196-1200.
36. Mazzone M, Dettori D, Leite de Oliveira R, Loges S, Schmidt T, et al. (2009) Heterozygous deficiency of PHD2 restores tumor oxygenation and inhibits metastasis via endothelial normalization. Cell 136: 839-851.
37. Edwards MM, Lefebvre O (2013) Laminins and retinal vascular development. Cell Adh Migr 7: 82-89.
38. Dorrell MI, Aguilar E, Friedlander M (2002) Retinal vascular development is mediated by endothelial filopodia, a preexisting astrocytic template and specific R-cadherin adhesion. Invest Ophthalmol Vis Sci 43: 3500-3510.
39. Fruttiger M (2007) Development of the retinal vasculature. Angiogenesis 10: 77-88.

40. Sapieha P (2012) Eyeing central neurons in vascular growth and reparative angiogenesis. Blood 120: 2182-2194.
41. Weidemann A, Krohne TU, Aguilar E, Kurihara T, Takeda N, et al. (2010) Astrocyte hypoxic response is essential for pathological but not developmental angiogenesis of the retina. Glia 58: 1177-1185.
42. Scott A, Powner MB, Gandhi P, Clarkin C, Gutmann DH, et al. (2010) Astrocyte-derived vascular endothelial growth factor stabilizes vessels in the developing retinal vasculature. PLoS One 5: e11863.
43. Okabe K, Kobayashi S, Yamada T, Kurihara T, Tai-Nagara I, et al. (2014) Neurons Limit Angiogenesis by Titrating VEGF in Retina. Cell 159: 584-596.
44. Lang RA (1997) Apoptosis in mammalian eye development: lens morphogenesis, vascular regression and immune privilege. Cell Death Differ 4: 12-20.
45. Marquardt T, Ashery-Padan R, Andrejewski N, Scardigli R, Guillemot F, et al. (2001) Pax6 is required for the multipotent state of retinal progenitor cells. Cell 105: 43-55.
46. Binet F, Mawambo G, Sitaras N, Tetreault N, Lapalme E, et al. (2013) Neuronal ER Stress Impedes Myeloid-Cell-Induced Vascular Regeneration through IRE1α Degradation of Netrin-1. Cell Metabolism 17: 353-371.
47. Fruttiger M, Calver AR, Kruger WH, Mudhar HS, Michalovich D, et al. (1996) PDGF mediates a neuron-astrocyte interaction in the developing retina. Neuron 17: 1117-1131.
48. Diez-Roux G, Lang RA (1997) Macrophages induce apoptosis in normal cells in vivo. Development 124: 3633-3638.
49. Caprara C, Thiersch M, Lange C, Joly S, Samardzija M, et al. (2011) HIF1A is essential for the development of the intermediate plexus of the retinal vasculature. Invest Ophthalmol Vis Sci 52: 2109-2117.
50. Olsson AK, Dimberg A, Kreuger J, Claesson-Welsh L (2006) VEGF receptor signalling - in control of vascular function. Nat Rev Mol Cell Biol 7: 359-371.
51. Carmeliet P, Ferreira V, Breier G, Pollefeyt S, Kieckens L, et al. (1996) Abnormal blood vessel development and lethality in embryos lacking a single VEGF allele. Nature 380: 435-439.
52. Stalmans I, Ng YS, Rohan R, Fruttiger M, Bouche A, et al. (2002) Arteriolar and venular patterning in retinas of mice selectively expressing VEGF isoforms. J Clin Invest 109: 327-336.
53. Nakamura-Ishizu A, Kurihara T, Okuno Y, Ozawa Y, Kishi K, et al. (2012) The formation of an angiogenic astrocyte template is regulated by the neuroretina in a HIF-1-dependent manner. Dev Biol 363: 106-114.
54. Stahl A, Connor KM, Sapieha P, Chen J, Dennison RJ, et al. (2010) The mouse retina as an angiogenesis model. Invest Ophthalmol Vis Sci 51: 2813-2826.
55. Garrett KL, Shen WY, Rakoczy PE (2001) In vivo use of oligonucleotides to inhibit choroidal neovascularisation in the eye. J Gene Med 3: 373-383.
56. Schwesinger C, Yee C, Rohan RM, Joussen AM, Fernandez A, et al. (2001) Intrachoroidal neovascularization in transgenic mice overexpressing vascular endothelial growth factor in the retinal pigment epithelium. Am J Pathol 158: 1161-1172.

57. Baffi J, Byrnes G, Chan CC, Csaky KG (2000) Choroidal neovascularization in the rat induced by adenovirus mediated expression of vascular endothelial growth factor. Invest Ophthalmol Vis Sci 41: 3582-3589.
58. Wang F, Rendahl KG, Manning WC, Quiroz D, Coyne M, et al. (2003) AAV-mediated expression of vascular endothelial growth factor induces choroidal neovascularization in rat. Invest Ophthalmol Vis Sci 44: 781-790.
59. Tobe T, Ortega S, Luna JD, Ozaki H, Okamoto N, et al. (1998) Targeted disruption of the FGF2 gene does not prevent choroidal neovascularization in a murine model. Am J Pathol 153: 1641-1646.
60. Yamada H, Yamada E, Kwak N, Ando A, Suzuki A, et al. (2000) Cell injury unmasks a latent proangiogenic phenotype in mice with increased expression of FGF2 in the retina. J Cell Physiol 185: 135-142.
61. Korte GE, Reppucci V, Henkind P (1984) RPE destruction causes choriocapillary atrophy. Invest Ophthalmol Vis Sci 25: 1135-1145.
62. Kurihara T, Westenskow PD, Bravo S, Aguilar E, Friedlander M (2012) Targeted deletion of Vegfa in adult mice induces vision loss. J Clin Invest 122: 4213-4217.
63. Ohno-Matsui K, Hirose A, Yamamoto S, Saikia J, Okamoto N, et al. (2002) Inducible expression of vascular endothelial growth factor in adult mice causes severe proliferative retinopathy and retinal detachment. Am J Pathol 160: 711-719.
64. Heckenlively JR, Hawes NL, Friedlander M, Nusinowitz S, Hurd R, et al. (2003) Mouse model of subretinal neovascularization with choroidal anastomosis. Retina 23: 518-522.
65. Smith LE (2004) Pathogenesis of retinopathy of prematurity. Growth Horm IGF Res 14 Suppl A: S140-144.
66. Aiello LP, Pierce EA, Foley ED, Takagi H, Chen H, et al. (1995) Suppression of retinal neovascularization in vivo by inhibition of vascular endothelial growth factor (VEGF) using soluble VEGF-receptor chimeric proteins. Proc Natl Acad Sci U S A 92: 10457-10461.
67. Shima DT, Gougos A, Miller JW, Tolentino M, Robinson G, et al. (1996) Cloning and mRNA expression of vascular endothelial growth factor in ischemic retinas of Macaca fascicularis. Invest Ophthalmol Vis Sci 37: 1334-1340.
68. Das A, Stroud S, Mehta A, Rangasamy S (2014) New treatments for diabetic retinopathy. Diabetes Obes Metab.
69. Zheng Y, He M, Congdon N (2012) The worldwide epidemic of diabetic retinopathy. Indian J Ophthalmol 60: 428-431.
70. Klein R, Klein BE, Moss SE, Davis MD, DeMets DL (1984) The Wisconsin epidemiologic study of diabetic retinopathy. III. Prevalence and risk of diabetic retinopathy when age at diagnosis is 30 or more years. Arch Ophthalmol 102: 527-532.
71. Klein R, Klein BE, Moss SE, Davis MD, DeMets DL (1984) The Wisconsin epidemiologic study of diabetic retinopathy. II. Prevalence and risk of diabetic retinopathy when age at diagnosis is less than 30 years. Arch Ophthalmol 102: 520-526.
72. Lutty GA (2013) Effects of diabetes on the eye. Invest Ophthalmol Vis Sci 54: Orsf81-87.
73. Tarr JM, Kaul K, Chopra M, Kohner EM, Chibber R (2013) Pathophysiology of diabetic retinopathy. ISRN Ophthalmol 2013: 343560.

74. Choudhuri S, Dutta D, Sen A, Chowdhury IH, Mitra B, et al. (2013) Role of N-epsilon- carboxy methyl lysine, advanced glycation end products and reactive oxygen species for the development of nonproliferative and proliferative retinopathy in type 2 diabetes mellitus. Mol Vis 19: 100-113.
75. Sasaki M, Ozawa Y, Kurihara T, Kubota S, Yuki K, et al. (2010) Neurodegenerative influence of oxidative stress in the retina of a murine model of diabetes. Diabetologia 53: 971-979.
76. (1991) Fundus photographic risk factors for progression of diabetic retinopathy. ETDRS report number 12. Early Treatment Diabetic Retinopathy Study Research Group. Ophthalmology 98: 823-833.
77. Fong DS, Barton FB, Bresnick GH (1999) Impaired color vision associated with diabetic retinopathy: Early Treatment Diabetic Retinopathy Study Report No. 15. Am J Ophthalmol 128: 612-617.
78. Regan D, Neima D (1984) Low-contrast letter charts in early diabetic retinopathy, ocular hypertension, glaucoma, and Parkinson's disease. Br J Ophthalmol 68: 885-889.
79. Newman EA (2013) Functional hyperemia and mechanisms of neurovascular coupling in the retinal vasculature. J Cereb Blood Flow Metab 33: 1685-1695.
80. Ryden L, Grant PJ, Anker SD, Berne C, Cosentino F, et al. (2013) ESC Guidelines on diabetes, pre-diabetes, and cardiovascular diseases developed in collaboration with the EASD: the Task Force on diabetes, pre-diabetes, and cardiovascular diseases of the European Society of Cardiology (ESC) and developed in collaboration with the European Association for the Study of Diabetes (EASD). Eur Heart J 34: 3035-3087.
81. Abcouwer SF (2013) Direct effects of PPARalpha agonists on retinal inflammation and angiogenesis may explain how fenofibrate lowers risk of severe proliferative diabetic retinopathy. Diabetes 62: 36-38.
82. Frank RN (1975) Visual fields and electroretinography following extensive photocoagulation. Arch Ophthalmol 93: 591-598.
83. Lains I, Figueira J, Santos AR, Baltar A, Costa M, et al. (2014) Choroidal thickness in diabetic retinopathy: the influence of antiangiogenic therapy. Retina 34: 1199-1207.
84. Foxton RH, Finkelstein A, Vijay S, Dahlmann-Noor A, Khaw PT, et al. (2013) VEGF-A Is Necessary and Sufficient for Retinal Neuroprotection in Models of Experimental Glaucoma. The American Journal of Pathology 182: 1379-1390.
85. Santos AR, Gomes SC, Figueira J, Nunes S, Lobo CL, et al. (2014) Degree of decrease in central retinal thickness predicts visual acuity response to intravitreal ranibizumab in diabetic macular edema. Ophthalmologica 231: 16-22.
86. Hayman SR, Leung N, Grande JP, Garovic VD (2012) VEGF inhibition, hypertension, and renal toxicity. Curr Oncol Rep 14: 285-294.
87. Gurevich F, Perazella MA (2009) Renal effects of anti-angiogenesis therapy: update for the internist. Am J Med 122: 322-328.
88. Sheetz MJ, Aiello LP, Davis MD, Danis R, Bek T, et al. (2013) The effect of the oral PKC beta inhibitor ruboxistaurin on vision loss in two phase 3 studies. Invest Ophthalmol Vis Sci 54: 1750-1757.

89. Clermont A, Chilcote TJ, Kita T, Liu J, Riva P, et al. (2011) Plasma kallikrein mediates retinal vascular dysfunction and induces retinal thickening in diabetic rats. Diabetes 60: 1590-1598.
90. Sfikakis PP, Grigoropoulos V, Emfietzoglou I, Theodossiadis G, Tentolouris N, et al. (2010) Infliximab for diabetic macular edema refractory to laser photocoagulation: a randomized, double-blind, placebo-controlled, crossover, 32-week study. Diabetes Care 33: 1523-1528.
91. Joussen AM, Poulaki V, Mitsiades N, Kirchhof B, Koizumi K, et al. (2002) Nonsteroidal anti-inflammatory drugs prevent early diabetic retinopathy via TNF-alpha suppression. Faseb j 16: 438-440.
92. Gardiner TA, Gibson DS, de Gooyer TE, de la Cruz VF, McDonald DM, et al. (2005) Inhibition of tumor necrosis factor-alpha improves physiological angiogenesis and reduces pathological neovascularization in ischemic retinopathy. Am J Pathol 166: 637-644.
93. Zhou J, Wang S, Xia X (2012) Role of intravitreal inflammatory cytokines and angiogenic factors in proliferative diabetic retinopathy. Curr Eye Res 37: 416-420.
94. Feng Y, Busch S, Gretz N, Hoffmann S, Hammes HP (2012) Crosstalk in the retinal neurovascular unit - lessons for the diabetic retina. Exp Clin Endocrinol Diabetes 120: 199-201.
95. Tanigami H, Okamoto T, Yasue Y, Shimaoka M (2012) Astroglial integrins in the development and regulation of neurovascular units. Pain Res Treat 2012: 964652.
96. Stanimirovic DB, Friedman A (2012) Pathophysiology of the neurovascular unit: disease cause or consequence[quest]. J Cereb Blood Flow Metab 32: 1207-1221.
97. Sarkar S, Raymick J, Mann D, Bowyer JF, Hanig JP, et al. (2014) Neurovascular changes in acute, sub-acute and chronic mouse models of Parkinson's disease. Curr Neurovasc Res 11: 48-61.
98. Liu R, Li JZ, Song JK, Zhou D, Huang C, et al. (2014) Pinocembrin improves cognition and protects the neurovascular unit in Alzheimer related deficits. Neurobiol Aging 35: 1275-1285.
99. Iadecola C, Nedergaard M (2007) Glial regulation of the cerebral microvasculature. Nat Neurosci 10: 1369-1376.
100. Kern TS (2014) Interrelationships between the Retinal Neuroglia and Vasculature in Diabetes. Diabetes Metab J 38: 163-170.
101. Buerk DG, Riva CE, Cranstoun SD (1995) Frequency and luminance-dependent blood flow and K+ ion changes during flicker stimuli in cat optic nerve head. Invest Ophthalmol Vis Sci 36: 2216-2227.
102. Falsini B, Riva CE, Logean E (2002) Flicker-evoked changes in human optic nerve blood flow: relationship with retinal neural activity. Invest Ophthalmol Vis Sci 43: 2309-2316.
103. Riva CE, Logean E, Falsini B (2005) Visually evoked hemodynamical response and assessment of neurovascular coupling in the optic nerve and retina. Prog Retin Eye Res 24: 183-215.
104. Formaz F, Riva CE, Geiser M (1997) Diffuse luminance flicker increases retinal vessel diameter in humans. Curr Eye Res 16: 1252-1257.
105. Bill A, Sperber GO (1990) Aspects of oxygen and glucose consumption in the retina: effects of high intraocular pressure and light. Graefes Arch Clin Exp Ophthalmol 228: 124-127.

106. Kondo M, Wang L, Bill A (1997) The role of nitric oxide in hyperaemic response to flicker in the retina and optic nerve in cats. Acta Ophthalmol Scand 75: 232-235.
107. Mishra A, Newman EA (2011) Aminoguanidine reverses the loss of functional hyperemia in a rat model of diabetic retinopathy. Front Neuroenergetics 3: 10.
108. Schmidt KG, Bergert H, Funk RH (2008) Neurodegenerative diseases of the retina and potential for protection and recovery. Curr Neuropharmacol 6: 164-178.
109. Abcouwer SF, Gardner TW (2014) Diabetic retinopathy: loss of neuroretinal adaptation to the diabetic metabolic environment. Ann N Y Acad Sci 1311: 174-190.
110. Mishra A, Newman EA (2010) Inhibition of inducible nitric oxide synthase reverses the loss of functional hyperemia in diabetic retinopathy. Glia 58: 1996-2004.
111. De Bock K, Georgiadou M, Schoors S, Kuchnio A, Wong BW, et al. (2013) Role of PFKFB3-driven glycolysis in vessel sprouting. Cell 154: 651-663.
112. Stapor P, Wang X, Goveia J, Moens S, Carmeliet P (2014) Angiogenesis revisited - role and therapeutic potential of targeting endothelial metabolism. J Cell Sci 127: 4331-4341.
113. Galvan-Pena S, O'Neill LA (2014) Metabolic reprograming in macrophage polarization. Front Immunol 5: 420.
114. Tannahill GM, Curtis AM, Adamik J, Palsson-McDermott EM, McGettrick AF, et al. (2013) Succinate is an inflammatory signal that induces IL-1beta through HIF-1alpha. Nature 496: 238-242.
115. Joyal JS, Omri S, Sitaras N, Rivera JC, Sapieha P, et al. (2012) Neovascularization in retinopathy of prematurity: opposing actions of neuronal factors GPR91 and semaphorins 3A. Acta Paediatr 101: 819-826.
116. Sapieha P, Sirinyan M, Hamel D, Zaniolo K, Joyal JS, et al. (2008) The succinate receptor GPR91 in neurons has a major role in retinal angiogenesis. Nat Med 14: 1067-1076.
117. Saint-Geniez M, Jiang A, Abend S, Liu L, Sweigard H, et al. (2013) PGC-1alpha regulates normal and pathological angiogenesis in the retina. Am J Pathol 182: 255-265.
118. Neu J, Afzal A, Pan H, Gallego E, Li N, et al. (2006) The dipeptide Arg-Gln inhibits retinal neovascularization in the mouse model of oxygen-induced retinopathy. Invest Ophthalmol Vis Sci 47: 3151-3155.
119. Bain JR, Stevens RD, Wenner BR, Ilkayeva O, Muoio DM, et al. (2009) Metabolomics Applied to Diabetes Research: Moving From Information to Knowledge. Diabetes 58: 2429-2443.
120. Friedrich N (2012) Metabolomics in diabetes research. J Endocrinol 215: 29-42.
121. Nikolskiy I, Siuzdak G, Patti GJ (2015) Discriminating precursors of common fragments for large-scale metabolite profiling by triple quadrupole mass spectrometry. Bioinformatics.
122. Zhu ZJ, Schultz AW, Wang J, Johnson CH, Yannone SM, et al. (2013) Liquid chromatography quadrupole time-of-flight mass spectrometry characterization of metabolites guided by the METLIN database. Nat Protoc 8: 451-460.

123. Cho K, Mahieu N, Ivanisevic J, Uritboonthai W, Chen YJ, et al. (2014) isoMETLIN: a database for isotope-based metabolomics. Anal Chem 86: 9358-9361.
124. Barba I, Garcia-Ramirez M, Hernandez C, Alonso MA, Masmiquel L, et al. (2010) Metabolic fingerprints of proliferative diabetic retinopathy: an 1H-NMR-based metabonomic approach using vitreous humor. Invest Ophthalmol Vis Sci 51: 4416-4421.
125. Li X, Luo X, Lu X, Duan J, Xu G (2011) Metabolomics study of diabetic retinopathy using gas chromatography-mass spectrometry: a comparison of stages and subtypes diagnosed by Western and Chinese medicine. Mol Biosyst 7: 2228-2237.
126. Aiello LP, Avery RL, Arrigg PG, Keyt BA, Jampel HD, et al. (1994) Vascular endothelial growth factor in ocular fluid of patients with diabetic retinopathy and other retinal disorders. N Engl J Med 331: 1480-1487.
127. Skarnes WC, Rosen B, West AP, Koutsourakis M, Bushell W, et al. (2011) A conditional knockout resource for the genome-wide study of mouse gene function. Nature 474: 337-342.
128. Nishida A, Furukawa A, Koike C, Tano Y, Aizawa S, et al. (2003) Otx2 homeobox gene controls retinal photoreceptor cell fate and pineal gland development. Nat Neurosci 6: 1255-1263.
129. Roger JE, Hiriyanna A, Gotoh N, Hao H, Cheng DF, et al. (2014) OTX2 loss causes rod differentiation defect in CRX-associated congenital blindness. J Clin Invest 124: 631-643.
130. Westenskow PD, McKean JB, Kubo F, Nakagawa S, Fuhrmann S (2010) Ectopic Mitf in the Embryonic Chick Retina by Co-transfection of β-Catenin and Otx2. Investigative Ophthalmology & Visual Science 51: 5328-5335.
131. Kawaguchi Y, Cooper B, Gannon M, Ray M, MacDonald RJ, et al. (2002) The role of the transcriptional regulator Ptf1a in converting intestinal to pancreatic progenitors. Nat Genet 32: 128-134.
132. Haase VH, Glickman JN, Socolovsky M, Jaenisch R (2001) Vascular tumors in livers with targeted inactivation of the von Hippel-Lindau tumor suppressor. Proc Natl Acad Sci U S A 98: 1583-1588.
133. Ryan HE, Poloni M, McNulty W, Elson D, Gassmann M, et al. (2000) Hypoxia-inducible factor-1alpha is a positive factor in solid tumor growth. Cancer Res 60: 4010-4015.
134. Gruber M, Hu CJ, Johnson RS, Brown EJ, Keith B, et al. (2007) Acute postnatal ablation of Hif-2alpha results in anemia. Proc Natl Acad Sci U S A 104: 2301-2306.
135. Gerber HP, Hillan KJ, Ryan AM, Kowalski J, Keller GA, et al. (1999) VEGF is required for growth and survival in neonatal mice. Development 126: 1149-1159.
136. Buch T, Heppner FL, Tertilt C, Heinen TJ, Kremer M, et al. (2005) A Cre-inducible diphtheria toxin receptor mediates cell lineage ablation after toxin administration. Nat Methods 2: 419-426.
137. Madisen L, Zwingman TA, Sunkin SM, Oh SW, Zariwala HA, et al. (2010) A robust and high-throughput Cre reporting and characterization system for the whole mouse brain. Nat Neurosci 13: 133-140.
138. Muzumdar MD, Tasic B, Miyamichi K, Li L, Luo L (2007) A global double-fluorescent Cre reporter mouse. Genesis 45: 593-605.

139. Smith LE, Wesolowski E, McLellan A, Kostyk SK, D'Amato R, et al. (1994) Oxygen-induced retinopathy in the mouse. Invest Ophthalmol Vis Sci 35: 101-111.
140. Aguilar E, Dorrell MI, Friedlander D, Jacobson RA, Johnson A, et al. (2008) Chapter 6. Ocular models of angiogenesis. Methods Enzymol 444: 115-158.
141. Westenskow PD, Kurihara T, Bravo S, Feitelberg D, Sedillo ZA, et al. (2015) Performing subretinal injections in rodents to deliver retinal pigment epithelium cells in suspension. J Vis Exp: 52247.
142. Byrne LC, Khalid F, Lee T, Zin EA, Greenberg KP, et al. (2013) AAV-mediated, optogenetic ablation of Muller Glia leads to structural and functional changes in the mouse retina. PLoS One 8: e76075.
143. Banin E, Dorrell MI, Aguilar E, Ritter MR, Aderman CM, et al. (2006) T2-TrpRS inhibits preretinal neovascularization and enhances physiological vascular regrowth in OIR as assessed by a new method of quantification. Invest Ophthalmol Vis Sci 47: 2125-2134.
144. McVicar CM, Hamilton R, Colhoun LM, Gardiner TA, Brines M, et al. (2011) Intervention with an erythropoietin-derived peptide protects against neuroglial and vascular degeneration during diabetic retinopathy. Diabetes 60: 2995-3005.
145. Zhang L, Conejo-Garcia JR, Yang N, Huang W, Mohamed-Hadley A, et al. (2002) Different effects of glucose starvation on expression and stability of VEGF mRNA isoforms in murine ovarian cancer cells. Biochem Biophys Res Commun 292: 860-868.
146. Murakami Y, Matsumoto H, Roh M, Suzuki J, Hisatomi T, et al. (2012) Receptor interacting protein kinase mediates necrotic cone but not rod cell death in a mouse model of inherited degeneration. Proc Natl Acad Sci U S A 109: 14598-14603.
147. Wen ZH, Su YC, Lai PL, Zhang Y, Xu YF, et al. (2013) Critical role of arachidonic acid-activated mTOR signaling in breast carcinogenesis and angiogenesis. Oncogene 32: 160-170.
148. Tautenhahn R, Patti GJ, Rinehart D, Siuzdak G (2012) XCMS Online: A Web-Based Platform to Process Untargeted Metabolomic Data. Anal Chem 84: 5035-5039.
149. Patti GJ, Tautenhahn R, Rinehart D, Cho K, Shriver LP, et al. (2013) A View from Above: Cloud Plots to Visualize Global Metabolomic Data. Anal Chem 85: 798-804.
150. Huang X, Chen YJ, Cho K, Nikolskiy I, Crawford PA, et al. (2014) X(13)CMS: Global Tracking of Isotopic Labels in Untargeted Metabolomics. Anal Chem 86: 1632-1639.
151. Storkebaum E, Quaegebeur A, Vikkula M, Carmeliet P (2011) Cerebrovascular disorders: molecular insights and therapeutic opportunities. Nat Neurosci 14: 1390-1397.
152. Metea MR, Newman EA (2007) Signalling within the neurovascular unit in the mammalian retina. Exp Physiol 92: 635-640.
153. Otani A, Dorrell MI, Kinder K, Moreno SK, Nusinowitz S, et al. (2004) Rescue of retinal degeneration by intravitreally injected adult bone marrow-derived lineage-negative hematopoietic stem cells. J Clin Invest 114: 765-774.

154. Stanimirovic DB, Friedman A (2012) Pathophysiology of the neurovascular unit: disease cause or consequence? J Cereb Blood Flow Metab 32: 1207-1221.
155. Sakowski SA, Heavener SB, Lunn JS, Fung K, Oh SS, et al. (2009) Neuroprotection using gene therapy to induce vascular endothelial growth factor-A expression. Gene Ther 16: 1292-1299.
156. Ayton LN, Guymer RH, Luu CD (2013) Choroidal thickness profiles in retinitis pigmentosa. Clin Experiment Ophthalmol 41: 396-403.
157. Coscas F, Puche N, Coscas G, Srour M, Francais C, et al. (2014) Comparison of macular choroidal thickness in adult onset foveomacular vitelliform dystrophy and age-related macular degeneration. Invest Ophthalmol Vis Sci 55: 64-69.
158. Dhoot DS, Huo S, Yuan A, Xu D, Srivistava S, et al. (2013) Evaluation of choroidal thickness in retinitis pigmentosa using enhanced depth imaging optical coherence tomography. Br J Ophthalmol 97: 66-69.
159. Jonas JB, Forster TM, Steinmetz P, Schlichtenbrede FC, Harder BC (2014) Choroidal thickness in age-related macular degeneration. Retina 34: 1149-1155.
160. Lee JY, Lee DH, Lee JY, Yoon YH (2013) Correlation between subfoveal choroidal thickness and the severity or progression of nonexudative age-related macular degeneration. Invest Ophthalmol Vis Sci 54: 7812-7818.
161. Ma Y, Kawasaki R, Dobson LP, Ruddle JB, Kearns LS, et al. (2012) Quantitative analysis of retinal vessel attenuation in eyes with retinitis pigmentosa. Invest Ophthalmol Vis Sci 53: 4306-4314.
162. Pennesi ME, Nishikawa S, Matthes MT, Yasumura D, LaVail MM (2008) The relationship of photoreceptor degeneration to retinal vascular development and loss in mutant rhodopsin transgenic and RCS rats. Exp Eye Res 87: 561-570.
163. Bhutto I, Lutty G (2012) Understanding age-related macular degeneration (AMD): relationships between the photoreceptor/retinal pigment epithelium/Bruch's membrane/choriocapillaris complex. Mol Aspects Med 33: 295-317.
164. McLeod DS, Grebe R, Bhutto I, Merges C, Baba T, et al. (2009) Relationship between RPE and choriocapillaris in age-related macular degeneration. Invest Ophthalmol Vis Sci 50: 4982-4991.
165. Rishi P, Rishi E, Mathur G, Raval V (2013) Ocular perfusion pressure and choroidal thickness in eyes with polypoidal choroidal vasculopathy, wet-age-related macular degeneration, and normals. Eye (Lond) 27: 1038-1043.
166. Sohrab M, Wu K, Fawzi AA (2012) A pilot study of morphometric analysis of choroidal vasculature in vivo, using en face optical coherence tomography. PLoS One 7: e48631.
167. Kurihara T, Westenskow PD, Bravo S, Aguilar E, Friedlander M (2012) Targeted deletion of Vegfa in adult mice induces vision loss. The Journal of Clinical Investigation 122: 4213-4217.
168. Saint-Geniez M, Kurihara T, Sekiyama E, Maldonado AE, D'Amore PA (2009) An essential role for RPE-derived soluble VEGF in the maintenance of the choriocapillaris. Proc Natl Acad Sci U S A 106: 18751-18756.
169. Alm A (1992) Ocular Circulation, in Adler's Physiology of the Eye. In: Hart WM, editor. Adler's Physiology of the Eye. St Louis
: Mosby

. pp. 198-227.
170. Alm A, Bill A (1973) Ocular and optic nerve blood flow at normal and increased intraocular pressures in monkeys (Macaca irus): a study with radioactively labelled microspheres including flow determinations in brain and some other tissues. Exp Eye Res 15: 15-29.
171. Laughlin SB, de Ruyter van Steveninck RR, Anderson JC (1998) The metabolic cost of neural information. Nat Neurosci 1: 36-41.
172. Punzo C, Xiong W, Cepko CL (2012) Loss of Daylight Vision in Retinal Degeneration: Are Oxidative Stress and Metabolic Dysregulation to Blame? The Journal of Biological Chemistry 287: 1642-1648.
173. Okabe K, Kobayashi S, Yamada T, Kurihara T, Tai-Nagara I, et al. (2014) Neurons limit angiogenesis by titrating VEGF in retina. Cell 159: 584-596.
174. Usui Y, Westenskow PD, Kurihara T, Aguilar E, Sakimoto S, et al. (2015) Neurovascular crosstalk between interneurons and capillaries is required for vision. JCI In Press.
175. Johnson CH, Ivanisevic J, Benton HP, Siuzdak G (2015) Bioinformatics: the next frontier of metabolomics. Analytical chemistry 87: 147-156.
176. Tautenhahn R, Cho K, Uritboonthai W, Zhu Z, Patti GJ, et al. (2012) An accelerated workflow for untargeted metabolomics using the METLIN database. Nat Biotech 30: 826-828.
177. Cravatt BF, Prospero-Garcia O, Siuzdak G, Gilula NB, Henriksen SJ, et al. (1995) Chemical characterization of a family of brain lipids that induce sleep. Science 268: 1506-1509.
178. Ezzili C, Otrubova K, Boger DL (2010) Fatty acid amide signaling molecules. Bioorganic & medicinal chemistry letters 20: 5959-5968.
179. Guan X, Cravatt BF, Ehring GR, Hall JE, Boger DL, et al. (1997) The sleep-inducing lipid oleamide deconvolutes gap junction communication and calcium wave transmission in glial cells. The Journal of cell biology 139: 1785-1792.
180. Boger DL, Henriksen SJ, Cravatt BF (1998) Oleamide: an endogenous sleep-inducing lipid and prototypical member of a new class of biological signaling molecules. Current pharmaceutical design 4: 303-314.
181. Hamberger A, Stenhagen G (2003) Erucamide as a modulator of water balance: new function of a fatty acid amide. Neurochem Res 28: 177-185.
182. Mitchell CA, Davies MJ, Grounds MD, McGeachie JK, Crawford GJ, et al. (1996) Enhancement of neovascularization in regenerating skeletal muscle by the sustained release of erucamide from a polymer matrix. J Biomater Appl 10: 230-249.
183. Wakamatsu K, Masaki T, Itoh F, Kondo K, Sudo K (1990) Isolation of fatty acid amide as an angiogenic principle from bovine mesentery. Biochem Biophys Res Commun 168: 423-429.
184. Anglin EJ, Cheng L, Freeman WR, Sailor MJ (2008) Porous silicon in drug delivery devices and materials. Adv Drug Deliv Rev 60: 1266-1277.
185. Mears AJ, Kondo M, Swain PK, Takada Y, Bush RA, et al. (2001) Nrl is required for rod photoreceptor development. Nat Genet 29: 447-452.
186. Roger JE, Ranganath K, Zhao L, Cojocaru RI, Brooks M, et al. (2012) Preservation of cone photoreceptors after a rapid yet transient degeneration and remodeling in cone-only Nrl(−/−) mouse retina. The Journal of neuroscience : the official journal of the Society for Neuroscience 32: 528-541.

187. Czyzyk TA, Ning Y, Hsu MS, Peng B, Mains RE, et al. (2005) Deletion of peptide amidation enzymatic activity leads to edema and embryonic lethality in the mouse. Dev Biol 287: 301-313.
188. Chang B, Hawes NL, Pardue MT, German AM, Hurd RE, et al. (2007) Two mouse retinal degenerations caused by missense mutations in the beta-subunit of rod cGMP phosphodiesterase gene. Vision Res 47: 624-633.
189. Bowes C, Li T, Danciger M, Baxter LC, Applebury ML, et al. (1990) Retinal degeneration in the rd mouse is caused by a defect in the beta subunit of rod cGMP-phosphodiesterase. Nature 347: 677-680.
190. Farjo R, Skaggs JS, Nagel BA, Quiambao AB, Nash ZA, et al. (2006) Retention of function without normal disc morphogenesis occurs in cone but not rod photoreceptors. J Cell Biol 173: 59-68.
191. Farrell EK, Merkler DJ (2008) Biosynthesis, degradation and pharmacological importance of the fatty acid amides. Drug Discov Today 13: 558-568.
192. Klimczak RR, Koerber JT, Dalkara D, Flannery JG, Schaffer DV (2009) A novel adeno-associated viral variant for efficient and selective intravitreal transduction of rat Muller cells. PLoS One 4: e7467.
193. Skorupa A, Urbach S, Vigy O, King MA, Chaumont-Dubel S, et al. (2013) Angiogenin induces modifications in the astrocyte secretome: relevance to amyotrophic lateral sclerosis. J Proteomics 91: 274-285.
194. Steidinger TU, Standaert DG, Yacoubian TA (2011) A neuroprotective role for angiogenin in models of Parkinson's disease. Journal of Neurochemistry 116: 334-341.
195. Subramanian V, Crabtree B, Acharya KR (2008) Human angiogenin is a neuroprotective factor and amyotrophic lateral sclerosis associated angiogenin variants affect neurite extension/pathfinding and survival of motor neurons. Human Molecular Genetics 17: 130-149.
196. Wu D, Yu W, Kishikawa H, Folkerth RD, Iafrate AJ, et al. (2007) Angiogenin loss-of-function mutations in amyotrophic lateral sclerosis. Ann Neurol 62: 609-617.
197. Skeie JM, Zeng S, Faidley EA, Mullins RF (2011) Angiogenin in age-related macular degeneration. Mol Vis 17: 576-582.
198. Skorupa A, King MA, Aparicio IM, Dussmann H, Coughlan K, et al. (2012) Motoneurons secrete angiogenin to induce RNA cleavage in astroglia. J Neurosci 32: 5024-5038.
199. Braas KM, Harakall SA, Ouafik L, Eipper BA, May V (1992) Expression of peptidylglycine alpha-amidating monooxygenase: an in situ hybridization and immunocytochemical study. Endocrinology 130: 2778-2788.
200. Milgram SL, Kho ST, Martin GV, Mains RE, Eipper BA (1997) Localization of integral membrane peptidylglycine alpha-amidating monooxygenase in neuroendocrine cells. Journal of Cell Science 110: 695-706.
201. Grimm C, Hermann DM, Bogdanova A, Hotop S, Kilic U, et al. (2005) Neuroprotection by hypoxic preconditioning: HIF-1 and erythropoietin protect from retinal degeneration. Semin Cell Dev Biol 16: 531-538.
202. Yu DY, Yu PK, Cringle SJ, Kang MH, Su EN (2014) Functional and morphological characteristics of the retinal and choroidal vasculature. Prog Retin Eye Res 40: 53-93.
203. Dorrell MI, Aguilar E, Scheppke L, Barnett FH, Friedlander M (2007) Combination angiostatic therapy completely inhibits ocular and tumor angiogenesis. Proc Natl Acad Sci U S A 104: 967-972.

204. Stone J, Dreher Z (1987) Relationship between astrocytes, ganglion cells and vasculature of the retina. J Comp Neurol 255: 35-49.
205. Fujitani Y, Fujitani S, Luo H, Qiu F, Burlison J, et al. (2006) Ptf1a determines horizontal and amacrine cell fates during mouse retinal development. Development 133: 4439-4450.
206. Chien CL, Liem RK (1995) The neuronal intermediate filament, alpha-internexin is transiently expressed in amacrine cells in the developing mouse retina. Exp Eye Res 61: 749-756.
207. Cringle SJ, Yu PK, Su EN, Yu DY (2006) Oxygen distribution and consumption in the developing rat retina. Invest Ophthalmol Vis Sci 47: 4072-4076.
208. Stone J, Itin A, Alon T, Pe'er J, Gnessin H, et al. (1995) Development of retinal vasculature is mediated by hypoxia-induced vascular endothelial growth factor (VEGF) expression by neuroglia. J Neurosci 15: 4738-4747.
209. Bai Y, Ma JX, Guo J, Wang J, Zhu M, et al. (2009) Muller cell-derived VEGF is a significant contributor to retinal neovascularization. J Pathol 219: 446-454.
210. Park HY, Kim JH, Park CK (2014) Neuronal cell death in the inner retina and the influence of vascular endothelial growth factor inhibition in a diabetic rat model. Am J Pathol 184: 1752-1762.
211. Vinores SA, Kuchle M, Derevjanik NL, Henderer JD, Mahlow J, et al. (1995) Blood-retinal barrier breakdown in retinitis pigmentosa: light and electron microscopic immunolocalization. Histol Histopathol 10: 913-923.
212. Klaassen I, Van Noorden CJ, Schlingemann RO (2013) Molecular basis of the inner blood-retinal barrier and its breakdown in diabetic macular edema and other pathological conditions. Prog Retin Eye Res 34: 19-48.
213. Stem MS, Gardner TW (2013) Neurodegeneration in the pathogenesis of diabetic retinopathy: molecular mechanisms and therapeutic implications. Curr Med Chem 20: 3241-3250.
214. Barber AJ, Lieth E, Khin SA, Antonetti DA, Buchanan AG, et al. (1998) Neural apoptosis in the retina during experimental and human diabetes. Early onset and effect of insulin. J Clin Invest 102: 783-791.
215. Arden GB, Wolf JE, Tsang Y (1998) Does dark adaptation exacerbate diabetic retinopathy? Evidence and a linking hypothesis. Vision Res 38: 1723-1729.
216. Du Y, Veenstra A, Palczewski K, Kern TS (2013) Photoreceptor cells are major contributors to diabetes-induced oxidative stress and local inflammation in the retina. Proc Natl Acad Sci U S A 110: 16586-16591.
217. Arden GB (2001) The absence of diabetic retinopathy in patients with retinitis pigmentosa: implications for pathophysiology and possible treatment. Br J Ophthalmol 85: 366-370.
218. Gastinger MJ, Singh RS, Barber AJ (2006) Loss of cholinergic and dopaminergic amacrine cells in streptozotocin-diabetic rat and Ins2Akita-diabetic mouse retinas. Invest Ophthalmol Vis Sci 47: 3143-3150.
219. Kern TS, Barber AJ (2008) Retinal ganglion cells in diabetes. J Physiol 586: 4401-4408.
220. Fong DS, Ferris FL, 3rd, Davis MD, Chew EY (1999) Causes of severe visual loss in the early treatment diabetic retinopathy study: ETDRS report no. 24. Early Treatment Diabetic Retinopathy Study Research Group. Am J Ophthalmol 127: 137-141.

221. Cheung N, Wong IY, Wong TY (2014) Ocular anti-VEGF therapy for diabetic retinopathy: overview of clinical efficacy and evolving applications. Diabetes Care 37: 900-905.
222. Robinson R, Barathi VA, Chaurasia SS, Wong TY, Kern TS (2012) Update on animal models of diabetic retinopathy: from molecular approaches to mice and higher mammals. Dis Model Mech 5: 444-456.
223. Roberts LD, Koulman A, Griffin JL (2014) Towards metabolic biomarkers of insulin resistance and type 2 diabetes: progress from the metabolome. Lancet Diabetes Endocrinol 2: 65-75.
224. Ivanisevic J, Zhu ZJ, Plate L, Tautenhahn R, Chen S, et al. (2013) Toward 'omic scale metabolite profiling: a dual separation-mass spectrometry approach for coverage of lipid and central carbon metabolism. Anal Chem 85: 6876-6884.
225. Huang X, Chen YJ, Cho K, Nikolskiy I, Crawford PA, et al. (2014) X13CMS: global tracking of isotopic labels in untargeted metabolomics. Anal Chem 86: 1632-1639.
226. Xia JG, Psychogios N, Young N, Wishart DS (2009) MetaboAnalyst: a web server for metabolomic data analysis and interpretation. Nucleic Acids Res 37: W652-W660.
227. Metea MR, Newman EA (2006) Glial cells dilate and constrict blood vessels: a mechanism of neurovascular coupling. J Neurosci 26: 2862-2870.
228. Bringmann A, Pannicke T, Grosche J, Francke M, Wiedemann P, et al. (2006) Muller cells in the healthy and diseased retina. Prog Retin Eye Res 25: 397-424.
229. Patel C, Rojas M, Narayanan SP, Zhang W, Xu Z, et al. (2013) Arginase as a mediator of diabetic retinopathy. Front Immunol 4: 173.
230. Narayanan SP, Suwanpradid J, Saul A, Xu Z, Still A, et al. (2011) Arginase 2 deletion reduces neuro-glial injury and improves retinal function in a model of retinopathy of prematurity. PLoS One 6: e22460.
231. Narayanan SP, Xu Z, Putluri N, Sreekumar A, Lemtalsi T, et al. (2014) Arginase 2 deficiency reduces hyperoxia-mediated retinal neurodegeneration through the regulation of polyamine metabolism. Cell Death Dis 5: e1075.
232. Liu W, Glunde K, Bhujwalla ZM, Raman V, Sharma A, et al. (2012) Proline oxidase promotes tumor cell survival in hypoxic tumor microenvironments. Cancer Res 72: 3677-3686.
233. Zheng L, Mackenzie ED, Karim SA, Hedley A, Blyth K, et al. (2013) Reversed argininosuccinate lyase activity in fumarate hydratase-deficient cancer cells. Cancer Metab 1: 12.
234. Narayanan SP, Rojas M, Suwanpradid J, Toque HA, Caldwell RW, et al. (2013) Arginase in retinopathy. Prog Retin Eye Res 36: 260-280.
235. Suwanpradid J, Rojas M, Behzadian MA, Caldwell RW, Caldwell RB (2014) Arginase 2 deficiency prevents oxidative stress and limits hyperoxia-induced retinal vascular degeneration. PLoS One 9: e110604.
236. Glanville NT, Anderson GH (1984) Altered methionine metabolism in streptozotocin-diabetic rats. Diabetologia 27: 468-471.
237. Bringmann A, Grosche A, Pannicke T, Reichenbach A (2013) GABA and Glutamate Uptake and Metabolism in Retinal Glial (Muller) Cells. Front Endocrinol (Lausanne) 4: 48.

238. Reichenbach A, Fuchs U, Kasper M, el-Hifnawi E, Eckstein AK (1995) Hepatic retinopathy: morphological features of retinal glial (Muller) cells accompanying hepatic failure. Acta Neuropathol 90: 273-281.
239. Marc RE, Jones BW, Watt CB, Vazquez-Chona F, Vaughan DK, et al. (2008) Extreme retinal remodeling triggered by light damage: implications for age related macular degeneration. Mol Vis 14: 782-806.
240. Braissant O, Henry H, Loup M, Eilers B, Bachmann C (2001) Endogenous synthesis and transport of creatine in the rat brain: an in situ hybridization study. Brain Res Mol Brain Res 86: 193-201.
241. Moxon-Lester L, Takamoto K, Colditz PB, Barnett NL (2009) S-adenosyl-L-methionine restores photoreceptor function following acute retinal ischemia. Vis Neurosci 26: 429-441.
242. Mai M, Tonjes A, Kovacs P, Stumvoll M, Fiedler GM, et al. (2013) Serum levels of acylcarnitines are altered in prediabetic conditions. PLoS One 8: e82459.
243. Bi HC, Pan YZ, Qiu JX, Krausz KW, Li F, et al. (2014) N-methylnicotinamide and nicotinamide N-methyltransferase are associated with microRNA-1291-altered pancreatic carcinoma cell metabolome and suppressed tumorigenesis. Carcinogenesis.
244. Gonzalez-Dominguez R, Garcia A, Garcia-Barrera T, Barbas C, Gomez-Ariza JL (2014) Metabolomic profiling of serum in the progression of alzheimer's disease by capillary electrophoresis - mass spectrometry. Electrophoresis.
245. Sampey BP, Freemerman AJ, Zhang J, Kuan PF, Galanko JA, et al. (2012) Metabolomic Profiling Reveals Mitochondrial-Derived Lipid Biomarkers That Drive Obesity-Associated Inflammation. Plos One 7.
246. Xia J, Wang Z, Zhang F (2014) Association between Related Purine Metabolites and Diabetic Retinopathy in Type 2 Diabetic Patients. Int J Endocrinol 2014: 651050.
247. Lee JJ, Yang IH, Kuo HK, Chung MS, Chen YJ, et al. (2014) Serum uric acid concentration is associated with worsening in severity of diabetic retinopathy among type 2 diabetic patients in Taiwan-A 3-year prospective study. Diabetes Res Clin Pract.
248. Gruber J, Tang SY, Jenner AM, Mudway I, Blomberg A, et al. (2009) Allantoin in human plasma, serum, and nasal-lining fluids as a biomarker of oxidative stress: avoiding artifacts and establishing real in vivo concentrations. Antioxid Redox Signal 11: 1767-1776.
249. Madsen-Bouterse SA, Kowluru RA (2008) Oxidative stress and diabetic retinopathy: pathophysiological mechanisms and treatment perspectives. Rev Endocr Metab Disord 9: 315-327.
250. Fong DS, Aiello L, Gardner TW, King GL, Blankenship G, et al. (2003) Diabetic retinopathy. Diabetes Care 26: 226-229.
251. Nguyen TT, Kawasaki R, Wang JJ, Kreis AJ, Shaw J, et al. (2009) Flicker light-induced retinal vasodilation in diabetes and diabetic retinopathy. Diabetes Care 32: 2075-2080.
252. Lott MEJ, Slocomb JE, Shivkumar V, Smith B, Quillen D, et al. (2013) Impaired Retinal Vasodilator Responses in Prediabetes and Type 2 Diabetes. Acta ophthalmologica 91: e462-e469.
253. Pardue MT, Barnes CS, Kim MK, Aung MH, Amarnath R, et al. (2014) Rodent Hyperglycemia-Induced Inner Retinal Deficits are Mirrored in Human Diabetes. Translational Vision Science & Technology 3: 6.

254. Usui Y, Westenskow PD, Kurihara T, Aguilar E, Sakimoto S, et al. (2015) Neurovascular crosstalk between interneurons and capillaries is required for vision. The Journal of Clinical Investigation 125: 0-0.
255. Osaadon P, Fagan XJ, Lifshitz T, Levy J (2014) A review of anti-VEGF agents for proliferative diabetic retinopathy. Eye (Lond) 28: 510-520.
256. Rosenfeld PJ, Shapiro H, Tuomi L, Webster M, Elledge J, et al. (2011) Characteristics of patients losing vision after 2 years of monthly dosing in the phase III ranibizumab clinical trials. Ophthalmology 118: 523-530.
257. Georgalas I, Papaconstantinou D, Papadopoulos K, Pagoulatos D, Karagiannis D, et al. (2014) Renal Injury Following Intravitreal Anti-VEGF Administration in Diabetic Patients with Proliferative Diabetic Retinopathy and Chronic Kidney Disease - A Possible Side Effect? Curr Drug Saf 9: 156-158.
258. Frank RN (2004) Diabetic retinopathy. N Engl J Med 350: 48-58.
259. Keenan HA, Sun JK, Levine J, Doria A, Aiello LP, et al. (2010) Residual insulin production and pancreatic ss-cell turnover after 50 years of diabetes: Joslin Medalist Study. Diabetes 59: 2846-2853.
260. Tessari P, Cecchet D, Cosma A, Puricelli L, Millioni R, et al. Insulin resistance of amino acid and protein metabolism in type 2 diabetes. Clinical Nutrition 30: 267-272.
261. Cohen LH, Noell WK (1960) Glucose catabolism of rabbit retina before and after development of visual function. J Neurochem 5: 253-276.
262. Barderas MG, Laborde CM, Posada M, de la Cuesta F, Zubiri I, et al. (2011) Metabolomic profiling for identification of novel potential biomarkers in cardiovascular diseases. J Biomed Biotechnol 2011: 790132.
263. Wikoff WR, Gangoiti JA, Barshop BA, Siuzdak G (2007) Metabolomics identifies perturbations in human disorders of propionate metabolism. Clin Chem 53: 2169-2176.
264. Feng S, Du YQ, Zhang L, Zhang L, Feng RR, et al. (2015) Analysis of Serum Metabolic Profile by Ultra-performance Liquid Chromatography-mass Spectrometry for Biomarkers Discovery: Application in a Pilot Study to Discriminate Patients with Tuberculosis. Chin Med J (Engl) 128: 159-168.
265. Lawton KA, Brown MV, Alexander D, Li Z, Wulff JE, et al. (2014) Plasma metabolomic biomarker panel to distinguish patients with amyotrophic lateral sclerosis from disease mimics. Amyotroph Lateral Scler Frontotemporal Degener 15: 362-370.
266. Hasko G, Sitkovsky MV, Szabo C (2004) Immunomodulatory and neuroprotective effects of inosine. Trends Pharmacol Sci 25: 152-157.
267. Sun JK, Keenan HA, Cavallerano JD, Asztalos BF, Schaefer EJ, et al. (2011) Protection from retinopathy and other complications in patients with type 1 diabetes of extreme duration: the joslin 50-year medalist study. Diabetes Care 34: 968-974.
268. Fong DS, Aiello LP, Ferris FL, 3rd, Klein R (2004) Diabetic retinopathy. Diabetes Care 27: 2540-2553.
269. Lytvyn Y, Perkins BA, Cherney DZ (2015) Uric Acid as a Biomarker and a Therapeutic Target in Diabetes. Can J Diabetes.
270. Markowitz CE, Spitsin S, Zimmerman V, Jacobs D, Udupa JK, et al. (2009) The treatment of multiple sclerosis with inosine. J Altern Complement Med 15: 619-625.

271. Sato T, Kusaka S, Hashida N, Saishin Y, Fujikado T, et al. (2009) Comprehensive gene-expression profile in murine oxygen-induced retinopathy. Br J Ophthalmol 93: 96-103.
272. Yoshida S, Yoshida A, Ishibashi T, Elner SG, Elner VM (2003) Role of MCP-1 and MIP-1alpha in retinal neovascularization during postischemic inflammation in a mouse model of retinal neovascularization. J Leukoc Biol 73: 137-144.
273. Ishida S, Usui T, Yamashiro K, Kaji Y, Amano S, et al. (2003) VEGF164-mediated inflammation is required for pathological, but not physiological, ischemia-induced retinal neovascularization. J Exp Med 198: 483-489.
274. Hasko G, Kuhel DG, Nemeth ZH, Mabley JG, Stachlewitz RF, et al. (2000) Inosine Inhibits Inflammatory Cytokine Production by a Posttranscriptional Mechanism and Protects Against Endotoxin-Induced Shock. The Journal of Immunology 164: 1013-1019.
275. Tambuyzer BR, Ponsaerts P, Nouwen EJ (2009) Microglia: gatekeepers of central nervous system immunology. J Leukoc Biol 85: 352-370.
276. Santiago AR, Baptista FI, Santos PF, Cristovao G, Ambrosio AF, et al. (2014) Role of microglia adenosine A(2A) receptors in retinal and brain neurodegenerative diseases. Mediators Inflamm 2014: 465694.
277. Crehan H, Hardy J, Pocock J (2012) Microglia, Alzheimer's disease, and complement. Int J Alzheimers Dis 2012: 983640.
278. Huang T, Cui J, Li L, Hitchcock PF, Li Y (2012) The role of microglia in the neurogenesis of zebrafish retina. Biochem Biophys Res Commun 421: 214-220.
279. Hume DA, Perry VH, Gordon S (1983) Immunohistochemical localization of a macrophage-specific antigen in developing mouse retina: phagocytosis of dying neurons and differentiation of microglial cells to form a regular array in the plexiform layers. J Cell Biol 97: 253-257.
280. Phipps JA, Yee P, Fletcher EL, Vingrys AJ (2006) Rod photoreceptor dysfunction in diabetes: activation, deactivation, and dark adaptation. Invest Ophthalmol Vis Sci 47: 3187-3194.
281. Arden GB, Sidman RL, Arap W, Schlingemann RO (2005) Spare the rod and spoil the eye. The British Journal of Ophthalmology 89: 764-769.
282. Perron NR, Beeson C, Rohrer B (2013) Early alterations in mitochondrial reserve capacity; a means to predict subsequent photoreceptor cell death. J Bioenerg Biomembr 45: 101-109.
283. Ames A, 3rd, Li YY, Heher EC, Kimble CR (1992) Energy metabolism of rabbit retina as related to function: high cost of Na+ transport. J Neurosci 12: 840-853.
284. Abcouwer SF, Shanmugam S, Gomez PF, Shushanov S, Barber AJ, et al. (2008) Effect of IL-1beta on survival and energy metabolism of R28 and RGC-5 retinal neurons. Invest Ophthalmol Vis Sci 49: 5581-5592.
285. Ow YP, Green DR, Hao Z, Mak TW (2008) Cytochrome c: functions beyond respiration. Nat Rev Mol Cell Biol 9: 532-542.
286. Ferrick DA, Neilson A, Beeson C (2008) Advances in measuring cellular bioenergetics using extracellular flux. Drug Discov Today 13: 268-274.
287. Woollard KV, Kingaby RO, Lab MJ, Cole AW, Palmer TN (1981) Inosine as a selective inotropic agent on ischaemic myocardium? Cardiovasc Res 15: 659-667.

288. Paris LP, C.H. J, Aguilar E, Usui Y, Hoang LT, et al. (2015) In vivo global isotope metabolomics implicates the arginase pathway in ischemic retinopathy. Under peer review.
289. Akizu N, Cantagrel V, Schroth J, Cai N, Vaux K, et al. (2013) AMPD2 regulates GTP synthesis and is mutated in a potentially treatable neurodegenerative brainstem disorder. Cell 154: 505-517.
290. Ames BN, Cathcart R, Schwiers E, Hochstein P (1981) Uric acid provides an antioxidant defense in humans against oxidant- and radical-caused aging and cancer: a hypothesis. Proc Natl Acad Sci U S A 78: 6858-6862.
291. Harmsen E, de Tombe PP, de Jong JW, Achterberg PW (1984) Enhanced ATP and GTP synthesis from hypoxanthine or inosine after myocardial ischemia. Am J Physiol 246: H37-43.
292. Shafy A, Molinie V, Cortes-Morichetti M, Hupertan V, Lila N, et al. (2012) Comparison of the effects of adenosine, inosine, and their combination as an adjunct to reperfusion in the treatment of acute myocardial infarction. ISRN Cardiol 2012: 326809.
293. de Jong JW (2012) Myocardial Energy Metabolism: Springer Netherlands. 310 p.
294. Zhang W, Baban B, Rojas M, Tofigh S, Virmani SK, et al. (2009) Arginase activity mediates retinal inflammation in endotoxin-induced uveitis. Am J Pathol 175: 891-902.
295. Rosenfeld JL, Dutta SP, Chheda GB, Tritsch GL (1975) Purine and pyrimidine inhibitors of arginase. Biochim Biophys Acta 410: 164-166.
296. Nikolic J, Bjelakovic G, Stojanovic I (2003) Effect of caffeine on metabolism of L-arginine in the brain. Mol Cell Biochem 244: 125-128.
297. Henzi V, Reichling DB, Helm SW, MacDermott AB (1992) L-proline activates glutamate and glycine receptors in cultured rat dorsal horn neurons. Mol Pharmacol 41: 793-801.
298. Lai AK, Lo AC (2013) Animal models of diabetic retinopathy: summary and comparison. J Diabetes Res 2013: 106594.
299. Storey KB (2007) Anoxia tolerance in turtles: metabolic regulation and gene expression. Comp Biochem Physiol A Mol Integr Physiol 147: 263-276.
300. Hou B, You SW, Wu MM, Kuang F, Liu HL, et al. (2004) Neuroprotective effect of inosine on axotomized retinal ganglion cells in adult rats. Invest Ophthalmol Vis Sci 45: 662-667.
301. Muto J, Lee H, Lee H, Uwaya A, Park J, et al. (2014) Oral administration of inosine produces antidepressant-like effects in mice. Sci Rep 4: 4199.
302. Munoz Garcia D, Midaglia L, Martinez Vilela J, Marin Sanchez M, Lopez Gonzalez FJ, et al. (2014) Associated Inosine to interferon: results of a clinical trial in multiple sclerosis. Acta Neurol Scand.
303. Schwarzschild MA, Ascherio A, Beal MF, Cudkowicz ME, Curhan GC, et al. (2014) Inosine to increase serum and cerebrospinal fluid urate in Parkinson disease: a randomized clinical trial. JAMA Neurol 71: 141-150.
304. Scott A, Fruttiger M (2010) Oxygen-induced retinopathy: a model for vascular pathology in the retina. Eye (Lond) 24: 416-421.
305. Daniels IS, Zhang J, O'Brien WG, 3rd, Tao Z, Miki T, et al. (2010) A role of erythrocytes in adenosine monophosphate initiation of hypometabolism in mammals. J Biol Chem 285: 20716-20723.
306. Lakowski B, Hekimi S (1996) Determination of life-span in Caenorhabditis elegans by four clock genes. Science 272: 1010-1013.

307. Sohal RS, Weindruch R (1996) Oxidative Stress, Caloric Restriction, and Aging. Science (New York, NY) 273: 59-63.
308. Neary MT, Ng KE, Ludtmann MH, Hall AR, Piotrowska I, et al. (2014) Hypoxia signaling controls postnatal changes in cardiac mitochondrial morphology and function. J Mol Cell Cardiol 74: 340-352.
309. Aslami H, Juffermans NP (2010) Induction of a hypometabolic state during critical illness - a new concept in the ICU? Neth J Med 68: 190-198.
310. Aviado DM (1983) Inosine : a naturally occurring cardiotonic agent. J Pharmacol 14 Suppl 3: 47-71.
311. Mather KJ (2013) The vascular endothelium in diabetes--a therapeutic target? Rev Endocr Metab Disord 14: 87-99.
312. Ting HH, Timimi FK, Boles KS, Creager SJ, Ganz P, et al. (1996) Vitamin C improves endothelium-dependent vasodilation in patients with non-insulin-dependent diabetes mellitus. J Clin Invest 97: 22-28.
313. Pournaras CJ, Rungger-Brandle E, Riva CE, Hardarson SH, Stefansson E (2008) Regulation of retinal blood flow in health and disease. Prog Retin Eye Res 27: 284-330.
314. Fawzi AA, Chou JC, Kim GA, Rollins SD, Taylor JM, et al. (2014) Sildenafil attenuates vaso-obliteration and neovascularization in a mouse model of retinopathy of prematurity. Invest Ophthalmol Vis Sci 55: 1493-1501.
315. Giannecchini M, Matteucci M, Pesi R, Sgarrella F, Tozzi MG, et al. (2005) Uptake and utilization of nucleosides for energy repletion. Int J Biochem Cell Biol 37: 797-808.
316. Tozzi MG, Camici M, Mascia L, Sgarrella F, Ipata PL (2006) Pentose phosphates in nucleoside interconversion and catabolism. FEBS J 273: 1089-1101.
317. Jurkowitz MS, Litsky ML, Browning MJ, Hohl CM (1998) Adenosine, inosine, and guanosine protect glial cells during glucose deprivation and mitochondrial inhibition: correlation between protection and ATP preservation. J Neurochem 71: 535-548.
318. Litsky ML, Hohl CM, Lucas JH, Jurkowitz MS (1999) Inosine and guanosine preserve neuronal and glial cell viability in mouse spinal cord cultures during chemical hypoxia. Brain Res 821: 426-432.
319. Li P, Ogino K, Hoshikawa Y, Morisaki H, Cheng J, et al. (2007) Remote reperfusion lung injury is associated with AMP deaminase 3 activation and attenuated by inosine monophosphate. Circ J 71: 591-596.
320. Li P, Ogino K, Hoshikawa Y, Morisaki H, Toyama K, et al. (2013) AMP deaminase 3 plays a critical role in remote reperfusion lung injury. Biochem Biophys Res Commun 434: 131-136.
321. Seynaeve H, Vermeiren A, Leys A, Dralands L (1994) Four cases of Wolfram syndrome: ophthalmologic findings and complications. Bull Soc Belge Ophtalmol 252: 75-80.
322. Hansen L, Eiberg H, Barrett T, Bek T, Kjaersgaard P, et al. (2005) Mutation analysis of the WFS1 gene in seven Danish Wolfram syndrome families; four new mutations identified. Eur J Hum Genet 13: 1275-1284.
323. Marshall BA, Permutt MA, Paciorkowski AR, Hoekel J, Karzon R, et al. (2013) Phenotypic characteristics of early Wolfram syndrome. Orphanet J Rare Dis 8: 64.

324. Yu G, Yu ML, Wang JF, Gao CR, Chen ZJ (2010) WS1 gene mutation analysis of Wolfram syndrome in a Chinese patient and a systematic review of literatures. Endocrine 38: 147-152.
325. Barrett TG, Bundey SE, Macleod AF (1995) Neurodegeneration and diabetes: UK nationwide study of Wolfram (DIDMOAD) syndrome. Lancet 346: 1458-1463.
326. Homa K, Stefanski A, Zmyslowska A, Moleda P, Bryskiewicz ME, et al. (2014) False diagnosis of type 1 diabetes mellitus and its complications in Wolfram syndrome--is it the reason for the low number of reported cases of this abnormality? Endokrynol Pol 65: 398-400.
327. de Heredia ML, Cleries R, Nunes V (2013) Genotypic classification of patients with Wolfram syndrome: insights into the natural history of the disease and correlation with phenotype. Genet Med 15: 497-506.
328. Rigoli L, Lombardo F, Di Bella C (2011) Wolfram syndrome and WFS1 gene. Clin Genet 79: 103-117.
329. Smith CJ, Crock PA, King BR, Meldrum CJ, Scott RJ (2004) Phenotype-genotype correlations in a series of wolfram syndrome families. Diabetes Care 27: 2003-2009.
330. Ishihara H, Takeda S, Tamura A, Takahashi R, Yamaguchi S, et al. (2004) Disruption of the WFS1 gene in mice causes progressive beta-cell loss and impaired stimulus-secretion coupling in insulin secretion. Hum Mol Genet 13: 1159-1170.
331. Fonseca SG, Ishigaki S, Oslowski CM, Lu S, Lipson KL, et al. (2010) Wolfram syndrome 1 gene negatively regulates ER stress signaling in rodent and human cells. J Clin Invest 120: 744-755.
332. O'Sullivan-Murphy B, Urano F (2012) ER stress as a trigger for beta-cell dysfunction and autoimmunity in type 1 diabetes. Diabetes 61: 780-781.
333. Sandhu MS, Weedon MN, Fawcett KA, Wasson J, Debenham SL, et al. (2007) Common variants in WFS1 confer risk of type 2 diabetes. Nat Genet 39: 951-953.
334. Fawcett KA, Wheeler E, Morris AP, Ricketts SL, Hallmans G, et al. (2010) Detailed investigation of the role of common and low-frequency WFS1 variants in type 2 diabetes risk. Diabetes 59: 741-746.
335. Minton JA, Hattersley AT, Owen K, McCarthy MI, Walker M, et al. (2002) Association studies of genetic variation in the WFS1 gene and type 2 diabetes in U.K. populations. Diabetes 51: 1287-1290.
336. Fukuoka H, Kanda Y, Ohta S, Usami S (2007) Mutations in the WFS1 gene are a frequent cause of autosomal dominant nonsyndromic low-frequency hearing loss in Japanese. J Hum Genet 52: 510-515.
337. Abecasis GR, Altshuler D, Auton A, Brooks LD, Durbin RM, et al. (2010) A map of human genome variation from population-scale sequencing. Nature 467: 1061-1073.
338. Shearer AE, Eppsteiner RW, Booth KT, Ephraim SS, Gurrola J, 2nd, et al. (2014) Utilizing ethnic-specific differences in minor allele frequency to recategorize reported pathogenic deafness variants. Am J Hum Genet 95: 445-453.
339. Manaviat MR, Rashidi M, Mohammadi SM (2009) Wolfram Syndrome presenting with optic atrophy and diabetes mellitus: two case reports. Cases J 2: 9355.

340. Batstra MR, Aanstoot HJ, Herbrink P (2001) Prediction and diagnosis of type 1 diabetes using beta-cell autoantibodies. Clin Lab 47: 497-507.
341. Fishman L, Ehrlich RM (1986) Wolfram syndrome: report of four new cases and a review of literature. Diabetes Care 9: 405-408.
342. Pinelli L, Cirillo D, Gonfiantini E, Maffeis C, Olivieri A (1987) HLA haplotypes and Wolfram's syndrome. Diabetes Care 10: 791-792.
343. Cano A, Molines L, Valero R, Simonin G, Paquis-Flucklinger V, et al. (2007) Microvascular diabetes complications in Wolfram syndrome (diabetes insipidus, diabetes mellitus, optic atrophy, and deafness [DIDMOAD]): an age- and duration-matched comparison with common type 1 diabetes. Diabetes Care 30: 2327-2330.
344. Schafer SA, Mussig K, Staiger H, Machicao F, Stefan N, et al. (2009) A common genetic variant in WFS1 determines impaired glucagon-like peptide-1-induced insulin secretion. Diabetologia 52: 1075-1082.
345. Kinsley BT, Swift M, Dumont RH, Swift RG (1995) Morbidity and mortality in the Wolfram syndrome. Diabetes Care 18: 1566-1570.
346. Al-Till M, Jarrah NS, Ajlouni KM (2002) Ophthalmologic findings in fifteen patients with Wolfram syndrome. Eur J Ophthalmol 12: 84-88.
347. Micic S, Ilic V, Micic M, Genbacev O, Dotlic R (1983) Endocrine profile of 45 patients with Sertoli cell only syndrome. Andrologia 15: 228-232.
348. Noormets K, Koks S, Kavak A, Arend A, Aunapuu M, et al. (2009) Male mice with deleted Wolframin (Wfs1) gene have reduced fertility. Reprod Biol Endocrinol 7: 82.
349. Haghighi A, Haghighi A, Setoodeh A, Saleh-Gohari N, Astuti D, et al. (2013) Identification of homozygous WFS1 mutations (p.Asp211Asn, p.Gln486[ast]) causing severe Wolfram syndrome and first report of male fertility. Eur J Hum Genet 21: 347-351.
350. Lim LS, Ling LH, Ong PG, Foulds W, Tai ES, et al. (2014) Dynamic responses in retinal vessel caliber with flicker light stimulation in eyes with diabetic retinopathy. Invest Ophthalmol Vis Sci 55: 5207-5213.
351. Andreas Reichenbach AB (2010) Mueller cells in the healthy and diseased retina. New York: Springer. 395 p.
352. Fagan A, Asghar O, Pearce K, Stout M, Ray SG, et al. (2015) Medalists with extreme duration of type 1 diabetes exhibit only mild diastolic dysfunction and myocardial fibrosis. Diabetes Care 38: e5-6.
353. Ng SK, Wood JP, Chidlow G, Han G, Kittipassorn T, et al. (2014) Cancer-like metabolism of the mammalian retina. Clin Experiment Ophthalmol.
354. Vacanti NM, Divakaruni AS, Green CR, Parker SJ, Henry RR, et al. (2014) Regulation of substrate utilization by the mitochondrial pyruvate carrier. Mol Cell 56: 425-435.
355. Storey KB (2015) Regulation of hypometabolism: insights into epigenetic controls. J Exp Biol 218: 150-159.
356. Newby AC (1984) Adenosine and the concept of 'retaliatory metabolites'. Trends in Biochemical Sciences 9: 42-44.
357. Nascimento FP, Figueredo SM, Marcon R, Martins DF, Macedo SJ, Jr., et al. (2010) Inosine reduces pain-related behavior in mice: involvement of adenosine A1 and A2A receptor subtypes and protein kinase C pathways. J Pharmacol Exp Ther 334: 590-598.

358. Kaster MP, Budni J, Gazal M, Cunha MP, Santos AR, et al. (2013) The antidepressant-like effect of inosine in the FST is associated with both adenosine A1 and A 2A receptors. Purinergic Signal 9: 481-486.
359. Caldwell RB, Zhang W, Romero MJ, Caldwell RW (2010) Vascular dysfunction in retinopathy-an emerging role for arginase. Brain Res Bull 81: 303-309.
360. Tatsumi Y, Kanamori A, Nagai-Kusuhara A, Nakanishi Y, Agarwal N, et al. (2008) Nipradilol protects rat retinal ganglion cells from apoptosis induced by serum deprivation in vitro and by diabetes in vivo. Curr Eye Res 33: 683-692.
361. Kolaczkowska E, Kubes P (2013) Neutrophil recruitment and function in health and inflammation. Nat Rev Immunol 13: 159-175.

Chapter VII: Appendix

A. Appendix A

A.1. Additional data regarding "Photoreceptors generate erucamide for maintenance of the retinal vasculature"

The following data is related to the concepts presented in the section "**Photoreceptors generate erucamide for maintenance of the retinal vasculature"(Chapter IV A).** These additional experiments were performed to assess angiogenin's ocular effects in the the C57/Bl6 mouse eye.

Effects of angiogenin overexpression in the mouse eye

To assess angiogenin's effects on the adult mouse retina, angiogenin recombinant protein (500 ng) or angiogenin overexpressing ShH10 (an adenovirus – AAV – that specifically transfects Mueller cells and astrocytes) and their respective controls were intravitreally injected in adult C57/Bl6 mice. The subsequent retinal phenotype was evaluated by using the following techniques:

1. **Fundus photography (Micron III)**

Enhancing intravitreal levels of angiogenin (both through viral overexpression and through injection of the recombinant protein) induced rapid development of white-yellow, raised patchy lesions resembling those observed in retinal inflammatory processes. The fact that the lesions show a similar phenotype in virus and protein injected eyes and that there is no evidence of lesions in control AAV injected eyes shows that the effect is specifically induced by angiogenin.

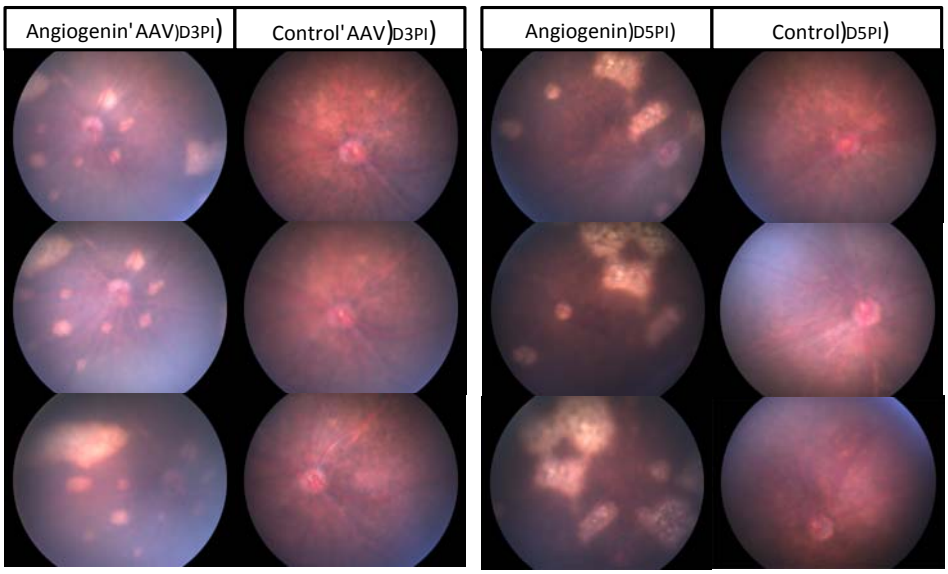

Figure 68 – Fundus lesions induced by angiogenin overexpression in the eye. Left side: representative images of retinas from eyes injected with angiogenin overexpression adenovirus (ShH10) and control adenovirus, at 3 days post injection; Right side: representative images of retinas from eyes injected with recombinant angiogenin protein and control protein at 5 days post-injection.

2. **Spectral Domain-OCT (Bioptigen**)

Cross sectional *in vivo* images of retinas from angiogenin-virus overexpressing injected eyes showed prominent subretinal and outer retinal lesions, consistent with inflammatory infiltrates and potential pathological neovascularization at these levels. Even though preretinal neovascularization was also observed, this only happened in rare cases and most lesions were actually seen at deeper retinal levels. Since angiogenin was delivered via intravitreal injection but angiogenin-induced lesions were mainly observed in the outer retina and subretinal space, it suggests that there is a higher sensitivity to its effects at this level, which could be explained by the presence of a specific receptor.

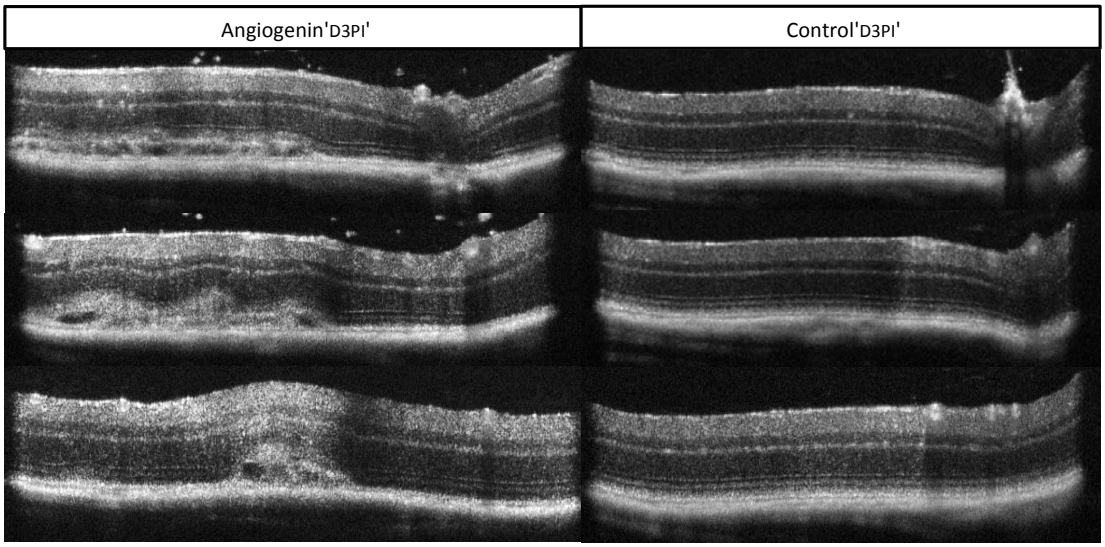

Figure 69 – Retinal lesions induced by intravitreal injections of angiogenin-overexpressing ShH10 showing prominent defects in the outer retina and in the subretinal space (3 days post injection).

3. **Gene expression: Angiogenesis and wound healing PCR arrays**

To assess inosine's effect on gene expression of genes involved in angiogenesis and fibrinolysis, PCR arrays were performed using retinal lysates from angiogenin and control injected eyes (ShH10) at 3 days post injection. Angiogenin overexpression in the retina affected expression of multiple genes in both pathways, suggesting that it induces an increase in fibrinolysis and matrix degradation that potentially facilitates and is associated with the growth of neovessels in undesired retinal locations. Moreover, angiogenin also elicited upregulation of inflammatory cytokines, such as Cxcl1 and Cxcl2, which are known to attract neutrophils with proangiogenic properties (via their receptor, CXCR2)[361].

Table 16 – Dysregulated gene expression levels of cytokines and angiogenic factors in Angiogenin-AAV injected eyes

Upregulated in ANG-AAV retinas				
Gene		**Fold change**	**P-value**	**Function**
Serpine 1 (PAI1)	Plasminogen activation inhibitor1	4.888473391	0.039845021	Anti-fibrinolysis
Plaur (uPAR)	Urokinase plasminogen activator receptor	12.22	0.04171	Profibrinolytic
Plat (tPA)	Tissue plasminogen activator	3.12	0.01463	Profibrinolytic
Timp1	Tissue inhibitor metalloprotease 1	3.02	0.02116	Extracelular matrix (ECM) degradation
Col5a3	Collagen type V Alpha 3	1.55	0.01228	Evidence of ECM degradation
Sphk1	Sphingosine kinase1	2.705879637	0.004637169	Possibly required for VEGFA induced tumor angiogenesis
Ctgf	Connective tissue growth factor	2.87	0.00594	Angiogenic modulator (regulates the balance between ECM synthesis and degradation)
STAT3	signal transducer and activator of transcription 3 (acute-phase response factor	2.41	0.03490	Mediates cellular responses to interleukins, and growth factors (e.g. FGF)
IL1b	Interleukin 1 beta	1.81	0.04170	Pro-inflammatory and proangiogenic cytokine
Cxcl1	chemokine (C-X-C motif) ligand 1	9.610077063	0.000246191	Attract neutrophils with proangiogenic properties; remodelling of connective tissue
Cxcl5	chemokine (C-X-C motif) ligand 5	1.974305618	0.052647881	
Tgfa	Transforming growth factor alpha	1.657044485	0.036907222	Promotes angiogenesis and cell growth
FGF2	Fibroblast growth factor 2	3.518054096	0.001789747	Proangiogenic factor
Downregulated genes in ANG-AAV retinas				
NOS3 (eNOS)	Endotelial nitric oxide synthase	1.681534447	0.030106684	Maintenace of antiproliferative environment in the vasculature
Kdr (VEGFR2)	VEGF receptor 2	1.651946159	0.008327158	Regulator of angiogenesis
Tek (Tie2)	Endothelial Tyrosine Kinase	1.503101048	0.02205797	Regulator of angiogenesis

4. **Protein: ELISA based angiogenesis array**

Levels of angiogenesis-related proteins were also assessed in retinal lysates from mice injected with angiogenin and control virus (3 days post injection). The upregulation of TIMP-1 was confirmed at the protein level and two cytokines were also found to be dysregulated: CCL5 (RANTES), a chemokine produced by T cells that attracts monocytes, memory T helper cells and eosinophils to the sites of inflammation; and CCL11, a chemokine that attracts eosinophils.

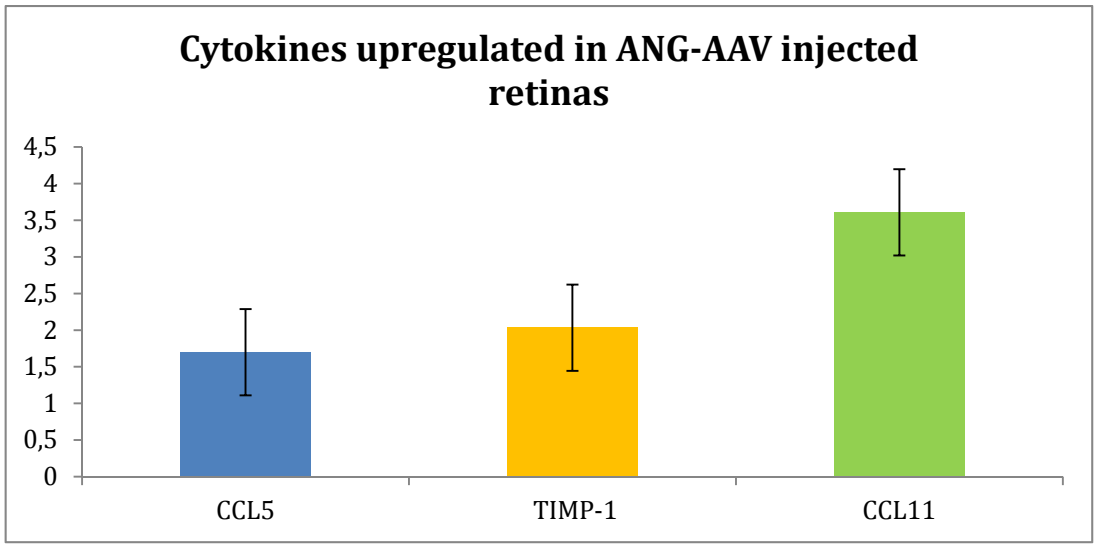

Figure 70 – Effects of angiogenin overexpression on protein levels of angiogenic factors in the retina (3 days post injection). Angiogenin -AAV injections increased production of TIMP-1, CCL5 and CCL11. (n=8; Two-tailed Student's t-test; values represent mean±SEM).

5. **Metabolomic analyses**

To further understand how angiogenin overexpression affected the ocular metabolic landscape, metabolomic analyses of angiogenin-AAV and control AAV injected eyes were performed 3 days post-injection. Angiogenin-AAV injected eyes showed a statistically significant ($p<0.01$) downregulation in levels of adenosine (6.7 fold), inosine (3 fold) and hypoxanthine (3 fold) when compared to control eyes, which further suggests that purine metabolism plays a central role in retinal pro-inflammatory and neurovascular diseases.

A.2. Additional data regarding "Neurovascular crosstalk between interneurons and capillaries is required for vision"

The following data is related to the section **"Neurovascular crosstalk between interneurons and capillaries is required for vision"** and presents additional figures that further illustrate and reinforce the concepts introduced in the main text.

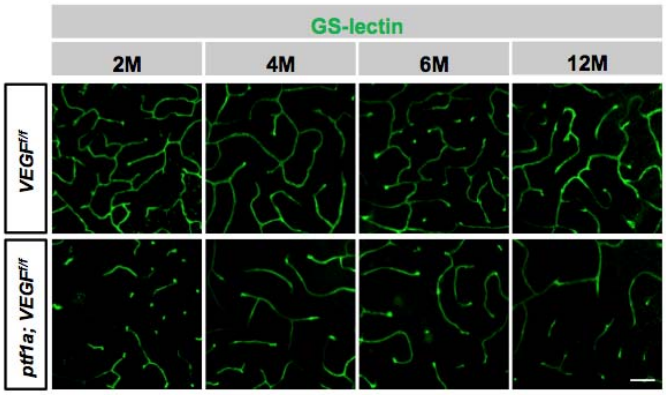

Figure 71 - Chronic intermediate plexus attenuation is observed in ptf1a-Cre; *VEGF* knockout mice. The intermediate plexus capillaries in the whole mount retinas of *VEGF*f/f or *ptf1a-Cre*; *VEGF*f/f mice at 2, 4, 6, 12 months. Scale bar: 50 µm.

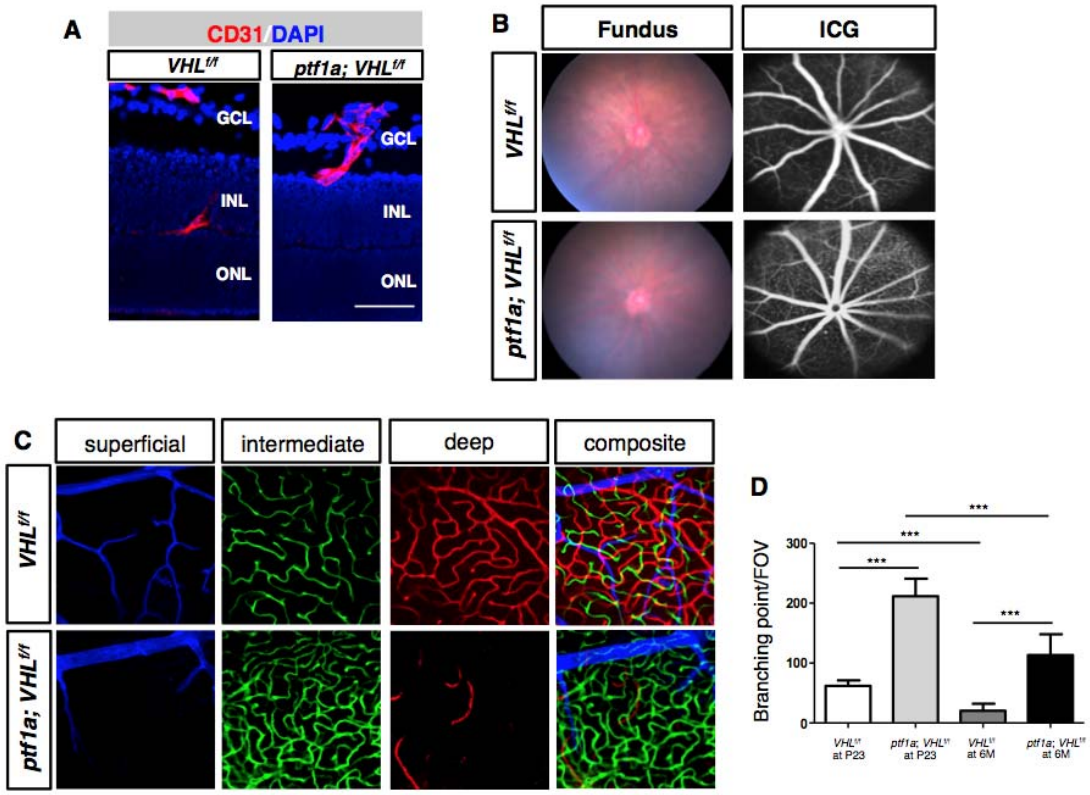

Figure 72 - Blood vessels do not advance to the OPL in *Vhl* mutants (A) Vessels sprout from the superficial plexus towards the OPL in controls (*VHL*f/f mice), but are directed towards the IPL in *ptf1a-Cre*; *VHL*f/f mice at P5 where *Vegfa* is most highly expressed. (B) In vivo imaging of the ocular fundus and indocyanine green angiography in *ptf1a-Cre*; *VHL*f/f mice and controls revealed dense vasculature. (C and D) The dense convoluted intermediate plexus, and attenuated superficial and deep plexuses persisted until as late as 20 months (C). Note that the abnormally high number of branching points persists in both groups longitudinally (D) (*n* = 4-5). ****P*<0.001; 2-tailed Student's *t* tests. Error bars indicate mean ± SD. Scale bar: 50 µm (A and C). GCL, ganglion cell layer; INL, inner nuclear layer; ONL, outer nuclear layer.

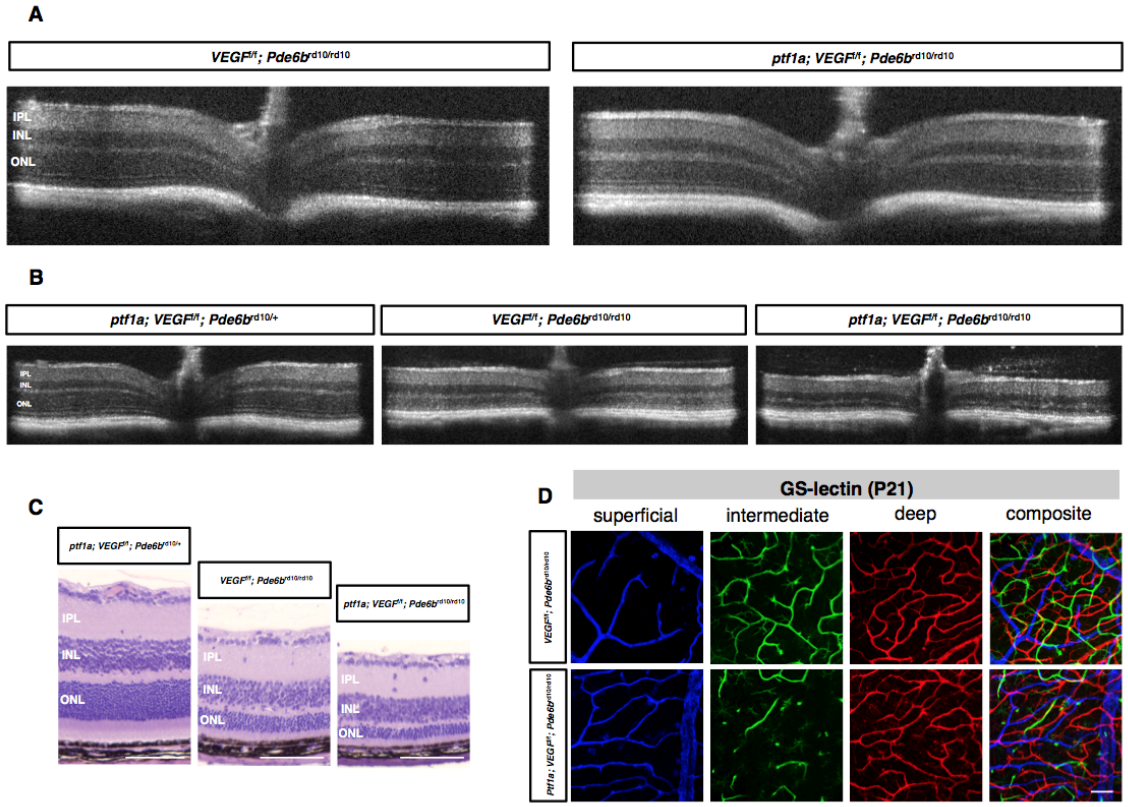

Figure 73 - Loss of VEGF in amacrine and horizontal cells accelerates photoreceptor atrophy in an animal model of retinal degeneration. (A) No degeneration (thinning of the ONL layer) is observed in SD-OCT images of P17 *ptf1a-Cre*; *VEGF*f/f; *Pde6b*rd10/rd10 mice compared with controls (*VEGF*f/f; *Pde6b*rd10/rd10). (B and C) Significant ONL thinning is observed in rd10 mice with impaired intermediate plexuses (*ptf1a-Cre*; *VEGF*f/f; *Pde6b*rd10/rd10) compared with rd10 mice (*VEGF*f/f; *Pde6b*rd10/ rd10), or with non-degenerating controls (one recessive *rd10* allele; *ptf1a-Cre*; *VEGF*f/f; *Pde6b*rd10/+) using OCT (B) and histology (C). (D) The integrity of the intermediate plexus is shown in P21 *ptf1a-Cre*; *VEGF*f/f; *Pde6b*rd10/rd10 mice (green) compared with controls (*VEGF*f/f; *Pde6b*rd10/rd10). Scale bar: 50 µm (C); 100 µm (D-F). IPL, inner plexiform layer; INL, inner nuclear layer; ONL, outer nuclear layer.

B. Appendix B

B.1. Additional data regarding "Inosine slows retinal metabolism in hypoxic conditions and prevents development of the most severe features of diabetic retinopathy"

Metabolic pathways of purine metabolism

The following schematics illustrate the most relevant metabolic pathways for understanding inosine metabolism.

The questionnaire provided to patients who accepted to be part of the MS-metabolomics blood serum study is also shown here (after the metabolic pathways).

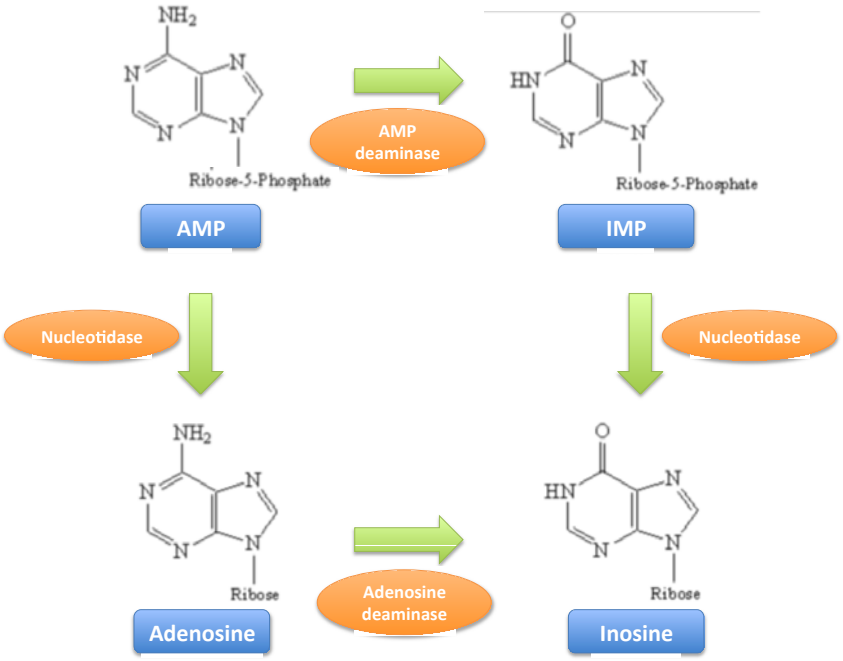

Figure 74 – Inosine production. Inosine can be produced both from Adenosine, by deamination (through AMP deaminase) and from Inosine-5-monophosphate (IMP), by cleavage of the phosphate group from the 5' C of the ribose (via 5' nucleotidase). AMP = adenosine monophosphate; IMP = inosine-5'-monophosphate.

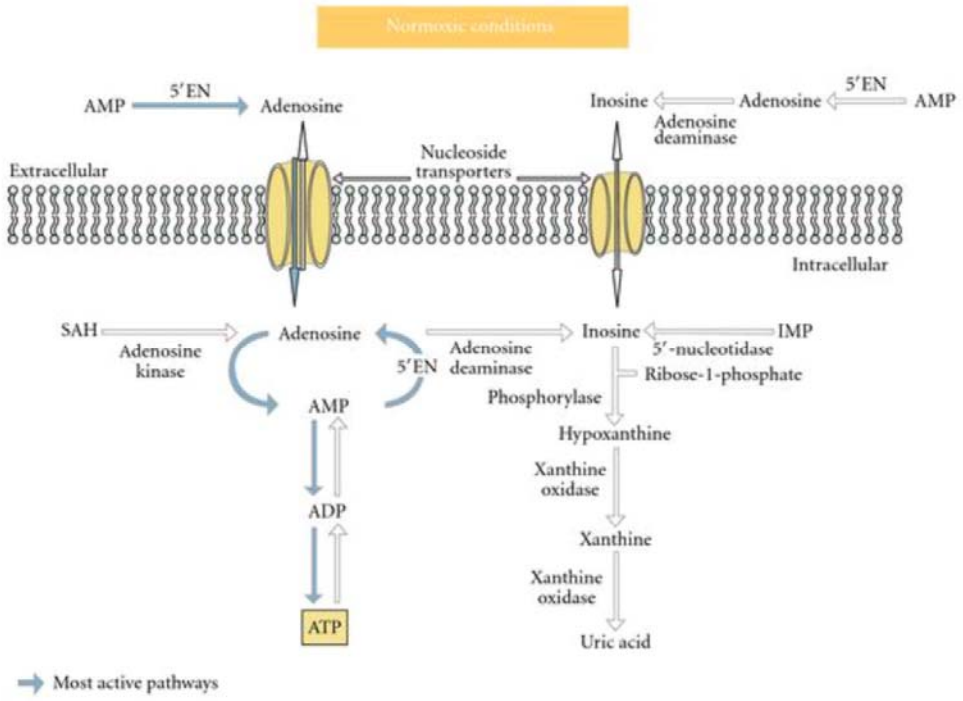

Figure 75 – Inosine metabolism in normoxic conditions (adapted from El Shafy et al[292]). Basal inosine levels in the plasma are practically undetectable (0.10 -0.1 um/l). In basal conditions, inosine is produced through deamination of adenosine by adenosine deaminase. Catabolism of inosine is performed by (a) purine nucleoside phosphorylase, yielding hypoxanthine, and by (b) xanthine oxidase, giving rise to uric acid.

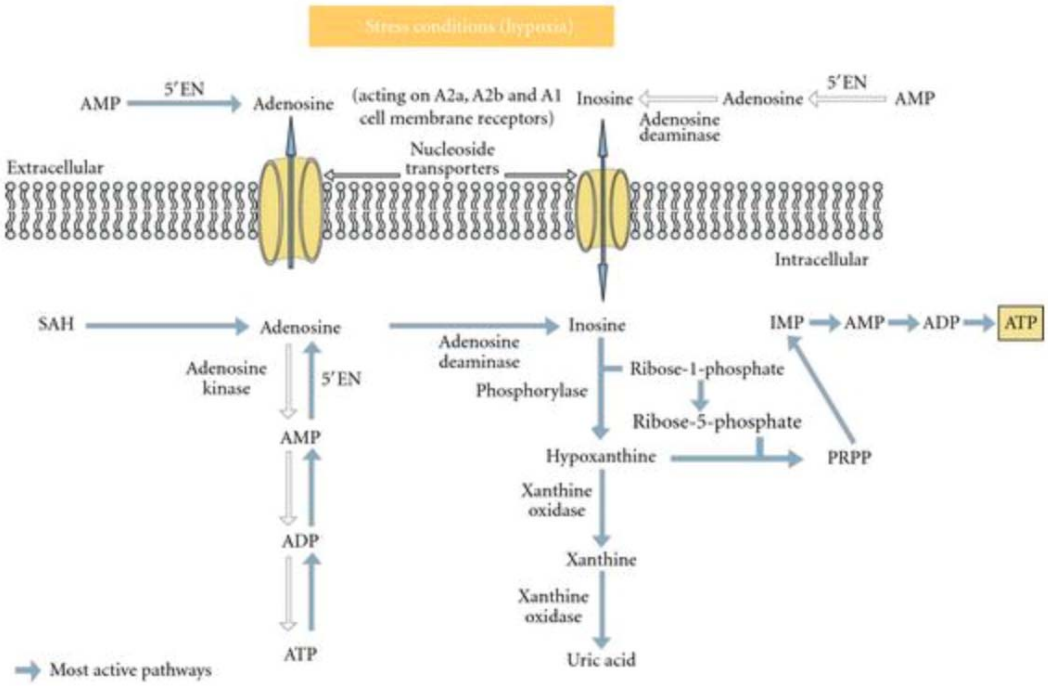

Figure 76 – Inosine metabolism in stress conditions (e.g. hypoxia). (adapted from El Shafy et al) [292] Under hypoxic conditions, due to ATP degradation, intracellular adenosine levels rise and so do those of inosine, which is shunted to the insterstitial space where it can reach concentrations greater than 1mM. Under hypoxic conditions, inosine can be greatly useful for the cell because (a) its phosphorylated ribose moiety can be used for anaerobic glycolysis (and the pentose phsophate pathway) for energy production[315] and (b) inosine can be used through the hypoxanthine-IMP-AMP pathway for ATP production.

Patient Data Collection Form for the Diabetic Retinopathy Study

Blood-borne infections

1. HBV/HCV/HIV infection:	☐ Not aware of ☐ Yes: Patient is excluded from the study.

Patient details

2. Patient study ID:	TK-
3. Date of blood sampling:	
4. Patient initials:	
5. DOB:	
6. Gender:	☐ Male ☐ Female
7. Ethnicity:	☐ White ☐ Hispanic ☐ Asian ☐ African-American ☐ Other
8. Weight (lbs):	
9. Height (ft, in):	

Diagnosis

10. Diabetic retinopathy stage:	☐ Mild NPDR ☐ Moderate NPDR ☐ Severe NPDR ☐ PDR Remarks:

Diabetes history

11. Type of diabetes:	☐ Type 1 diabetes mellitus ☐ Type 2 diabetes mellitus
12. Year of diabetes diagnosis:	
13. Latest HbA_{1c} (%):	Value: Date: ☐ HbA_{1c} not known
14. Oral antidiabetic therapy:	☐ No ☐ Yes, year of oral therapy start:
15. Insulin therapy:	☐ No ☐ Yes, year of insulin therapy start:
16. Type of insulin therapy:	☐ Conventional (fixed injection scheme) ☐ Intensive (meal-adapted injection scheme) by pen ☐ Intensive (meal-adapted injection scheme) by pump
17. Systemic diseases:	☐ Hypertension If yes: ☐ Antihypertensive therapy ☐ Hyperlipidemia If yes: ☐ Statin therapy ☐ Cardiovascular disease If yes: ☐ Myocardial infarction ☐ Cerebrovascular disease If yes: ☐ Stroke ☐ Diabetic nephropathy If yes: ☐ Renal dialysis therapy
18. Smoking:	☐ No ☐ Yes, pack years: